CONTENTS

Page

INTENTIONALLY LEFT BLANK

TABLES

Page

INTENTIONALLY LEFT BLANK

FIGURES

Page

FIGURES (Continued)

Page

FIGURES (Continued)

Page

INTENTIONALLY LEFT BLANK

2.3.7 Waste Form Degradation and Mobilization and Engineered Barrier System Flow and Transport

[NUREG-1804, Section 2.2.1.3.1.3: AC 1(1) to (5), (7), AC 2, AC 3(1) to (3), (5), AC 4, AC 5; Section 2.2.1.3.2.3: AC 1(2); Section 2.2.1.3.3.3: AC 1(1) to (10), (12), AC 2(1), (2), (4), AC 3(1) to (4), (6), AC 4, AC 5; Section 2.2.1.3.4.3: AC 1(1) to (6), (8), AC 2, AC 3(1) to (5), (8), (9), AC 4, AC 5(1) to (3)]

Section 2.3.7 outlines the models and analyses used to evaluate waste form degradation, fluid flow, and radionuclide transport in the Engineered Barrier System (EBS). This section addresses the requirements of proposed 10 CFR 63.114(a)(1) to (a)(7) and (b) regarding the abstraction of waste form degradation, fluid flow, and in-drift radionuclide transport in the performance assessment and specific acceptance criteria of NUREG-1804.

For the waste form degradation, EBS flow and transport analysis, this section presents the following:

- Data from the site, surrounding region, and laboratory studies; uncertainties and variabilities in parameter values; and alternative conceptual models used in the analyses
- Specific features, events, and processes (FEPs)
- Specific degradation, deterioration, and alteration processes, taking into consideration their effects on annual dose
- Technical bases for models used in the performance assessment.

The categories of information contained in this section, and the corresponding regulatory requirements and acceptance criteria (NUREG-1804), are provided in the table below. NUREG-1804, Section 2.2.1.3.1.3, Acceptance Criteria 1(7) and 3(5); Section 2.2.1.3.3.3, Acceptance Criteria 1(12) and 3(6); and Section 2.2.1.3.4.3, Acceptance Criteria 1(8) and 3(9) pertain to peer review, data qualification, and expert elicitation. Neither formal peer review nor expert elicitation was used in the development of information for the waste form degradation and mobilization and EBS flow and transport components of the total system performance assessment (TSPA). In addition, Section 2.3.7 does not discuss the approach used for data qualification. However, scientific analyses, model development, and data qualification activities were conducted in accordance with project procedures that comply with Quality Assurance Program requirements. The project procedures governing data qualification are consistent with NUREG-1298 (Altman et al. 1988). With regard to Acceptance Criterion 4(5) from NUREG-1804, Section 2.2.1.3.3.3, the equivalent continuum modeling approach (Pruess et al., 1990) is not used in the models described in Section 2.3.7.

NUREG-1804, Section 2.2.1.3.1.3, Acceptance Criterion 1(6), Section 2.2.1.3.3.3, Acceptance Criteria 1(11) and 3(5), NUREG-1804, Section 2.2.1.3.4.3, Acceptance Criterion 1(7) and 3(6) are not referenced below because they pertain to criticality, which is excluded from the TSPA. The information to screen criticality out as a scenario class is provided in Section 2.2.1.4.1. Similarly, NUREG-1804, Section 2.2.1.3.1.3 Acceptance Criterion 3(4) is not referenced in Section 2.3.7 because nondestructive examination of fabricated engineered barriers is addressed in Sections 1.5.2

and 2.3.6. Microbial effects on corrosion are addressed in Section 2.3.6, and other microbial effects are excluded (Table 2.2-5). Therefore, NUREG-1804 Section 2.2.1.3.3.3 Acceptance Criterion 2(5) and Section 2.2.1.3.4.3 Acceptance Criterion 3(7) are not referenced below. NUREG-1804, Section 2.2.1.3.4.3 Acceptance Criterion 5(4), on performance confirmation, is addressed by information provided in SAR Chapter 4 and is not referenced below.

SAR Section	Information Category	Proposed 10 CFR Part 63 Reference	NUREG-1804 Reference
2.3.7	Waste Form Degradation and Mobilization and Engineered Barrier System Flow and Transport	63.114(a)(1) 63.114(a)(2) 63.114(a)(3) 63.114(a)(4) 63.114(a)(5) 63.114(a)(6) 63.114(a)(7) 63.114(b) 63.342(c)	Section 2.2.1.3.1.3: Acceptance Criterion 1(1) Acceptance Criterion 1(2) Acceptance Criterion 1(3) Acceptance Criterion 1(4) Acceptance Criterion 1(5) Acceptance Criterion 1(7) Acceptance Criterion 2 Acceptance Criterion 3(1) Acceptance Criterion 3(2) Acceptance Criterion 3(3) Acceptance Criterion 3(5) Acceptance Criterion 4 Acceptance Criterion 5 Section 2.2.1.3.2.3: Acceptance Criterion 1(2) Section 2.2.1.3.3.3: Acceptance Criterion 1(1) Acceptance Criterion 1(2) Acceptance Criterion 1(3) Acceptance Criterion 1(4) Acceptance Criterion 1(5) Acceptance Criterion 1(6) Acceptance Criterion 1(7) Acceptance Criterion 1(8) Acceptance Criterion 1(9) Acceptance Criterion 1(10) Acceptance Criterion 1(12) Acceptance Criterion 2(1) Acceptance Criterion 2(2) Acceptance Criterion 2(4) Acceptance Criterion 3(1) Acceptance Criterion 3(2) Acceptance Criterion 3(3) Acceptance Criterion 3(4) Acceptance Criterion 3(6) Acceptance Criterion 4 Acceptance Criterion 5 Section 2.2.1.3.4.3: Acceptance Criterion 1(1) Acceptance Criterion 1(2) Acceptance Criterion 1(3) Acceptance Criterion 1(4)

SAR Section	Information Category	Proposed 10 CFR Part 63 Reference	NUREG-1804 Reference
2.3.7 (Continued)	Waste Form Degradation and Mobilization and Engineered Barrier System Flow and Transport (Continued)	63.114(a)(1) 63.114(a)(2) 63.114(a)(3) 63.114(a)(4) 63.114(a)(5) 63.114(a)(6) 63.114(a)(7) 63.114(b) 63.342(c)	Acceptance Criterion 1(5) Acceptance Criterion 1(6) Acceptance Criterion 1(8) Acceptance Criterion 2 Acceptance Criterion 3(1) Acceptance Criterion 3(2) Acceptance Criterion 3(3) Acceptance Criterion 3(4) Acceptance Criterion 3(5) Acceptance Criterion 3(8) Acceptance Criterion 3(9) Acceptance Criterion 4 Acceptance Criterion 5(1) Acceptance Criterion 5(2) Acceptance Criterion 5(3)
2.3.7.1	Summary and Overview	Not applicable	Not applicable
2.3.7.2	Summary of FEPs Evaluated in Waste Form Degradation and In-Drift Radionuclide Transport Models	63.114(a)(4)	Section 2.2.1.3.1.3: Acceptance Criterion 1(1) Section 2.2.1.3.3.3: Acceptance Criterion 1(1) Section 2.2.1.3.4.3: Acceptance Criterion 1(1)
2.3.7.3	Implementation of Conceptual Models	63.114(b) 63.342(c)	Section 2.2.1.3.1.3: Acceptance Criterion 1(1) Acceptance Criterion 1(2) Section 2.2.1.3.3.3: Acceptance Criterion 1(1) Acceptance Criterion 1(2) Section 2.2.1.3.4.3: Acceptance Criterion 1(1) Acceptance Criterion 1(2)
2.3.7.4	Radionuclide Inventory	63.114(a)(1) 63.114(a)(2) 63.114(a)(3) 63.114(a)(5) 63.114(a)(6) 63.114(a)(7) 63.114(b) 63.342(c)	Section 2.2.1.3.4.3: Acceptance Criterion 1(1) Acceptance Criterion 1(2) Acceptance Criterion 1(3) Acceptance Criterion 1(4) Acceptance Criterion 2(2) Acceptance Criterion 3(1) Acceptance Criterion 3(4) Acceptance Criterion 3(8) Acceptance Criterion 5(1)

SAR Section	Information Category	Proposed 10 CFR Part 63 Reference	NUREG-1804 Reference
2.3.7.5	In-Package Water Chemistry	63.114(a)(1) 63.114(a)(2) 63.114(a)(3) 63.114(a)(5) 63.114(a)(6) 63.114(a)(7) 63.114(b) 63.342(c)	Section 2.2.1.3.3.3: Acceptance Criterion 1(1) Acceptance Criterion 1(2) Acceptance Criterion 1(3) Acceptance Criterion 1(4) Acceptance Criterion 1(5) Acceptance Criterion 1(6) Acceptance Criterion 1(7) Acceptance Criterion 1(8) Acceptance Criterion 1(9) Acceptance Criterion 2(1) Acceptance Criterion 2(2) Acceptance Criterion 2(4) Acceptance Criterion 3(1) Acceptance Criterion 3(2) Acceptance Criterion 3(3) Acceptance Criterion 3(4) Acceptance Criterion 4(1) Acceptance Criterion 4(2) Acceptance Criterion 4(3) Acceptance Criterion 4(4) Acceptance Criterion 5
2.3.7.6	Commercial Spent Nuclear Fuel Cladding Degradation	63.114(a)(1) 63.114(a)(2) 63.114(a)(3) 63.114(a)(5) 63.114(a)(6) 63.114(a)(7)	Section 2.2.1.3.1.3: Acceptance Criterion 1(1) Acceptance Criterion 1(2) Acceptance Criterion 1(3) Acceptance Criterion 1(4) Acceptance Criterion 1(5) Acceptance Criterion 2 Acceptance Criterion 3(1) Acceptance Criterion 3(2) Acceptance Criterion 3(3) Acceptance Criterion 4 Acceptance Criterion 5 Section 2.2.1.3.2.3: Acceptance Criterion 1(2)

SAR Section	Information Category	Proposed 10 CFR Part 63 Reference	NUREG-1804 Reference
2.3.7.7	Commercial Spent Nuclear Fuel Degradation	63.114(a)(1) 63.114(a)(2) 63.114(a)(3) 63.114(a)(5) 63.114(a)(6) 63.114(a)(7) 63.114(b) 63.342(c)	Section 2.2.1.3.1.3: Acceptance Criterion 1(1) Acceptance Criterion 1(2) Acceptance Criterion 1(3) Acceptance Criterion 1(4) Acceptance Criterion 1(5) Acceptance Criterion 2 Acceptance Criterion 3(1) Acceptance Criterion 3(2) Acceptance Criterion 3(3) Acceptance Criterion 4 Acceptance Criterion 5 Section 2.2.1.3.2.3: Acceptance Criterion 1(2) Section 2.2.1.3.4.3: Acceptance Criterion 1(1) Acceptance Criterion 1(2) Acceptance Criterion 1(3) Acceptance Criterion 1(4) Acceptance Criterion 1(5) Acceptance Criterion 1(6) Acceptance Criterion 2 Acceptance Criterion 3(1) Acceptance Criterion 3(2) Acceptance Criterion 3(3) Acceptance Criterion 3(4) Acceptance Criterion 3(8) Acceptance Criterion 4 Acceptance Criterion 5(1) Acceptance Criterion 5(2) Acceptance Criterion 5(3)

SAR Section	Information Category	Proposed 10 CFR Part 63 Reference	NUREG-1804 Reference
2.3.7.8	U. S. Department of Energy Spent Nuclear Fuel Degradation	63.114(a)(1) 63.114(a)(2) 63.114(a)(3) 63.114(a)(5) 63.114(a)(6) 63.114(a)(7) 63.114(b) 63.342(c)	Section 2.2.1.3.1.3: Acceptance Criterion 1(1) Acceptance Criterion 1(2) Acceptance Criterion 1(3) Acceptance Criterion 1(4) Acceptance Criterion 1(5) Acceptance Criterion 2 Acceptance Criterion 3(1) Acceptance Criterion 3(2) Acceptance Criterion 3(3) Acceptance Criterion 4 Acceptance Criterion 5 Section 2.2.1.3.2.3: Acceptance Criterion 1(2) Section 2.2.1.3.4.3: Acceptance Criterion 1(1) Acceptance Criterion 1(2) Acceptance Criterion 1(3) Acceptance Criterion 1(4) Acceptance Criterion 1(5) Acceptance Criterion 1(6) Acceptance Criterion 2 Acceptance Criterion 3(1) Acceptance Criterion 3(2) Acceptance Criterion 3(3) Acceptance Criterion 3(4) Acceptance Criterion 3(8) Acceptance Criterion 4 Acceptance Criterion 5(1) Acceptance Criterion 5(2) Acceptance Criterion 5(3)

SAR Section	Information Category	Proposed 10 CFR Part 63 Reference	NUREG-1804 Reference
2.3.7.9	High-Level Radioactive Waste Glass Dissolution	63.114(a)(1) 63.114(a)(2) 63.114(a)(3) 63.114(a)(5) 63.114(a)(6) 63.114(a)(7) 63.114(b) 63.342(c)	Section 2.2.1.3.1.3: Acceptance Criterion 1(1) Acceptance Criterion 1(2) Acceptance Criterion 1(3) Acceptance Criterion 1(4) Acceptance Criterion 1(5) Acceptance Criterion 2 Acceptance Criterion 3(1) Acceptance Criterion 3(2) Acceptance Criterion 3(3) Acceptance Criterion 4 Acceptance Criterion 5 Section 2.2.1.3.2.3: Acceptance Criterion 1(2) Section 2.2.1.3.4.3: Acceptance Criterion 1(1) Acceptance Criterion 1(2) Acceptance Criterion 1(3) Acceptance Criterion 1(4) Acceptance Criterion 1(5) Acceptance Criterion 1(6) Acceptance Criterion 2 Acceptance Criterion 3(1) Acceptance Criterion 3(2) Acceptance Criterion 3(3) Acceptance Criterion 3(4) Acceptance Criterion 3(8) Acceptance Criterion 4 Acceptance Criterion 5(1) Acceptance Criterion 5(2) Acceptance Criterion 5(3)
2.3.7.10	Dissolved Radionuclide Concentration Limits	63.114(a)(1) 63.114(a)(2) 63.114(a)(3) 63.114(a)(5) 63.114(a)(6) 63.114(a)(7) 63.114(b) 63.342(c)	Section 2.2.1.3.4.3: Acceptance Criterion 1(1) Acceptance Criterion 1(2) Acceptance Criterion 1(3) Acceptance Criterion 1(4) Acceptance Criterion 1(5) Acceptance Criterion 1(6) Acceptance Criterion 2 Acceptance Criterion 3(1) Acceptance Criterion 3(2) Acceptance Criterion 3(3) Acceptance Criterion 3(4) Acceptance Criterion 3(8) Acceptance Criterion 4 Acceptance Criterion 5(1) Acceptance Criterion 5(2) Acceptance Criterion 5(3)

SAR Section	Information Category	Proposed 10 CFR Part 63 Reference	NUREG-1804 Reference
2.3.7.11	Colloidal Radionuclide Availability	63.114(a)(1) 63.114(a)(2) 63.114(a)(3) 63.114(a)(5) 63.114(a)(6) 63.114(a)(7) 63.114(b) 63.342(c)	Section 2.2.1.3.4.3: Acceptance Criterion 1(1) Acceptance Criterion 1(2) Acceptance Criterion 1(3) Acceptance Criterion 1(4) Acceptance Criterion 1(5) Acceptance Criterion 1(6) Acceptance Criterion 2 Acceptance Criterion 3(1) Acceptance Criterion 3(2) Acceptance Criterion 3(3) Acceptance Criterion 3(4) Acceptance Criterion 3(5) Acceptance Criterion 3(8) Acceptance Criterion 4 Acceptance Criterion 5(1) Acceptance Criterion 5(2) Acceptance Criterion 5(3)

SAR Section	Information Category	Proposed 10 CFR Part 63 Reference	NUREG-1804 Reference
2.3.7.12	Engineered Barrier System Flow and Transport Model	63.114(a)(1) 63.114(a)(2) 63.114(a)(3) 63.114(a)(5) 63.114(a)(6) 63.114(a)(7) 63.114(b) 63.342(c)	Section 2.2.1.3.3.3: Acceptance Criterion 1(1) Acceptance Criterion 1(2) Acceptance Criterion 1(3) Acceptance Criterion 1(4) Acceptance Criterion 1(5) Acceptance Criterion 1(6) Acceptance Criterion 1(7) Acceptance Criterion 1(8) Acceptance Criterion 1(9) Acceptance Criterion 1(10) Acceptance Criterion 2(1) Acceptance Criterion 2(2) Acceptance Criterion 2(4) Acceptance Criterion 3(1) Acceptance Criterion 3(2) Acceptance Criterion 3(3) Acceptance Criterion 3(4) Acceptance Criterion 4(1) Acceptance Criterion 4(2) Acceptance Criterion 4(3) Acceptance Criterion 4(4) Acceptance Criterion 5 Section 2.2.1.3.4.3: Acceptance Criterion 1(1) Acceptance Criterion 1(2) Acceptance Criterion 1(3) Acceptance Criterion 1(4) Acceptance Criterion 1(5) Acceptance Criterion 1(6) Acceptance Criterion 2 Acceptance Criterion 3(1) Acceptance Criterion 3(2) Acceptance Criterion 3(3) Acceptance Criterion 3(4) Acceptance Criterion 3(5) Acceptance Criterion 3(8) Acceptance Criterion 4 Acceptance Criterion 5(1) Acceptance Criterion 5(2) Acceptance Criterion 5(3)
2.3.7.13	Conclusions	Not applicable	Not applicable

In some instances, the acceptance criteria in the table above are addressed in multiple sections of the SAR. For example, acceptance criteria in NUREG-1804 Section 2.2.1.3.1.3 are addressed in Sections 2.3.6 and 2.3.7 since the EBS includes waste packages, drip shields, and waste forms. Acceptance criteria in NUREG-1804 Section 2.2.1.3.3.3 are addressed by one or more of Sections 2.2, 2.3.3 to 2.3.7, 2.3.11, and 2.4, as described more fully in Section 2.3.5.

2.3.7.1 Summary and Overview

This section describes processes initiated by the entry of water (as liquid or vapor) into the waste package, the degradation of the waste package internals and the waste form, and the subsequent release of radionuclides. This section also provides the models and parameters (and their associated uncertainty) for the calculation of radionuclide concentrations in the water, and radionuclide transport out of the waste package and through the invert. The abstractions presented here have been directly incorporated in the TSPA model described in SAR Section 2.4.

Spent nuclear fuel (SNF) and high-level radioactive waste (HLW) are emplaced within the repository in waste packages that are covered by drip shields. Release of radionuclides from within the waste package requires a breach of the waste package, degradation of the waste form, and a mechanism to transport material from the inside of the waste package. The rate of waste form degradation depends on the nature and condition of the waste form, the waste form temperature, and the chemical environment within the waste package. As degradation proceeds, sparingly soluble radionuclides may dissolve in water up to their solubility limits, which depend on the chemistry of the fluid. The concentrations of highly soluble radionuclides will depend on degradation rates of waste form materials. Radionuclides may also be mobilized by attachment to colloids present in the water that enters the waste package, and to colloids caused by the degradation of waste package internals and waste forms. Colloid-associated radionuclide concentrations will depend on the chemical composition of the water in the waste package, which is controlled largely by the degradation of the waste form.

The state of the waste package and drip shield affect flow and transport. When a drip shield is intact, only diffusive release is possible. When a waste package is cracked, only diffusive release is possible. When both have patch failures, advective releases are possible. The individual impacts on barrier capability are considered in a number of FEPs dealing with the physical form of the waste package and drip shield, and advection of liquids and solids (see Table 2.3.7-1, FEP 2.1.03.11.0A, and Table 2.2-5, FEPs 2.1.03.10.0A and 2.1.03.10.0B).

The processes and characteristics that have been determined to be important to the EBS capability, with respect to waste form degradation and mobilization and EBS flow and transport, include the following:

- **Advection of Liquids and Solids Through Cracks in the Drip Shield**—Any cracks that extend through the drip shield might allow the advective flow of water (Table 2.2-5), though the impacts of the latter on performance have been inconsequential. Cracks might form, for example, through mechanical damage caused by seismic activity. Advective flow is also possible after general corrosion failure of the drip-shield.

- **Advection of Liquids and Solids Through Cracks in the Waste Package**—Any cracks that extend through the waste package outer corrosion barrier and stainless steel inner vessel are expected to be of insufficient size and morphology to allow advection of water into the waste package. Advective water flow into the waste package is only possible when the degradation mode is by localized or general corrosion (Table 2.2-5). Although advective radionuclide transport does not occur through cracks, water vapor movement and diffusive transport through cracks does occur.

- **Chemical Characteristics of Water in Waste Package—**The alteration rate of different waste forms, the solubility of radionuclides, and the stability of colloids depend on the chemistry of the water inside a degraded waste package. Uncertainty in the in-package chemistry—in particular, the ionic strength and pH that have the most significant effect upon these coupled processes—has been considered in the abstraction models used in the TSPA and are presented in Section 2.3.7.5.

- **Radionuclide Solubility, Solubility Limits, and Speciation in the Waste Form and EBS—**The solubility of individual radionuclides has a significant effect on their release from the waste form to the edge of the waste package. Solubility models are presented in Section 2.3.7.10. The more soluble the radionuclide, generally the greater mass flux of that radionuclide that will be released by diffusive or advective release mechanisms from the waste form.

- **Sorption of Dissolved Radionuclides in the EBS**—Sorption occurs on various immobile and mobile (i.e., colloidal) phases in the waste package. The models used to evaluate this process are presented in Section 2.3.7.11. Sorption onto immobile phases, in particular the iron oxides generated from the corrosion of the structural and other support materials inside the waste package, significantly slows the release of dissolved and highly sorbing radionuclides, such as plutonium and americium.

- **Diffusion of Dissolved Radionuclides in the EBS**—The principal release mechanism of radionuclides from the waste package in the first several thousand years or longer is diffusion, which is in turn controlled by the degree of degradation of the waste package and the hydrologic characteristics that prevail within the waste package (Section 2.3.7.12).

- **Advection of Dissolved Radionuclides in the EBS**—Once radionuclides are released from the waste package by advection or diffusion, they are transported by advective and diffusive processes through the invert. Models used to describe this movement are presented in Section 2.3.7.12. In areas in which seepage or condensation takes place, or in zones where water flux is imbibed into the invert, the release will be dominated by advective transport from the invert into the fractured rock mass at the base of the invert.

- **Physical Form of the Waste Package and Drip Shield and Effects of Drip Shield on Flow**—The integrity of the waste package and drip shield over time will limit the access of water into waste packages and ultimately limit aqueous transport from failed waste packages (Section 2.3.4.1).

- **Unsaturated Flow in EBS**—Unsaturated flow occurs through the invert as a result of seepage or drift-wall condensation, imbibition from the host rock, or capillary condensation, and affects the release of radionuclides from the EBS (Section 2.3.7.12).

- **Chemical Characteristics of Water in Drifts**—The chemical makeup of water in the drift affects the corrosivity of EBS components and the transport characteristics of radionuclides (Section 2.3.5.1).

- **Chemical Interaction with Corrosion Products**—Sorption of dissolved radionuclides onto corrosion products contributes to the barrier capability by limiting transport (Section 2.3.7.12).

- **DOE SNF Degradation (Alteration, Dissolution, and Radionuclide Release)**—The degradation of DOE SNF affects the barrier capability of the waste form and the waste form internals by making available the radionuclides that are bound in the DOE SNF matrix (Section 2.3.7.8).

- **Commercial SNF Degradation (Alteration, Dissolution, and Radionuclide Release)**—The degradation of commercial SNF limits the availability of radionuclides present in the fuel matrix and in the gap and grain boundaries for subsequent transport from the package and is discussed in Section 2.3.7.7.

- **HLW Glass Degradation (Alteration, Dissolution, and Radionuclide Release)**—Kinetically-controlled degradation of HLW glass sets the rate at which radionuclides in the glass matrix are made available for interaction with fluids in the waste package and is discussed in Section 2.3.7.9.

- **Reaction Kinetics in Waste Package**—The rates at which individual components of the waste form degrade set limits on in-package chemistry, the dissolved concentrations of some radionuclides, the abundance of sorbing phases, and the overall availability of radionuclides leaching from fuels and glasses (Sections 2.3.7.5, 2.3.7.7 to 2.3.7.10, and 2.3.7.12).

- **Chemical Effects on Void Space in Waste Package**—The chemical and physical makeup of the void space inside breached waste packages is an important control over radionuclide stability and transport (Section 2.3.7.5).

Role of the Waste Form Degradation and Mobilization and Engineered Barrier System Flow and Transport Abstraction Models in the Total System Performance Assessment—Figure 2.3-2 provides a schematic representation of the TSPA model. The waste form degradation and the in-drift radionuclide transport submodels estimate the release of dissolved and colloidal radionuclides from the waste form. The submodels of the TSPA waste form degradation and mobilization component, and the associated information flows, are shown in Figures 2.3.7-1 through 2.3.7-7. Upstream estimates of waste package and drip shield degradation (Section 2.3.6) are combined with calculated physical and chemical conditions (Section 2.3.5) within the drift to set boundary conditions for the waste form degradation and radionuclide mobilization calculation. The estimated extent of waste form degradation and radionuclide mobilization is then used as input for the EBS transport calculation (Section 2.3.7.12). Each of the abstraction models is developed as a graph or a table.

2.3.7.2 Summary of FEPs Evaluated in Waste Form Degradation and In-Drift Radionuclide Transport Models

[NUREG-1804, Section 2.2.1.3.1.3: AC 1(1); Section 2.2.1.3.3.3: AC 1(1); Section 2.2.1.3.4.3: AC 1(1)]

FEPs relevant to this section are summarized in Tables 2.2-5 and 2.3.7-1. Some of the FEPs in Table 2.3.7-1 are also included in other models that provide inputs to the waste form degradation and in-drift transport models.

2.3.7.3 Implementation of Conceptual Models

[NUREG-1804, Section 2.2.1.3.1.3: AC 1(1), (2); Section 2.2.1.3.3.3: AC 1(1), (2); Section 2.2.1.3.4.3: AC 1(1), (2)]

The TSPA waste form degradation and mobilization and the EBS flow and transport models use the TSPA simulation tool GoldSim to predict the amounts of dissolved and colloidal radionuclides released over time from the waste form, through the corrosion products, out of the waste package, and through the invert.

Radionuclide inventory calculations are used to estimate the average radionuclide activity in the waste packages (Section 2.3.7.4). For each of the three primary waste types (commercial SNF, DOE SNF, and HLW), waste form degradation is modeled separately. The dose per waste package predicted from the commercial SNF degradation model bounds, or is representative of, the predicted dose per waste package calculated for naval SNF (Section 2.4.2.3.2.2.4), and is therefore used to represent the contribution of naval fuel.

Waste form degradation is analyzed using four models: (1) the in-package chemistry model evaluates the water chemistry inside waste packages (Section 2.3.7.5); (2) the commercial SNF degradation model predicts the degradation of fuel pellets (Section 2.3.7.7); (3) the DOE SNF degradation model evaluates the degradation rate of DOE SNF (Section 2.3.7.8); and (4) the HLW degradation model evaluates the degradation rate of the borosilicate glass encapsulating the HLW (Section 2.3.7.9). Although commercial SNF fuel rod cladding is expected to restrict radionuclide release, it is conservatively not included in the TSPA analyses (Section 2.3.7.6). Similarly, although DOE SNF cladding is expected to restrict radionuclide release, it is conservatively not included in the TSPA analyses. The effect of naval SNF structure on radionuclide release is accounted for in the assessment (Section 2.4.2.3.2.2.4) that justifies representing naval SNF waste packages with commercial SNF waste packages in the TSPA analyses.

The dissolved radionuclide concentration model determines the solubility of radionuclides for a particular water chemistry (Section 2.3.7.10), and the colloid model determines the mobilization of radionuclides attached to colloids (Section 2.3.7.11). Dissolved concentrations of highly soluble radionuclides (e.g. Tc and I) are calculated from waste form degradation rates (Section 2.4.2.2.1.1.3).

The EBS radionuclide flow and transport model (Section 2.3.7.12) predicts movement of dissolved and colloidal radionuclides through the waste form, out of the waste package, and through the invert.

These models depend on other models for key inputs, such as waste package surface temperatures (provided by the EBS thermal-hydrologic model, Section 2.3.5.4) and the time-dependent quantity of water seeping into the package.

Potential water flows are shown in Figure 2.3.7-8. The amount of water that can enter a waste package depends on (1) the time period assessed; and (2) the condition of the drip shields and waste packages. The time at which water may enter into the waste package and the specifics of degradation and transport are distinct for the nominal scenario class (Section 2.3.6); the early failure scenario class (Section 2.3.6); the seismic scenario class (Section 2.3.4); and the igneous scenario class (Section 2.3.11).

2.3.7.3.1 Nominal and Early Failure Scenario Classes

Prior to drip shield breach, any water seeping into the emplacement drifts or introduced into the drift walls as condensation (F_1) will be diverted away from the waste package (F_3) (Figure 2.3.7-8). Water vapor may only enter the waste package through stress corrosion cracks (Excluded FEP 2.1.03.10.0A, Advection of liquids and solids through cracks in the waste package, Table 2.2-5), and radionuclide release can only occur by diffusion through thin layers of water (Figure 2.3.7-9) (SNL 2007a, Section 6.3.4.5). After drip shield failure, advective flow through the drip shield can occur, and both diffusive and advective transport of radionuclides can occur, following waste package breach by general or localized corrosion. Advective transport is only expected to occur in a small fraction of the waste packages (other than those impacted by unlikely igneous events or faulting) failed by general corrosion (Section 2.4).

Manufacturing and handling defects may result in the early failure of waste packages (Section 2.3.6.6). An early failure is defined as the through-wall penetration of a waste package due to manufacturing or handling-induced defects, at a time earlier than would be predicted by mechanistic degradation models for a defect-free waste package. There are two early failure modeling cases: (1) one with early failure of the waste package, but with the drip shield intact yet undergoing general corrosion; and (2) the other with early failure of the drip shield with the waste package assumed to be failed by localized corrosion (Section 2.4.1). In the first case, releases are diffusive (until the drip shield fails). In the second case, the release would be both advective and diffusive.

2.3.7.3.2 Waste Form Degradation and Radionuclide Transport in the Seismic Scenario Class

Under the seismic scenario class (Section 2.3.4), a fraction of the drip shields and waste packages is assumed to be disrupted due to shaking, that is associated with unlikely seismic events. Seismic response (motion and rockfall) could cause drip shield and waste package damage, resulting in stress corrosion cracking of the waste package and drip shield. Rockfall can also lead to higher waste package and drip shield temperatures. Radionuclide transport through stress corrosion cracks may only occur through diffusion because the cracks are tight, tortuous, and will fill with precipitates. Radionuclide releases by diffusion will occur in a manner similar to the nominal scenario class. Once the drip shield fails (i.e., is initially breached), a portion of the total dripping flux can drip onto the waste package.

2.3.7.3.3 Waste Form Degradation and Radionuclide Transport in the Igneous Scenario

The igneous scenario class assumes eruptive and intrusive events (Section 2.3.11). In the volcanic eruption case, the associated waste form from impacted waste packages is transported to the surface. In the igneous intrusion case, a basalt dike intersects the repository (Section 2.3.11), and magma fills the drifts. The waste packages and drip shields are encapsulated in the magma and cease to perform their functions. The waste packages may slump or crack from the heat of the magma. As the magma cools, joints develop that eventually become pathways for groundwater movement once temperatures drop below 100°C. Any water moving through the cooled basalt can access radionuclides and transport them through the invert to the unsaturated zone (Figure 2.3.7-10). The water chemistry is modeled as pore water equilibrated with basalt.

2.3.7.4 Radionuclide Inventory

[NUREG-1804, Section 2.2.1.3.4.3: AC 1(1) to (4), AC 2(2), AC 3(1), (4), (8), AC 5(1)]

Determining the radionuclide inventory for use in the TSPA is a multistep process. First, a determination is made as to which radionuclides can exist within the SNF and HLW received at the repository. Then, a screening process is used to determine the radionuclides in terms of their potential contribution to the dose at the accessible environment. Those radionuclides shown to contribute only a small percentage of the potential dose (e.g., both 1% and 5% cutoffs were evaluated) are eliminated from further consideration (SNL 2007b, Section 6.2.6). Finally, the average initial inventory of radionuclides is estimated for each waste form and waste package type. The following sections describe the screening process and how the initial inventory estimates are developed.

2.3.7.4.1 Conceptual Description

[NUREG-1804, Section 2.2.1.3.4.3: AC 1(1) to (4)]

2.3.7.4.1.1 Waste Packaging and Waste Types to Be Disposed

Three types of waste are to be emplaced in the repository: commercial SNF, HLW, and DOE SNF (including naval SNF). These three types of waste will be placed in canisters, which in turn will be placed in waste packages. The waste package configurations that will be used for each waste form are shown in Figures 1.5.2-1 and 1.5.2-2. Additional details are provided in Section 1.5.2.

For the TSPA, one waste package category (consisting of two configurations) will contain only commercial SNF. The commercial SNF configurations are a medium transportation, aging, and disposal (TAD) canister and a small TAD canister. The medium TAD canister capacity is 21 pressurized water reactor (PWR) SNF assemblies or 44 boiling water reactor (BWR) SNF assemblies. The small TAD canister capacity is 12 PWR SNF assemblies, and the small TAD canister is longer than a medium TAD canister in order to dispose of the small fraction of PWR SNF assemblies that are too long to fit in the medium TAD canister. The design of the small TAD canister will not be completed prior to submission of the License Application. Small TAD canisters, however, make up a small fraction of the projected inventory. The small TAD canister estimated length was used in the calculation of the number of waste packages that would fill the repository

footprint for the TSPA. Because the small TAD canister contains less waste than the medium TAD, it is bounded by the performance of the medium TAD canister.

The second waste package category (consisting of three configurations) will contain codisposed wastes, consisting of HLW and DOE SNF in the same waste package. Two of the codisposal configurations are long and short packages, with five outer slots (that can hold 24-in.-diameter canisters of HLW or DOE SNF) surrounding a center slot (that can hold an 18-in.-diameter DOE SNF canister). Most codisposal waste packages will be loaded with a single 18-in.-diameter DOE SNF canister surrounded by five 24-in.-diameter HLW canisters. A small fraction of the codisposal waste packages will be loaded with an empty center slot and with the five outer slots holding four 24-in.-diameter HLW canisters and one 24-in.-diameter DOE SNF canister. The third codisposal configuration has four slots to load with two multicanister overpack canisters (which contain DOE SNF from Hanford) and two 24-in.-diameter HLW canisters.

The third waste package category (consisting of long and short configurations) contains naval SNF.

Commercial SNF is classified into two broad fuel categories: PWR and BWR fuels. Commercial nuclear power plants have used (and presently use) a variety of fuels and fuel configurations in their reactor cores. Most nuclear fuel is enriched uranium dioxide. Uranium dioxide fuel pellets are stacked in Zircaloy or stainless steel tubes (called cladding) that vary in size depending on reactor design. The stack of fuel pellets and associated cladding is called a fuel rod. Stainless steel cladding is no longer used and represents a small percentage of the overall inventory. Fuel rods are bundled into fuel assemblies using grid spacers that allow the flow of water between the rods within the assembly during reactor operation. The number of fuel rods per assembly varies depending on the core and reactor design. The radionuclide inventory within the commercial SNF varies depending on the history of usage and the fuel design.

Mixed oxide (MOX) fuel contains uranium and plutonium oxides. MOX waste also will be loaded into commercial SNF waste packages and, for the TSPA, its radionuclide content is added to the radionuclide inventory in the commercial SNF waste packages (SNL 2007c, Section 6.1.1).

Information regarding the design and performance of naval SNF and the naval spent fuel canister system is provided in Section 1.5.1.4. Commercial SNF waste packages are used to represent the naval SNF waste packages for all scenario classes in the TSPA as discussed in Section 2.3.7.3.

DOE SNF consists of many distinct types, and much like commercial SNF, radionuclide inventories for DOE SNF vary widely depending on the history and fuel design. The large variety of DOE SNF is indicative of the large number and variety of different research reactors. Section 1.5.1.3 provides a more detailed description of the DOE SNF. The DOE fuel assemblies and parts have been categorized by the size, shape, composition, and condition of the assemblies (Table 1.5.1-24; and DOE 2004, Appendix C and Table F-1). They will be packaged in long and short stainless steel canisters, which will then be loaded into the center slot of the codisposal waste packages (in most cases). There are also some 24-in.-diameter DOE SNF canisters that will be loaded in one of the five outer slots in the codisposal waste package. Also, a number of multicanister overpacks will be disposed of in codisposal waste packages with four outer slots and no central slot (two multicanister overpacks and two HLW canisters per waste package). Finally, a small amount of DOE SNF of

commercial origin may be shipped to the repository as uncanistered SNF in a cask. Once at the repository, this SNF would be removed from the cask and placed in TAD canisters.

The HLW in storage at DOE sites is primarily the result of reprocessing DOE SNF and other materials. HLW is immobilized by vitrification in a borosilicate glass. Borosilicate glass containing HLW will be shipped from four sites and delivered to the repository in either short or long stainless steel pour canisters. The Hanford Site will produce long (approximately 15-ft long) canisters. The Savannah River Site and Idaho National Laboratory will produce short (approximately 10-ft long) canisters. Additionally, a small amount of borosilicate glass containing HLW has been produced in short canisters at the West Valley Demonstration Project in New York, and is the result of reprocessing commercial SNF. Because the fuels reprocessed at each of these sites differ, the radionuclide inventory of the HLW (glass) will differ accordingly. The TSPA model uses an average inventory developed from the inventories from these multiple HLW sources, and uses a thermal source based on the most representative (Hanford and Savannah River Site) HLW (Section 2.3.7.4.2.3).

As described in Section 1.5.1, some excess DOE plutonium will be immobilized in lanthanide borosilicate glass. For the TSPA, the lanthanide borosilicate glass radionuclide inventory is conservatively added to the radionuclide inventory within the HLW canisters in the codisposal waste packages. That is, the HLW inventory in each codisposal waste package is that from the five (in most cases) HLW canisters plus a fraction of the total lanthanide borosilicate glass inventory, without reducing the HLW canister inventory in any waste package (SNL 2007c, Section 6.1.2). HLW canisters, will be disposed of in the outer five slots of codisposal waste packages, or in two of the four slots in the multicanister overpack codisposal waste packages.

2.3.7.4.1.2 Radionuclide Screening and Radionuclide Inventory

Radionuclides contained in the waste packages include fission products from reactor operations, actinides from neutron capture in uranium and plutonium, and activation products from neutron irradiation of structural materials and trace elements. Altogether, these fission products, actinides, and activation products constitute more than 100 radionuclides that may be collectively present in the waste packages at the time of repository closure. Many of the radionuclides have short half-life, low solubility and/or strongly sorbing characteristics, or are present in small quantities. Therefore, such radionuclides cannot be significant contributors to estimated dose. As a result, only a small subset of radionuclides needs to be considered in the evaluation of repository postclosure performance, and calculation of risk from that subset of radionuclides will result in essentially the same risk as would a calculation that includes all radionuclides. The following discussions and conclusions regarding the radionuclide screening process and radionuclide inventory development apply to commercial SNF and HLW, and to DOE (except naval) SNF and HLW. Section 2.3.7 of the Naval Nuclear Propulsion Program Technical Support Document addresses the development of the radionuclide inventory for a representative naval waste package to match the results of this screening process.

To determine the radionuclides that are most important to potential dose, two screening factors were calculated for each radionuclide: one for scenario classes and modeling cases involving groundwater transport (SNL 2007b, Section 1) (nominal, human-intrusion, seismic, early failure, and igneous intrusion; see Section 2.4.1.2); and one for the igneous eruptive modeling case, which

does not involve groundwater transport (Section 2.3.11; SNL 2007b, Section 1). The screening factors (NCRP 1996) are adjusted to reflect the local biosphere (SNL 2007b, Appendix A). The effects of inventory abundance, radionuclide longevity, element solubility, and element transport affinity (sorptivity) were considered. To evaluate inventory abundance, a screening calculation was performed for a broad range of commercial SNF (BWR, PWR, and MOX), HLW (Hanford, INL, Savannah River Site, West Valley, and lanthanide borosilicate glass), and DOE SNF (DOE SNF as a whole except for naval SNF, and U/Th Carbide DOE SNF separately) to determine those radionuclides present in sufficient quantities for 1,000,000 years after repository closure. The evaluation times were at 100, 200, 300, 500, 1,000, 2,000, 5,000, 10,000, 20,000, 30,000, 100,000, 300,000, and 1,000,000 years after emplacement. These sets of evaluation times capture the main features of the dominant radionuclides and their relative activities (SNL 2007b, Section 6.2.3). To address element solubility and transport affinity, the elements were evaluated in three solubility groups (high, medium, and low), and in three transport affinity groups (high, medium, and low). The isotopes in each group were compared to one another for relative importance.

Radionuclides were screened by calculating a radionuclide-screening product for each radionuclide. The radionuclide-screening product, which is roughly proportional to dose, is obtained by multiplying the screening factor for each radionuclide by the curie content of that radionuclide in the inventory. To evaluate the relative importance of each radionuclide for dose contribution calculations, the calculation of radionuclide screening factors considered consumption of locally produced vegetables, fish, meat, and milk; water consumption; inadvertent ingestion of soil; inhalation; and exposure to contaminated soil (SNL 2007b, Appendix A).

The screening products were ranked from largest to smallest and then summed, starting with the largest, until the screening products of each contributing radionuclide were included in the sum. For each waste type, time frame, solubility group, and transport affinity group, the radionuclides determined to contribute the first 95% of the summed radionuclide-screening products were considered potentially important and retained for analysis. Note that the 95% threshold does not directly correlate with actual calculated dose at the site boundary over the regulatory time period, but rather is based on a set of conservative hypothetical scenarios to ensure that appropriate attention is paid to those radionuclides that might affect actual TSPA doses (SNL 2007b, Section 6.2.1).

The results of the screening analysis are shown in Table 2.3.7-2. The table includes two radionuclides, ^{241}Pu and ^{245}Cm, that were added to capture the effect of their decay on the inventory of ^{241}Am (for ^{245}Cm) and the inventories of ^{241}Am and ^{237}Np (for ^{241}Pu) (SNL 2007b, Table 6-10). The radionuclides listed in Table 2.3.7-2 are a subset of those included in the radionuclide inventory tables in Section 1.5.1, because that section addresses radionuclides important for preclosure safety analysis in addition to those in Table 2.3.7-2 that are important for the TSPA.

The following radionuclides met the screening criteria but were eliminated from the screened-in list because they are short-lived daughters of included radionuclides that have a longer half life (greater than 180 days) and, hence, they are already included in the biological effects of the screened-in precursor radionuclides, as described in Section 2.3.10. The eliminated radionuclides are ^{225}Ac, ^{210}Bi, ^{239}Np, ^{210}Po, ^{223}Ra, ^{225}Ra, and ^{222}Rn (SNL 2007b, Table 6-10).

In contrast to prior TSPAs, ^{126}Sn and ^{79}Se are now screened in (SNL 2007b, Section 6.7.1). Although ^{94}Nb could be potentially important because of its significant ground shine exposure pathway in the igneous eruptive modeling case, it has been screened out because it did not meet the 95% screening criteria on which included that exposure pathway (SNL 2007b, Section 6.7.2). Earlier TSPAs have considered ^{94}Nb, and their results are consistent with screening it out in the current analysis.

10 CFR 63.331 specifically requires consideration of the combined activity of ^{226}Ra and ^{228}Ra in groundwater. Both radionuclides are already included in the TSPA because they met the screening criteria. Because ^{228}Ra is produced by the decay of ^{236}U and ^{232}Th, both ^{236}U and ^{232}Th should be included in the inventory, and both are included because they already met the screening criteria. ^{230}Th must also be included because it decays into ^{226}Ra (SNL 2007b, Table 4-4), and ^{230}Th is already included because it met the screening criteria (SNL 2007b, Table 6-8).

As shown in Table 2.3.7-2, 32 isotopes of 18 elements are included in the TSPA model for scenario classes or modeling cases involving groundwater transport. Table 2.3.7-2 also shows the 25 isotopes of 15 elements included in the TSPA for the igneous eruptive modeling case.

The result of the radionuclide screening analysis and the initial radionuclide inventory analysis is the radionuclide inventory (in terms of mass) of those radionuclides determined to be potentially important to dose. The result is shown in Tables 2.3.7-3 and 2.3.7-4 (SNL 2007d, Table 7-1[a]). Tables 2.3.7-3 and 2.3.7-4 are not directly comparable to the inventory tables listed in Section 1.5.1, because the inventories are at different points in time, and because the inventories in Tables 2.3.7-3 and 2.3.7-4 are on a per waste package basis. Table 2.3.7-5 (SNL 2008, Table 6.3.7-5) shows the inventory in a commercial SNF waste package (including MOX) and the inventory in a codisposal waste package (including DOE SNF and combined HLW and LaBS glass). This table shows the inventory in both grams and curies per waste package, at the repository closure date of 2117. Figures 2.3.7-11 and 2.3.7-12 show the decay of the radionuclide inventory in a commercial SNF waste package and in a codisposal waste package following closure.

The commercial SNF radionuclide quantities in Table 2.3.7-3 are for commercial SNF that is, on average, 23 years out of reactor on arrival at the repository, based on disposal rights (CRWMS M&O 2000a, Table 5, Case A - 63,000 MTU). For a later repository opening date than in previous TSPAs, use of the same waste stream at a later date, rather than an older waste stream due to decay, is conservative with respect to radionuclide inventory and heat. Waste will be emplaced for up to 50 years, depending on the amount of onsite aboveground aging required for the hottest waste packages. Ventilation will continue until the closure time used in the TSPA calculation, 2117, which is approximately 100 years after the start of emplacement. The radionuclide quantities shown in Tables 2.3.7-3 and 2.3.7-4 are at inventory times specific to the type of waste. The times of the waste form inventories are 2067 for commercial SNF (approximately 50 years after the start of emplacement), 2030 for HLW and DOE SNF, 2035 for MOX, and 2003 for lanthanide borosilicate glass. For the TSPA thermal calculation, it is assumed that the waste is emplaced simultaneously in 2067, and that it is 23 years old on-average at emplacement (SNL 2007d, Sections 6.4.1[a] and 7.1.1[a]). Waste that is 23 years old in 2067 has more radionuclide content than older waste, and hence is conservative with respect to radionuclide inventory and heat. HLW and DOE SNF radionuclide quantities in the above tables are those calculated at 2030 (SNL 2007d, Sections 6.4.1[a] and 7.1.1[a]). TSPA modeling of all three waste

sources will account for decay occurring from the time of emplacement (or inventory calculation) to repository closure, which is assumed to occur in 2117.

The inventories in Table 2.3.7-3 were developed based on a repository inventory of 70,000 metric tons of heavy metal (MTHM), with 90% being commercial SNF. Of the remaining 10%, two-thirds are allocated to HLW (glass), and one-third is allocated to DOE SNF. Because the HLW and DOE SNF allocations result in only partial filling of some codisposal waste packages, additional HLW is conservatively added to fill those waste packages for the purposes of calculation. The design for the subsurface does not identify a specific quantity as a contingency for drift length. The repository design contains about 4% more drift length than is needed to emplace the resulting quantity of waste packages, which is a contingency for the situation of unacceptable sections of some excavated drifts. For the purpose of the TSPA calculation, and to ensure that no potential location is ignored in the TSPA calculation, additional waste packages are conservatively added to fill all the emplacement drifts within the footprint (SNL 2007d, Section 5.14[a]). Section 1.3.1 presents the approach being taken in the design of the repository to designate which parts of the repository footprint will be allocated to contingency (only 70,000 MTHM will be emplaced, and some drift length will not be used, but will be excavated as contingency for unacceptable ground conditions found during repository construction). The resulting waste package count is 11,629, of which 8,213 are commercial SNF (including naval represented as commercial) waste packages, and 3,416 are codisposal waste packages that include both DOE SNF and HLW (SNL 2007d, Section 6.2[a]). See Section 1.3.2.4.3.1 for the total count of waste packages, and Table 1.5.2-2 for the fractional quantities of waste packages by type, that are being used in the design of the repository.

The inventories in Table 2.3.7-3 do not include approximately 47 MT of excess DOE plutonium that is currently planned to be disposed in the repository. Of the 47 MT, approximately 34 MT are planned to be converted into MOX fuel and eventually disposed of as commercial SNF; 13 MT are planned to be immobilized in a lanthanide borosilicate glass (LaBS glass) (SNL 2007c, Section 6.1). The inclusion of MOX SNF and LaBS glass HLW in the TSPA is accomplished by adding radionuclide-specific inventories to the inventories provided by *Initial Radionuclide Inventories* (SNL 2007d, Sections 5.7[a] and 6.4.1[a]), and the new radionuclides conservatively do not displace existing HLW or DOE SNF radionuclides. That is, the LaBS glass inventory is added to the HLW portion of the initial radionuclide inventory, and the MOX commercial SNF is added to the commercial SNF portion of the initial radionuclide inventory. The LaBS and MOX inventories are subject to the same uncertainty sampling applied to the HLW and commercial SNF radionuclide inventories, respectively. The total nominal inventories per waste package of MOX and LaBS glass HLW are shown in Table 2.3.7-4 (SNL 2007d, Table 7-1[a]).

The MOX radionuclide quantities are those calculated to exist in 2035, and the LaBS glass HLW radionuclide quantities are those calculated to have existed in 2003 (SNL 2007c, Section 7.1). Both will be decayed to the assumed date of 2117 for repository closure as part of the TSPA calculation.

2.3.7.4.2 Data and Data Uncertainty

[NUREG-1804, Section 2.2.1.3.4.3: AC 2(2), AC 3(1), (4), (8)]

In accordance with the Nuclear Waste Policy Act of 1982, as amended (Section 114), the inventory element of the TSPA model begins with an inventory of 70,000 MTHM. The total inventory is

allocated to 63,000 MTHM of commercial SNF and commercial HLW, and 7,000 MTHM of DOE SNF (including naval SNF) and DOE HLW (DOE 2008, Table 1; SNL 2007d, Section 1.1). The 7,000 MTHM of DOE SNF and DOE HLW is allocated to be 2/3 DOE HLW and 1/3 DOE SNF. When assigning waste to the available waste packages, the (DOE or DOE plus commercial) HLW allocation is exhausted before the DOE SNF allocation. The codisposal waste packages are filled with additional HLW for the purpose of the TSPA calculation, because (1) additional HLW is available; (2) it is unlikely that partially filled waste packages would be emplaced; and (3) the TSPA is based on full waste packages (SNL 2007d, Section 5.10[a]). This adds approximately 3,000 MTHM to the TSPA calculation (SNL 2007d, Section 6.2[a]). To emplace the nominal 70,000 MTHM of waste requires about 96% of the available emplacement drift length. To calculate the effect of waste in any of the available locations, the TSPA fills the additional drift length with waste packages, for calculational purposes only, for a grand total of 11,629 waste packages (8,213 commercial SNF and naval SNF waste packages, and 3,416 codisposal waste packages). The added waste packages are distributed proportionally by type such that the fractional representation of any waste package type is the same for the 70,000 MTHM set of waste packages and the full-footprint set of waste packages. The 108 drifts in the TSPA calculation contain 76,223 MTHM of modeled waste, with the excess above the 70,000 MTHM emplacement limit about equally divided between additional waste packages and additional HLW in otherwise partially-filled codisposal waste packages (SNL 2007d, Table 6-2[a], and Sections 5.10[a] and 5.14[a]).

There are three sources of uncertainty with respect to the radionuclide inventory. The first is the computational method and nuclear data used to predict radionuclide inventories (e.g., isotopic neutron cross section or decay half-life). The second source of uncertainty is the existence and condition of records kept for SNF and HLW materials (e.g., burnup history or batch compositions). The third source of uncertainty involves future decisions that may influence the creation, packaging, or shipment of waste; this can be thought of as a heterogeneity uncertainty. Uncertainty multipliers from the combined three sources of uncertainty are developed from sensitivity studies and are applied to the inventory of radionuclides for each waste type (commercial SNF, HLW, and DOE SNF) (SNL 2007d, Section 6.6), as described below and shown in Table 2.3.7-6.

2.3.7.4.2.1 Commercial SNF Inventory Data and Data Uncertainty

The amount of commercial SNF and commercial HLW allocated to be disposed at Yucca Mountain will be 63,000 MTHM. Although the commercial allocation includes commercial HLW, the TSPA models commercial HLW as part of the larger quantity of DOE HLW. Similarly, naval SNF is part of the DOE SNF allocation, but is modeled in the TSPA using commercial SNF as a representative surrogate as described in Sections 1.5.1 and 2.4.2.3.2.2.4. The radionuclide inventory received at the repository is dependent on the burnup of the fuel and the time since reactor discharge. Because nuclear fuel technology has improved as the industry has matured, the burnup of fuel has increased. Uncertainty exists regarding the timing or sequence in which fuel will be shipped to Yucca Mountain. If the oldest fuel is shipped to the repository first, the average burnup of the fuel to be disposed would be about 36 GWd/MTHM (SNL 2007d, Tables 6-6 and 6-7, 1999 Case C, and 2002 Case A). However, if the youngest shippable fuel is sent first, the average burnup would be about 49 GWd/MTHM (SNL 2007d, Tables 6-6 and 6-7, 2002 Case D). The nominal inventory given in Table 2.3.7-3 is based on initial shipment of 10-year-old fuel first, resulting in an average burnup of

38 GWd/MTHM (SNL 2007d, Tables 6-6 and 6-7, 1999 Case A). Different receipt scenarios are accounted for through uncertainty distributions on total inventory (SNL 2007d, Section 6.6).

An analysis of the uncertainty associated with the computational method and nuclear data, which also includes uncertainty in commercial SNF burnup history (based on the differences between measured and calculated isotope quantities), has provided correction factors to represent the minimum and maximum ratios of 0.89 to 1.08 for the inventory of commercial SNF (SNL 2007d, Section 6.6.1).

No uncertainty modifier was applied for the records of commercial SNF materials, because NRC regulations for commercial fuel require extensive historical records of burnup and/or batch configuration, and because burnup history record uncertainty (1.89%) is included in the uncertainty associated with computational method and nuclear data (SNL 2007d, Section 6.6.1).

The uncertainty due to heterogeneity of waste in the repository average inventories was investigated by comparing average burnups of three 1999 arrival forecasts and four 2002 arrival forecasts (SNL 2007d, Section 6.6.1). The 2002 forecasts account for a younger fuel population. The minimum and maximum ratios of the projected average burnups for these cases over the inventory given in Table 2.3.7-3 are 0.95 and 1.29 (SNL 2007d, Table 6-7). When multiplied by the minimum and maximum inventory ratios of 0.89 and 1.08 for the computational method, a range of 0.85 to 1.40, as shown in Table 2.3.7-6, is obtained (SNL 2007d, Section 6.6.1). Because the radionuclide inventories (except that of ^{238}U) are highly burnup-dependent, they are correlated and should not be sampled independently. Therefore, an uncertainty multiplier is sampled and applied to the radionuclide inventories, except ^{238}U, in the TSPA. A uniform distribution was selected because it equally weights the possible values. The ^{238}U uncertainty is small and not modeled in the TSPA (SNL 2007d, Section 6.6.1). The inventory of ^{238}U has much less relative uncertainty than the other radionuclides, because it is the dominant isotope in the initial fuel and changes little during reactor operation.

2.3.7.4.2.2 U.S. Department of Energy SNF Inventory Data and Data Uncertainty

The naval SNF inventory portion of DOE SNF is discussed in Section 1.5.1.4 and in Section 2.3.7 of the Naval Nuclear Propulsion Program Technical Support Document. The DOE is responsible for storage and final disposition of nuclear fuel that spans several decades of nuclear research and defense-related material production within the United States. The SNF presently in DOE custody consists of several hundred different fuel types (see Table 1.5.1-23). Although the historical data (e.g., fuel fabrication, operations, and storage records) are incomplete or of uncertain quality for some of these fuels, conservative assumptions based on available information can be made regarding the nature of the fuel.

The fuel information available at DOE storage sites depends on the records requirements and the intended disposition path at the time the fuel was placed into storage. These requirements and disposition paths were often unique to each of the DOE storage sites and evolved over time. As a result, the availability and completeness of the radionuclide inventories and associated documentation varies considerably for DOE SNF. Detailed characterization of these fuels is not necessary, however, because a conservative source term estimate is used for these fuels for repository design and analyses.

A conservative estimate of the radionuclide inventory in SNF was developed for each of the DOE SNF storage sites. The inventory was generated from calculational techniques and relevant experimental data and confirmatory studies (DOE 2003, p. 14). The result of this work is a database with over 500 entries. Each DOE SNF entry includes the radionuclide inventory, the number of assemblies, and the number and type of canisters that will contain the DOE SNF.

The inventory estimates (DOE 2003, Appendix C) provide both a nominal and a bounding radionuclide inventory estimate for each DOE SNF entry. Both the nominal and bounding inventory per waste package for the weighted average of the DOE SNF waste were analyzed to determine uncertainty in the DOE SNF radionuclide inventory (SNL 2007d, Section 6.6.2).

A range of total DOE SNF inventory (0.45 to 2.9 times the nominal inventory) was established:

- The nominal inventory (Table 2.3.7-3) includes conservative assumptions (SNL 2007d, Section 6.6.2) applied to the small percentage of fuel for which little information is available (0.31%). These assumptions include beginning-of-life inventory being double the end-of-life value, and use of activity per unit mass values for each radionuclide being the maximum of the highest value for that radionuclide in any of the well-characterized DOE SNF types. These assumptions result in 38% of the assumed total inventory being contained in 0.31% of the fuel, resulting in a potential overestimation of the total curie inventory by about 38%.

- The best estimate inventory has a ratio of 0.62 to the nominal inventory (SNL 2007d, Section 6.6.2). The best estimate inventory is lower than the nominal inventory, because the conservatism of the nominal inventory is replaced by the assumption that the small percentage of fuel for which little information is available (0.31%) has the same inventory as the average of the remaining fuel, rather than 38% of the assumed total inventory.

- The bounding radionuclide inventory is assumed to be as much as twice the nominal inventory per waste package (SNL 2007d, Section 6.6.2).

The inventory per waste package is also affected by the number of DOE SNF canisters that will be used to dispose of the inventory. The range of canister counts is 2,500 to 5,000, with a best estimate of 3,607. The lower bound for the inventory-per-package multiplier is the best estimate (0.62) times 3,607/5,000, which is 0.45. The upper bound is the upper bound inventory (1.99) times 3,607/2,500, which is 2.9. Like commercial SNF, the uncertainties of the DOE SNF radionuclide inventories are correlated, and an uncertainty multiplier is defined to capture the uncertainty for all radionuclides except ^{238}U. The DOE SNF multiplier is taken from a triangular distribution with a minimum of 0.45, a best estimate value of 0.62 times nominal, and a maximum of 2.90, as shown in Table 2.3.7-6. It is applied to the nominal values for DOE SNF grams per waste package in Table 2.3.7-3 for all isotopes except ^{238}U (SNL 2007d, Section 6.6.2). A triangular distribution is appropriate because only a best estimate and endpoint values are available. A cumulative distribution function for a triangular distribution is determined by simple mathematical formulas (Evans et al. 1993, p. 149), providing a reasonable probability distribution between the endpoints.

2.3.7.4.2.3 HLW Inventory Data and Data Uncertainty

The uncertainty of HLW radionuclide inventory is primarily due to heterogeneity uncertainty, that is based on uncertainty in the number of canisters that will be used to package the known HLW total inventory. Because the heterogeneity uncertainty is much larger than the uncertainty in the overall inventory, the heterogeneity uncertainty discussed below is essentially the same as the overall uncertainty.

The radionuclide inventory of the HLW is summarized in Table 2.3.7-3. The HLW radionuclide inventory (in curies per canister for each radionuclide) is evaluated for the borosilicate glass to be produced at the four sites that will be supplying HLW to the repository. The great majority of the HLW inventory will be received from Savannah River and Hanford. The weighted average of the total inventory is dominated by the radioactive material to be received from these two sites; therefore, the canisters from the Idaho National Laboratory and West Valley Demonstration Project are treated as similar to those from Savannah River and Hanford (SNL 2007d, Section 6.6.3).

Radiological compositions of HLW canisters to be received from the Savannah River Site are shown in Table 2.3.7-7 (SNL 2007d, Table 4-9, Appendix 1).

Data on HLW to be received from the Hanford site (Hamel 2003) include HLW canister production estimates for the Hanford Waste Treatment and Immobilization Plant, and include the program case (maximum expected production of canisters with the least effective waste loading), planning case (nominal expected production), and the technology case (minimum expected HLW canister production with the maximum waste loading). Table 2.3.7-8 summarizes canister production estimates for the three waste loading cases and three canister glass fill percentages.

The uncertainty in the repository average inventory per HLW canister is directly related to the uncertainty in the number of canisters into which the total HLW inventory is placed. The uncertainty of radionuclide loading per HLW canister applies to all isotopes equally. Therefore, an uncertainty multiplier is used to represent the uncertainty in the HLW inventory per canister. The minimum inventory per waste package is 0.7 times the nominal value, based on the nominal canister count of 9,202 divided by the maximum count of 13,205 (Tables 2.3.7-6 and 2.3.7-8) (SNL 2007d, Section 6.6.3). The maximum inventory per waste package is 1.3 times the nominal value, based on the nominal canister count of 9,202 divided by the minimum count of 7,071 (Table 2.3.7-8) (SNL 2007d, Section 6.6.3). Because of potential technological advancement in radionuclide glass loading, it is prudent to overestimate the upper limit, and a ratio of 1.5 is used instead of 1.3 (Table 2.3.7-6) (SNL 2007d, Section 6.6.3). With the nominal, maximum, and minimum values defined, a triangular distribution is used for the HLW uncertainty multiplier for use by the TSPA. This multiplier is to be applied to the nominal HLW inventories shown in Table 2.3.7-3 for all isotopes (including ^{238}U) (SNL 2007d, Section 6.6.3). The uncertainty multiplier is taken from a triangular distribution with a minimum of 0.70, best estimate value of 1, and a maximum of 1.5, as shown in Table 2.3.7-6. A triangular distribution is appropriate because only a best estimate and endpoint values are available. The cumulative distribution function for a triangular distribution is determined by simple mathematical formulas (Evans et al. 1993, p. 149), providing a reasonable probability distribution between the endpoints.

2.3.7.4.3 Abstraction and Results

[NUREG-1804, Section 2.2.1.3.4.3: AC 5(1)]

The radionuclide inventories for a representative commercial SNF waste package and for a representative codisposal waste package were derived by averaging the radionuclide inventories in each of the commercial SNF and codisposal waste package configurations over the number of waste packages per configuration, the results of which are shown in Table 2.3.7-3 (SNL 2007d, Table 7-1[a]). The initial mass of each radionuclide shown in Table 2.3.7-3 is supplemented by the MOX and LaBS glass inventory (SNL 2007c, Section 7.1), as shown in Table 2.3.7-4 (SNL 2007d, Table 7-1[a]). Each of the five waste form inventories is then adjusted from the time of the inventory (2003 for lanthanide borosilicate glass, 2030 for HLW and DOE SNF, 2035 for MOX, and 2067 for commercial SNF) until the 2117 TSPA calculation start time (SNL 2007d, Section 7.1.1[a]). These values are then used to initialize source terms during each TSPA model realization. The initial masses are then adjusted to account for uncertainty by applying the multipliers shown in Table 2.3.7-6.

Note that the DOE HLW allocation of 4,667 MTHM (Dreyfus 1995; Lytle 1995) would not fill the codisposal waste packages used in the TSPA, based on the "historic method" for counting MTHM per HLW canister (2.28 MTHM per West Valley canister and 0.5 MTHM per DOE HLW canister) (DOE 1985, Table 1-1). The TSPA was calculated assuming full codisposal waste packages, thus providing an extra margin of conservatism and preventing the underestimation of risk due to HLW (SNL 2007d, Section 5.10[a]). The use of a higher MTHM due to the larger number of HLW canisters or the inclusion of MOX and LaBS glass inventory in no way implies that the LA is requesting to dispose of more than 70,000 MTHM. The addition of the MOX and LaBS glass inventory in the TSPA provides conservatism for analytical purposes only.

2.3.7.5 In-Package Water Chemistry

[NUREG-1804, Section 2.2.1.3.3.3: AC 1(1) to (9), AC 2(1), (2), (4), AC 3(1) to (4), AC 4(1) to (4), AC 5]

Water chemistry within the waste packages and pathways must be evaluated because it controls waste form degradation (Sections 2.3.7.7 and 2.3.7.9), radionuclide solubilities (Section 2.3.7.10), and the suspension stabilities of colloids (Section 2.3.7.11).

2.3.7.5.1 Conceptual Description of the In-Package Water Chemistry

[NUREG-1804, Section 2.2.1.3.3.3: AC 1(1) to (4)]

In the event of waste package breach, the stainless steel inner vessel and, in the case of commercial SNF waste packages, the TAD canister itself, are modeled as breaching simultaneously. Water may then enter as a vapor (or possibly as a liquid) that is assumed to condense on the internal surfaces. Liquid water can only persist inside the package in non-negligible quantities once the emplacement drift environment has cooled to below roughly 100°C. Humid-air corrosion may nevertheless occur and is accounted for in waste form degradation models. Aqueous chemistry and, potentially, radionuclide transport from the package can only begin once appreciable liquid water is present (SNL 2007e, Section 6.10.9.1[a]). The in-package chemistry model is then implemented when advection into the package is greater than 0.1 L/yr or, in the absence of advection, when continuous thin layers of liquid water are calculated to exist inside of a breached waste form at temperatures less

than 100°C, relative humidity > 95% (SNL 2007e, Section 6.10.9.1[a]). Water will adsorb from the vapor phase to the surfaces of degraded waste package materials with increasing relative humidity. A relative humidity of 95% corresponds to a calculated water thickness on the commercial SNF corrosion products of approximately 5 to 9 monolayers of water (SNL 2007a, Table 6.5-8). Lower relative humidities would result in fewer monolayers of water and fewer connected surface films, and negligible diffusion of radionuclides.

Access of oxygen and carbon dioxide to the waste package internals upon breach is assumed (the partial pressure of oxygen is assumed to be 0.2 atm). Subsequent waste form degradation will involve oxidation of fuels, steels, and, in the case of co-disposal packages, HLW glass as well. Waste form degradation will consume water while reducing the available void space inside the waste package – which may impede additional reaction by preventing further access of water and oxygen. Corrosion product buildup is conservatively assumed to not prevent reaction (SNL 2007e, Section 5.2). The surface areas of the reactants within the breached waste package are fixed, and do not vary with time until the respective material is completely dissolved (SNL 2007e, Section 5.2). This tends to maximize the impact of waste form degradation on in-package chemistry (SNL 2007e, Section 5.2).

The in-package chemistry model predicts pH and ionic strength inside breached packages. Hydrogen ion concentrations and ionic strength are critical indicators of, respectively, radionuclide solubilities and colloid stability. For these reasons pH and ionic strength are the primary outputs of the in-package chemistry calculation. In-package pH is controlled largely by mineral precipitation and dissolution reactions and ambient carbon dioxide levels. Ionic strength depends more on the water balance inside the package. After breach, fuel and steels are oxidized to secondary oxides whose presence anchors in-package pH close to neutral through solubility reactions. Stainless steel will corrode to iron(III) and chromium(III) oxides and $NiFe_2O_4$. UO_2 will oxidize to schoepite or other uranium oxides. Subsequent dissolution of the steel and fuel alteration products will limit the pH range inside the package. For example, schoepite dissolution at high pH consumes hydroxyls; at low pH, schoepite dissolution consumes protons. $NiFe_2O_4$ dissolves and consumes acidity at $pH < 7$. The net effect will be to keep pH close to the solubility minima of the fuel and steel corrosion products which, depending on ambient carbon dioxide levels, are near neutral. Solutions in contact with HLW glass are able to achieve higher pH. Subsequent contact with altered fuel tends to force pH back towards neutral because of schoepite dissolution. As the fluid flux increases, there is less interaction between the water and the waste package contents and pH and ionic strength approach that of the incoming water. The model also predicts maximum dissolved fluoride levels that might prevail inside the various waste packages (SNL 2007e, Section 6.10.3[a]).

2.3.7.5.2 Data and Data Uncertainty of the In-Package Water Chemistry

[NUREG-1804, Section 2.2.1.3.3.3: AC 2(1), (2), (4), AC 3(1) to (4)]

The in-package chemistry model uses a reaction-path calculation to predict the broad chemical features (e.g., pH and ionic strength) of in-package fluids. The TSPA uses these outputs to predict the dissolved and colloidal radionuclide concentrations in the waste package and their transport from the waste package. The primary data inputs that the in-package chemistry calculation relies on include (1) the masses, surface areas, and degradation rates of the fuels and waste glass; (2) the thermodynamic data that is used to calculate the stabilities of dissolved, aqueous, and gas phase

species inside the waste package; (3) input fluid chemistries; and (4) the masses, surface areas, and degradation rates of the steels in the waste package.

The commercial SNF degradation rate is the product of the fuel surface area and the surface area-normalized dissolution rate. The latter depends on pH, carbonate levels, and the oxygen partial pressure. The surface area and dissolution rate, and their associated uncertainties, are discussed in Section 2.3.7.7. The largest uncertainty is the reactive surface area. In addition to this and to uncertainties in the commercial SNF rate law (which are quantified), there are also uncertainties associated with the potential ability of species dissolved in solution (e.g. Ca^{++} and SiO_2^{aq}) and trace impurities present in the fuel to inhibit commercial SNF dissolution by stabilizing the reacting commercial SNF surface (which are not quantified) which might lead to model overestimates of commercial SNF degradation. DOE SNF is assumed to degrade instantaneously upon breach (Section 2.3.7.8), and thereby anchor in-package pH close to neutral upon onset of dissolution.

HLW degradation depends upon the glass surface area and the surface area-normalized glass dissolution rate. The dissolution rate varies as a function of pH, being lowest at ~ pH 9. The individual uncertainties associated with the HLW degradation model are discussed in Section 2.3.7.9. Foremost among these is the surface area of the glass and how it might change over time. Degradation of glass often leads to the formation of non-stoichiometric silica-rich "leach layers" that, once accumulated in sufficient abundance, might inhibit the movement of reactants to the glass surface and products away from the glass.

The thermodynamic database "data0.ymp.R5," allows the calculation of mineral and gas solubilities, the chemical state of dissolved species, and (in part), the dissolution rates of solids whose rate laws include an affinity function. Uncertainty is implicit in the thermodynamic database, as it was built from the accumulation of a large number of experimental measurements, each with their own associated uncertainty. The free energies of common minerals (such as calcite and quartz) are known to considerable precision at 25°C—as are those of their dissolved components. The free energies of, for example, multi-oxide clay minerals and some of the less common minerals and aqueous species are less predictable. With a few exceptions, the thermodynamic properties of species become more uncertain at temperatures higher than 25°C. In the absence of experimental data, the thermodynamic properties of many species were estimated using models that carry with them their own uncertainty. The general role of uncertainty in thermodynamic databases, and the individual uncertainties that are part of this database, are discussed in detail in the documentation for the chosen thermodynamic database (SNL 2007f). Uncertainty is minimized in this and other similar situations by using experimental data and natural analogue evidences to guide secondary phase selection in the calculations (SNL 2007e, Sections 6.3.1.3.6[a] and 7.4.3).

There is considerable uncertainty in the chemical composition of fluids likely to enter breached waste packages. Scoping calculations indicate that the chemistries of fluids that are used at the starting point of the in-package chemistry calculation have little impact on the chemistry of fluids that ultimately leave the package (SNL 2007e, Section 6.6.2[a]). Because the uncertainty of this specific input has little impact on the uncertainty of the output, it has little impact on potential radionuclide releases.

Degradation rates for waste package materials (SNL 2007e, Table 4-9[a]) are uncertain by several orders of magnitude. For example, the minimum and maximum corrosion rates that the in-package chemistry model uses for the primary components (all in microns/yr) are as follows:

- Aluminum Alloy: 0.4, 110.9
- 316L Stainless Steel: 0.0007, 14.8
- 304L Stainless Steel: 0.001, 39.1.

Steel corrosion typically results in the formation of a passivating metal oxide surface film whose stability controls long-term dissolution and whose stability can be affected by ambient fluid chemistry. Passivating surface layers control rates by preventing the access of water and oxygen to the underlying material. Steel corrosion rates measured in brines differ from rates measured in dilute solutions. Increasing temperature leads to enhanced corrosion. Experimentally measured corrosion rates tend to decrease over time, presumably due in part to extensive passive layer formation. To ensure that the entire potential ranges of rates were considered in the in-package chemistry calculations, all experimental conditions documented in *Aqueous Corrosion Rates for Waste Package Materials* (BSC 2004a) were included when determining the minimum and maximum values. The mid-range values are selected median measurements reported for low temperature conditions ("ambient" or ~25°C). The low temperature conditions are used for the mid-range measurements because low temperatures will prevail over the regulatory period. The minimum and maximum rate measurements for a given material differ by several orders of magnitude; thus, the mid-range measurements were chosen such that the minimum, maximum, and mid-range values are roughly representative of lognormal distributions. Because it is not clear whether measurements from salt water or fresh water experiments are more appropriate for the application, measurements from all water types were considered. A more sophisticated approach to selecting degradation rates is unjustified for the in-package chemistry abstractions as degradation rates have little effect on the pH abstraction and only a minor effect on the ionic strength abstraction, and then only under liquid influx conditions. This effect is accounted for by adjusting the degradation rates to minimum and maximum values to account for uncertainty in the liquid influx ionic strength abstraction. The pH abstraction is not sensitive to metal degradation rates because the pH abstraction only determines the minimum and maximum pH values.

2.3.7.5.3 Model and Model Uncertainty

[NUREG-1804, Section 2.2.1.3.3.3: AC 1(1) to (9), AC 4(1) to (4), AC 5]

Interaction of fluid with waste form internals is modeled as occurring in two cells: Cell 1 includes fuel elements and some metals; Cell 2 contains only corrosion products and steels. Each cell is modeled as a batch reactor (SNL 2007a, Section 6.5.2.5). Codisposal fuel elements are further subdivided into Cell 1a, containing HLW glass, and Cell 1b, containing SNF. Solubility and dissolution reactions dominate in Cell 1; adsorption reactions dominate in Cell 2. The behavior of the latter is considered in Section 2.3.7.12. The Cell 1 model considers both water vapor influx and liquid water influx.

- The vapor influx submodel describes a case in which water vapor enters a breached waste package, is conservatively assumed to condense on the internal surfaces, and then reacts with the waste forms and metal alloys of the waste package. There is no egress of liquid water in this case, but transport of radionuclides out of the waste package may occur via

diffusion if continuous diffusion pathways exist (i.e., if RH is greater than 95%) (Section 2.3.7.5.1) (SNL 2007e, Sections 6.3 and 6.3[a]).

- The liquid influx submodel describes a case in which liquid water in equilibrium with atmospheric oxygen and carbon dioxide enters a breached waste package, reacts with the waste forms and metal alloy components, and then exits the waste package. Transport of water out of the waste package is by advection.

Water in the vapor influx case would initially be very dilute, whereas the liquid influx water would contain a variety of dissolved and particulate components from the geologic media through which the water had passed.

The in-package chemistry model is applied to two representative waste packages: (1) a 21-PWR commercial SNF waste package; and (2) a 2-MCO/2-DHLW. Cell 1a is referred to as 2-DHLW; Cell 1b is referred to as 2-MCO waste package containing N Reactor SNF—a metallic uranium fuel that makes up a sizeable fraction of the total DOE SNF—to represent the codisposal packages. MCO refers to multi-canister overpack co-disposal waste, which is usually uranium metal SNF. In codisposal packages radionuclides are envisioned to be transported from Cell 1a to 1b and then into Cell 2 (SNL 2007a, Section 6.5.2.1.2). Cell 1a will likely be alkaline due to glass degradation; Cell 1b pH will be near neutral because of schoepite solubility. Splitting of Cell 1 is done because of the difference in chemical environment. Moving radionuclides from Cell 1a into 1b, as opposed to the other way around, should not greatly affect the actual amount of radionuclides that move into Cell 2. The most numerous codisposal waste package in the design for the repository is the 5-DHLW/DOE Long. This waste package contains five HLW glass canisters identical to the glass canisters in the 2-MCO/2-DHLW waste package. These canisters are placed radially around a core compartment that contains DOE SNF. Although this waste package is the most numerous of the codisposal waste packages, the total mass of uranium in all of the 2-MCO/2-DHLW waste packages exceeds the total uranium mass in all of the 5-DHLW/DOE Long Codisposal waste packages. Because of the latter, the in-package chemistry model simulates the 2-MCO/2-DHLW waste package. The chemistry of the fluids inside of a 2-MCO/2-DHLW package containing N Reactor fuel is not expected to be materially different from the chemistry of fluids inside of a 5-DHLW/DOE Long Codisposal waste package containing Three Mile Island SNF (uranium oxide fuel)—the co-disposal waste package that is used in radionuclide transport calculations: Cell 1a of each configuration will likely have an alkaline pH caused by DOE HLW glass degradation; the pH in Cell 1b in each package will be controlled by solubility equilibria with schoepite and steel corrosion products (Section 2.3.7.5.3.1). Although N Reactor fuel is uranium metal and Three Mile Island SNF is uranium oxide, both alter rapidly to schoepite–a primary control over pH under both vapor and seepage scenarios. Ionic strength is controlled largely by the formation of hydrated alteration products–namely, schoepite and iron corrosion products. These will be the same in either package type; hence, the ionic strength trends should be similar. The calculated ionic strengths at a given point in time in the two packages will differ because the two packages possess different proportions of materials. The difference is likely to be within the order of magnitude uncertainty associated with predicted in-package ionic strengths. The reasonableness of the 2-MCO model for other codisposal fuel types is outlined further in *In-Package Chemistry Abstraction* (SNL 2007e, Section 6.6.6[a]).

The submodels of the in-package chemistry model include the following:

- Reaction-path tracking of the in-package chemical system.
- Conservation of mass.
- Kinetic dissolution of the waste package components and N Reactor U-metal fuel using linear rate laws.
- Equilibrium precipitation and dissolution of metal corrosion products and secondary mineral phases.
- Effect of variable input fluid compositions on the resulting fluid composition.
- Water ingress of 0.1 to 1,000 L/yr for the liquid influx model. This range is thought to bound that likely to exist in the mountain. The vapor case assumes equilibrium with local relative humidity.

The in-package chemistry model uses EQ6 (Wolery and Daveler 1992), which is a chemical reaction path equilibrium computer code, to model the batch reactor chemistry for a range of in-package environments.

For the vapor influx case, the simulations are divided into two relative humidity ranges. The high range, corresponding to an ionic strength of one molal or below, is simulated using the EQ6 batch reactor and the B-dot equation for the calculation of activity coefficients. This range is simulated by degrading small amounts of cell materials (proportional to their relative reaction rates) into one liter of water and then incrementally removing water from the reactor. Water (as pure H_2O) is removed independent of time, so additional degradation is not allowed during water removal. As the activity of water decreases, the ionic strength increases. The simulations end when the ionic strength reaches one molal. Regardless of the amount of degradation allowed in the initial liter of water, the same water compositions are obtained for a given equilibrium activity of water.

Above one molal ionic strength, when humidities are low, EQ6 simulations of the in-package chemistry model are not performed. Instead, the in-package chemistry vapor influx case uses a correlation between ionic strength and relative humidity, as calculated from results in the *In-Drift Precipitates/Salts Model* (SNL 2007g) to develop the high ionic strength abstractions.The vapor influx submodel examines the in-package water chemistry when a waste package breaches and water vapor enters the package. The vapor influx submodel assumes water vapor equilibration between the breached waste package and the drift. The waste package relative humidity is then used to calculate the ionic strength of fluids inside the package.

The liquid influx submodel examines in-package chemistry following the ingress of liquid water. As water flows through, accumulates in, and exits the waste package void space, it reacts with the internal components of the waste package and deposits corrosion products and secondary mineral phases.

The key components for the liquid influx submodel are as follows:

- The liquid influx submodel is treated using a solid-centered-flow-through option in EQ6, which simulates a single-cell well-mixed batch reactor (SNL 2007e, Section 6.3.1.1[a]). That is, dripping water flows into a single cell at a specified rate while reactants are added to the cell at their degradation rate(s), chemical reactions take place, products precipitate and redissolve, and effluent exits the waste package (Wolery and Daveler 1992, p. 46, Figure 5).

- The water flow rate is varied over a range of rates at which water could enter a waste package. The ratio of the water volume to the volume of waste package materials is examined in sensitivity studies. At the maximum water-to-reactant ratio, the water volume is equal to that of the void space, which is calculated to be more than 50% of the waste package. To examine a range of conditions, the ratio of water to reactants is lowered to represent a condition in which capillary forces cause a water film to cover the waste package materials. For the base case, a water volume equal to approximately 0.5 the void space is used to examine a ratio between the two extremes. The impact of varying this ratio is examined in a sensitivity analysis (SNL 2007e, Section 6.6.1[a]).

2.3.7.5.3.1 Results and Abstraction

The waste package must breach for water in the form of vapor or dripping water to enter the package, and the interior temperature of the waste package must be below the boiling temperature of water so that appreciable liquid water may exist for the aqueous chemical reactions to begin.

The applicable temperature range for the in-package chemistry model abstraction is 25°C to 100°C (above which liquid water is modeled as not present), and the applicable carbon dioxide fugacity range is 10^{-4} to $10^{-1.5}$ atm (SNL 2007e, Section 1[a]). While the boiling point of pure water at the repository elevation is approximately 96°C, the value of 100°C is used to reflect possible higher boiling points of the dilute groundwater compositions that may enter the waste package (SNL 2007e, Section 1[a]). As soon as liquid water comes in contact with the reactive components in the waste package (e.g., carbon steel or stainless steel), the ionic strength of the solution will increase and the boiling point will increase.

Figures 2.3.7-13 through 2.3.7-18 show base case pH and ionic strength trends for the waste form cells of commercial SNF packages, and codisposal packages. These and the other results discussed in this section are for Cell 1 (commercial SNF), or Cells 1a (multicanister overpacks) and 1b (HLW). The base case in-package chemistry liquid influx runs assume a liquid flux of 1 L/yr and P_{CO_2} = 10^{-3} atmospheres (SNL 2007e, Section 6.3.1.2[a]). Calculations are stopped once steady-state concentrations are observed. Figures 2.3.7-14 and 2.3.7-17 show that base case in-package commercial SNF and 2-MCO cells pH values remain between 5 and 8, and are largely independent of input fluid composition. The HLW pH values are somewhat higher because of glass degradation (SNL 2007e, Section 6.10.1[a]) and the absence of schoepite. The sharp peak at ~ 2000 years in Figure 2.3.7-18 occurs as the last of the fuel dissolves, and the in-package fluids are then diluted by incoming fluids. Input fluid compositions for these calculations are given in Tables 2.3.7-9, 2.3.7-10, and 2.3.7-11. The basalt water compositions are used as inputs for the igneous scenario class. In the figures, time periods of greater than ~ 40 years are most relevant to

repository performance. The insensitivity of the calculated pH to input fluid compositions reflects the solids-dominated nature of waste form degradation. The primary control over pH in the commercial SNF and 2-MCO cells is the redissolution of oxidized uranium and steel corrosion products and equilibration with CO_2. In the 2-DHLW packages, redissolution of steel corrosion products sets lower limits for pH; atmospheric CO_2 provides some base-buffering capacity. The general insensitivity of model outputs to seepage chemistry suggest that the pH trends outlined here would envelope the fluid chemistries produced by seepage of EBS fluids (Section 2.3.5) into breached waste packages (SNL 2007e, Section 6.6.2[a]).

The pH trends shown in Figures 2.3.7-14, 2.3.7-15, and 2.3.7-17, along with non-base case results (that often defined lower pH trajectories), were generalized by using EQ6 to numerically calculate pH buffer capacity in each of the respective altered waste form cells, and to thus establish cell specific pH ranges (SNL 2007e, Section 6.3.4.3[a]). This involved building a series of simulations wherein acid and base were numerically titrated into altered cells to predict likely in-package pH ranges. The latter were found to tightly bound the pH trends shown in Figures 2.3.7-14, 2.3.7-15, and 2.3.7-17, and the trends observed in sensitivity runs performed at different P_{CO_2} values and material degradation rates. The bounds established by the pH titration calculations define the ranges used by the TSPA (SNL 2007e, Section 6.10.1[a]). These are shown for commercial SNF, 2-DHLW, and 2-MCO cells in Figures 2.3.7-19, 2.3.7-20, and 2.3.7-21. In each case, the lower pH limit is set by dissolution of $NiFe_2O_4$ (produced by corrosion of stainless steel), which is insensitive to P_{CO_2} (SNL 2007e, Section 6.3.4.1[a]). The upper pH limit is set by schoepite dissolution and CO_2 equilibration. Maximum pH decreases with increasing P_{CO_2} values (note that pH values are plotted as a function of pCO_2; the negative logarithm of the partial pressure of carbon dioxide) (SNL 2007e, Section 6.10.1.1[a]). Vapor influx pH trajectories describe a pH range similar to that defined by the liquid influx calculations (SNL 2007e, Section 6.10.1.2[a]).

The pH trajectories calculated using materials degradation rates that varied by roughly two orders of magnitude around the base case values likewise fall within the bounds shown in Figures 2.3.7-19, 2.3.7-20, and 2.3.7-21. This correspondence emphasizes that, just as fuel and steel corrosion reactions do not greatly affect pH (except for DOE HLW), the corrosion products that are produced buffer pH. Because no central pH tendency is observed, pH values are assumed to be uniformly distributed between the two limits (SNL 2007e, Section 6.10.9[a]).

Ionic strength trends reach maximal values (most apparent in Figures 2.3.7-13 and 2.3.7-18). The maxima become higher and larger and shift to longer times when the liquid influx is decreased (SNL 2007e, Section 6.10.2[a]). The peak becomes higher because less water is available for dissolving solids. The peak becomes larger and moves farther out in time because low liquid influxes hinder complete flushing of salts from the cells. Figures 2.3.7-22, 2.3.7-23, and 2.3.7-24 show ionic strength trends for, respectively, commercial SNF, 2-DHLW, and 2-MCO cells as a function of liquid water flux. For vapor influx conditions, ionic strength and pH are calculated as a function of relative humidity and are shown in Figure 2.3.7-25. The latter values were calculated using EQ6 and the B-dot equation to calculate activity coefficients of dissolved species. When the ionic strength exceeds 1 M (at RHs less than ~ 98.5%) a Pitzer approach is used to calculate pH and a correlation between the vapor pressure above divalent cation/monovalent anion salts and ionic strength is used to estimate in-package ionic strengths (SNL 2007e, Section 6.10.2.2[a]).

The in-package chemistry model also provides fluoride levels to the TSPA, so that the effect of actinide-fluoride complexes on solubilities can be assessed. Some fluoride may exist in the waste glass (SNL 2007e, Section 6.10.3[a]). Otherwise, fluoride comes from liquid influxes that might be concentrated by consumption by fuel degradation reactions. Because of the latter, fluoride levels tend to correlate with ionic strength. The fluoride abstraction is therefore defined for discrete ionic strength intervals as right-triangular distributions. Zero is the minimum value. The maximum fluoride values (F_{max}), which are set conservatively high, are:

- **Commercial SNF**—ionic strength < 0.2, F_{max} = 0.25 mM and ionic strength ≥ 0.2 with F_{max} = 2.5 mM
- **2-DHLW**—F_{max} = 0.25 mM
- **2-MCO**—ionic strength < 0.004 with F_{max} = 0.25 mM and ionic strength ≥ 0.004 with F_{max} = 10 mM.

At low ionic strength, the fluoride concentration either remains in the vicinity of the concentration in the liquid influx, or falls below the liquid influx concentration due to mineral precipitation. At high ionic strength for the commercial SNF cell, and especially for the 2-MCO cell, fluoride often concentrates as water is consumed by degradation reactions. However, at high ionic strength in the 2-DHLW cell, fluoride precipitation prevents the fluoride concentration from ever increasing much above the incoming concentration.

Fluorine was included in the estimated composition of the HLW glass used in the parent document. That composition was hypothetical and based on the analyses of the radionuclide sludges that had fluoride from hydrofluoric acid used to dissolve the wastes. However, including fluorine in 2-DHLW in-package chemistry simulations does not result in higher aqueous fluoride concentrations because of mineral precipitation. Fluoride never substantially exceeds the incoming concentration in the liquid influx simulations, and is always below 0.01 mM in the vapor influx simulations.

For the solubility calculation, single fluoride distributions were defined for discrete ionic strength intervals. These distributions were defined to be right-triangular with a zero value for the minimum and apex and a conservatively high value for the maximum. This distribution is justified based on conservative arguments as long as the maximum fluoride values are set conservatively high, which they are (SNL 2007e, Section 6.10.3[a]).

Again, the discussion in this section has outlined the controls over fluid chemistry in Cell 1 (or Cell 1a and 1b), where the fuel and/or HLW glass reside. Cell 2 is made up of corrosion products that sorb radionuclides and moderate the pH of incoming fluids through surface protonation-deprotonation reactions. The controls over radionuclide sorption and fluid chemistry in Cell 2 are described in greater detail in Section 2.3.7.12 and *EBS Radionuclide Transport Abstraction* (SNL 2007a, Section 6.5.2.4). In short, several dozen Cell 1 chemistries were numerically equilibrated with Cell 2 corrosion product assemblages and the sorption of the various radionuclides was quantified. The Cell 2 pH was also calculated in each scenario, and its

value was found to depend upon carbon dioxide levels and the amount of dissolved uranium (SNL 2007a, Equation 6.5.2.4.6-2):

$$pH = 4.5342 + 0.6312(pCO_2) - 0.3805\log_{10}[U] - 0.0254(\log_{10}[U])^2 + E \quad \text{(Eq. 2.3.7-1)}$$

where, pCO_2 is the negative log of the in-drift CO_2 partial pressure (bars), $[U]$ is the dissolved concentration of uranium in mol/L, and E is the error term (pH_Cell_2_Regression_Error) defined by a normal distribution with mean of zero and standard deviation of 0.32 truncated at ± 2 standard deviations. Cell 2 pH values are between 6 and 8.5. The pH is lower at higher carbon dioxide levels (lower pCO_2s). The pH is higher when uranium levels are lower. The ionic strength for the corrosion products domain is assumed to be the same as that computed for the upstream domain by the in-package chemistry model.

2.3.7.5.3.2 Validation

There are no natural analogues to which one can compare estimated in-package chemistry values. Many uranium ore bodies are located below the water table under a reducing environment, yet the Yucca Mountain repository is assumed to be oxidizing. Because stainless steels only became widely available in the early part of the twentieth century, there are no ancient artifacts that one can consider as a natural analogue. All of the natural materials have deficiencies preventing them from being considered an analogue; for example, iron-rich meteorites are seldom found in saturated environments and, unlike stainless steel, they have very low chromium contents.

Confidence is built in the in-package chemistry model by showing that the predicted secondary phases are correct, and that the predicted pH ranges are consistent with those observed in qualitatively similar soils and groundwaters (SNL 2007e, Section 7.4[a]). The primary phases predicted to form in the model and control pH are ferric oxyhydroxides (goethite, etc.) and spinels (trevorite, $NiFe_2O_4$, etc.) from stainless steel corrosion, and schoepite from the degradation of spent nuclear fuel. (SNL 2007e, Section 6.3.4.1[a]). Iron-based alloys and minerals are observed in nature and in experiments to corrode to metal oxides whose specific identities depend upon the particular conditions of corrosion and the composition of the steel. Hematite and goethite are routinely observed as the most common iron oxides in soil (Schwertmann and Taylor 1995), and are observed in the corrosion products in both natural analogues (Johnson and Francis 1980) and laboratory experiments (Kim 1999). Analyses of oxide coatings on stainless steels under very aggressive conditions (e.g., low pH nitric acid solutions, induced potentials, PWR environment) show that inverse chromium or nickel-iron spinels are the major components (Wang et al. 2001; Da Cunha Belo et al. 1998). Schoepite is observed as an alteration product in experiments (BSC 2004b; SNL 2007h; Wronkiewicz et al. 1996) and at the Peña Blanca natural analogue (Langmuir 1997, p. 513; Palache et al. 1944).

The minimum pH values inside the degrading waste form cell are predicted to be around 5. The chemical makeup of the waste form corrosion products will be dominated by metal oxides and hydroxides similar to natural soils. Natural soil and groundwaters typically only become more acidic than pH 5 when high levels of organic acids are present, or when reduced sulfur is oxidized. The release of the relatively small amounts of reduced sulfur from stainless steels in the package is

too slow to exceed the pH-buffering capacity of the corrosion products themselves (SNL 2007e, Section 7.4.5.2[a]). The pH ranges in the commercial SNF and 2-MCO waste form cell abstractions are consistent with the pH range of 5.9 to 8.2 observed in UO_2 degradation experiments conducted at Argonne National Laboratory (Wronkiewicz et al. 1996). The experiments involved slowly dripping J-13 well water, pre-equilibrated with crushed tuff at 90°C, onto UO_2 pellets encased in Zircaloy-metal sleeves and maintained in 90°C unsaturated environment over a period of ten years at near atmospheric CO_2 levels. The higher pH range (7.5 to 8.5) seen in the glass-containing 2-DHLW simulations is similar to the pH range observed in groundwaters in contact with basalt and basalt glass (the latter is an appropriate natural analogue for nuclear waste glass; see Ewing and Haaker 1979). Hem (1995) gives the analyses of two basalt groundwaters and one water from a tuff containing the basaltic mineral olivine. The basalt waters have pH values of 7.8 and 7.9 (Hem 1995, Table 12, Analyses 4 and 5) and water from an olivine tuff has a pH of 8.2 (Hem 1995, Table 16, Analysis 3). In short, the elevated pH values predicted by the codisposal waste package Cell 1a HLW glass simulations in the in-package chemistry model are corroborated by natural observations documented in the peer-reviewed literature (Vernaz and Goden 1992). This observation provides confidence that the estimates of pH in the solutions in contact with HLW glass will be greater than those associated with codisposal waste package Cell 1b containing DOE SNF. Because the DOE SNF degradation model is very similar to that of commercial SNF, the fluids exiting codisposal waste package Cell 1b will be modified to be very similar to those exiting the commercial SNF Cell 1.

2.3.7.6 Commercial Spent Nuclear Fuel Cladding Degradation

[NUREG-1804, Section 2.2.1.3.1.3: AC 1(1) to (5), AC 2, AC 3(1) to (3), AC 4, AC 5; Section 2.2.1.3.2.3: AC 1(2)]

Commercial SNF presently in service uses Zircaloy cladding. Earlier fuels, roughly 1% of those going into the repository, used stainless steel cladding. The fuel cladding protects the fuel pellets from contact with the surrounding environment and provides structural integrity for the fuel. As long as it remains intact, the cladding prevents the release of radionuclides.

In the TSPA, the Zircaloy and stainless-steel spent-fuel cladding is assumed to be failed upon emplacement (Table 2.2-3). Although the cladding is expected to retard radionuclide release and transport, this ability is conservatively not included in the TSPA analyses. This conservative approach is taken because the effort involved in onsite cladding inspection outweighs the potential barrier benefit that cladding will provide at Yucca Mountain. The effect of naval SNF structure on the release and transport of radionuclides is accounted for in the assessment (Section 2.4.2.3.2.2.4) that justifies representing naval SNF waste packages with commercial SNF waste packages in the TSPA.

Despite its absence in the TSPA calculations, commercial SNF cladding will be a long-term feature of Yucca Mountain. It is therefore useful to briefly document the technical basis for cladding behavior in the repository. The as-received cladding condition is a useful predictor of long-term cladding integrity as cladding flaws (small cracks or holes in the cladding) tend to focus subsequent axial splitting—"cladding unzipping"—and oxidation of the underlying fuel. Nuclear utility and government experience point to an as-received cladding failure percentage at the repository of between 0.01 and 1.0%, with an expected failure rate of 0.1% (S. Cohen & Associates 1999). The failed rate of stainless steel cladding is similar (S. Cohen & Associates 1999). As-received cladding

flaws might arise during the course of reactor operation, storage, handling, and transport. After arrival at Yucca Mountain, new cladding flaws may occur during handling in the surface facilities.

After waste package breach, cladding will fail by mechanical action from seismic or volcanic events, and/or by long-term chemical degradation. Both stainless steel and Zircaloy form passive oxide surface layers that are typically resistant to chemical oxidation. Likely modes of chemical degradation include stress corrosion cracking of stainless steel and halide attack on Zircaloy cladding. Corrosion of stainless steel will result in the accumulation of iron oxides that tend to sorb radionuclides.

2.3.7.7 Commercial Spent Nuclear Fuel Degradation

[NUREG-1804, Section 2.2.1.3.1.3: AC 1(1) to (5), AC 2, AC 3(1) to (3), AC 4, AC 5; Section 2.2.1.3.2.3: AC 1(2); Section 2.2.1.3.4.3: AC 1(1) to (6), AC 2, AC 3(1) to (4), AC 4, (8), AC 5(1) to (3)]

The commercial SNF model predicts the rate at which radionuclides are released from spent fuel into the Cell 1 of a breached waste package.

2.3.7.7.1 Conceptual Description of Commercial Spent Nuclear Fuel Degradation

[NUREG-1804, Section 2.2.1.3.1.3: AC 1(1) to (5); Section 2.2.1.3.4.3: AC 1(1) to (4)]

The availability of individual radionuclides for dissolution once the waste package and fuel cladding are breached is limited by the structure, microstructure, and physicochemical properties of the irradiated fuel, as well as by the distribution of radionuclides in the fuel rods. Most radionuclides, and essentially all of the rare earth and actinide radionuclides, are retained in the fluorite structure of the UO_2 matrix. Transition metals (molybdenum, technetium, ruthenium, rhodium, and protactinium) are partly partitioned into metallic phases embedded in fuel grains and at the fuel grain boundaries. The part of the radionuclide inventory present either as a solid solution in the fuel matrix or embedded as discrete phases in the fuel grains is not available for dissolution until the fuel matrix is dissolved, or otherwise altered, and is referred to as the matrix inventory. A fraction of the fission gases and more mobile fission product elements (cesium, iodine, strontium, and technetium) migrate out of the matrix during in-reactor operations. The radionuclides of these elements accumulate in the gap region (i.e., the interface between the pellets and the cladding, the rod plenum regions, and pellet fracture surfaces), while some accumulate at fuel grain boundaries. The radionuclide inventory that is not a part of the matrix is called the gap and grain boundary inventory, and can be released rapidly once the cladding is breached (BSC 2004b).

Once the waste package and cladding have been breached, oxidation and degradation of the commercial SNF matrix will proceed. If the temperatures exceed approximately 100°C at low relative humidities, the degradation will occur via solid-state reactions associated with dry oxidation (BSC 2004b). The presence of water vapor complicates the oxidation process by facilitating formation of hydrated oxidation products. Not only are the reaction products different in the presence of water vapor, but the rates and mechanisms for reaction differ as well (Aronson 1958, p. 94; Taylor et al. 1989); McEachern and Taylor 1998, Section 2.2). Humidity can influence oxidation by forming hydrated uranyl phases (e.g., by hydrous disproportionation of U_3O_8), by supporting oxidative dissolution in water films that form on the surface at higher relative

humidities, by enhancing grain-boundary oxidation in SNF, and by supporting radiolytic processes at grain boundaries. Because gas-phase diffusion is rapid along the connected porosity at SNF-grain boundaries, the oxidation of SNF can be considered to proceed simultaneously at grain boundaries throughout the fuel when it is exposed to humid air. This grain-boundary corrosion and associated decohesion of the fuel grains is modeled to occur rapidly if commercial SNF pellets are exposed to humid air at temperatures greater than 100°C (BSC 2004b, Section 6.2.2.2). The effects on the fuel matrix include some bulk oxidation of the grains and a large increase in the specific surface area of the fuel as it disaggregates into grain-sized powders.

Because of these complexities, an instantaneous radionuclide release rate model is used for any fuel that is first exposed by a waste-package breach at temperatures greater than 100°C when it is subsequently contacted by water after the temperature drops below 100°C (BSC 2004b, Section 6.2.2.2).

The commercial SNF corrosion process in humid air at temperatures less than 100°C is best characterized as an oxidative dissolution process in a film of water at the fuel surface, rather than an interaction between water vapor and oxygen in the air that accelerates the solid-state oxidation process. Thus, the commercial SNF degradation model discussed below assumes that oxidation followed by dissolution of commercial SNF in water at temperatures below 100°C is the degradation process relevant to repository conditions (BSC 2004b, Section 6.2.2.2).

The long-term oxidative dissolution of UO_2 (and SNF) under neutral to basic conditions involves oxidation of a thin layer of the UO_2 at the surface–water interface to a higher oxide UO_{2+x} (e.g., U_3O_7), followed by further oxidation and dissolution of this layer. Based on the results of x-ray photoelectron spectroscopy analyses, it has been shown that the corrosion of unirradiated UO_2 fuel in near-neutral–to–alkaline solutions proceeds in two stages. The first stage is the rapid formation of a surface UO_{2+x} film that achieves a limiting composition of $UO_{2.33}$. The second stage involves the further oxidation of the $UO_{2.33}$ film at the film–water interface to form soluble secondary uranium(VI) phases (e.g., $UO_3 \cdot xH_2O$, hydrated schoepite). Under acidic and complexing (carbonate/bicarbonate) conditions that promote rapid dissolution of this layer, the solid surface is found to be less oxidized. For both acidic and alkaline conditions, the overall oxidative dissolution process involves a coupled series of redox, surface complexation and dissolution, and precipitation reactions, with the overall reactions depending on the water chemistry environment. The rate of the overall oxidative dissolution process is controlled by water chemistry factors that promote oxidation of uranium(IV) to uranium(VI), and also promote dissolution of the oxidized uranium(VI) species. Under hydraulically unsaturated conditions in which limited volumes of water are available, uranium(VI) alteration phases are precipitated onto the corroding surfaces. These alteration phases can influence the rate of the oxidative dissolution process by inhibiting the mass transport of oxidizing agents (e.g., dissolved oxygen) to the underlying corroding surface (BSC 2004b, Section 6.2.2.3). This effect is conservatively not included in the model (BSC 2004b, Section 6.4.1.5).

2.3.7.7.2 Data and Data Uncertainty

[NUREG-1804, Section 2.2.1.3.1.3: AC 2, AC 3(1) to (3); Section 2.2.1.3.4.3: AC 1(2), (4), AC 2, AC 3(1) to (4), (8)]

Several different tests on SNF have been conducted by various researchers to provide data that form the basis for the commercial SNF degradation model (Gray et al. 1992; Gray and Wilson 1995; Stout and Leider 1998; CRWMS M&O 2000b; Thomas 2003; Goldberg 2003). These tests are summarized below (BSC 2004b).

Gray et al. (1992) measured the gap and grain boundary inventories of cesium, strontium, iodine, and technetium. Tests were run on light water reactor SNF, and results were given in terms of the percentage of total inventory of these four radionuclides in the gap region and percentage of the total inventory in the grain boundaries. The data from these tests were used to develop the model for release of the gap and grain boundary inventory are described in *CSNF Waste Form Degradation: Summary Abstraction* (BSC 2004b), Section 6.3.1.

Environmental factors that influence the oxidative dissolution rate of the commercial SNF matrix are temperature, dissolved oxygen concentration, pH, and carbonate concentration (Shoesmith 2000; Jegou et al. 2001, Section 8.2.3). Commercial SNF, in the form of grain-sized powders, was tested in single-pass, flow-through dissolution studies to provide the parametric dependence of the matrix dissolution rate over a range of conditions for each of these factors. This range of conditions spans the anticipated conditions at the repository (Gray and Wilson 1995). In these studies, the principal test response was the specific oxidative dissolution rate of the matrix. The data set spans a wide range of dissolution conditions, with pH ranging from 2 to 10.3, the oxygen partial pressure ranging from 0.002 to 0.2 atm, the temperature ranging from 25°C to 75°C, and carbonate and bicarbonate concentrations up to 2×10^{-2} mol/L (BSC 2004b).

Unirradiated UO_2 was also tested in flow-through dissolution studies under alkaline conditions (Stout and Leider 1998; Tait and Luht 1997; De Pablo et al. 1999). The UO_2 data are pertinent because the dissolution behavior of unirradiated UO_2 is likely to be similar to the behavior of commercial SNF after the ^{137}Cs and ^{90}Sr have decayed and the associated radiolysis effects are no longer present (BSC 2004b). The corrosion rates of unirradiated UO_2 and commercial SNF demonstrate no significant difference under air-saturated groundwater conditions (Serrano et al. 1998; Jegou et al. 2001, p. 542; Shoesmith 2000, Figure 29).

Additional long-term tests have been conducted to corroborate the model through examination of oxidative dissolution of (1) unirradiated UO_2 fuel pellets (Wronkiewicz et al. 1996); (2) irradiated commercial SNF pellet fragments (CRWMS M&O 2000b; Thomas 2003; Wilson 1990a; Wilson 1990b); and (3) fuel rod segments (Goldberg 2003; Forsyth 1997; Cunnane et al. 2003, Section 2a) under test conditions and configurations relevant to exposure scenarios in the repository.

In the long-term tests conducted on unirradiated UO_2 fuel pellets exposed to periodic dripping of simulated groundwater at 90°C, a layer of uranium(VI) alteration phases accumulated on the corroding UO_2 surfaces after about two years, and inhibited uranium release. The paragenetic sequence of these alteration phases was found to be similar to that observed in superficial weathering zones of natural uraninite deposits (Wronkiewicz et al. 1996), indicating that the

laboratory test results are relevant to very long-term alteration of UO_2 under oxidizing and hydraulically unsaturated conditions.

The long-term tests on irradiated commercial SNF pellet fragments from which cladding had been removed examined the corrosion and fractional radionuclide release rates (CRWMS M&O 2000b; Thomas 2003). These fragments were exposed to one of two unsaturated test conditions (high drip rate or low drip rate) with water that had been equilibrated with tuff at 90°C. All tests were run at 90°C. Some have been run for more than nine years. These tests were designed to emulate a scenario in which dripping water in a breached waste package reacts with the fuel, dissolves soluble components, and forms solid corrosion products.

The fuel rod segment tests included five tests conducted on short (1.4-in. to 3.7-in.) segments of fuel rods. In the tests, water that had been equilibrated with tuff at 90°C was allowed to percolate at 90°C under a low hydraulic head through the fuel rod segment, with the effluent used to determine radionuclide release. The test configuration, matrix, and methodology are described in the data report (Goldberg 2003), together with the data. Alteration mineralogy information observed in testing is consistent with natural analogue evidences. This is particularly important for modeling system behavior several thousand years after breach, when all of the fuel will be degraded.

2.3.7.7.3 Model, Model Uncertainty, Abstraction, and Results

[NUREG-1804, Section 2.2.1.3.1.3: AC 1(1) to (5), AC 4, AC 5; Section 2.2.1.3.4.3: AC 1(1) to (6), AC 4, AC 5(1) to (3)]

To provide abstractions to the TSPA, the radionuclide inventory in commercial SNF rods is divided into two fractions: (1) the combined gap and grain boundary inventory; and (2) the matrix inventory (BSC 2004b, Section 1). Separate models are developed for estimating radionuclide releases from the gap and grain boundary, and from the matrix, because the processes that control these releases are different.

2.3.7.7.3.1 Model for Release of Gap and Grain Boundary Inventory

Release of the gap inventory is assumed to be instantaneous upon breach (BSC 2004b, Section 1). Although there is some uncertainty regarding the applicable degradation and release mechanisms for the grain boundary inventory, they are conservatively combined with the gap inventory in estimating the instantaneous release fraction (BSC 2004b, Section 1).

The gap and grain boundary inventory available for instantaneous release is expressed as a fraction of the total inventory of radionuclide *i* in the fuel (BSC 2004b, Section 1):

$$I_i^G = f_i \times I_i \qquad \text{(Eq. 2.3.7-2)}$$

where

I_i^G = gap and grain boundary inventory of radionuclide i available for instantaneous release (g)

f_i = instantaneous release fraction

I_i = total inventory of radionuclide i in the fuel (g).

The gap and grain boundary inventories of cesium, strontium, iodine, and technetium (and their release fractions) are given as a triangular distribution based on data collected. The total inventory of each radionuclide i in the fuel (I_i) is addressed in Section 2.3.7.4. The empirical probability distributions for instantaneous release fractions of ^{137}Cs, ^{129}I, ^{99}Tc, and ^{90}Sr are shown in Table 2.3.7-12, and were derived from measured gap and grain boundary inventories (BSC 2004b, Table 8-1). The qualified data set is limited, which prevents development of statistical distributions for each of the gap inventory elements based on statistical analysis. However, the model for the gap and grain boundary inventories has been validated using available literature data.

As shown in Table 2.3.7-12, most of the inventory of volatile radionuclides remains in the matrix. This is especially true for ^{99}Tc and ^{90}Sr, where, at most, 0.26% and 0.25% of the inventory is modeled in the gap and grain boundary, respectively. The radionuclide with the highest fraction of inventory in the gap and grain boundary is ^{129}I, where a maximum of 26.75% of the inventory is modeled in the gap and grain boundary.

2.3.7.7.3.2 Model of Radionuclide Release from Matrix

The matrix radionuclide inventory cannot be released into the water until the matrix degrades. Degradation results from oxidative dissolution of the fuel matrix in a film of water on the fuel surfaces. The process of oxidative dissolution begins with the oxidation of uranium(IV) to uranium(VI), followed by the dissolution of uranium(VI) in the film of water. The fractional radionuclide release rate from the commercial SNF matrix is modeled as equal to the fractional rate of oxidative dissolution of the matrix (BSC 2004b, Section 1).

The rate of radionuclide release from the matrix is expressed as (BSC 2004b, Section 1):

$$R_i = I_i^M \times F_i \qquad \text{(Eq. 2.3.7-3)}$$

where

R_i = rate of release of radionuclide i from the matrix (g/day)
I_i^M = matrix inventory of radionuclide i (g)
F_i = fractional release rate of any radionuclide i (1/day).

The radionuclide release rate given in Equation 2.3.7-3 is used in the TSPA model to provide the mass of a particular radionuclide available for dissolution during a particular period of time

(BSC 2004b, Section 1). The concentration of a given radionuclide in water exiting the waste form is equal to the dissolved concentration of that radionuclide plus the concentration of that radionuclide attached to or embedded in colloids. The dissolved concentration of a given radionuclide is taken to be equal to its elemental solubility limit, as apportioned among the various isotopes of that element, if the fractional release rate of that radionuclide saturates the available solution volume (SNL 2008, Section 6.3.7.5.3).

The following model for radionuclide release from the fuel matrix calculates F; the matrix inventory of radionuclides is given in Section 2.3.7.4 (assuming otherwise stoichiometric dissolution of the commercial SNF means F_i and F are equivalent). The equations describing the model for radionuclide release from the fuel matrix are given as a piecewise-continuous function over the acidic and basic pH regimes (BSC 2004b, Section 6.4.1). For pH ≥ 6.8:

$$\log(F) = \log(A) + a_0 + a_1 \times 1/T + a_2 \times p\mathrm{CO}_3 + a_3 \times p\mathrm{O}_2 \qquad \text{(Eq. 2.3.7-4)}$$

For pH < 6.8:

$$\log(F) = \log(A) + a_0 + a_1 \times 1/T + a_3 \times p\mathrm{O}_2 + a_4 \times \mathrm{pH} \qquad \text{(Eq. 2.3.7-5)}$$

where

F	=	fractional dissolution rate of the fuel (per day)
a_0, a_1, a_2, a_3, and a_4	=	model parameters determined by regression analyses from experimental data (Tables 2.3.7-13 and 2.3.7-14)
A	=	effective specific surface area of the fuel (m^2/mg)
T	=	temperature (K)
$p\mathrm{CO}_3$	=	negative log of the total carbonate molar concentration
$p\mathrm{O}_2$	=	negative log of the oxygen partial pressure (atmosphere)
pH	=	negative log of the hydrogen ion molar concentration.

Thus, the degradation of commercial SNF is a function of temperature, surface area, pH, $p\mathrm{CO}_3$, and $p\mathrm{O}_2$. The uncertainty associated with the reactive surface area (A) is treated by TSPA with a triangular distribution between log(A) = – 7.3 and – 5.4, with an apex at – 6.7 (BSC 2004b, Section 8.1). A more detailed discussion of the uncertainties in the model parameters is provided in (BSC 2004b, Section 8.1). The validity range is from 15 to 65 GWd/MTHM for burnup, 2 to 10.3 for pH, 0.002 to 0.2 atm for oxygen partial pressure, carbonate and bicarbonate concentrations up to 2×10^{-2} mol/L, and 25°C to 100°C for temperatures (BSC 2004b, Section 8.2). A bounding

instantaneous degradation model is used for any fuel exposed by a waste package breach at temperatures greater than 100°C (BSC 2004b, Section 8.1). Results of tests conducted on commercial SNF (Section 2.3.7.7.2) were used to determine the values of the model parameters (A, a_0, a_1, a_2, a_3, and a_4) for both alkaline conditions and acidic conditions (BSC 2004b). This reflects the functional dependence of the commercial SNF degradation rate on these environmental factors. The parameter values for both alkaline and acidic conditions are given in Tables 2.3.7-13 and 2.3.7-14, respectively. The acidic conditions model is used when the pH is less than 6.8, and the alkaline conditions model is used when the pH is equal to or greater than 6.8 (BSC 2004b, Section 8.1). The alkaline conditions model is not sensitive to pH (i.e., $a_4 = 0$ in the alkaline conditions model). The regression analyses indicated that pH was not a significant factor influencing the dissolution rate under alkaline conditions; therefore, it was removed from the alkaline conditions model (see Figure 2.3.7-26 for a plot of the alkaline dissolution rate data and model). In addition, carbonate concentrations are very low under acidic conditions. Therefore, total carbonate concentration was removed from the acidic conditions model (i.e., $a_2 = 0$ in the acidic-conditions model) (BSC 2004b, Section 6.4.1.2) (BSC 2004b, Sections 6.4.1.3 and 8.1). Figure 2.3.7-26 gives a picture of the model fit to the (alkaline) data. Tables 2.3.7-15, 2.3.7-16, and 2.3.7-17 provide the data that are used as the basis for the model (BSC 2004b, Tables 4-2, 4-3, and 4-4). The uncertainty in model predicted rates at a given temperature and oxygen level is roughly an order of magnitude in either direction (BSC 2004b, Section 8.2 provides a more detailed discussion of the uncertainty), suggesting that most of the data points in Figure 2.3.7-26 fall within the range of values predicted by the model.

The model was compared to two sets of published literature data on the fractional release rates of radionuclides measured under air-saturated dissolution conditions: the Nevada Nuclear Waste Storage Investigations Series 3 batch test data (Wilson 1990b), and the extensive commercial SNF test results published by the Swedish SNF corrosion program (Forsyth 1997; Röllin et al. 2001). Comparisons of the model-calculated results to the Nevada Nuclear Waste Storage Investigations Series 3 experimental data show that the model gives slightly higher rates, but the agreement is well within an order of magnitude (BSC 2004b, Section 7.1.2) (Table 2.3.7-18). The agreement with the Forsyth data is excellent, and well within the modeling uncertainty range (BSC 2004b, Section 7.1.2) (Table 2.3.7-19). Röllin et al. (2001) provide single-pass flow-through data on the oxidative dissolution rate of commercial SNF under acidic conditions. The results (Röllin et al. 2001, Figure 9) show a coefficient of –0.6 for dependence on pH. Although this reflects a greater dependence on pH than does the –0.34 coefficient (Table 2.3.7-14) in the base-case acid model, the dissolution rates presented are comparable to those calculated by the acidic conditions model (BSC 2004b, Section 7.1.2). The results outlined above, and considered in further detail in BSC 2004b, Section 7.1.2, suggest that the model-calculated fractional release rates are consistent with experimentally measured fractional release rates in the literature. Similarly, gap inventories are validated by comparison with published fuel rod segment test data (BSC 2004b, Table 7-3).

2.3.7.8 U. S. Department of Energy Spent Nuclear Fuel Degradation

[NUREG-1804, Section 2.2.1.3.1.3: AC 1(1) to (5), AC 2, AC 3(1) to (3), AC 4, AC 5; Section 2.2.1.3.2.3: AC 1(2); Section 2.2.1.3.4.3: AC 1(1) to (6), AC 2, AC 3(1) to (4), (8), AC 4, AC 5(1) to (3)]

2.3.7.8.1 Conceptual Description

[NUREG-1804, Section 2.2.1.3.1.3: AC 1(1) to (5); Section 2.2.1.3.4.3: AC 1(1) to (4)]

The 34 distinct forms of DOE SNF are divided into the following eleven groups, according to fuel type for postclosure modeling (see Section 1.5.1 for a more detailed description of the DOE SNF, and Section 1.5.2 for the waste package configurations):

1. Naval SNF canister placed in naval short and long waste package configurations

2. Plutonium/uranium alloy in long and short 18-in.-diameter canisters (to be placed in 5-DHLW/DOE long and short codisposal waste packages)

3. Plutonium/uranium carbide in long and short 18-in.-diameter canisters (to be placed in 5-DHLW/DOE long and short codisposal waste packages)

4. Mixed oxide and plutonium oxide in long and short 18-in.-diameter canisters (to be placed in 5-DHLW/DOE long and short codisposal waste packages)

5. Thorium/uranium carbide in long and short 18-in.-diameter canisters (to be placed in 5-DHLW/DOE long and short codisposal waste packages)

6. Thorium/uranium oxide in long and short 18-in.-diameter canisters (to be placed in 5-DHLW/DOE long and short codisposal waste packages), and in multicanister overpacks to be placed in 2-MCO/2-DHLW waste packages).

7. Uranium metal in long and short 18-in.-diameter canisters (to be placed in 5-DHLW/DOE long and short codisposal waste packages), and in multicanister overpacks to be placed in 2-MCO/2-DHLW waste packages).

8. Uranium oxide in long and short 18-in.-diameter canisters (to be placed in 5-DHLW/DOE long and short codisposal waste packages), and in multicanister overpacks to be placed in 2-MCO/2-DHLW waste packages).

9. Aluminum-based fuel in long and short 18-in.-diameter canisters (to be placed in 5-DHLW/DOE long and short codisposal waste packages), and in short 24-in.-diameter canisters (to be placed in 4-DHLW/1-DOE-SNF short waste packages)

10. Miscellaneous fuel in long and short 18-in.-diameter canisters (to be placed in 5-DHLW/DOE long and short codisposal waste packages)

11. Uranium-zirconium hydride (U-ZrHx) in short 18-in.-diameter canisters (to be placed in 5-DHLW/DOE long and short codisposal packages) (DOE 2004, Table F-1).

The degradation rates of these fuel types vary over a wide range (Table 2.3.7-20). DOE SNF types, except for Naval SNF, are modeled as degrading instantaneously upon waste package breach (BSC 2004c, Sections 6.2 and 8.1). This is a conservative treatment and is validated by corroboration of model results with the alternative mathematical model (BSC 2004c, Section 7). Commercial SNF waste packages are used to represent the naval SNF waste packages for all scenario classes in the TSPA as discussed in Section 2.3.7.3 (BSC 2004c, Sections 6.2 and 8.1).

2.3.7.8.2 Data and Data Uncertainty

[NUREG-1804, Section 2.2.1.3.1.3: AC 2, AC 3(1) to (3); Section 2.2.1.3.4.3: AC 2, AC 3(1) to (4), (8)]

DOE SNF is grouped into eleven types; Group 1 (naval SNF), and Groups 2 through 11 (DOE SNF in 18-in.-diameter × 10- or 15-ft-long canisters, in 24-in.-diameter × 10- or 15-ft-long canisters, or in multicanister overpacks) (DOE 2004, Table F-1).

DOE SNF Group 1 (Naval SNF)—Commercial SNF waste packages are used to represent the naval SNF waste packages for all scenario classes in the TSPA as discussed in Section 2.3.7.3. The radionuclide releases from naval SNF waste packages are considerably less than releases from commercial SNF waste packages; accordingly, the use of this surrogate is conservative (BSC 2004c, Section 6.2).

DOE SNF Groups 2 through 11—For Groups 2, 3, 4, 7, 8, and 10, the mass fractional degradation rates at 50°C are high enough compared to the long time frames of the TSPA representation that the fuels can be treated as degrading effectively instantaneously. The remaining Groups (5, 6, 9, and 11) have small inventories such that an instantaneous degradation treatment is appropriate. This upper-limit model is chosen because most of the best-estimate models (other than Group 7) are currently based on limited and unqualified corrosion, dissolution, or oxidation data, and because the degradation of most of the DOE SNF inventory is effectively instantaneous (BSC 2004c, Section 6.2).

2.3.7.8.3 Model, Model Uncertainty, Abstraction, and Results

[NUREG-1804, Section 2.2.1.3.1.3: AC 1(1) to (5), AC 4, AC 5; Section 2.2.1.3.4.3: AC 1(1) to (6), AC 4, AC 5(1) to (3)]

DOE SNF Group 1 (Naval SNF)—Commercial SNF waste packages are used to represent the naval SNF waste packages for all scenario classes in the TSPA as discussed in Section 2.3.7.3 (BSC 2004c, Section 6.2).

DOE SNF Groups 2 through 11—These groups are modeled as dissolving or degrading instantaneously. This conservative approach does not require confirmatory data. Validation is based on the fact that the best estimate degradation rates (i.e., the alternative mathematical model)

for the uranium metal-based fuels, which comprise approximately 85% of the mass, indicate that complete degradation will occur in less than one year after exposure (i.e., the degradation is effectively instantaneous relative to geologic timeframes). The instantaneous release model is bounding, yet reasonable compared to the alternative mathematical model and is, therefore, validated through corroboration (BSC 2004c, Section 7).

2.3.7.9 High-Level Radioactive Waste Glass Dissolution

[NUREG-1804, Section 2.2.1.3.1.3: AC 1(1) to (5), AC 2, AC 3(1) to (3), AC 4, AC 5; Section 2.2.1.3.2.3: AC 1(2); Section 2.2.1.3.4.3: AC 1(1) to (6), AC 2, AC 3(1) to (4), (8) AC 4, AC 5(1) to (3)]

2.3.7.9.1 Conceptual Description

[NUREG-1804, Section 2.2.1.3.1.3: AC 1(1) to (5); Section 2.2.1.3.4.3: AC 1(1) to (4)]

The glass dissolution model provides the TSPA with a means for abstracting release rates of radionuclides in high level radioactive waste glass. Glass dissolution can be modeled as being congruent. All the constituents enter solution in proportion to the glass composition, followed by precipitation of saturated mineral phases (Grambow et al. 1986; BSC 2004d, Sections 1.2 and 6.3.1). Some elements reach saturation relatively early in the dissolution process, and may scavenge other elements that are released from the glass matrix (e.g., iron as the mineral ferrihydrite). Waste glass dissolution therefore contains kinetic (e.g., dissolution rate) and thermodynamic (e.g., mineral solubility) features. The effect of the barrier capability of the canisters that contain the glass is conservatively not included in the analysis.

While the dissolution mechanism may involve a series of chemical reactions, only one of these is rate-limiting. Many experiments over the past 20 years have suggested that the kinetics are controlled by a single dissolved species, orthosilicic acid (H_4SiO_4) (also referred to as aqueous silica). Orthosilicic acid is present in groundwater and is introduced into solution as the glass dissolves (e.g., Advocat et al. 1999; Bourcier 1994; Grambow et al. 1986; Knauss et al. 1990; McGrail et al. 1998). The release of soluble components into solution slows as the concentration of orthosilicic acid increases (e.g., Grambow et al. 1986; BSC 2004d, Sections 1.2 and 6.3.1; Chick and Pederson 1984).

As glass reacts with solution and elements reach saturation with respect to mineral phases, precipitation occurs. For the most part, precipitation occurs on the surface of the reacting glass, and forms what is known as the alteration rind (Figure 2.3.7-27). Elements from the dissolving glass must diffuse through this layer. For some elements like boron there is no significant transport control across this rind. However, other elements either sorb or precipitate in this layer. The glass dissolution rate is used to determine the thickness of the rind. The release of a specific element into the solution outside the rind depends on either the dissolution rate of glass, or the element's solubility-limited concentration, and on the rate of diffusion through the rind (BSC 2004d, Section 6.5.3.3).

Dissolution studies conducted with a wide range of borosilicate glass compositions and using various test methods have confirmed that the forward dissolution rate depends on the solution pH

and temperature (e.g., Abraitis et al. 2000; Advocat et al. 1999; BSC 2004d, Section 7.2; Knauss et al. 1990; McGrail et al. 1998). The general form for the glass dissolution rate is:

$$\text{rate}_G = k_0 \times 10^{\eta \text{pH}} \times \exp(-E_a/RT) \times (1 - Q/K) \qquad \text{(Eq. 2.3.7-6)}$$

where

rate_G = glass dissolution rate (g glass/(m^2·day))

k_0 = intrinsic glass dissolution rate (g glass/(m^2·day))

η = pH dependence (dimensionless)

E_a = effective activation energy (kJ/mol)

R = gas constant (8.314 J/mol·K)

T = absolute temperature (K)

$(1 - Q/K)$ = affinity term (dimensionless)

Q = the ion activity product; in this case, the activity of H_4SiO_4

K = the equilibrium constant for the rate limiting step; in this case, the activity of H_4SiO_4 at saturation with the glass.

2.3.7.9.2 Data and Data Uncertainty

[NUREG-1804, Section 2.2.1.3.1.3: AC 2, AC 3(1) to (3); Section 2.2.1.3.4.3: AC 1(2), (4), AC 2, AC 3(1) to (4), (8)]

Test methods have been developed in which the solution concentration of dissolved silica is maintained low enough that the value of the affinity term remains nearly one throughout the test (i.e., far from equilibrium conditions). By controlling the pH and temperature in those tests, values of k_0, η, and E_a have been determined for several glasses.

The dissolution rates of several borosilicate glass compositions have been observed to increase as the solution pH decreases from near-neutral (Abraitis et al. 2000; Knauss et al. 1990). The same rate equation was used to model the results in acidic and alkaline solutions with different parameter values. Figure 2.3.7-28 shows the pH-dependent glass degradation rates at 70°C and 90°C that were used to build the glass degradation model. They also give an idea of the uncertainty in degradation rates and temperature dependence.

Similar parameter values have been measured for different glass compositions. This is consistent with the rate-limiting step in the dissolution mechanism in alkaline solutions of all borosilicate waste glasses being similar. Differences in glass composition do not affect the rate limiting step and

are contained in the k_0 term. Since the effects of glass composition on the glass dissolution rate are small, the k_0 and chemical affinity terms were combined in the glass dissolution model as a single term, which is referred to as the effective dissolution rate coefficient, k_E (BSC 2004d, Sections 6.4 and 6.5). This term was also used to represent the effects of the water contact mode (e.g., humid air, dripping water, or immersion (BSC 2004d, Section 6.3)) on the dissolution rate. The value of k_E was determined by using the degradation rates measured in tests simulating particular water-contact conditions. The use of those parameter values to represent a range of waste glass compositions was validated by comparison with corresponding values determined from literature data (BSC 2004d). As with the commercial SNF degradation model, the glass degradation model is built from data describing degradation rates and surface areas. A mosaic of overlapping studies emphasizes the fairly predictable behavior of dissolving glass and the rates involved.

2.3.7.9.3 Model, Model Uncertainty, Abstraction and Results

[NUREG-1804, Section 2.2.1.3.1.3: AC 1(1) to (5), AC 4, AC 5; Section 2.2.1.3.4.3: AC 1(1) to (6), AC 4, AC 5(1) to (3)]

The release rate of radionuclides due to HLW glass degradation that is provided to TSPA is calculated as the product of three terms (BSC 2004d, Section 6.5). These are:

$$R_i = \text{rate}_G \times S \times I_i \qquad \text{(Eq. 2.3.7-7)}$$

where

R_i	=	release rate of radionuclide i from HLW glass (g radionuclide$_i$/day)
rate_G	=	specific degradation rate of the glass (g glass/(m^2·day))
S	=	surface area of glass contacted by water (m^2)
I_i	=	grams of radionuclide i per gram of glass (Section 2.3.7.4).

The radionuclide release rate given in Equation 2.3.7-7 is used in the TSPA to estimate the mass of a particular radionuclide i available for dissolution into water in the codisposal waste package during a particular period of time. The concentration of a given radionuclide i in water exiting Cell 1 is equal to the concentration of that radionuclide dissolved in solution plus the concentration of that radionuclide attached to or embedded in colloids. The maximum concentration of a given radionuclide that can dissolve in solution is equal to its elemental solubility limit, as apportioned among the various isotopes of that element. Radionuclides released from the glass in excess of the solubility limit may be associated with colloids or remain with the glass as insoluble residue. The water volume available for dissolution is equal to the volume of water contained in the alteration rind (SNL 2008, Sections 6.3.7.4.3.2 and 6.3.7.4.3.3).

Mathematical expressions for the specific degradation rate of the glass and the surface area of the glass contacted by water are given in Equation 2.3.7-8 and Equation 2.3.7-9, respectively. The inventory of radionuclides in HLW glass canisters is discussed in Section 2.3.7.4.

The specific degradation rate of the glass is given as (BSC 2004d, Section 6.5.1):

$$\text{rate}_G = k_E \times 10^{\eta \text{pH}} \times \exp(-E_a/RT) \qquad \text{(Eq. 2.3.7-8)}$$

where

k_E = glass degradation rate coefficient (g glass/(m^2·day))
η = pH dependence coefficient (dimensionless)
E_a = effective activation energy (kJ/mol)
R = gas constant (8.314 J/mol·K)
T = absolute temperature (K).

Note that Equation 2.3.7-8 is the same as Equation 2.3.7-6, except k_E has been substituted for $k_0 \times (1 - Q/\text{K})$. The value of k_E accounts for the effects of glass composition, including heterogeneity of the waste inventory, as well as the effects of the affinity term and water-contact mode. The model requires specification of three parameter values (k_E, η, and E_a) and is a function of pH and temperature. From 100°C to 125°C, a conservative pH of 10 is used (BSC 2004d, Section 5.2). Values of the three parameters and their distributions are shown in Table 2.3.7-21 (BSC 2004d, Table 8-1). Note that the most probable surface areas and rates are chosen to be the minimal values, reflecting the fact that—over time—degradation rates of glasses tend to decrease as the surface becomes covered with alteration products. This is routinely seen in the field where glass degradation rates measured over longer time-spans are typically slower than those measured in the laboratory (e.g. Zoitos et al. 1989, White and Brantley 2003, and Gordon and Brady 2003). Alternative conceptual models for glass degradation were considered as well and are documented in BSC 2004d, Section 6.4. Specifically, a diffusion-controlled glass rate law and a glass rate law that was independent of glass composition were considered. The first envisions overall rate control being exerted by diffusion of reactants and products through a non-stoichiometric leach layer. This model was not used because independent evidence for the leach layer is weak, and the model predicts rates that are close to those predicted by the existing model. The composition-independent glass dissolution model presumes that the composition of the waste glass does not affect its long-term durability—a conclusion that is at odds with the general dependency of silicate dissolution rates on composition.

The equation used to calculate the glass surface area contacted by water as glass dissolves accounts for an increase in surface area from cracking and a loss in surface area due to dissolution (BSC 2004d):

$$S = f_{\text{exposure}} \times S_{sp} \times (M_0 - \Sigma M) \qquad \text{(Eq. 2.3.7-9)}$$

where

S = surface area available for reaction in the current time step (m^2)
f_{exposure} = exposure factor (dimensionless)

S_{sp} = specific surface area (m^2/kg)
M_0 = initial mass of glass (kg)
$\sum M$ = total mass of glass degraded in all previous time steps (kg).

The surface area is greater than the geometric surface area of the glass cylinder by an exposure factor ($f_{exposure}$) because glass cracks from thermal and mechanical stresses generated as glass cools in the pour canisters. A range of values from 4 to 17 is used to account for variations in the degree of cracking of different glass logs and the accessibility of water to tight cracks (BSC 2004d, Section 6.6, Table 6-14). The minimum value of $f_{exposure}$ is 4 (conservatively based upon the highest observed experimental evidence), and the maximum value is 17 to account for extreme cracking (Bickford and Pellarin 1987; Sené et al. 1999).

The volume, thickness, and water content of the alteration rind are calculated in terms of the mass of HLW glass that reacts (BSC 2004d, Appendix D). The volume of the alteration layer is equal to the mass of glass reacted divided by the glass density. The volume of water in the layer is the volume of the layer times its porosity. The thickness of the layer is obtained by solving for the change in radius of the right cylinder of glass with an initial radius of 0.3 m (BSC 2004d, Appendix D).

The parameter values used in the HLW glass dissolution model are shown in Table 2.3.7-21. These parameter values were calculated from glass dissolution test data (BSC 2004d, Section 6.5). In addition, the results of vapor hydration tests indicated that a relative humidity of at least 44% is required for degradation to occur. Therefore, the glass degradation rate equation is applied only when the relative humidity is above 44%. Otherwise, the glass degradation rate is set to zero.

2.3.7.9.3.1 Uncertainty in the HLW Glass Dissolution Model

Uncertainty in the HLW glass dissolution model is represented by a statistical treatment of the range of values and distributions assigned to the degradation rate coefficients (k_E) (BSC 2004d, Section 8.2.2). The distributions of k_E also account for uncertainty in the glass dissolution rate model coefficients, η and E_a, by covering the range of solution exposure conditions from thin water films to free flowing bulk solutions and conservatively treating the high-temperature vapor hydration test results as applying to lower temperatures (BSC 2004d, Section 8.2.2).

Uncertainty in glass dissolution test results is accounted for by conservatively using the release rate of boron to represent the glass dissolution rate (BSC 2004d, Section 8.2.3). Because boron is the most rapidly released structural element of borosilicate waste glass, it bounds selective leaching, and the release of boron is a conservative treatment of the dissolution rate and the release rates of all radionuclides (BSC 2004d, Section 8.2.3). Tests have shown that technetium, which bonds weakly to the glass, is released nearly stoichiometrically with boron, while other radionuclides (e.g., plutonium and americium) are released much more slowly than boron (e.g., Bazan et al. 1987; Bibler and Jurgensen 1988; Ebert et al. 1996). In addition, this treatment is conservative because transport of radionuclides through the alteration rind is controlled by their individual solubilities and propensities for colloid formation.

2.3.7.9.3.2 Model Validation

The model is validated by comparison with literature values that were not used to develop or calibrate the model (BSC 2004d, Section 7.1), and by comparison with dissolution rates of seabed basaltic glasses, which are used as natural analogues for waste glasses. The dissolution rates for basaltic glasses covered in sediment and exposed to Si-saturated seawater at about 3°C and pH 7 to 9 are bounded by the glass degradation model. The activation energy for glass degradation under alkaline conditions is also similar to that measured when basaltic glass is dissolved in seawater (BSC 2004d, Section 7.2). Other parameters in the glass degradation rate law are likewise broadly consistent with published values (BSC 2004d, Sections 7.3 and 7.4). These comparisons demonstrate that an appropriate level of confidence exists in the glass degradation model (BSC 2004d, Section 7.5).

Dissolution rates calculated using the HLW glass degradation model with the minimum and maximum values of k_E were compared directly with the dissolution rate of natural analogue basalt glasses recovered from the seabed (BSC 2004d, Section 7.2). The dissolution rates of several basalt glasses were calculated based on the thickness of the layer of palagonite that forms as an alteration phase in vesicles and vugs in the glass and the independently determined age (Grambow et al. 1986, pp. 268 and 269, Table 2, Figure 3). These specimens had been exposed to silica-saturated seawater at about 3°C at pH 7 to 9. The dissolution rates of these basalt glasses were about 10^{-7} m per 1,000 years, which is equivalent to 6×10^{-7} g/(m^2·day) for a basalt density of 2.5 g/cm^3. The respective minimum and maximum dissolution rates calculated using the HLW glass degradation model at 3°C are 6.62×10^{-9} and 1.16×10^{-5} g/(m^2·day) at pH 7, and 6.33×10^{-8} and 1.11×10^{-4} g/(m^2·day) at pH 9 (BSC 2004d, Appendix B, Table B-4). Thus, the model bounds the long-term dissolution rate of basalts at both pH limits, providing further confidence in the model (BSC 2004d, Section 7.2).

2.3.7.10 Dissolved Radionuclide Concentration Limits

[NUREG-1804, Section 2.2.1.3.4.3: AC 1(1) to (6), AC 2, AC 3(1) to (4), (8), AC 4, AC 5(1) to (3)]

The dissolved radionuclide concentration model estimates concentrations of dissolved radionuclides as a function of water chemistry under the conditions likely to prevail inside breached waste packages (Section 2.3.7.5) (SNL 2007h).

2.3.7.10.1 Conceptual Description

[NUREG-1804, Section 2.2.1.3.4.3: AC 1(1) to (6)]

The dissolved concentration model uses the chemical speciation code EQ3–NR to estimate the solubilities of radionuclides as a function of pH, carbon dioxide levels, fluoride levels, and ionic strength inside breached waste packages and the invert. Solubilities are mapped over a large range of potential fluid compositions and are provided to the TSPA in the form of lookup tables or single values. These are applicable in all scenario classes that involve groundwater transport of radionuclides. The conceptual description, data, and data uncertainty are more fully developed for each radionuclide in the following sections.

2.3.7.10.2 Data and Data Uncertainty

[NUREG-1804, Section 2.2.1.3.4.3: AC 2, AC 3(1) to (4), (8)]

Four types of uncertainty are associated with the dissolved concentrations calculation: 1) in the thermodynamic data supporting the EQ3NR calculations; 2) due to variations in the chemistry of the water in which dissolution is occurring; 3) in the temperature; and 4) in activity coefficients. For some elements, the identities of the solubility controlling phases existing over the repository lifetime are also uncertain. Uncertainties in solubility limits due to uncertainties in thermodynamic data and in the chemistry of the water into which dissolution occurs are included as variables in the solubility expressions given for the actinide elements. Temperature uncertainties are treated as bounding or limiting conditions on the solubility limits given. Activity coefficient uncertainties are also treated as bounding conditions when the ionic strength of the solutions does not exceed 1 molal (the nominal limit of applicability of the EQ3NR modeling code) (Wolery 1992, p. 38) and the supporting database *Data0.ymp.R2*). Additional activity coefficient uncertainty in solutions with ionic strengths from 1 molal to 3 molal is treated by augmenting the uncertainty applied to the solubility to account for thermodynamic data uncertainty (SNL 2007h, Section 6.3.3).

Critical to the evaluation of radionuclide solubilities is identification of the solubility-controlling solid(s). This is typically based on laboratory or field observation. The chosen value can result in several orders of magnitude difference in the final result. For this reason, a closer examination of solids identification is warranted. Thermodynamic data on actinide solids are derived from laboratory solubility measurements and from direct thermochemical measurements (Nordstrom and Munoz 1986, Chapter 11). The thermodynamic properties of the minerals uraninite (UO_2), thorianite (ThO_2), and analogous phases have been well defined using thermochemical techniques. However, other phases such as NpO_2 and PuO_2 have not. Solubility studies of actinide dioxide (Grenthe et al. 1992, Section v3.2.3.3; Guillaumont et al. 2003, Section 9.3.2.2; Hummel et al. 2002; Neck and Kim 2001), using over and under saturation tests at pH greater than 3 to 5 (depending on reference), indicate that the dissolved actinide concentrations are not controlled by high temperature crystalline phases, but solids (such as hydrated or amorphous phases) are considerably more soluble. Hummel et al. (2002, Figure 3.2.2) clearly show the solubility calculated from the thermodynamic properties of the high temperature mineral form of ThO_2 is 8 orders of magnitude lower than concentrations measured in laboratory experiments at pH values above about 6. Similarly, Figure 3.2.3 of the report by Hummel et al. (2002) shows the calculated solubility of the high temperature mineral form of UO_2 is 6 orders of magnitude lower than concentrations measured in laboratory experiments at pH values above about 3. The more soluble phases leading to the higher, laboratory measured concentrations are not well defined crystallographically. However, solubility values are reproducible and these solubility values do not change over a period of several years (the time scale of laboratory experiments). The most-stable solid would be selected as the controlling phase, because thermodynamically less stable phases would ultimately be replaced by the most-stable phase. However, it cannot be demonstrated that the thermodynamically most-stable solid appears under the expected repository conditions. This fact makes identification of the controlling solid purely from thermodynamic considerations unreliable. To use a more stable phase (rather than the first formed, less stable phase) as the controlling phase for solubility calculations, it is necessary to demonstrate that the less stable mineral(s) is replaced by the more stable mineral(s) in a shorter period than the characteristic time scale of the problem.

For some elements, the identification of controlling solids for the repository by experiments has yet to be reported (e.g., protactinium), or experimental observations are not conclusive (e.g., plutonium). For situations like these, a conservative approach is, as suggested by Bruno et al. (1997, p. 81), to choose the amorphous solids (oxide or hydroxide) as their controlling solids. Also, the radiation associated with spent nuclear fuel could damage the lattice structure of solids and make it less crystalline (Rai and Ryan 1982, p. 216). It is well known that radioactive decay, especially alpha decay, can damage the crystal structure of plutonium solids. Rai and Ryan (1982) reported in an experiment lasting 1,266 days that $^{238}PuO_2$(c) (c = crystalline) was found to convert to an amorphous form of PuO_2, which has higher solubility than PuO_2(c). In waste forms, the fraction of isotope ^{238}Pu in the total plutonium inventory is small (SNL 2007d, Table 7-1), so crystal structure damage is not expected to occur rapidly enough to be significant. However, over the regulatory time period, it is reasonable to expect that PuO_2(c) would gradually convert to a PuO_2(am). Therefore, this phenomenon is recognized, and the uncertainty it introduces to radionuclide solubility is addressed.

Freshly precipitated solids tend to be fine particles with a large specific surface area. The extra surface energy given by the large surface area makes fresh precipitates more soluble. However, with time, the freshly precipitated fine particles go through a process called aging in which particle size increases. As a result, an aged precipitate has a lower solubility than the freshly precipitated solid. Aging could be a long-lasting process. For example, in a study lasting 1,266 days, Rai and Ryan (1982) observed continuous aging of $PuO_2{\cdot}xH_2O$ (amorphous). As solubility experiments usually last less than a year, it is reasonable to expect that the measured solubility is actually an upper limit. Therefore, because of aging, a solid's real solubility could be lower than its measured solubility.

In fact, aging and decay effects (radiation damage) have opposite effects on solubility. Aging could make a radionuclide less soluble if the starting material is an amorphous solid. Decay effects could make a radionuclide more soluble, provided the initial material is a crystalline solid. Therefore, it is reasonable to speculate that the real controlling material may contain both amorphous and crystalline phases. Indeed, Rai and Ryan (1982, p. 214) found that "the solubility of $^{239}PuO_2$ and $^{239}PuO_2{\cdot}xH_2O$ tend to merge; most, if not all, of the effect is due to decreased solubility of $PuO_2{\cdot}xH_2O$ with time." While there is not enough information to define the thermodynamic properties of this intermediate solid quantitatively and, consequently, to calculate solubility controlled by it, the uncertainty can be bounded by use of the amorphous and crystalline phases. A more detailed discussion of all uncertainties in the dissolved concentrations calculation can be found in SNL 2007h (, Section 6.3.3). Figure 2.3.7-29 compares the solubility of crystalline and hydrated, aged PuO_2. The latter solubility is used by the TSPA to estimate plutonium levels.

Direct inputs for the individual concentration models include the thermodynamic databases "data0.ymp.R2" and "data0.ymp.R4" (SNL 2007h), with supplemental data from a review and compilation by the Nuclear Energy Agency (Guillaumont et al. 2003) and representative J-13 well water chemistry. Table 2.3.7-22 gives the composition of the J-13 water used in the solubility calculations. J-13 water has historically been used to consider fluid-waste interaction at Yucca Mountain. It should be noted, however, that the output of the dissolved concentrations model are insensitive to the starting water composition, except for those components (e.g., fluoride, carbonate) whose levels are uncertain and whose effects are treated explicitly. The principal properties of the water to which the solubilities show sensitivity are pH, CO_2 fugacity (fCO_2), and fluoride concentration. The effects of varying pH and fCO_2 values are directly considered, and

values of calculated radionuclide concentrations are presented in lookup tables for a range of pH and fCO_2 values. The effects of different fluoride concentrations are uncertain and are addressed through the use of uncertainty coefficients, ε_2, discussed below. Lastly, there is an implicit uncertainty in the supporting thermodynamic database that translates into uncertainties in the predicted radionuclide solubility limits.

2.3.7.10.3 Model, Model Uncertainty, Abstraction and Results

[NUREG-1804, Section 2.2.1.3.4.3: AC 3(1) to (4), AC 4, (8), AC 5(1) to (3)]

Using the thermodynamic equilibrium computer code EQ3NR and the thermodynamic database "data0.ymp.R2" and "data0.ymp.R4," solubility limits are determined considering (1) controlling solid phases, (2) water chemistry (Section 2.3.7.5), and (3) temperature (SNL 2007h, Section 8.1 and Appendix VI). These limits form the abstraction that is provided to the TSPA (R5 data is used for tin solubility calculations).

Solubility is determined by the controlling solid phases (the solid phases that would precipitate from solution at higher concentrations). The use of the most thermodynamically stable phase results in the lowest solubility, which in some cases—because of slow precipitation kinetics of the stable phase—underpredicts observed solubilities. In some cases, it therefore may be necessary to select less stable solid phases on the bases of laboratory or natural analogue evidence to ensure that the modeled solubilities are representative or bounding. When such evidence is unavailable or inconclusive, less stable solids were chosen based on the Ostwald step rule (Langmuir 1997, p. 324). Therefore, the solubility models are either supported by direct observations or are conservative (SNL 2007h, Section 6.3.2).

Atmospheric oxidizing conditions are conservatively assumed, and all solubilities except those of plutonium and neptunium (Sections 2.3.7.10.3.1 and 2.3.7.10.3.2) were calculated with an fO_2 of 0.2 bar (SNL 2007h, Section 5.1). Radiolysis has the potential for increasing the redox potential near the fuel, and for lowering the pH. The specific impacts of radiolysis are outlined in excluded FEP 2.1.13.01.0A, Radiolysis, Table 2.2-5. Local radiolytic production of oxidized species and/or nitric acid is likely to be limited by the presence of steel and fuel corrosion products.

To estimate the effects of changing temperature on actinide solubilities, calculations were made at 60°C (SNL 2007h, Appendix VI). Plutonium, neptunium, uranium, thorium, americium, and protactinium solubilities at higher temperatures were lower than those at 25°C (SNL 2007h, Table 6.3-4). Radium solubilities are higher at 100°C; the higher value was therefore used in place of the lower, 25°C radium value. Because the TSPA implements only one temperature for solubility, all solubilities used in the TSPA model were calculated for 25°C (ambient temperatures are expected to go no lower than 23-24°C; hence 25°C is a reasonable lower bound). Because the solubilities for these radionuclides are lower at higher temperatures, this approach is conservative (SNL 2007h, Sections 6.3.3.3 and 6.4.2.2 and Appendix VI).

The dissolved concentrations model outputs have three forms: (1) lookup tables as a function of pH and fCO_2 along with associated uncertainty terms, (2) a constant for specified pH intervals; and (3) no solubility limit (e.g., the release is set by the SNF or HLW degradation rate). With the exception of curium and actinium, these elements are the complete set of elements corresponding to the radionuclides listed in Table 2.3.7-2. Transport of actinium is not modeled because of its

extremely short half-life (around 22 years) (SNL 2007h, Section 6.10). Actinium dose is calculated instead by assuming secular equilibrium with ^{231}Pa. Curium is only included so as to account for effects of its decay on the inventory of ^{241}Am (SNL 2008, Section 6.3.7.5). The solubility model output form that applies for each element is identified below:

- Lookup tables as a function of pH and fCO_2—plutonium, neptunium, uranium, thorium, americium, tin, and protactinium
- Constant for specified pH range—radium
- No solubility limit—technetium, carbon, iodine, cesium, selenium, chlorine, and strontium concentrations are limited by waste form degradation rate.

Lookup tables were calculated for plutonium, neptunium, uranium, thorium, americium, tin, and protactinium. Results of the EQ3NR calculations for these elements (with the exception of tin) are shown in Figures 2.3.7-29 to 2.3.7-33 (SNL 2007h). (Thermodynamic data are not available in the thermodynamic databases "data0.ymp.R2" for protactinium, and neptunium is used as an analogue for the purposes of solubility calculations, as described in Section 2.3.7.10.3.6 below). The solubilities of these radioelements generally increase with increasing pH under alkaline conditions, while under acid conditions they increase with decreasing pH. This U-shape (or V-shape) curve is typical for actinides. Minimum solubility generally is reached at neutral to mildly basic pH, which is also generally the pH range predicted by the in-package chemistry model (Section 2.3.7.5.1). The solubilities of radioelements increase with fCO_2, which is approximated by pCO_2.

The dissolved concentration for plutonium, neptunium, uranium, thorium, americium, tin, and protactinium is expressed as (SNL 2007h, Section 8.1.2):

$$[RN] = 10^{s} \times 10^{(\varepsilon_1)} + (\varepsilon_2 \times N) \qquad \text{(Eq. 2.3.7-10)}$$

where

RN = the solubility limit of the element used in the TSPA (mg/L)

S = solubility calculated as a function of pH and CO_2 level with the speciation code, EQ3NR

ε_1 = the uncertainty associated with the equilibrium constant

ε_2 = the uncertainty associated with the effect of the dissolved F^- concentration

N = pH dependence of ε_2 ($N = 1$ for protactinium).

Uncertainty associated with the equilibrium constant, K, of the reaction between controlling solids and aqueous species is captured by the uncertainty term ε_1. This uncertainty is derived from the

standard-state Gibbs free energy of formation ($\Delta_f G^0$) of the species involved in the dissolution reaction. Uncertainties in $\Delta_f G^0$ values are taken from various sources (SNL 2007h, Section 6.3.3.1), and correspond to the 95% confidence interval (2σ in a normal distribution). The uncertainty in the $\Delta_f G^0$ value is directly propagated to the uncertainty in the log(K) value. Therefore, the uncertainties in the $\Delta_f G^0$ values for all of the aqueous species of a given element are examined, and the largest value associated with any aqueous species selected as the 2σ value for a normal distribution (SNL 2007h, Section 6.3.3.1). The potential impact of high ionic strengths on radionuclide solubilities was accounted for by increasing the uncertainty in the radionuclide solubility products to account for ionic strength-dependent changes in aqueous actinide activity coefficients (SNL 2007h, Section 6.3.3.4).

Uncertainty associated with the effects of F^- concentration is captured by the uncertainty term ε_2. The source of fluoride for commercial SNF waste packages is groundwater, but in codisposal waste packages, HLW glass releases fluoride as it dissolves. To evaluate the effects of fluoride content on solubilities, calculations for a range of pH values at a single fCO_2 were made at higher fluoride contents for each type of waste and water influx condition. Maximum fluoride levels are calculated by concentrating fluoride-containing seepage fluids; the highest fluoride level is 10 mM. In general, increased fluoride concentration is associated with increased radionuclide solubility, as shown in Figure 2.3.7-34 for thorium. For each element, the largest difference between the base-case solubility and the solubility associated with increased fluoride concentration was used to establish the uncertainty distribution for ε_2. This difference is the maximum and least likely value of the triangular distribution of ε_2 that has a minimum and most probable value of zero (SNL 2007h, Section 6.5.3.4.3). This was done because only the relatively high fluoride concentrations significantly increase actinide solubility levels. In the TSPA, the sampled values for the ε_2 term for each actinide should be perfectly correlated, since the uncertainty represented is epistemic uncertainty in the fluoride concentrations in seepage waters.

2.3.7.10.3.1 Plutonium

The solubility of plutonium is expected to be controlled by a hydrated plutonium dioxide PuO_2(hyd, aged) (SNL 2007h, Section 6.4.2.5.1). The amorphous precipitate is observed in experimental studies to be the first solid phase formed, and it has been shown to gradually convert to the more crystalline, less soluble form over time (SNL 2007h, Section 6.5.3.1).

Plutonium solubility is sensitive to small changes in redox potential (Eh), so a more detailed analysis of the redox state is warranted. The plutonium solubility calculated at an fO_2 of 0.2 bar is significantly above the measured solubility from experiments originally open to the air (Figure 2.3.7-35). Therefore, the redox potential that best fits the data (Equation 2.3.7-11) was established for modeling purposes (SNL 2007h, Appendix V.5). The redox potential is modeled as:

$$Eh = 1.10 - 0.0592\ pH \qquad \text{(Eq. 2.3.7-11)}$$

The modeled redox potential is less than the theoretical air-water value, but still higher than redox potentials measured in natural waters at the Yucca Mountain Project (SNL 2007h, Figure 6.5-6) and

is expected to be conservative for seepage, and as well the interior of a breached waste package (SNL 2007h, Appendix V). The results are shown in Figure 2.3.7-36.

Figure 2.3.7-37 presents plutonium solubility at $\log(fCO_2) = -3.5$ bar and the Eh calculated using Equation 2.3.7-11 and compares it against the laboratory data upon which the model is based, showing good agreement. In addition, Figure 2.3.7-38 plots the model against data from Pacific Northwest Laboratory and Argonne National Laboratory spent fuel leaching experiments that validate the model (Wilson 1990a; Wilson 1990b (Series 2 and Series 3 tests, respectively); CRWMS M&O 2000b and CRWMS M&O 2000c for Argonne National Laboratory high-drip and low-drip tests). The good match between the model results and the experimental results, which were not used to develop the model, builds confidence in the use of the plutonium solubility component of the TSPA model (SNL 2007h, Section 7.2.2). High fluoride levels can raise the solubility of plutonium, though the effect is seen primarily at pH values unexpected inside the package (SNL 2007h, Table 6.5-3)

2.3.7.10.3.2 Neptunium

Several studies concerning neptunium-bearing phases that could form under repository conditions have been conducted. Several types of solubility-controlling phases have been examined. One is pure neptunium phases, consisting primarily of neptunium oxides, hydroxides, and carbonates. The other is neptunium-bearing uranium phases, wherein neptunium constitutes a minor element component in solid solutions.

NpO_2–$NaNpO_2CO_3$ are assumed to be the controlling phases inside corroding waste packages. Additionally, the Np_2O_5–$NaNpO_2CO_3$ solubility model is used for the invert (SNL 2007h, Section 6.6 and Appendix IV). The presence of reduced metals and fuels in the package is expected to result in NpO_2 limiting levels of dissolved neptunium. The more oxidized Np_2O_5 might limit dissolved levels inside the package once the steels and fuels have been completely oxidized. More oxidizing conditions should also prevail in the invert. The TSPA tracks the persistence of electron donors (metals, fuels) over time. From onset of breach until all of the metals and fuel are corroded, NpO_2 limits dissolved neptunium concentrations. Once metal/fuel oxidation is complete Np_2O_5 equilibria dictates dissolved neptunium levels (Section 2.4.1).

Figure 2.3.7-39 plots the NpO_2 model results and the Np_2O_5 model results at $\log fCO_2 = -3.5$ against experimental data from Pacific Northwest Laboratory and Argonne National Laboratory that validate the models (Wilson 1990a; Wilson 1990b (Series 2 and Series 3 tests, respectively); CRWMS M&O 2000b; CRWMS M&O 2000c; and Thomas 2003 and for Argonne National Laboratory high-drip and low-drip tests). The figure shows that the results of both models demonstrate them to be bounding when compared to experimental data that were not used to develop the models. This builds confidence in the use of the neptunium solubility component of the TSPA model (SNL 2007h, Section 7.2.3). Note that the NpO_2 model and the Np_2O_5 model include $NaNpO_2CO_3$ at high pH values, and are termed the NpO_2–$NaNpO_2CO_3$ and Np_2O_5–$NaNpO_2CO_3$ models. Unlike uranium and thorium, neptunium solubilities (both NpO_2 and Np_2O_5) are relatively insensitive to dissolved fluoride levels.

An alternative conceptual model for neptunium-dissolved concentrations is based on incorporation of neptunium into secondary uranium phases (e.g., the neptunyl ion substituting for the uranyl ion

in the mineral structure) (SNL 2007h, Section 6.6.1). By comparing the neptunium-to-uranium ratio in solution versus the ratio in the fuel, an incorporation ratio of neptunium into the uranium phases can be estimated. Additional information has been presented by Burns et al. (2004) showing that pentavalent neptunium is correlated with uranophane and Na-compreignacite in experiments forming those phases in the presence of dissolved neptunium. Although the observations of Burns et al. (2004) provide evidence for the likely incorporation of Np^{5+} into uranophane and Na-compreignacite, uncertainty exists in the effect of environmental variables on the rate of incorporation. As a result, for the purposes of the TSPA, this alternative model is not used. Instead, the conservative solubility limits based on the NpO_2–$NaNpO_2CO_3$ and Np_2O_5–$NaNpO_2CO_3$ models are used.

2.3.7.10.3.3 Uranium

Uranium solubility has been shown to be controlled by different solid phases, depending on the composition of water in the system (SNL 2007h, Sections 6.7.1 and 6.7.4). When the water is low in silica, as is the case for water in contact with commercial SNF waste packages, schoepite, a hydrated uranium oxide mineral phase, is the controlling phase. When the water contains appreciable amounts of silica, as is the case for water in contact with HLW glasses in codisposal packages, or in the case of an igneous intrusive event, the uranyl silicate mineral Na-boltwoodite controls uranium solubility. The choice of uranium-controlling phases is corroborated by comparison with phases found in laboratory studies (Wronkiewicz et al. 1996, Table 5) and reported in the literature from a natural analogue site (SNL 2007h, Section 7.2.4). The model used in the TSPA contains both controlling solid phases, depending on the waste type and scenario class (SNL 2007h, Sections 6.7.1 and 6.7.4). At higher fCO_2 levels and basic pH, a uranium carbonate phase ($Na_4UO_2(CO_3)_3$) is solubility-controlling (SNL 2007h, Section 6.7.4).

The effect of elevated fluoride on uranium solubility was investigated and found to be significant at pH between 4 and 7. An uncertainty factor is contained in the uranium solubility model to account for the sensitivity to fluoride concentration (SNL 2007h, Sections 6.7.5.3 and 6.7.6).

2.3.7.10.3.4 Thorium

The amorphous form of ThO_2 has been selected as the controlling solid phase for thorium solubility over the expected range of repository conditions (SNL 2007h, Section 6.8.2). The minimum thorium concentration modeled is 6.36×10^{-4} mg/L at an fCO_2 of 10^{-5} bar and a pH of 6.25. At this pH and low fCO_2, the impact of F^- and SO_4^{2-} complexes is minimal, and the hydroxyl complex $Th(OH)_3CO_3^-$ dominates. This solubility should therefore represent the experimental solubility of amorphous thorium dioxide in pure water at moderate to high pH values. Hummel et al. (2002, Section 5.21) have summarized data from a number of studies of thorium solubility in pure water. From the results of these studies, Neck and Kim (2001) calculated that, at pH values above 6, the solubility of thorium dioxide in pure water is $10^{-8.5\pm0.6}$ mol/L (Neck and Kim 2001, Section 3.1). The minimum solubility modeled in *Dissolved Concentration Limits of Elements with Radioactive Isotopes* (SNL 2007h, Section 7.2.5.1) of 2.7×10^{-9} mol/L (equals $10^{-8.6}$ mol/L) is close to the mean and well within the uncertainty of the measured values. The above comparison validates that the thorium solubility model compares favorably with test data and is adequate for use in the TSPA model. Figure 2.3.7-32 shows pH and CO_2-dependent thorium solubilities, and highlights the

importance of thorium-carbonate complexation at the pH values likely to prevail inside the package. Increasing pH and/or CO_2 levels cause sharp increases in dissolved thorium.

2.3.7.10.3.5 Americium

$AmOHCO_3$ was chosen as the controlling solid phase in all calculations of americium solubility (SNL 2007h, Section 6.9). The choice of this mineral is based on the studies by Nitsche, Gatti et al. (1993) and Nitsche, Roberts et al. (1994), which identify $AmOHCO_3$ as the solid phase precipitated from water corresponding to the water used in these calculations at a pH range of 5.9 to 8.4 and temperatures from 25°C to 90°C. This is the most likely controlling phase under the range of environmental variables of interest to this analysis. Thus, the model of americium solubility is consistent with experimental data generated and is adequate for use in the TSPA model. Above and below this pH range, americium solubility becomes very high, depending on fCO_2. The solubility of americium is somewhat sensitive to dissolved fluoride levels. From pH 6 to 7, maximum in-package fluoride levels could raise dissolved americium levels by roughly an order of magnitude. The effect decreases at higher pH. Above pH 8, fluoride does not significantly change calculated americium levels.

2.3.7.10.3.6 Protactinium

Thermodynamic data for protactinium are sparse, so neptunium and thorium are used as analogues for the purpose of solubility calculations. Baes and Mesmer (1986, Section 9.1), Shibutani et al. (1998), and Yui et al. (1999) describe extraction of some thermodynamic data from limited experimental data for protactinium behavior in solutions of several types at a range of pH values. Protactinium occurs in aqueous solution as both protactinium(IV) and protactinium(V). The solution properties of protactinium are similar to those of other actinides in the same oxidation states. Based on considerations of chemical analogy, protactinium solubility should range from above that of thorium(IV) to below that of neptunium(V). Under the widest range of pH and fCO_2 conditions, Np_2O_5 solubility is greater than that of ThO_2(am) (am = amorphous). The base-case protactinium solubility is taken as equal to that of Np_2O_5, with the solubility difference from the ThO_2(am) analogue accommodated in the ε_1 uncertainty term (SNL 2007h, Section 6.11.2).

2.3.7.10.3.7 Radium

The solubility limit of radium is based on the solubility of pure $RaSO_4$, and is modeled as a piecewise function of pH (SNL 2007h, Table 6.12-1). For slightly alkaline (J-13 well water) and acidified Yucca Mountain waters, the calculated radium solubility ranges from 9.1×10^{-3} to 1.9×10^{-2} mg/L. Thus, a constant solubility of 8.5×10^{-2} mg/L is recommended for radium for pH values from 3 to 7.75. Under more alkaline conditions, pH from 7.75 to 9.75, calculated solubility ranges from 0.1 to 47.9 mg/L. For this pH range, a constant value of 47.9 mg/L is recommended. Above a pH of 9.75, there is no solubility limit (SNL 2007h, Section 6.12), and the concentration is controlled by the dissolution rate of the waste form.

2.3.7.10.3.8 Technetium, Carbon, Iodine, Cesium, Strontium, Selenium, and Chlorine

For technetium, carbon, iodine, cesium, strontium, selenium, and chlorine, no solubility-controlling solid will exist in the repository, and the release of these five elements will be controlled by the

dissolution rate of waste forms in addition to the availability of connected water films inside the package and diffusion, rather than by solubility (SNL 2007h, Sections 6.14 to 6.18, 6.20, and 6.21). This treatment tends to greatly overpredict the release of carbon from breached waste packages and the invert, because it neglects retardation of carbon movement due to the formation of carbonate minerals and sorption onto metal oxides, and as such, is a conservative approach.

2.3.7.11 Colloidal Radionuclide Availability

[NUREG-1804, Section 2.2.1.3.4.3: AC 1(1) to (6), AC 2, AC 3(1) to (5), (8), AC 4, AC 5(1) to (3)]

Colloids are 1 nm to 2 μm sized particles that have the potential to remain suspended, and therefore be transported, in solution. Colloids are of concern because they have the potential to facilitate transport of otherwise low solubility, highly sorbing radionuclides. Suspension of low solubility radionuclides on colloids may increase the mobile concentrations of those radionuclides above the solubility limits.

2.3.7.11.1 Conceptual Description

[NUREG-1804, Section 2.2.1.3.4.3: AC 1(1) to (6)]

The colloid model (1) identifies the types of colloids likely to be present in the waste package and their absolute abundances; (2) establishes colloid pH and ionic strength-dependent stability ranges; and (3) calculates the amount of radionuclides that each colloid type is able to transport. Due to their complexity and/or uncertainty, some processes were not incorporated into the model, including colloid filtration, colloid straining, and colloid sorption to the air–water interface. Exclusion of these processes is conservative, as their inclusion would result in slower colloid migration with respect to radionuclide transport by colloids (Excluded FEP 2.1.09.20.0A, Filtration of colloids in EBS, Table 2.2-5).

The stability of colloidal suspensions is controlled by electrostatic and chemical processes at the colloid-solution interface that determine the balance between attractive and repulsive forces between adjacent colloids. Higher ionic strengths weaken repulsive forces between colloids, causing colloidal suspensions to become unstable and to agglomerate. Repulsion is also minimal, and agglomeration is favored, when the pH is near the pH of zero point of charge of a particular colloid. High temperatures and low humidity in a breached waste package would favor high-ionic strength solutions that would destabilize colloids. The ionic strength threshold depends on the colloid mineral phase and pH of the solution, as these largely determine the colloid surface charge.

Colloid sorption, filtration, and straining were not modeled in the EBS transport calculation (Excluded FEP 2.1.09.20.0A, Filtration of colloids in EBS, Table 2.2-5), in part because of the difficulty in accurately anticipating the paths colloids might follow particularly as the waste form degrades over time from metal + fuel to corrosion products + oxidized fuel. Unlike the unsaturated zone—where the matrix is fairly well understood and unlikely to change over time—the physical characteristics of the EBS will be materially different in the future.

There are two types of radionuclide-bearing colloids: those formed from hydrolysis of dissolved radionuclides (often called true colloids), and colloidal particles of other materials with attached radionuclides (called pseudocolloids). True colloids of trace radionuclides, such as plutonium, are

not expected to form in the repository, because the large abundance of other sorbing materials will prevent the radionuclides from becoming saturated and nucleating free-floating particles. Instead, plutonium is seen as inclusions in waste form corrosion products that can be mobilized as colloids; plutonium and other radionuclides can also be sorbed onto the waste form corrosion colloids themselves. For the glass waste form, radionuclide inclusions are seen in clay corrosion product colloids. For commercial SNF, plutonium- and americium-rich regions are seen in a layer at the corroding surface, associated with an actinide- and rare earth element-containing zirconium phase that may also move as a colloid. Uranium phases may do likewise. For DOE SNF, which comprises a small fraction of the repository inventory, the uranium metal fuels alter to hydrated and/or oxidized secondary phases that might ultimately be transported as a colloid. Iron oxyhydroxide colloids are expected to form from corrosion of the waste package materials, and will be potentially able to sorb, and transport, radionuclides.

To summarize, the main colloid sources in the repository, their radionuclide interactions, estimated concentrations, and stabilities are as follows:

1. Glass waste form colloids that contain plutonium and americium, and are also able to sorb radionuclides. Their concentrations are estimated from laboratory tests performed at Argonne National Laboratory. Because they form from glass weathering, their stability is modeled as being that of a montmorillonite clay.

2. Plutonium-rich zirconium oxide (Pu/Zr) particles whose levels are estimated from lab tests on spent fuel and whose stability is modeled as being that of ZrO_2.

3. DOE and commercial SNF waste form colloids that are oxidized uranium phases that are able to sorb radionuclides. Their levels are estimated on the basis of lab tests on spent fuel. Their stability is modeled as being that of meta-autunite, which is a mineral whose surface chemistry is thought to be similar to uranophane.

4. Iron oxide steel corrosion colloids that can sorb radionuclides. Their levels are estimated from lab tests and groundwater analyses. Their stability is modeled from measurements on hematite colloids.

5. Clay colloids from groundwater seepage that are able to sorb radionuclides. Levels are estimated from groundwater analyses. Their stability is assumed to be that of montmorillonite.

Absent from the list above are microbes and humic acids, (Excluded FEP 2.1.09.13.0A, Complexation in EBS, Table 2.2-5), that are occasionally seen to transport otherwise insoluble compounds in the subsurface. Previous analyses (BSC 2004e, Section 6.5.3) evaluated the potential for biocolloidal transport of radionuclides and suggested it to be limited due, in part, to low microbial activity, and negligible compared to groundwater colloids.

To estimate colloidal radionuclide fluxes: (1) the TSPA uses input pH and ionic strengths to determine the stability of each colloid type; (2) the concentration(s) of the stable colloid types are then estimated; and (3) surface equilibria are then used to calculate the amount of radionuclides sorbed onto each of the stable colloids (except the Pu/Zr-particles, which carry radionuclides in their

structure but do not sorb radionuclides). The glass waste form colloids and the DOE SNF and commercial SNF uranophane colloids are distinct in that they carry radionuclides in their structure that cannot exchange with solution, in addition to radionuclides sorbed to their surfaces, which can exchange with solution.

2.3.7.11.2 Data and Data Uncertainty

[NUREG-1804, Section 2.2.1.3.4.3: AC 2, AC 3(1) to (4), (8)]

Data from both laboratory experiments and literature sources have been used in developing the colloid model. Measurements of colloid concentrations, studies of colloid suspension stability, and experiments to determine radionuclide sorption properties are discussed in the remainder of this section.

There are several sources of data uncertainty (SNL 2007i, Section 6.6). The parameters developed in this model analysis are in some cases based on data that are not specific to the Yucca Mountain site. The colloid model maps these parameters to Yucca Mountain conditions through bounding assumptions and/or probability distributions that account for the data uncertainty.

2.3.7.11.2.1 Tests on Commercial Spent Nuclear Fuel, U. S. Department of Energy Spent Nuclear Fuel, and High-Level Radioactive Waste Glass

Formation and Identification—Tests of commercial SNF and DOE SNF have been performed at Argonne National Laboratory and Pacific Northwest National Laboratory to examine the alteration products formed as well as the release of dissolved and colloid-associated radionuclides (SNL 2007i, Sections 6.3.3, 6.3.4, 6.3.5, and 6.3.6). Testing was designed to simulate a variety of repository-relevant water-exposure conditions for several waste forms spanning a range of fuel burnups and compositions. Observations from the commercial SNF tests showed that alteration products formed that included low concentrations of uranium-based oxyhydroxide colloids (mostly meta-schoepite and metastudtite); and uranium-based silicates might also be expected to form from Si-rich solutions (SNL 2007i, Section 6.3.2.5). Analysis of plutonium-bearing solids from spent fuel corrosion tests, including dynamic flow-through and drip tests, suggests that the plutonium is located in nanocrystalline particles that also contain rare earths and zirconium (Buck, Hanson et al. 2004).

Drip tests and immersion tests on HLW have been conducted at Argonne National Laboratory (CRWMS M&O 2001). The drip tests were designed to be relevant to dripping conditions that could occur within a breached waste package. Waste form colloids were determined to be smectite clay that contain measurable quantities of plutonium and americium (SNL 2007i, Sections 5.4 and 6.3.2.2). Plutonium-bearing smectite colloids formed from the degradation of HLW are incorporated into the colloid model.

Stability and Concentration—The saturated tests on HLW glass performed at Argonne National Laboratory were used to estimate the concentration of actinide-bearing colloids resulting from the degradation of HLW glass (CRWMS M&O 2001, Section 6.3.1). Generally, the ionic strength at which smectite colloids are destabilized occurs at higher ionic strengths, as shown in Figure 2.3.7-40.

An experimental investigation of the stability of montmorillonite (a smectite clay) suspensions as a function of pH and ionic strength in an NaCl solution resulted in suspensions becoming unstable and flocculating at pH 2, 4, and 8 in 0.01 mol/L, 0.225 mol/L, and 0.375 mol/L NaCl solutions, respectively.

Uncertainties—Uncertainties associated with these data include measurement uncertainties and experimental factors and the application of these results to repository conditions. Additionally, uncertainties during the measurement of colloids formed from the various waste forms arise in the determination of mass, calculation of volume, determination of particle sizes by filtration, and measurement of concentrations by the various detection methods employed.

2.3.7.11.2.2 Tests to Examine Colloid Generation from Steel Corrosion

Corrosion of carbon steel was investigated in a set of bench-scale experiments in which water was introduced to a small carbon steel container designed with the approximate geometry of a waste package, but at 1/70 scale. The tests yielded data on alteration phases from corrosion of carbon steel. Products resulting from corrosion of the steel were characterized by quantity and the produced mineralogy. Two configurations were used for the disposition of water in the container: (1) a bathtub configuration, in which water was introduced into a hole at the top of the container and exited from an opening on the side of the container after it accumulated along the bottom; and (2) a flow-through configuration, in which water was introduced into a hole at the top of the container and directly exited from a hole at the bottom. Water with a repository-relevant chemical composition was used in the experiments. To establish the total amount of corrosion material goethite, lepidocrocite, maghemite, and magnetite (among others) transported out of the vessels, the effluent was passed through a microfiltration system capable of separating particles of 0.1 μm and larger (SNL 2007i, Section 6.3.8).

Stability and Concentration—From the log-normal distribution of the miniature waste package corrosion tests results, a geometric average concentration of 3.69 mg/L was determined for the four-week-long experiments (SNL 2007i, Section 6.3.8).

Iron oxyhydroxide colloid suspensions are minimally stable at near-neutral pH, with the degree to which they are stable depending on mineralogy and water composition. At higher or lower pH, however, iron oxyhydroxide colloid suspensions are stable; the exact pH limits depend upon ionic strength. Experimental data show that, for a given ionic strength, iron oxyhydroxide stability increases as pH both increases and decreases away from the pH range of minimum stability (Liang and Morgan 1990). In general, the higher the ionic strength, the wider the pH range in which iron oxyhydroxide colloid suspensions are unstable.

Uncertainties—Measurements of corrosion colloids produced in the steel corrosion experiments described above have uncertainties related to the measurement of colloid mass using filtration techniques, and possibly are related to remobilization of colloid suspensions from high ionic strength, flow rate, and/or coating of particles (thereby changing surface characteristics). To use the results of the corrosion experiments to estimate corrosion colloid quantities for use in the colloid model, values and ranges were developed that simultaneously incorporated the experimental uncertainties and maintained realism based on measurements in groundwater. The range of values for iron oxyhydroxide colloids concentration (0.3 to 30 mg/L, which was chosen

so that the maximum value bounded experimental values) was greater than natural iron oxyhydroxide colloid levels found in groundwater, and reflects the large masses of steel corrosion products anticipated in the repository. Additionally, the value is consistent with maximum colloid values of all types observed in groundwater.

2.3.7.11.2.3 Tests to Characterize Seepage Water Colloids

Colloid concentrations in saturated zone groundwater were used in the colloid model to estimate the colloid concentrations in seepage water that could enter a breached waste package.

There is a wide range in natural groundwater colloid concentrations in the Yucca Mountain vicinity over a relatively narrow range of groundwater ionic strength. The colloid concentration data were collected from nine different sources (SNL 2007i, Section 6.3.11). Measured concentrations range from near zero to several hundred milligrams per liter. Montmorillonite was used to model groundwater colloids at the site, although, in reality, ambient colloids are likely a mixture of clays, primary silicates, and iron oxides (note that "montmorillonite" and "smectite" are terms that are here used interchangeably to identify 2:1 clay minerals). Weathering of tuff produces clay minerals. In addition, montmorillonite was preferred over primary silicates, as it has a higher sorptive potential. Montmorillonite was chosen over iron oxide groundwater colloids because the mass of iron oxides in the package is both large and treated separately.

Stability—Seepage water colloids are modeled as montmorillonite; thus stability considerations are the same as those for waste form colloids derived from the degradation of HLW glass (Section 2.3.7.11.2.1).

Uncertainties—Factors that contribute to uncertainty in the concentrations of colloids in the groundwater samples used in the colloid model include (1) field sampling techniques; (2) factors affecting the quantities of particles suspended in the water samples, including additives introduced in the wells during the drilling process itself; and (3) errors inherent in the laboratory methods used to measure the quantities of colloids suspended in the water samples, such as filter ripening and interference and detection limitations for dynamic light scattering measurement techniques. To account for this uncertainty, mass concentrations used to establish the groundwater colloid concentration parameters were pooled using groundwater samples extracted primarily in the vicinity of Yucca Mountain. A cumulative distribution function was developed to accommodate the variable colloid concentrations and the uncertainty in groundwater sample collection.

As with the smectite HLW glass-derived colloids, the chief sources of uncertainty in the prediction of smectite seepage water colloids stability as a function of pH and ionic strength are associated with (1) experimental measurement uncertainties (e.g., detection limitations, quantification methods, interferences); (2) the extrapolation of laboratory data reported in the literature or DOE-supported experimental work to conditions (e.g., solution chemistry) expected in the postclosure repository environment; and (3) uncertainties related to calculations of ionic strength and pH, which are used as inputs to the colloid model from other TSPA models (e.g., in-package chemistry model, Section 2.3.7.5).

2.3.7.11.2.4 Radionuclide Sorption Data

Reversible sorption onto montmorillonite and uranophane colloids is modeled for plutonium, americium, uranium, neptunium, thorium, protactinium, cesium, radium, and tin. The radionuclide sorption distribution coefficients (K_d) were obtained from various data sources and measurements, including colloid-specific tests performed at Los Alamos National Laboratory and by Torstenfelt et al. (1982), Bradbury and Baeyens (2005), Pabalan and Turner (1997), Tachi et al. (2001), and others. Uncertainty distributions were developed and are given in *Waste Form and In-Drift Colloids-Associated Radionuclide Concentrations: Abstraction and Summary* (SNL 2007i, Tables 6-9 and 6-15). Radionuclide K_ds for montmorillonite sorption and uncertainty distributions are shown in Figures 2.3.7-41 and 2.3.7-42. Actinide sorption onto uranyl phases is shown in further detail in *Waste Form and In-Drift Colloids-Associated Radionuclide Concentrations: Abstraction and Summary* (SNL 2007i, Section 6.3.2.6).

A simplified competitive sorption model is used to model reversible sorption of radionuclides onto iron oxyhydroxide (as hematite) colloids. The model is based in part on the assumption that the available sorption sites can be partitioned linearly among the radionuclides based on their K_d values and their concentrations in solution. The model requires surface area and site density values for the sorbent colloids. Radionuclide sorption onto smectite (as montmorillonite) and uranophane (as meta-autunite) is modeled using K_ds.

Uncertainties—K_d value parameters established for the colloids in this analysis rely heavily on experimental work conducted at Los Alamos National Laboratory and on peer reviewed literature, in some cases for "analogues" of the colloids phases modeled. Corroborative data and model results reported in literature were evaluated to support the limited available data (SNL 2007i, Section 6.3.12.1). Within specific experimental data sets, results were subject to experimental measurement uncertainties (e.g., detection limitations, quantification methods, and interferences).

2.3.7.11.3 Model and Model Uncertainty

[NUREG-1804, Section 2.2.1.3.4.3: AC 4]

The model abstraction that the TSPA uses estimates the stability threshold of the five colloid types identified above as a function of pH and ionic strength using the Derjaguin, Landau, Verwey, and Overbeek model. The Derjaguin, Landau, Verwey, and Overbeek theory calculates the electrostatic and van der Waals forces between colloidal particles and predicts a stability ratio, W, which is related to the difference in the rate constants of rapid (van der Waals dominated attraction) and slow coagulations (Honig et al. 1971). Published zeta potential measurements are used as input in the Derjaguin, Landau, Verwey, and Overbeek model. The Derjaguin, Landau, Verwey, and Overbeek-predicted colloid stability thresholds are then parameterized as a function of pH and ionic strength for each colloid type, and validated where possible against independently measured colloid stabilities. The threshold relationships are as follows:

1. Montmorillonite (glass waste form colloids and groundwater colloids);
   $I_{threshold} = (-0.008 \times pH^2) + (0.12 \times pH) - 0.03$ (Figure 2.3.7-40).

2. ZrO_2 (Pu/Zr-particles);
   pH 4 – 7; $I_{threshold} = (0.0089 \times pH^3) - (0.1466 \times pH^2) + (0.7462 \times pH) - 1.092$;

when pH > 9.3, $I_{threshold} = (0.087362 \times pH^3) - (2.4078 \times pH^2) + (22.126 \times pH) - 67.791$;
from pH 7 to 9.3 the colloids are unstable at all ionic strengths (Figure 2.3.7-43).

3. Meta-autunite (DOE SNF and commercial SNF uranophane colloids);
$I_{threshold} = (-0.008 \times pH^2) + (0.14 \times pH) - 0.4$ (Figure 2.3.7-44).

4. Iron oxides; pH 4.5 – 8.4, $I_{threshold} = -0.013 \times pH + 0.11$;
when pH 9.4 – 10.4, $I_{threshold} = (-0.0017 \times pH^2) + (0.0327 \times pH) + 0.158$;
from pH 8.4 to 9.4 the colloids are unstable at all ionic strengths (Figure 2.3.7-45).

Meta-autunite (a uranium phosphate) is used as an analogue for uranophane (a uranium silicate) because the crystallochemical origins of meta-autunite and uranophane surface charge are similar (SNL 2007i, Section 5.6).

Once the TSPA determines that a particular colloid type is stable, the concentration of the colloid in solution must be estimated:

1. **Groundwater Colloids**—A cumulative distribution function was built from colloid levels measured in the Yucca Mountain area and from the Idaho National Laboratory. It extends from 0.001 to 200 mg/L (SNL 2007i, Figure 6.24).

2. **Glass Waste Form Colloids**—A triangular distribution was fit to laboratory measurements of plutonium-bearing glass waste form colloid levels (minimum: 5×10^{-9} mol/L plutonium; mode: 2×10^{-8} mol/L plutonium; maximum: 2.5×10^{-8} mol/L plutonium) (SNL 2007i, Section 6.3.2.2).

3. **Pu/Zr-Particles**—A range of 10^{-10} to 5.0×10^{-6} mol/L plutonium was developed from spent fuel test data; the associated americium range is calculated on the basis of the plutonium/americium ratio in the inventory at each time step in the TSPA iterations (SNL 2007i, Section 6.3.2.4).

4. **DOE SNF and Commercial SNF Uranophane Colloids**—A cumulative distribution from 0.001 to 200 mg/L was developed by comparison with groundwater smectite data, and confirmed against laboratory test results (SNL 2007i, Section 6.3.2.6. Low concentrations of actinides observed in SNF colloid tests are assumed to only associate on the surface of these colloids.)

5. **Iron Oxides**—A cumulative distribution was developed to describe a range from 0.001 to 30 mg/L for colloids generated by corrosion of stainless steel and a truncated log normal distribution with a mean of 3.69 mg/L and a range from 0.3 to 30 mg/L for colloids generated by corrosion of carbon steel (SNL 2007i, Section 6.3.8).

If a colloid is deemed unstable, the concentration is set to a very low nonzero value, which is typically 10^{-6} mg/L.

The last remaining task of the colloid model is to provide surface equilibria that allow radionuclides to be apportioned onto colloids. A K_d approach is used to predict reversible radionuclide uptake by groundwater, glass waste form, and uranophane colloids. Distribution functions were fit to literature measurements of radionuclide uptake by montmorillonite (for groundwater and glass waste form colloids) and uranophane (SNL 2007i, Sections 6.3.12.1 and 6.3.2.6 respectively). A more elaborate surface complexation model is used to calculate the competitive radionuclide uptake by iron oxide corrosion products and mobile iron oxide corrosion product colloids. This model also explicitly considers the kinetics of plutonium and americium attachment and detachment from iron oxide colloids. The iron oxide surface complexation model, and kinetic approach, are described in detail in Section 2.3.7.12.1. The site-limited K_d model of radionuclide uptake by montmorillonite and uranophane is presented here.

All strongly sorbing elements that have been screened in for the TSPA (SNL 2007b, Tables 7-1 and 6-3)—Actinium, americium, cesium, protactinium, lead, plutonium, radium, tin, and thorium, as well as the moderately sorbing elements neptunium and uranium—were considered for reversible sorption onto colloidal montmorillonite and uranophane. Of these, actinium and lead were eliminated because the TSPA does not consider them for transport but uses secular equilibrium with their parents.

When sorption and desorption are relatively fast, radionuclide sorption is controlled by local chemical equilibria and is most simply described using effective distribution coefficients (K_d values) (Langmuir 1997, p. 354):

$$S = K_d \times C \qquad \text{(Eq. 2.3.7-12)}$$

where

S = mass of a solute adsorbed on a unit mass of solid (mg/g)
K_d = mass-based distribution coefficient (mL/g)
C = concentration of the adsorbing solute in solution (mg/mL).

To account for competition between sites, and in recognition of the limited number of sorption sites on montmorillonite and uranophane, the approach is modified to allow linear partitioning of radionuclides based on their sampled K_d values and their concentrations in solution. Specifically, both sides of Equation 2.3.7-12 are summed over all sorbing radionuclides to estimate the maximum amount of radionuclides sorbed by both montmorillonite and uranophane. The latter value is then normalized to the number of available sites on montmorillonite and uranophane, which are estimated from their surface areas (10 to 100 m^2/g and 30 m^2/g, respectively) and site densities (2.3 and 2.0 sites/nm^2, respectively). Surface areas for montmorillonite are from Pabalan and Turner (1997); the uranophane surface area is from Ilton et al. (2006). Site densities for montmorillonite are from Pabalan and Turner (1997); the uranophane source is SNL 2007i, Table 6-24.

Table 2.3.7-23 provides the K_d ranges used in the TSPA calculation of montmorillonite (smectite) and uranophane colloidal radionuclide fluxes. Ranges are drawn from literature values of Lu et al.

(2000); Bradbury and Baeyens (2005); Bradbury and Baeyens (2006); Pabalan and Turner (1997); Tachi et al. (2001); Kim et al. (2006); Burns (1999); Douglas et al. (2005); Douglas et al. (2002); and McNamara et al. (2005). The model assumes thorium and protactinium sorption to be identical to that of americium.

2.3.7.11.3.1 Validation

The three pillars of the colloid model—stability, concentration, and sorption—are supported by comparison with independent observations in the technical literature that corroborate the model values. The specific supporting evidences are outlined in *Waste Form and In-Drift Colloids-Associated Radionuclide Concentrations: Abstraction and Summary* (SNL 2007i, Table 7-1), and are reviewed briefly below.

Validation of the Derjaguin, Landau, Verwey, and Overbeek prediction of montmorillonite and iron oxide stability comes from corroborating experimental data of, respectively, Tombácz et al. (1990) and Liang and Morgan (1990). Secondary corroboration of the smectite stability relationship comes from the data of Jara et al. (2005), which bounds model predictions. Additional validation of the iron oxide colloid stability model comes from the data from Madden et al. (2006).

Data from Mertz et al. (2000) were used to validate the zeta potential data from Zheng et al. (2006) that were used to develop the stability relation for uranophane colloids. Surface potential models calculated from the data of Schindler et al. (2004) agree qualitatively with the data used to establish the uranium(VI) colloid phase submodel. Hsu et al. (1988) published electro-mobility data for various forms of cerium oxide that agree qualitatively with the values published by Bitea et al. (2003), which were used to develop the Pu-Zr stability model.

The Derjaguin, Landau, Verwey, and Overbeek theory works best when predicting the behavior of colloids in dilute electrolyte solutions, but is less useful for concentrated brines. For this reason, the colloid model cannot readily explain the presence of suspended aggregates of particles in the relatively high ionic strength experiments performed by Zarrabi et al. (2003). The possibility of resuspension of colloids by high ionic strength brines might be countered by settling upon mixing with more dilute waters in the unsaturated zone.

The DOE HLW glass test data used in the model is supported by similar results observed in other alkali borosilicate glass testing programs; in particular, in corrosion tests on plutonium-, americium-, and thorium-doped alkali-borosilicate waste glasses (Ménard et al. 1998; Pirlet 2001; Vernaz and Gordon 1992).

The commercial SNF derived colloids model has been validated using the four intermittent long-term drip tests conducted on spent nuclear fuel fragments at 90°C (Finn et al. 1994; Mertz et al. 2003), spent fuel studies presented by Grambow et al. (1996), natural analogue studies (van Middlesworth and Wood 1998; Murakami et al. 1997), tests on uranium oxide (UO_2) ceramic pellets (Wronkiewicz et al. 1996), and tests on uranium metal fuels (Mertz et al. 2000), Kaminski et al. 2005).

The K_d ranges chosen for radionuclides attached to smectite and uranophane come from the peer-reviewed literature cited above. Additional confidence for these values comes from

independent overlapping K_d compilations of the EPA (EPA 1999a; EPA 2004) and Honeyman and Ranville (2002). The EPA studies (EPA 1999a; EPA 2004) reviewed published literature to predict K_d ranges for thorium, uranium, plutonium, americium, neptunium, radium, strontium, and cesium in soils. Honeyman and Ranville (2002) reviewed colloid-facilitated radionuclide transport and radionuclide sorption. Table 2.3.7-24 provides Honeyman and Ranville's (2002) groundwater colloid-actinide K_ds for comparison with the model montmorillonite (smectite) K_ds in Table 2.3.7-23.

2.3.7.11.3.2 Alternative Conceptual Models

Two alternatives were considered. The first uses a different waste form corrosion methodology for bounding colloid formation from glass. The second considers air-water limitations on the release of particles from a weathered waste form surface under unsaturated flow conditions. The principal bases and screening assessments for each are provided in *Waste Form and In-Drift Colloids-Associated Radionuclide Concentrations: Abstraction and Summary* (SNL 2007i, Table 6-19). The air-water limited alternative conceptual model, described by Buck, McNamara et al. (2004), investigates the processes whereby colloid generation at, and mobilization from, the surface of degrading waste is primarily related to flow rate at the waste surface and the attachment of colloids to air-water interfaces. The supporting concepts and data from the peer-reviewed literature that support this alternative model were developed in the context of deposition and remobilization of existing colloids under conditions of moderate to high fluid flow. The model suggests that, unless high flows are present, mobile colloid generation would be negligible owing to the strong and irreversible attachment of hydrophobic colloids to air bubbles on the surface of waste package components. This suggests that the conceptual model that the TSPA presently uses provides a conservative assessment of colloidal transport. The alternative conceptual model was not implemented, in part, because all of the data that are needed to implement it do not exist.

2.3.7.12 Engineered Barrier System Flow and Transport Model

[NUREG-1804, Section 2.2.1.3.3.3: AC 1(1) to (10), AC 2(1), (2), (4), AC 3(1) to (4), AC 4, AC 5; Section 2.2.1.3.4.3: AC 1(1) to (6), AC 2, AC 3(1) to (5), (8), AC 4(1) to (4), AC 5(1) to (3)]

The EBS flow and transport model estimates transport of radionuclides through the degraded waste package and waste form and invert, using inputs from models of drift seepage (Section 2.3.3), in-drift chemical environment (Section 2.3.5), waste package and drip shield degradation (Section 2.3.6), in-package chemistry, dissolved concentrations, and colloids. The EBS flow and transport model uses drift seepage and in-drift chemical environment inputs to anticipate the composition of fluids entering the invert from outside the waste package. Waste package and drip shield degradation information ultimately defines the nature and extent of fluid flow into and around breached waste packages. The in-package chemistry, dissolved concentrations, and colloid models provide the information needed to predict the concentrations of dissolved and colloidal radionuclides advecting and/or diffusing inside the waste package and through the invert.

For water to contact the fuel elements, the waste package must first be breached. This can occur through stress corrosion cracking (possibly initiated by seismic activity), through general corrosion (Section 2.3.6), through seismic damage (Section 2.3.4), or by igneous activity (Section 2.3.11). In the last case, the waste package and drip shield are assumed to provide no protection from basalt,

or seeping groundwater, or water vapor (SNL 2007a, Section 1). Water will be able to diffuse through non-igneous breaches into the waste package, and can do this in the presence of an intact drip shield. The waste package exterior will witness advective fluid flow only if the drip shield fails–possibly due to seismic activity. Seismic-induced shearing of the package or general corrosion can provide pathways for advective fluxes of water into a breached waste package; stress corrosion cracks cannot (Section 2.3.6). The drip shield is expected to fail from general corrosion after about 200,000 years in the nominal scenario, but failure due to seismic damage is statistically expected to occur before that time. Until drip shield failure, water vapor can only diffuse into a breached waste package. More generally, a strictly diffusive transport scenario is one in which the drip shield has not failed and the RH is greater than 95% (Section 2.3.7.5.1).

2.3.7.12.1 Conceptual Description

[NUREG-1804, Section 2.2.1.3.3.3: AC 1(1) to (10); Section 2.2.1.3.4.3: AC 1(1) to (6)]

The EBS flow and transport model considers (1) flow pathways within the EBS; and (2) radionuclide transport along specific flow pathways. Eight flow pathways within the EBS are considered in the model; fluxes corresponding to these pathways are designated *F*1 through *F*8 in Figure 2.3.7-8 (SNL 2007a, Section 6.3.1). *F*4, *F*6, and *F*8 are transport pathways for radionuclides (SNL 2007a, Section 6.3.1).

The primary source of water in the EBS is seepage flux. The seepage flux is combined with condensation flux on the drift walls, resulting in the total dripping flux, *F*1. Condensation under the drip shield is excluded from the EBS flow and transport model, based on low consequence (Table 2.2-5). The total dripping flux is potentially split between the amount (some, or all) diverted by the drip shield (*F*3) and the amount (if any) passing through breaches in the drip shield (*F*2) that might result from corrosion or seismic damage. It is assumed that any water that passes through breaches in the drip shield falls onto the waste package, and this flux is potentially split between the amount (some, or all) that is diverted by intact portions of the waste package (*F*5) and the amount (if any) that makes it past the waste package outer corrosion barrier (*F*4) (SNL 2007a, Sections 1 and 6.3.1.1). Radionuclides released from a degraded waste package are transported from the waste package via the flow pathway for flux *F*4. Water diverted by intact drip shield or waste package surfaces mixes with the flux through the waste package, resulting in the total flux into the invert (*F*6). The flow pathway for flux *F*7 represents imbibition flux of water from the unsaturated zone matrix into the invert. The total advective flux that enters the unsaturated zone is *F*8. Flow is modeled as quasi-steady state; thus, the flux out of the waste package (*F*4) is equal to the flux in, and the flux leaving the invert (*F*8) is equal to the sum of the total dripping flux (*F*1) and the imbibition flux (*F*7). The magnitudes of fluxes *F*1 through *F*8, as they are implemented in the TSPA, are spatially and temporally variable. The fluxes change temporally in response to changes in boundary conditions (e.g., the climate state) (BSC 2004f and SNL 2007a, Section 6.3.2.1).

In the case where no seepage occurs into the drift, and condensation on drift walls also does not take place, the total dripping flux (*F*1) is zero. In this case, *F*2 through *F*6 are also zero. There is no advection through the EBS, except possibly for the imbibition flux in the invert. Even if seepage or drift wall condensation does occur, if the drip shield is intact ($F2 = 0$) or the waste package is breached, there are no advective releases from the waste package ($F4 = 0$), and only diffusive releases will occur if the RH exceeds 95%.

After drip shield and waste package breach (general corrosion or rupture), the EBS flow and transport model considers both advective and diffusive transport of radionuclides along flow pathways for fluxes $F4$, $F6$, and $F8$. The model considers the transport of both dissolved and colloidal radionuclides. Advective transport occurs when dissolved or colloidal radionuclides are carried by liquid flow. Diffusive transport is due to concentration gradients along a flow pathway, and can occur without liquid flow. Advective and diffusive transport can take place simultaneously along a given pathway. When flux $F2 = 0$, radionuclide release from a degraded waste package will be limited to diffusive transport.

Subcomponents of the EBS flow and transport model account for the following:

- Temperature and water content-dependent diffusion within a degraded waste form and waste package
- Advection within a degraded waste form and waste package and the invert
- Competitive equilibrium sorption-desorption of radionuclides onto/off of surface sites exposed on fixed corrosion products and colloids in a degraded waste package
- Temperature and water content-dependent invert diffusion
- Reversible sorption onto crushed invert tuff.

The submodels use estimations of time-dependent corrosion product mass and water saturation to estimate sorptive surface areas, and effective radionuclide diffusion coefficients. Water adsorption isotherms and waste form surface areas are used to calculate the in-package water saturation as a function of relative humidity which, in turn, affects diffusion. When advective flow into the waste package occurs, the water saturation is simply set to 1.0. Central to the diffusive and advective transport calculation is the modeled partitioning of radionuclides onto mobile colloids and stationary corrosion products and the clear identification of which reactions will prevail inside the waste package. It is important to emphasize that Cell 1 contains waste fuel and/or glass. Cell 2 consists of steel and corrosion products. Dissolved and colloidal radionuclides are envisioned to move from Cell 1 to Cell 2 and then into the drift. All dissolved radionuclides start from Cell 1. Glass waste form colloids (montmorillonite) enter solution in Cell 1a. Pu/Zr and SNF uranophane colloids enter solution in Cell 1 or Cell 1b, depending on if the package is commercial SNF or codisposal. Clay colloids from groundwater seepage enter Cell 1 or 1a first, depending on package type. Iron oxide corrosion colloids enter solution in Cell 2. This means that radionuclide sorption by montmorillonite colloids (from the glass waste form or seepage) occurs in Cell 1 or Cell 1a. Radionuclide sorption by uranophane colloids occurs in Cell 1 or Cell 1b. Radionuclide sorption by iron oxide corrosion product colloids occurs in Cell 2. Lastly, radionuclide sorption onto stationary corrosion products occurs in Cell 2.

Radionuclide sorption by montmorillonite and uranophane colloids is calculated using the reversible, site-limited K_d model described in Section 2.3.7.11. Radionuclide sorption to iron oxide corrosion products (stationary and colloidal) is calculated in the following fashion:

1. Dissolution of fuel (and possibly glass) and/or solubility reactions control radionuclide levels in Cell 1.

2. Corrosion products accumulate over time in Cell 2, and are assumed to be a mixture of goethite and ferrihydrite and other oxides (SNL 2007a Section 6.3.4.2.1).

3. A range of Cell 1 fluid compositions—which varied in equilibrium CO_2 levels, pH, ionic strength, and radionuclide solubility-limiting phase saturation state—was used as input to a surface complexation model that equilibrated solutions with a range of Cell 2 corrosion product masses, goethite/ferrihydrite mixing ratios, and site densities (SNL 2007a, Sections 6.3.4.2.3 and 6.5.2.4.2). The output sorbed to dissolved radionuclide ratios were used to calculate site-limited, competitive model K_ds.

4. Model K_ds were regressed to build a multivariable response surface that the TSPA uses to estimate K_d and Cell 2 pH values as functions of CO_2 levels and corrosion product surface properties.

5. The kinetic sorption model, described in *EBS Radionuclide Transport Abstraction* (SNL 2007a, Section 6.3.1.2), incorporates a backward rate constant to allow slow desorption of plutonium and americium from stationary corrosion products. The forward rate constant is a sampled parameter; the backward rate constant is computed by dividing the forward rate constant by the K_d value derived from surface complexation-based modeling. The calculation of competitive sorption of radionuclides onto iron oxyhydroxide colloids does not allow radionuclide desorption (SNL 2007a, Section 6.5.1.2). The overall calculation of plutonium and americium mass balances is done inside of the TSPA. Allowing desorption from stationary corrosion products would tend to maximize advective plutonium and americium dose. Preventing plutonium and americium desorption from colloidal corrosion products would tend to maximize predicted colloidal plutonium and americium doses.

The elements considered for corrosion product competitive sorption calculations are uranium, neptunium, plutonium, americium, thorium, and nickel. The competitive sorption calculations are done using single-site surface complexation reactions in PHREEQC V. 2.11. Explicit consideration of plutonium and americium sorption kinetics was driven by (1) their potential importance to colloidal dose; and (2) greater availability of sorption kinetics data. Th sorption kinetics were not considered for corrosion product competitive sorption calculations because of relative unimportance to dose and lack of data. The same sorption K_d correlations used in the unsaturated zone transport model (Section 2.3.8) are also used to describe radionuclide adsorption on invert crushed tuff.

2.3.7.12.2 Data and Data Uncertainty

[NUREG-1804, Section 2.2.1.3.3.3: AC 2(1), (2),(4), AC 3(1) to (4); Section 2.2.1.3.4.3: AC 1(1) to (6), AC 2, AC 3(1) to (5), (8)]

The total dripping flux (*F*1) includes seepage and condensation, which are input to the EBS transport model within the TSPA framework. The imbibition flux (*F*7) is provided by the multiscale model within the TSPA. Water fluxes *F*2 through *F*6 depend on the total dripping flux. The flux leaving the invert (*F*8) is dependent on both the total dripping flux and the imbibition flux (Figure 2.3.7-8) (SNL 2007a, Figure 6.3-1). Diffusion through the invert also depends on the temperature and saturation in the drift (SNL 2007a, Section 6.3.4.1), which are provided to TSPA by the multiscale model (SNL 2007a). Because these other models account for uncertainty in their calculations, the associated uncertainties are propagated through the EBS flow and transport model.

Diffusion through waste package corrosion products depends on the water saturation, porosity, temperature, and relative humidity. The relative humidity inside a degraded waste package is taken to be the same as in the drift. As a reasonable upper bound on the porosity of waste package corrosion products, a fixed value of 40% is used in the transport model (SNL 2007a, Section 6.3.4.3.4.2). An upper bound would tend to result in maximal diffusive and advective fluxes. The effective water content is calculated for the corrosion products in no-seep locations using the relative humidity and the specific surface area of waste package corrosion products. Iron oxides and oxyhydroxides—such as goethite, ferrihydrite (hydrous ferrous oxide), hematite, as well as nickel and chromium oxides—will form inside the breached waste package from corrosion of the steel. The effective water content of corroded commercial spent nuclear fuel is calculated using the relative humidity and the specific surface areas of surrogate materials, including UO_2, ThO_2, PuO_2, CeO_2, and ZrO_2. The effective water content of corroded HLW glass is calculated using the relative humidity and glass specific surface area. The effective water content of DOE SNF is calculated using the relative humidity of the codisposal waste package and the same surrogate materials as for commercial SNF.

The mass of iron-bearing corrosion products that can form in the waste packages is calculated using design information representing the TAD (with 21-PWR canister) and long 5-DHLW/DOE codisposal waste package types (SNL 2007a, Section 6.3.3.1). These two waste package types are considered in development of the EBS transport model, because they are the most common types of commercial SNF and codisposal packages and, together, comprise 56% of the packages. It is important to emphasize, again, that while the in-package chemistry calculation (Section 2.3.7.5) also uses the 21-PWR TAD canister to model commercial SNF degradation, it uses the 2-MCO/2-DHLW assemblage to consider fluid chemistry in codisposal packages. The 2-MCO/2-DHLW package was chosen because the N Reactor fuel it contains accounts for the greatest actinide mass in co-disposal packages (SNL 2007e, Section 4.1.4[a]). SNL 2007e, Section 6.6.6[a]) explains why the chemistries inside of 2-MCO/2-DHLW packages will prevail inside the other co-disposal packages as well (Section 2.3.7.5.3). For the TSPA, the TAD and the long 5-DHLW/DOE codisposal waste package types are used to represent all waste packages, and are called the commercial SNF and codisposal waste packages, respectively (SNL 2007a, Section 6.3.3.1).

The pore volume of the corrosion products (which provides the saturated water volume) depends on the porosity, density, and mass of corrosion products as a function of time since the waste package

was breached (SNL 2007a, Section 6.5.2.2). The time-dependent mass of corrosion products is estimated from the total mass and estimated lifetimes for each of the predominant types of steel comprising the waste package internal components and inner vessel. Values for a TAD/21-PWR waste package are used as representative because this is the most common type of waste package in the repository. The lifetimes of steel internal components are obtained from the maximum thickness for each type of steel and the corrosion rates based on one year of exposure. The corrosion rate for each type of steel is uncertain, and each is represented by a truncated lognormal distribution (SNL 2007a, Section 6.3.4.3.4.3). The distribution ranges are from 29.53–130.02 μm/yr (A516) and 0.037–0.51 μm/yr (stainless steel) (SNL 2007a, Table 4.1-1). High corrosion rates favor accumulation of radionuclide-sorbing corrosion products, but also the adsorption of water and the formation of water films through which radionuclides might be transported more rapidly.

For the waste form and corrosion product domains, the effective diffusion coefficient in each domain is estimated using Archie's Law, which calculates effective radionuclide diffusion coefficients from free water diffusion coefficients as a function of volumetric water content (porosity and water saturation) and temperature. The diffusion coefficient in the corrosion products is assumed to be that of unconsolidated sand (SNL 2007a, Section 6.3.4.3.5). An unconsolidated sand is a reasonable proxy for an assemblage of iron oxides in an open drift that are periodically disaggregated by seismic events. Effective radionuclide diffusion coefficients in the invert were estimated by fitting Archie's Law to diffusion measurements from granular material (including tuff), and then adjusted for temperature and volumetric water content (SNL 2007a, Section 6.3.4.1.1).

Data from breached full-scale drip shield experiments (BSC 2003) are used to represent uncertainty in the drip shield and waste package flux-splitting algorithms. The data include water mass that flows through breaches in the drip shield, drip splash radius, and location of drips relative to breaches (SNL 2007a, Section 6.3.2). These breaches do not include cracks; these were artificial holes created in a scaled drip shield.

To provide an accurate concentration boundary condition at the invert-unsaturated zone interface, a portion of the unsaturated zone is modeled in the implementation of the EBS flow and transport model. This calculation requires unsaturated zone properties as input data.

The EBS flow and transport model is largely built on data feeds describing the corrosion rates of engineered materials, water adsorption, and radionuclide adsorption to stationary and colloidal particles. A common uncertainty in each of these data feeds is the reactive material surface area—particularly as breached waste packages evolve over time. Recognizing the uncertainty in the data, and incorporating it into the rates and isotherms used in the model, are important steps in bounding the overall process. Corroborating these measurements where possible with independent or field observations of, for example, colloid levels, sorption coefficients, and diffusion coefficients, also helps to minimize the overall uncertainty.

2.3.7.12.3 Model and Model Uncertainty

[NUREG-1804, Section 2.2.1.3.3.3: AC 1(1) to (10), AC 4(1) to (4), AC 5; Section 2.2.1.3.4.3: AC 1(1) to (6), AC 4, AC 5(1) to (3)]

In order to develop the flow and transport model for the EBS, a number of assumptions were made (SNL 2007a, Section 5). The most important of these are as follows:

- **Total Dripping Flux onto Drip Shield and Waste Package**—The source of dripping seepage and condensation at the roof of the drift is assumed to be fixed, and partial coverage by fallen rock is assumed to not divert any dripping flux from the waste package or drip shield. Further, all dripping seepage is assumed to fall on the crown of the drip shield or, if the drip shield is not present or is breached, on the crown of the waste package. This simplification bounds the upper limits of the dripping flux that will encounter the waste package.

- **Water Evaporation off a Drip Shield or Waste Package**—No evaporation of dripping seepage or condensation flux from the surface of a drip shield or waste package is allowed. This maximizes the amount of water available for interaction with the waste forms. It addresses the uncertainty of the residence time of liquid water on the surface, and the potential effect of dripping water on the local relative humidity.

- **Consumption of Water by Chemical Reactions**—Chemical reactions in the EBS, including those inside the waste package, are assumed to neither produce nor consume water. This assumption provides for a reasonable upper bound on the amount of water potentially available for advective and diffusive transport and release of radionuclides.

- **Continuous Thin Water Films**—Humidity inside the waste package is assumed to produce a continuous thin film of adsorbed water on corrosion products inside the waste package. Above a relative humidity threshold value of 95%, this water is assumed to behave as bulk liquid, allowing dissolved and colloidal radionuclides to diffuse through it. This assumption provides for an upper bound for radionuclide transport. At temperatures of 100°C or greater, the films are assumed to evaporate, so that no significant transport of radionuclides can occur, nor can water accumulate. This provides an upper bound on ease of diffusive transport from the package.

- **Corrosion Products**—For the purposes of estimating water saturation (for no-seep locations) and radionuclide sorption-desorption in commercial SNF waste packages and in codisposal waste packages, the metals contained in all internal waste package components (including carbon steel and stainless steel) are assumed to degrade to goethite, ferrihydrite (hydrous ferric oxide, abbreviated as HFO), NiO, and Cr_2O_3-like phases in corrosion products produced by steel degradation (SNL 2007a Section 6.3.4.2.1). These phases are those observed in corrosion tests.

- **Invert**—Because corrosion products in the invert are localized (SNL 2007a, Section 5.6), only the crushed tuff ballast is considered for invert transport. This provides a lower bound on invert retardation.

- **Water Vapor Access**—The waste package inner barrier is assumed to be breached immediately after the waste package outer corrosion barrier (SNL 2008). This simplification results in an upper bound on radionuclide transport.

2.3.7.12.3.1 EBS Flow

The model for EBS flow and transport involves three physical domains: (1) the waste form (e.g., fuel rods or HLW with some corrosion products); (2) waste package corrosion products; and (3) the invert. The unsaturated zone immediately underlying the invert is conceptualized as a dual continuum. The waste form and waste package corrosion product domains comprise the pathway for flux *F*4 (Figure 2.3.7-8). The invert comprises the pathway for flux *F*6.

The invert domain is modeled as being in close and direct contact with the waste package. The invert thickness varies because of the curvature of the bottom surface. Water and radionuclides are conservatively assumed to pass directly from the waste package to the invert. The emplacement pallet is not considered in the transport path length (SNL 2007a, Section 6.3.1.1). The final output from the EBS flow and transport model is the mass flux of radionuclides from the EBS into the unsaturated zone.

Flow Through and Around the Drip Shield—Water that falls onto the drip shield due to seepage (Section 2.3.3) and condensation (Section 2.3.5.4.2) either flows through a corrosion patch or a tear in the drip shield or is diverted around the drip shield. Water that has seeped into the drift or condensed on the walls of the drift above the drip shield will fall on the crown of the drip shield as droplets (SNL 2007a, Section 6.3.2.4). Water that falls onto the drip shield can either penetrate the drip shield through corrosion patches or drain along the sides of the drip shield. The function of the drip shield for the seismic scenario class, including the potential for stress corrosion cracking, is discussed in Sections 2.3.4 (also Excluded FEP, 2.1.03.02.0B, Stress corrosion cracking of drip shields, Table 2.2-5).

Breached drip shield experiments performed to discern the realistic behavior of dripping water on a drip shield with corrosion patches (BSC 2003) suggest that the main mechanism for water to enter breaches in the drip shield is through rivulets originating in a splash area around the point of impact. These observations were used to develop a submodel for EBS flow, which calculates the flux through the drip shield, *F*2, as a function of total dripping flux, *F*1.

Flow Through and Around the Waste Package—The conceptual model for advective liquid flow through the waste package assumes flow through breaches of restricted size (e.g., general corrosion patches) that penetrate the waste package wall. The function of the waste package for the seismic disruptive scenario class, including the potential for stress corrosion cracking, is discussed in Sections 2.3.4. All water that penetrates through breaches in the drip shield is conservatively assumed to contact the waste package (SNL 2007a, Section 5.1). Conservation of mass dictates that the flux diverted by the waste package, *F*5, is $F2 - F4$ (Figure 2.3.7-8).

Flow Into and Out of the Invert—From mass balance, the flux into the top surface of the invert is $F6 = F3 + F4 + F5$. The flux out of the invert is $F8 = F6 + F7$. Of the advective flux out of the invert, an amount equal to the imbibition flux, *F*7, flows into the unsaturated zone matrix. The remainder, *F*6, flows into the unsaturated zone fractures. The volume of the invert is equal to its

cross-sectional area (i.e., the area of a segment of a circle) times the axial length, for example, the length of a waste package (SNL 2007a, Section 6.5.2.3). The TSPA assumes that invert hydrologic properties consistent with design specifications for the invert are modeled as a single continuum porous medium.

2.3.7.12.3.2 EBS Transport

Radionuclides mobilized from the waste form can be transported out of the waste package, downward through the invert, and into the unsaturated zone, as shown in Figure 2.3.7-9. The occurrence of diffusion and/or advection depends on the types of penetrations in the drip shield and waste package, and on local seepage and drift wall condensation conditions. Advective release of radionuclides could occur through breaches in the waste package wall, which are caused by localized or general corrosion, in addition to breach or dislocation of the drip shield. Diffusion can occur through stress corrosion cracks, as well as through breaches caused by general corrosion patches (SNL 2007a, Section 6.3.4).

Thermal-hydrologic-chemical controls over the transport of dissolved and colloidal radionuclides have been included in radionuclide transport calculations. The effect of temperature variations on the EBS flow and transport model is explicitly included in the calculation of diffusion coefficients.

In-Package Diffusion—In commercial SNF waste packages, the waste form domain consists of fuel rods and some corrosion products. The reacted SNF constitutes a porous rind that is modeled as saturating quickly and completely in contact with dripping water. In the no-drip case, saturation is a function of the relative humidity in the waste package. The volume of the rind is modeled as a function of time. Its porosity is uncertain (SNL 2007a, Section 6.3.4.6.1). Radionuclides dissolve in the water that partially or fully saturates the pore volume of the rind (SNL 2007a, Section 6.3.4.6).

After the codisposal waste package is breached, the HLW eventually degrades to a clay-like material. Although the steel support framework inside the waste package corrodes, the general cylindrical shape of the canisters is retained (SNL 2007a, Section 6.5.2.1.2). Water saturation in all packages in the no-drip case is estimated by calculating water uptake onto waste package solids as a function of relative humidity (e.g., SNL 2007a, Section 6.3.4.3.1).

The effective diffusion coefficient for corrosion products in commercial SNF and codisposal waste packages is calculated as a function of water content and temperature (SNL 2007a, Section 6.5.2.1.1.2). When dripping water enters a breached waste package directly, full saturation of the corrosion products is assumed. For commercial SNF waste packages, the diffusive area of the corrosion products domain for diffusion to the invert domain is the total area of all waste package breaches, including corrosion patches and stress corrosion cracks. The diffusive path length—excluding the outer corrosion barrier—is approximately the combined thickness of the TAD canister and the inner vessel. The diffusive path length through the outer corrosion barrier is the thickness of the outer corrosion barrier. The diffusive area for the path through the outer corrosion barrier of the waste package is taken to be the minimum of the total area of all waste package breaches and the surface area of the commercial SNF waste package. The areas of the ends of the inner vessel are relatively small, and are not included in the calculation.

The diffusive area between the corrosion products domain and the invert domain in codisposal packages is the total area of all breaches in the Alloy 22 outer corrosion barrier of the waste package. The diffusive area and path lengths in the corrosion products domain in a codisposal waste package are treated identically to those in the commercial SNF corrosion products domain. The diffusive area for the path, excluding the outer corrosion barrier, is given by the outer surface area of the inner vessel. The diffusive area for the path through the outer corrosion barrier of the waste package is taken to be the minimum of total area of all waste package breaches and the surface area of the codisposal waste package. The length of the diffusive path, excluding the outer corrosion barrier, is the thickness of the inner vessel. The length of the diffusive path through the outer corrosion barrier is the thickness of the waste package outer corrosion barrier.

For commercial SNF waste packages, the diffusive area of the waste form domain is the total exposed surface area of all of the SNF fuel rods. The diffusive path length is the inside radius of the TAD canister. The diffusive area is the inside surface area of the TAD canister. Consistent with the treatment for the commercial SNF waste form domain, radionuclides will tend to diffuse radially outward from the HLW glass waste form domain. The diffusive path length is the inside radius of the inner vessel of a codisposal waste package. The diffusive area is the inside surface area of the inner vessel (the minor contributions of the ends are not accounted for). Similarly, radionuclides will tend to diffuse radially outward from the DOE SNF waste form domain. The maximum diffusive path length is the inside radius of the DOE SNF standard canister. The diffusive area is the surface area of the DOE SNF standard canister (again, the minor contributions of the ends are not accounted for).

Corrosion Product Formation—The mass of waste package corrosion products available for sorbing radionuclides has been estimated using the iron content of stainless steel and carbon steel, and the masses of these materials in two representative waste package types (the 21-PWR/44-BWR TAD and the 5-DHLW/DOE Long Codisposal waste packages) (SNL 2007a, Section 6.3.4.3.4.1). There is only stainless steel in a 21-PWR/44-BWR TAD waste package. The steel that degrades in the model to form the corrosion product domain of a 5-DHLW/DOE Long Codisposal waste package is 30% low carbon steel; the remainder is stainless (SNL 2007a, Tables 6.3-8 and 6.3-9). The model allows the amount of radionuclide-sorbing corrosion products to increase over time, but says little about transport pathways. The analysis was performed assuming that borated stainless steel absorber plates would be included in the waste packages for criticality control.

The mass of corrosion products in each domain is obtained as a function of time by linearly interpolating from the time of waste package breach over the lifetime of carbon steel and stainless steel components. The lifetimes are computed by dividing the maximum thickness for each type of steel by the sampled (single-side) corrosion rate of that steel (SNL 2007a, Section 6.5.2.2.1). The total mass of corrosion products in domain n is the mass of corrosion products from carbon steel and stainless steel summed over the four types of corrosion products. The total surface area of corrosion products is obtained by multiplying the total calculated mass of each corrosion product type by the sampled value for its specific surface area (the distribution was built from an analysis of literature values) (SNL 2007a, Section 6.5.2.2 and Appendix K). Figure 2.3.7-46 shows the cumulative distribution function descriptions of HFO and Goethite surface areas.

Water Content of Corrosion Products—The total water content of corrosion products is used to calculate the dissolved radionuclide mass retained in the waste package. Water content is estimated from the known mass, density, and porosity of corrosion products (SNL 2007a Sections 6.3.4.1.1 and 6.5.2.2.1). Uncertainty in the water saturation of the corrosion products is provided for in 1) the sampled specific surface area of the corrosion products components; 2) the relative proportions of goethite and HFO in the iron corrosion products; and 3) in the sampled Frenkel-Halsey-Hill adsorption isotherm parameters for generic corrosion products (SNL 2007a Section 6.5.2.1.1.2).

Several uncertain parameters are associated with this submodel. The corrosion rates of carbon and stainless steel are uncertain. The uncertainty is accounted for by considering distributions (SNL 2007a, Section 6.3.4.3.4.3). The carbon steel and stainless steel corrosion rate ranges used in the EBS flow and transport model are, respectively, 25 to 135 microns/yr and 0.01 to 0.51 microns/yr and were fit by Bayesian updating (SNL 2007a, Appendix F). The in-package chemistry analysis considered a wider set of corrosion rates, and ultimately used a stainless steel rate range that was more than an order of magnitude wider than each end of the EBS range. The more detailed analysis of stainless steel corrosion rates in the Radionuclide Transport Abstraction is warranted because steel corrosion rates are directly related to the rate at which radionuclide-sorbing corrosion products are formed. Outputs of the in-package chemistry model – pH and ionic strength – are insensitive to steel degradation rates (Section 2.3.7.5.2).

The corrosion products may be finely powdered with a high specific surface area, or they can agglomerate into an impermeable mass with low specific surface area. The morphology of corrosion products resulting from extensive corrosion of stainless steel is not well characterized, simply because stainless steel corrodes so slowly that no samples have corroded extensively under low-temperature atmospheric conditions since stainless steel was invented, less than a century ago. Lamination and flaking of corrosion products is expected to occur due to seismic activity and rockfall that will jar the waste packages and knock loose any corrosion products that would normally adhere to internal component surfaces. At the same time, the surface area is likely to vary depending on the corrosion history. The corrosion product surface areas are represented as truncated lognormal distributions, and were developed from an analysis of published measurements (SNL 2007a, Section 6.3.4). The goethite surface area range is 14.7 to 110 m^2/gm; the mean is 51.42 m^2/gm. The ferrihydrite surface area range is 68 to 600 m^2/gm; the mean is 275.6 m^2/gm.

Colloidal Transport—Five types of colloids are anticipated to exist in the EBS (Section 2.3.7.11). Their stability and mass will depend on the ionic strength and pH of the groundwater or of the waste package and invert (SNL 2007i, Section 1), as discussed in Section 2.3.7.11. Reversible, competitive sorption onto montmorillonite and uranophane colloids is modeled using K_ds from the literature (SNL 2007a, Section 6.3.4.4). Radionuclide uptake by iron oxide corrosion products is predicted using the surface complexation approach described above. Colloidal transport of radionuclides occurs by advection and diffusion. Advection moves colloids (and the associated radionuclides) at approximately the same velocity as the liquid flux through the EBS. Longitudinal dispersion, which could potentially enable colloids to travel faster than the bulk average liquid velocity, does not need to be included because of the short travel distance through the EBS. Colloid diffusion rates are calculated from hydrodynamic theory on the basis of temperature and particle radius (Stokes-Einstein relationship) (SNL 2007a, Section 6.3.4.4).

Radionuclides in Cell 2 may sorb onto fixed corrosion products from the degradation of waste package internal components, as well as onto mobile colloids. Competitive sorption onto corrosion product colloids is modeled in the same manner as for sorption onto stationary corrosion products, where the forward rate constant for irreversible sorption onto corrosion product colloids is identical to the forward rate constant onto stationary corrosion products. The backward rate constant for stationary corrosion products is calculated by dividing the forward rate constant by the K_d derived from the competitive sorption (surface complexation) model (SNL 2007a, Section 6.5.2.4.6).

Invert Water Chemistry—The TSPA estimates invert chemistry in order to calculate solubility and colloid suspension stability within the invert. Invert chemistry is represented by the seepage evaporation abstraction (Section 2.3.5.5.2). For the igneous intrusion modeling case, the water chemistry is modeled as being that of waters in contact with basalt (Section 2.3.11.3.3.9).

Linear sorption of dissolved radionuclides onto the crushed tuff material in the invert is included in the EBS transport model. Radionuclide sorption onto iron corrosion products in the invert is not included in the EBS transport model. Corrosion products have high affinities for sorption of certain radionuclides; however, in the invert, the corrosion products will be localized and widely spaced. Therefore, for radionuclide sorption in the invert, K_d values for crushed tuff are more representative than those for corrosion products.

Invert-Unsaturated Zone Boundary Condition—Radionuclide transport transitions from the EBS to the unsaturated zone at the drift wall interface below the invert. The radionuclide mass flux may enter fractures or the matrix of the host rock at this interface. Transport at the interface may be predominantly advective or diffusive, depending on the flow of water through the EBS.

In the TSPA, a far-field zero-concentration boundary condition is used to represent diffusive behavior at the interface between the EBS transport model and the unsaturated zone far field (SNL 2007a, Section 6.5.2.6). The far-field boundary condition is implemented by specifying an effective zero-concentration boundary at approximately three drift diameters below the invert-unsaturated zone boundary in the unsaturated zone (SNL 2007a, Section 6.5.2.6). This boundary condition does not impact the length of the transport pathway in the unsaturated zone transport model; rather, it provides a more realistic calculation of the radionuclide concentration gradient and, therefore, of the diffusive radionuclide flux across the drift wall into the fractures and matrix of the unsaturated zone.

In the EBS-unsaturated zone interface model, the near-field unsaturated zone domain is modeled as a dual continuum of overlapping unsaturated zone-matrix and unsaturated zone-fracture media. This approach is consistent with the dual-permeability modeling approach used by the unsaturated zone transport model (Section 2.3.8). Matrix and fracture continua in the host rock are represented by a two-dimensional vertical array of cells that are oriented parallel to a cross section of a drift and located immediately beneath a drift (Figure 2.3.7-47). As shown in the figure, the invert is in direct communication with the cells representing the rock immediately below the drift (the middle column of zones). The advective flux is only applied vertically downward (SNL 2007a, Sections 6.3.4 and 6.5.2.6). Diffusive transport of radionuclides occurs between the middle zone and the left and right zones in the figure. A "collector cell" at the bottom of the array simulates a zero-concentration boundary (SNL 2007a, Section 6.5.2.6).

The mass fluxes of water and radionuclides from the invert are admitted into the top layer of the middle zone in the unsaturated zone. Interaction of water with engineered materials should change fluid compositions little, since the majority of engineered materials are low solubility iron and steels. Radionuclide sorption onto iron (and copper) corrosion products outside of the waste package will tend to lower the levels of radionuclides that move from the invert to the unsaturated zone. The invert advective liquid flux (*F*8), except for the portion contributed by the imbibition flux (*F*7), flows entirely into the top middle unsaturated zone fracture cell. All the water that is imbibed from the rock matrix by the invert (*F7*) is assumed to flow subsequently into the unsaturated zone matrix, along with any condensation and seepage flux. The diffusive flux from the invert goes into both unsaturated zone continua, and is partitioned based on the concentration gradients and effective diffusion coefficients. The advective flux flowing through the unsaturated zone fracture cells in the middle zone is given by the greater of the advective flux out of the invert and the steady state unsaturated zone fracture flux (SNL 2007a, Section 6.5.2.6). The advective flux in the two outer zones is given by the steady-state unsaturated zone flux in each continuum at the repository horizon (SNL 2007a, Section 6.5.2.6).

For diffusive mass transport, the effective diffusion coefficient for the matrix continuum is calculated using a method developed in *Radionuclide Transport Models under Ambient Conditions* (SNL 2007j), wherein the tortuosity of the rock type is determined based on experimental work (Reimus et al. 2007, Equation 2) while the free water diffusion coefficient is species dependent. Multiplying the tortuosity with the free water diffusion coefficient gives the effective diffusion coefficient.

The mass fluxes from the invert to the unsaturated zone fractures and matrix are passed to the unsaturated zone transport model for TSPA calculations (Section 2.3.8). This partitioning is time-dependent and captures the temporal processes active in the EBS, such as variations in the rates of radionuclide release from the EBS, and changes in seepage or condensation flux in the drift. The partitioning is computed by solving mass transport equations for the EBS and part of the unsaturated zone as a coupled system, using a modeling approach consistent with other models of the host rock (Sections 2.3.5 and 2.3.8).

2.3.7.12.3.3 Model Uncertainties

Transport is affected by the parameters that define the physicochemical environment, including the porosity and pore volume, water saturation, interfacial diffusive areas, diffusive path lengths, and diffusion coefficients. Uncertainty in the EBS flow and transport model is represented by a range of values and distributions assigned to these parameters. The TSPA implements the correlated K_d values from the unsaturated zone model (Section 2.3.8) to predict sorption in the invert.

Invert Diffusion Coefficient—The invert diffusion coefficient was derived from measured values of diffusion coefficients in various granular materials, including tuff. The data are scattered, particularly at lower values of volumetric water content. The use of electrical conductivity measurements as an analogue for diffusivity becomes more uncertain at low water content, due to uncertainty in the electrical connectivity between electrodes and the porous material. The reported uncertainty approximates a normal distribution for the residuals in the statistical fit to the experimental data. Uncertainty in the porosity of the invert is subsumed by the

greater uncertainty associated with the measurements of the diffusion coefficient; thus, the porosity uncertainty is accounted for in the diffusion coefficient (SNL 2007a, Section 6.3.4).

In-Package Diffusion Model—The corrosion rates for carbon steel and stainless steel are represented with uncertainty using one-year exposure data. Empirical cumulative distribution functions are sampled in the TSPA. In view of the range in the measured data, even among multiple samples under identical conditions, uncertainty exists in corrosion rates.

The specific surface areas of corrosion product components account for the uncertainty in the estimated surface area of corrosion products that is available for water adsorption inside a breached waste package. The calculated masses of corrosion products are multiplied by the specific surface areas to compute the bulk surface areas. Saturation is calculated from relative humidity in no-drip environments, and is set at 100% in drip environments. Again, the likelihood of advective flow occurring depends on the nature of the breach. The uncertainties are associated with the morphology of corrosion products and their surface area, including effects from seismic events, collapse of waste package internal structures, and changes in seepage rates. The nature of corrosion products formed under the conditions in a breached waste package in a humid environment from a mixture of various types of steel is uncertain. Truncated lognormal (goethite and ferrihydrite), uniform (NiO) and log-uniform (Cr_2O_3) distributions are appropriate for these parameters (SNL 2007a, Section 6.5.2.2).

Invert-Unsaturated Zone Boundary Condition Implementation in the TSPA—The EBS-unsaturated zone boundary condition implementation is applied when the EBS transport abstraction is discretized and implemented in GoldSim (Section 2.4). This model provides the radionuclide concentration boundary condition at the invert-unsaturated zone boundary such that the far-field concentration is approximately zero. To compute this boundary condition, a portion of the unsaturated zone is modeled, so input parameters for the unsaturated zone are used and, therefore, become EBS transport input parameters. The uncertainty in sampled parameters is discussed in Section 2.3.8.5.2.

2.3.7.12.3.4 Model Validation

A number of lines of independent evidence either provide corroborative support to important features of the EBS flow and transport model, or provide evidence that the model is conservative.

Invert Diffusion Properties—The invert diffusion coefficient submodel has two components: (1) radionuclide-specific diffusion coefficients; and (2) adjustments to account for the effects of water content of a porous medium and of temperature. The effect of invert water content on radionuclide diffusion is estimated from the effect of water content on electrical conductivity, using electrical conduction as an analogue for molecular diffusion. While the analogue is known to be valid in fully saturated media, its application to unsaturated media, particularly at very low moisture contents, is supported by few data. To address this uncertainty, diffusive tracer concentrations in tuff cubes were measured directly, using laser ablation combined with inductively coupled plasma-mass spectrometry (SNL 2007a, Section 7.2.2), to corroborate the electrical analogues. The data from the direct measurements of diffusive transport show that the diffusion coefficient within a single grain of crushed tuff is as small as five orders of magnitude less than predicted by the invert diffusion properties submodel. This difference suggests that the

invert diffusion properties submodel overestimates releases of radionuclides from the EBS (SNL 2007a, Section 7.2.2).

In-Package Diffusion—Two modeling studies (EPRI 2000; Lee et al. 1996) provide corroborative support of the in-package diffusion submodel. The Electric Power Research Institute (EPRI 2000) source-term model, COMPASS2000, implements five compartments: waste, corrosion product, canister, invert, and near-field rock, of which two (corrosion product and canister) are analogous to portions of the in-package diffusion submodel. Mass balances in each compartment account for diffusion and advection, radioactive decay and in-growth, sorption, dissolution, and precipitation (SNL 2007a, Section 7.2.1.1).

In the EPRI model, EBS transport parameters are assigned fixed values. Both the corrosion product and corroded canister compartments have a porosity of 0.42 (EPRI 2000, p. 6-21), which is in close agreement with the porosity of corrosion products (0.4) used in the in-package diffusion submodel. The EPRI value accounts for the volume occupied by the oxide. A lower value for porosity overestimates releases of radionuclides (SNL 2007a, Section 7.2.1.1).

The EPRI model assumes a fixed water saturation of 0.35 in both the corrosion products and corroded canister compartments (EPRI 2000, pp. 6 to 21). This value is appropriate for scenarios involving advective transport, but overestimates releases of radionuclides for the expected large fraction of the repository where no dripping flux is expected, and where the only water present is adsorbed water. The in-package diffusion submodel specifically applies to those regions, and provides a more complex estimate of saturation as a function of relative humidity (SNL 2007a, Section 7.2.1.1), and a connected water film threshold at RH greater than 95% (Section 2.3.7.5.1).

The EPRI model uses a fixed value for the effective diffusion coefficient of approximately 4.6×10^{-4} m^2/yr in both the corrosion products and corroded canister compartments (EPRI 2000, pp. 6 to 22), which converts to approximately 1.5×10^{-11} m^2/s. For diffusion through a fully degraded waste package, this value corresponds to a relative humidity of 97.9%. When the humidity is 100%, the EPRI diffusion model and the in-package diffusion submodel agree well (SNL 2007a, Section 7.2.1.1).

The EPRI model also specifies fixed diffusive lengths, which are defined as the distance from the center of the compartment to the interface of the two contacting compartments. For the corrosion product compartment, the diffusion length is 0.046 m; for the canister compartment, the diffusion length is 0.025 m (EPRI 2000, pp. 6 to 22). In a degraded waste package, these are reasonable values comparable to those used in the in-package diffusion submodel. For the conditions assumed in the EPRI model, when the waste package is extensively corroded, the in-package diffusion submodel agrees with the EPRI model. Differences occur primarily where the in-package diffusion submodel provides increased realism (e.g., saturation that depends on relative humidity and corrosion product accumulation, radionuclide-specific diffusion coefficients) in the diffusive release calculation (SNL 2007a, Section 7.2.1.1).

Lee et al. (1996) developed a model for steady-state and quasi-transient diffusive releases from breached waste packages into the invert. The waste package is approximated by an equivalent spherical configuration, and the underlying invert is represented by a spherical shell surrounding the waste package. The model of Lee et al. (1996) is appropriately applied to the late stages of waste

package degradation, when the waste form has become a mass of porous corrosion products (SNL 2007a, Section 7.2.1.2).

The assumption of Lee et al. (1996) that the waste (the radionuclide source) is uniformly distributed inside the waste package restricts the applicability of the model and comparison to the in-package diffusion submodel to later time frames, when the waste package has corroded extensively. The objective of the in-package diffusion submodel is to provide more realism at earlier and intermediate times, when the waste cannot yet be considered a uniform porous medium. Lee et al. (1996, p. 5-67) compute a diffusion coefficient for the porous corrosion products filling the perforations (SNL 2007a, Section 7.2.1.2) of 4.4×10^{-7} cm^2/s, which is comparable to the value used for the in-package diffusion submodel (SNL 2007a, Section 7.2.1.2).

Sorption onto Corrosion Products—Validation of the competitive surface complexation model involves comparison with recent tabulations of K_ds measured in the laboratory (EPA 1999b; EPA 2004). The EPA (EPA 1999b and EPA 2004) compiled K_ds for actinides (and other inorganic contaminants) measured on a large number of soils, rocks, and single mineral phases, and considers the general controls over sorption. This dataset and critical analysis set some limits on the ranges of K_ds that might be expected and their functional dependencies on, for example, pH and P_{CO_2}. The comparison assumes that soil K_ds at pH 7 to 9 should be broadly similar to but lower than iron oxide K_ds, because of the relatively high surface areas of the latter (SNL 2007a, Section 7.2.3).

There are some obstacles to the comparison of the competitive surface complexation model and EPA compilation K_ds. The competitive surface complexation model predicts actinide K_ds only for iron (hydr)oxides, albeit for a wide range of available site densities. The EPA compilation typically provides K_ds for multimineralic soils that contain both clays and primary minerals (e.g., quartz, feldspars), as well as iron oxides and coatings and, possibly, organic matter. While the competitive surface complexation model considers competition with other surface species explicitly, the EPA compilation incorporates competition only implicitly and probably with less competition by surface-bound actinides. Competitive surface complexation model K_ds were calculated for P_{CO_2} values, ranging from 10^{-4} to 10^{-2} atmosphere. Most soil K_ds are measured under ambient levels, $P_{CO_2} \sim 10^{-3.5}$ atmosphere, which would tend to result in lower adsorption of those actinides that form carbonate complexes. Finally, although the EPA compilation considers sorption to pH values as low as 3, the comparison here will focus on the more repository relevant pH values of 6 to 9.

The EPA compilation uranium K_ds decrease from 10^2 to 10^6 mL/g^{-1} at pH 6 to < 0.4 to 7,900 mL/g^{-1} at pH 9. The low end is for single mineral quartz substrates; the high end is for ferrihydrite (and kaolinite), which is probably more analogous to the competitive surface complexation model conditions. The competitive surface complexation model K_ds ranges from $10^{0.5}$ to $10^{5.5}$ at pH 7 to 10^2 to 10^6 at pH 8. From pH 7 to 9, the range of competitive surface complexation model predicted uranium K_ds tend to overlap the range of EPA soil uranium K_ds. Below pH 7, the competitive surface complexation model predicts lower uranium K_ds.

There are very large uncertainties in plutonium sorption measurements (EPA 1999b). Redox is often unmeasured and/or poorly controlled. Depending on the plutonium valence state, solubilities may be exceeded in sorption experiments. Moreover, a number of minerals are able to shift the valence state of plutonium during the sorption process. Although soil iron oxides are known to sorb

plutonium, the relationship between iron content and plutonium uptake is unclear (EPA 1999b). The EPA review of literature plutonium K_ds points to values between 10 and 10^5 mL/g. This range is compared with competitive surface complexation model K_ds of about 10^0 to $10^{5.5}$ mL/g in Figure 2.3.7-48.

The EPA (2004) quotes Thibault et al. (1990), who report a range of 0.4 to 2,575 mL/g from a compilation of soil (sand, silt, clay only). Jerden and Kropf (2007) measured K_ds for neptunium sorption on goethite at pH 6 to 9 of 10^3 to 10^5 m/Lg. The competitive surface complexation model predicted neptunium K_ds of $10^{-0.5}$ to 10^6 mL/g. The EPA (2004) quotes Thibault et al. (1990), who report a range of 8.2 to 400,000 mL/g from a compilation of soil (sand, silt, and clay only) americium K_ds values and notes a clear correlation between soil K_ds and soil iron/americium oxide content. Lu et al. (2000) reported americium K_ds for colloidal hematite as high as 10^7 mL/g. The competitive surface complexation model predicted K_ds from 10^{-1} to $10^{7.5}$ mL/g. In general, competitive surface complexation model predictions of actinide uptake are broadly consistent with compilations of soil K_ds for the actinides considered. Soil K_ds for a given pH tend to vary by 2 to 4 orders of magnitude, while competitive surface complexation model predicted K_ds vary by 3 to 4 orders of magnitude for a given pH. The larger uncertainty for the competitive surface complexation model results is expected, because it reflects the combination of effects due to uncertainty in such various input parameters as dissolved concentrations, sorption sites, and P_{CO_2}.

2.3.7.12.3.5 Alternative Conceptual Models

The bathtub model is an alternative conceptual EBS flow model (SNL 2007a, Section 6.6.1), in which seepage collects within the waste package before being released to the EBS. It is only applicable to late times when breach is due to general corrosion. This alternative flow path was screened out because the natural system transport pathways and the variability of waste package corrosion rates would dampen any pulse in release rates caused by filling, and emptying, of a breached waste package (SNL 2007a, Section 6.6.1.2.3).

Limited Water Vapor Diffusion into the Waste Package—As long as the inside of the waste package is at least slightly warmer than the outside, condensation is not inevitable. Another alternative conceptual model accounts for the resistance to diffusion of water vapor into a waste package through stress corrosion cracks (SNL 2007a, Section 6.6.2). In the base model, there is no limit to the amount of water vapor available to adsorb onto surfaces within a waste package, which is assumed to create a continuous pathway for diffusive transport of radionuclides out of the waste package if the RH is greater than 95%. This applies to the in-package diffusion submodel. However, the base model currently used in the TSPA overestimates releases of radionuclides, particularly when the only breaches in a waste package are small stress corrosion cracks. If the diffusion rate is limited, the rate of steel corrosion is limited by the rate of diffusion of water vapor. The result is that less water is available to adsorb and form a continuous thin liquid film on corrosion products, and no water would be available for radionuclide transport, because all water is consumed by the corrosion process as quickly as it diffuses into the waste package. This could prevent formation of a diffusive path until all of the internal steel components are substantially corroded, which could delay diffusive release of radionuclides until that time. During this delay, radioactive decay would decrease the quantities of radionuclides in the waste package, ultimately reducing releases to the environment (SNL 2007a, Section 6.4.2).

This alternative conceptual model is not used for the TSPA because of the associated uncertainties, which make it unclear whether the model sufficiently bounds the expected behavior. For example, adsorption is typically a fast process, so the assumption that no water is physically adsorbed until all steel is corroded may not be valid. Some water may be adsorbed, even if there is a delay caused by the water consumption from corrosion. In addition, the corrosion rates used are for aqueous conditions. However, if there is significant water consumption from corrosion, rates for a low-humidity gaseous environment are more appropriate. Yet these rates would increase the time required for complete corrosion of the steel, which leads to greater uncertainty about the suitability of the assumption (SNL 2007a, Section 6.6.2).

Limited Oxygen Diffusion into the Waste Package—In this alternative conceptual model, a film of adsorbed water does not form on the surface of corrosion products if the rate of water consumption by corrosion reactions is greater than the rate of diffusion of water vapor into the waste package. Until a film of water forms on internal corrosion products surfaces, diffusive releases of radionuclides through the adsorbed water cannot occur (according to the in-package diffusion submodel). Depending on how oxygen competes with water vapor in diffusing through stress corrosion cracks and reacting with steel, the time required for all internal components to react and stop consuming water could be altered. Then, diffusive releases through the film of adsorbed water, as calculated by the in-package diffusion submodel, could begin at a different time than predicted by the water vapor-limited diffusion model alone (SNL 2007a, Section 6.6.2).

Although this alternative conceptual model represents a more complete mass balance of available reactants, it is not used in the TSPA because it significantly increases uncertainties. It has the same weaknesses described for the previous alternative conceptual model, which limits the water vapor diffusion rate.

Dual-Continuum Invert—In this alternative conceptual model (SNL 2007a, Sections 6.4.3 and 6.6.3), the invert is conceptualized as overlapping dual continua and modeled using a dual-permeability approach. The invert design (SNL 2007a, Section 6.6.3) uses crushed tuff as the invert ballast material. This material is comprised of two pore spaces: (1) intragranular pore space (tuff particle matrix); and (2) intergranular pore space. In the dual-permeability approach, flow and transport occur in both pore spaces, and mass transfer takes place between the two pore spaces. Although radionuclide transport by advection and diffusion can occur in both pore spaces, flow and transport processes in each of these two pore spaces are generally different. Advective transport depends on the liquid flux through each of these pore spaces. Diffusive transport through each of these pore spaces depends on the diffusive properties associated with each pathway. For this alternative conceptual model, the invert is modeled as a dual continuum in which one continuum is represented by the intergranular pore space, and the other continuum is represented by the intragranular pore space.

Whereas the base model, as shown in Figure 2.3.7-8, is a single-continuum invert model and has a single advective flow path (pathway for flux *F*8) from the invert to the unsaturated zone, the dual-continuum invert model has two potential advective flow pathways:

- **Flux from the Intragranular Invert Continuum to the Unsaturated Zone**—Advective flux from the invert intragranular continuum flows directly into the unsaturated zone matrix.

- **Flux from the Intergranular Invert Continuum to the Unsaturated Zone**—All advective flux from the invert intergranular continuum flows directly into the unsaturated zone fractures.

In the alternative model described here, no advective flux occurs between the two invert continua. Thus, the flux through the invert intragranular continuum (tuff particle matrix) is identical to the imbibition flux, *F*7. Ignoring three-dimensional effects (e.g., flow along the axis of the drift), the quasi-steady-state flux through the intergranular invert continuum is equal to the seepage flux, *F*1.

Diffusive transport in the alternative conceptual model can occur from the corrosion product domain into each of the two invert continua, between the two invert continua, and from each invert continuum to each unsaturated zone continuum (matrix and fractures). The invert-unsaturated zone boundary condition is implemented in the TSPA with modifications that account for the four connections, with diffusive fluxes from each invert continuum to both unsaturated zone fractures and matrix (SNL 2007a, Section 6.6.3.3).

This alternative conceptual model is not used for the TSPA, due to insufficient data to validate diffusion coefficients in each continuum, and because the single-continuum approach adequately represents the invert behavior based on the available information. Furthermore, there are insufficient data to confirm whether the dual-continuum model is a bounding approach with respect to chemical behavior information.

Alternative Single-Continuum Invert Diffusion Coefficient Model—As an alternative to the Archie's Law approach for determination of the diffusion coefficient for the single-continuum invert, diffusion through the crushed tuff invert ballast was modeled using an approach that has been applied to diffusion in soils (SNL 2007a, Section 6.6.4.1). Studies generally show that the bulk diffusion coefficients of soils at a high water content decline with the moisture content (Nye 1979; Olesen et al. 1999). The studies also show that, below a critical moisture content, the diffusion coefficient for granular materials becomes negligible (So and Nye 1989).

This alternative conceptual model considers an alternative to Archie's Law for determining the diffusion coefficient in the crushed tuff invert. Despite the potential for increased accuracy at low water content, compared to the base case single-continuum model using Archie's Law, insufficient data exist to validate diffusion behavior at very low water contents. In addition, the alternative conceptual model does not provide an upper bound on the diffusion coefficient, as does the Archie's Law approach. Therefore, invert diffusion coefficients are computed in the TSPA using Archie's Law (SNL 2007a, Section 6.6.4.3).

Alternative Dual-Continuum Invert Diffusion Coefficient Model—In general, the literature supports a dual continuum picture of the diffusive conductance by the invert granular material (SNL 2007a, Section 6.6.4.2). For example, Roberts and Lin (1997) observed multiple conduction pathways in their measurements of the electrical conductance of unsaturated tuff samples. Their measurements indicated conduction by adsorbed water on the solid surfaces of the tuff samples and conduction by water within the tuff rock. These measurements support a dual continuum picture of the tuff samples in which the water on the surface of the samples corresponds to the intergranular continuum, and the water within the samples corresponds to the intragranular continuum.

An alternate approach models the invert as a dual continuum comprised of two pore spaces: intragranular pore space (tuff particle matrix), and intergranular pore space. Despite the potential for increased accuracy compared to the base case single-continuum model using Archie's Law, insufficient data exist to validate diffusion behavior at very low water contents. In addition, this alternative conceptual model does not provide an upper bound on the diffusion coefficient, as does the Archie's Law approach.

2.3.7.13 Conclusions

2.3.7.13.1 Summary of Significant Processes for EBS Capability

The waste form degradation and mobilization models and the EBS flow and transport model described in this section include features and processes that contribute to the barrier capability of the EBS, which is described in Section 2.1.2.2. Some features and processes make significant contributions to the overall barrier capability of the EBS. Features that are significant include the drip shields, waste packages, waste forms and waste package internals, and ballast in the emplacement drift inverts. The processes and characteristics that are considered to be potentially important to the barrier capability include the following.

- **Advection of Liquids and Solids through Cracks in the Drip Shield**—Any cracks that extend through the drip shield are expected to be of insufficient size and morphology to allow the advective flow of water to impact repository performance (see Table 2.2-5).

- **Advection of Liquids and Solids through Cracks in the Waste Package**—Any cracks in the waste package are expected to be of insufficient size and morphology to allow for any advection of water into the waste package sufficient to adversely affect repository performance (see Table 2.2-5).

- **Chemical Characteristics of Water in Waste Package**—The alteration rate of different waste forms, the solubility of radionuclides, and the stability of colloid suspensions are dependent on the chemistry of the water inside a degraded waste package that may come into contact with the waste forms. Uncertainties in the in-package chemistry—in particular, the ionic strength and pH that have the most significant effect on these coupled processes—have been considered in the abstraction models used in the TSPA that are presented in Section 2.3.7.5.

- **Radionuclide Solubility, Solubility Limits, and Speciation in the Waste Form and EBS**—The solubility of radionuclides has a significant effect on the rate of release of radionuclides from the waste form to the edge of the waste package. Solubility models are presented in Section 2.3.7.10. The more soluble the radionuclide, generally the greater mass flux of that radionuclide that will be released by diffusive or advective release mechanisms from the waste form.

- **Sorption of Dissolved Radionuclides in the EBS**—Sorption occurs on various immobile phases in the waste package. Reversible and irreversible sorption occurs on mobile (e.g., colloidal) phases in the waste package. The models used to evaluate this process are presented in Section 2.3.7.12. Reversible sorption on the corrosion products inside the waste package can significantly reduce the release rate of dissolved radionuclides.

- **Diffusion of Dissolved Radionuclides in the EBS**—The principal release mechanism of radionuclides from the waste package is through diffusion. This diffusion is controlled by the degree of degradation of the waste package and the hydrologic characteristics within the waste package, which, in turn, are a function of the type of waste (Section 2.3.7.12).

- **Advection of Dissolved Radionuclides in the EBS**—Once radionuclides are released from the waste package, the dominant transport process through the invert is advection into the fractures and matrix of the unsaturated zone. Models used for these transport processes are presented in Section 2.3.7.12. In areas of seepage, the release is dominated by advective transport from the invert into the fractures of the rock mass at the base of the invert.

- **Physical Form of the Waste Package and Drip Shield and Effects of Drip Shield on Flow**—The integrity of the waste package and drip shield over time will limit the access of water to waste packages and ultimately limit aqueous transport from failed waste packages (Section 2.3.4.1).

- **Unsaturated Flow in EBS**—Unsaturated flow occurs through the invert as a result of seepage or drift-wall condensation, imbibition from the host rock, or capillary condensation, and affects the release of radionuclides from the EBS (Section 2.3.7.12).

- **Chemical Characteristics of Water in Drifts**—The chemical makeup of water in the drift affects the corrosivity of EBS components and the transport characteristics of radionuclides (Section 2.3.5.1).

- **Chemical Interaction with Corrosion Products**—Sorption of dissolved radionuclides onto corrosion products contributes to the barrier capability by limiting transport (Section 2.3.7.12).

- **DOE SNF Degradation (Alteration, Dissolution, and Radionuclide Release)**—The degradation of DOE SNF affects the barrier capability of the waste form and the waste form internals by making available radionuclides bound in the DSNF matrix (Section 2.3.7.8).

- **Commercial SNF Degradation (Alteration, Dissolution, and Radionuclide Release)**—The degradation of commercial SNF limits the availability of radionuclides present in the fuel matrix and in the gap and grain boundaries for subsequent transport from the package and is discussed in Section 2.3.7.7.

- **HLW Glass Degradation (Alteration, Dissolution, and Radionuclide Release)**—Kinetically-controlled degradation of HLW glass sets the rate at which radionuclides in the glass matrix are made available for interaction with fluids in the waste package and is discussed in Section 2.3.7.9.

- **Reaction Kinetics in Waste Package**—The rates at which individual components of the waste form degrade set limits on in-package chemistry, the dissolved concentrations of some radionuclides, the abundance of sorbing phases, and the overall availability of radionuclides leaching from fuels and glasses (Sections 2.3.7.5, 2.3.7.7 to 2.3.7.10, and 2.3.7.12).

- **Chemical Effects on Void Space in Waste Package**—The chemical and physical makeup of the void space inside breached waste packages is an important control over radionuclide stability and transport (Section 2.3.7.5).

2.3.7.13.2 Summary of Key Uncertainties Associated with EBS Capability

As discussed throughout Section 2.3.7, there are uncertainties associated with the barrier capability of the EBS. These uncertainties arise from uncertainties in the various models used to analyze the processes and in the test data. These uncertainties are incorporated probabilistically in the TSPA by using ranges of parameter values for the initial radionuclide inventories, for representing the chemical characteristics of fluids that can contact the waste form, for the rates of the various degradation and transport processes, and for the dissolved concentration limits. The ranges of parameters and process rates used in the performance model are based on the results of testing and analysis, as well as on the fundamental physical principles that apply. The key uncertain parameters that are provided to the TSPA include the following:

- Uncertainty multipliers for the initial mass of each radionuclide per waste package (Table 2.3.7-6)

- In-package pH and ionic strength (Section 2.3.7.5)

- Porosity in the commercial SNF rind (Section 2.3.7.12.3.2)

- Instantaneous release fractions for gap and grain boundary inventory (Table 2.3.7-12)

- Fuel specific surface area (A) (Table 2.3.7-13)

- HLW glass degradation rate coefficients (k_E) (Section 2.3.7.9.3.1 and Table 2.3.7-21)

- HLW glass surface area exposure coefficient (Section 2.3.7.9.3.1 and Table 2.3.7-21)

- Uncertainty associated with the equilibrium constants in the dissolved concentration model (Section 2.3.7.10)
- Uncertainty associated with the effect of the dissolved F concentration on radioelement solubility (Section 2.3.7.10)
- Sorption coefficients for reversible radionuclide (plutonium, americium, thorium, protactinium, cesium) sorption onto colloids (Section 2.3.7.11.2.4)
- Irreversible sorption rate constants (plutonium, americium) for immobile and colloidal corrosion products (Section 2.3.7.12.1)
- Drip shield flux splitting uncertainty factor (Section 2.3.7.12.1); this parameter is an input to a mass balance equation (SNL 2007a, Equation 6.3.2.4-2)
- Waste package flux splitting uncertainty factor (Section 2.3.7.12.1); this parameter is an input to a mass balance equation (SNL 2007a, Equation 6.3.3.2.5-1)
- The stainless steel corrosion rate for waste package internals (Section 2.3.7.12.3.2)
- The specific surface area of iron oxide corrosion products (Section 2.3.7.12.3.2)
- Invert diffusion coefficient for radionuclide diffusion (Section 2.3.7.12.3.3).

2.3.7.13.3 Summary of Key Conservatisms in Models Used to Assess EBS Capability

In addition to the parameter uncertainties above, a variety of uncertainties in the data from the tests measuring degradation and transport processes, as well as uncertainties in the conceptual and numerical models used to analyze the processes, are addressed by making bounding estimates and conservative assumptions in the waste form degradation and mobilization models and in the EBS flow and transport models described in this section. These assumptions generally lead to faster waste form degradation, higher radionuclide concentrations, and faster release times from the EBS. These assumptions include the following.

Secondary Phases of Uranium—Neither neptunium nor other radionuclides are incorporated into secondary phases of uranium (SNL 2007h, Section 6.6.1). Neptunium would likely be incorporated into secondary phases; however, experimental data are lacking to confirm this phenomenon with sufficient reliability (SNL 2007h, Section IV.3.3). This conservatism results in the overestimation of aqueous neptunium concentrations. Section 2.3.7.10 provides more information on the secondary phases of uranium.

Solubility versus Temperature—The solubility of actinides at 25°C is used for all temperatures. Because actinide solubilities decrease with increasing temperature, however, this conservatism simplifies the model approach (SNL 2007h, Section 6.3.3.3). This conservatism may result in the overestimation of aqueous radioactive element concentrations at times when the temperatures exceed 25°C. Section 2.3.7.10 provides more information on solubility and temperature.

Commercial SNF Failed Cladding—Although Commercial SNF cladding is expected to limit the amount of water or moist air that can contact the fuel pellets, thus limiting the interaction of fuel pellets and the environment, it is conservatively not included in the TSPA analyses (SNL 2007k, Section 6.1.4). In reality, cladding may provide some protection.

Stainless Steel-Cladding Fuel—The stainless steel-cladding fuel rods are modeled as 100% failed upon emplacement in waste packages. The stainless steel-cladding inventory is approximately 1.0% of the commercial SNF inventory (SNL 2007k, Section 6.2.2).

DOE Spent Nuclear Fuel Cladding—No credit is taken for DOE SNF cladding. This simplified modeling approach is used because there is no technical basis for giving credit for DOE SNF cladding, and the recommended DOE SNF release model is an upper limit model invoking the complete exposure of DOE SNF upon exposure of DOE SNF cladding to groundwater (BSC 2004c, Section 8.1). Furthermore, a significant fraction of the uranium metal SNF (DOE SNF Group 7), the representative DOE SNF used in the TSPA model, is visibly damaged and much of the rest could have small pinholes/cracks in the cladding (BSC 2004c, Section 6.1.7).

Degradation of DOE Spent Nuclear Fuel—A constant degradation rate is used that conservatively bounds degradation of metallic uranium present in N Reactor fuel; upon waste package breach, degradation of DOE SNF occurs in one timestep of the TSPA. Little quality-level data exists on DOE SNF fuel, so a conservative approach is used to bound uncertainty in the characteristics of the DOE SNF fuel (BSC 2004c, Section 8.1). Section 2.3.7.8 provides more information on the degradation of DOE SNF.

DOE Spent Nuclear Fuel and High-Level Waste Inventories—The number of packages and inventory are overestimated for DOE SNF and HLW (SNL 2007d, Section 5.2), particularly when the upper end of the uncertainty limits of the per-package inventory is sampled. Section 2.3.7.4 provides more information on HLW and DOE SNF inventories.

Degradation of Commercial Spent Nuclear Fuel Waste Above 100°C—If the waste package fails while the waste package surface temperature exceeds 100°C, it is assumed that degradation of commercial SNF would be rapid with respect to the time period of the evaluation (essentially instantaneous) and all radionuclides would be available for release upon contact with water (BSC 2004b, Section 8.1).

All Dripping Water Falls on Drip Shields—All seepage into the drifts, not just seepage above the drip shields, is assumed to fall on the drip shields. This conservative approach is taken to simplify the modeling approach, and because the uncertainty in the seepage locations is difficult to quantify (SNL 2007a, Section 5.1). This conservative approach will increase the seepage flux contacting the drip shield. Section 2.3.7.12.3 provides more information on dripping water onto drip shields.

Dripping on the Waste Package—All the dripping water penetrating a drip shield falls on the crown of the waste package. This conservative approach is taken to simplify the modeling approach, and because the uncertainty in the seepage locations is difficult to quantify (SNL 2007a, Section 5.1). Section 2.3.7.12.3 provides more information on dripping on waste packages.

No Evaporation of the Seepage Water from the Surfaces of the Drip Shields—A reduction in the quantity of water flux through the drip shields reduces the potential for advective transfer and subsequent release and transport of radionuclides from the waste packages (SNL 2007a, Section 5.2). Not accounting for evaporation from the drip shield surface tends to increase the seepage flux falling on the waste packages. Section 2.3.7.12.3 provides information on the lack of evaporation of the seepage water from the surfaces of drip shields.

No Evaporation of the Seepage Water from the Waste Packages—Transport within the waste package is not possible if evaporation eliminates liquid fluxes and effective water saturation (SNL 2007a, Section 5.3). Ignoring evaporation on the waste package surface tends to increase the potential for advective and diffusive transport of radionuclides. Section 2.3.7.12.3 provides more information on the lack of evaporation of the seepage water from the waste packages.

Transport from Waste Package to Invert—The presence of emplacement pallets for waste packages is conservatively not included to allow water and radionuclides to pass directly from the waste package to the invert without increasing the transport distance (SNL 2007a, Section 6.3.1.1). In the one dimensional vertical diffusive and advective transport model for the EBS, the breach is always conservatively located at the base of the waste package. However, the transport path length inside the waste package, from the waste form to the breach point, is sampled and can be as much as the radius of the waste package. This conservatism leads to a shortened advective flow path and increases the concentration gradient for diffusion. Section 2.3.7.12.3.2 provides more information on the transport from waste package to invert.

Invert Corrosion Products—Corrosion products in the invert are not uniformly distributed, and hence are not modeled. By assuming that there are no corrosion products in the invert, there will be no sorption or delay of radionuclides by invert corrosion products (SNL 2007a, Section 5.6). Not taking credit for the reversible and irreversible sorption of radionuclides onto the invert corrosion products will tend to increase the mass flux of radionuclides through the invert.

Physical Filtration of Colloids is Not Modeled—By assuming there is no filtration of colloids, the model will tend to overestimate the colloid mass flux and colloid facilitated radionuclide transport in the EBS. Section 2.3.7.11 provides more information on the physical filtration of colloids.

Colloid Retardation—Colloid retardation due to sorption at the air-water interface, interaction with microbes and organic components, and gravitational settling is not modeled. Not including colloid retardation tends to increase the colloid mass flux and the colloid facilitated radionuclide transport in the EBS (SNL 2007i, Section 5.4). Section 2.3.7.11 provides more information on colloid retardation.

2.3.7.13.4 Summary of Consistency Between TSPA Model Abstractions and Process Models

There is a general conceptual and numerical consistency between the TSPA and process models. This section outlines the consistency in assumptions and boundary conditions used in various process models and abstractions in Section 2.3.7 and other sections, and discusses why the differences are appropriate in the context of specific applications. It also identifies differences.

In-Package Chemistry—Although the in-package chemistry model does not explicitly model the evaporated brines discussed in Section 2.3.5.5 and *Engineered Barrier System: Physical and Chemical Environment Model* (SNL 2007l), thermally perturbed and evolved waters were used in sensitivity analyses (SNL 2007e, Section 6.6.2).

Waste Form Temperature versus Waste Package Surface Temperature—The TSPA model treats waste form temperature as if it were the same as the waste package surface temperature (Section 2.4.2.3.1.5). It is expected that waste form temperatures would be higher than waste package surface temperatures, and the effect of hotter temperatures are not included in the waste form submodels. However, the assumption of rapid commercial SNF degradation at temperatures above 100°C reduces the significance of the temperature difference between the waste form and waste package (SNL 2008, Section 6.3.7.7.1). Note, however, that as long as decay heat exists, condensation of water on waste forms is unlikely.

2.3.7.13.5 Summary of Key Outputs Provided to the TSPA

The radionuclide inventory abstraction (Section 2.3.7.4.3) provides the TSPA waste form degradation and mobilization model component with the initial radionuclide inventories and the loading uncertainties for a representative commercial SNF waste package configuration and a representative codisposal waste package designed to hold both DOE SNF and HLW. The radionuclide inventories are summarized in Table 2.3.7-5.

The in-package water chemistry model provides the TSPA waste form degradation and mobilization model component with simplified expressions to define pH and ionic strength inside a failed waste package (Section 2.3.7.5 and SNL 2007e, Section 1).

The commercial SNF degradation abstraction provides the TSPA waste form degradation and mobilization model component with parameters representing the radionuclides available for instantaneous release from the gap and grain boundary inventory and expressions and parameter values used to calculate the radionuclide release from the fuel matrix (Section 2.3.7.7 and BSC 2004b, Section 1).

The DOE SNF degradation abstraction provides the TSPA waste form degradation and mobilization model component with an instantaneous degradation rate for DOE SNF Groups 2 and 3. Commercial SNF waste packages are used to represent the naval SNF waste packages for all scenario classes in the TSPA, as discussed in Section 2.3.7.3.

The high-level radioactive waste glass dissolution abstraction provides the TSPA waste form degradation and mobilization model component with a simplified expression for the high-level radioactive waste dissolution rate, an expression for the glass surface area contacted by water, an expression for the radionuclide release rate from the glass, and parameters to evaluate the expressions.

The dissolved radionuclide concentration limits abstraction (Section 2.3.7.10.3) provides the TSPA waste form degradation and mobilization model component with solubility outputs in three forms:

- Lookup tables for elements whose solubility is a function of pH and fCO_2. These elements include plutonium, neptunium, uranium, thorium, americium, tin, and protactinium,
- Radium solubility that is a function of pH only (constant solubility limit for two intervals),
- No solubility limit for technetium, carbon, iodine, cesium, selenium, chlorine, and strontium.

For neptunium solubility, lookup tables are provided for two different solubility controlling phases: Np_2O_5 and NpO_2. The Np_2O_5 based abstraction is applied to the invert and inside the waste package when all reducing materials are fully corroded and the NpO_2 based abstraction is applied to the waste package in the presence of reductants (fuel, carbon steel, and stainless steel). At high pH values, $NaNpO_2CO_3$ is used as the solubility controlling phase in both the waste package and the invert.

For uranium solubility, lookup tables are provided for two distinct environments and related scenario classes:

1. Commercial SNF waste packages that are breached in the nominal, early waste package failure, and seismic scenario classes,
2. Codisposal waste packages breached under all scenario classes, commercial SNF waste packages breached in the course of the igneous intrusion modeling case.

The colloidal radionuclide availability abstraction provides the TSPA waste form degradation and mobilization model component with criteria, parameters, and expressions to calculate the following:

- Concentrations of HLW glass waste form colloids
- Concentrations of commercial SNF and DOE SNF colloids (two types)
- Concentrations of seepage water colloids
- Concentration of iron oxyhydroxide colloids
- Concentration of americium and plutonium irreversibly attached within waste form colloids (HLW glass colloids and one type of commercial SNF colloid)
- Radionuclide mass concentration reversibly attached to waste form colloids

- Radionuclide mass concentration reversibly attached to iron oxyhydroxide colloids
- Radionuclide mass concentration reversibly attached to seepage water colloids.

The EBS radionuclide flow and transport abstraction provides the TSPA EBS flow model component and the EBS transport model component with the following:

- Functions and flux splitting algorithms for:
  - Flow through and around the drip shield
  - Flow through and around the waste package
  - Flow into and out of the invert.
- Continuum one-dimensional mass balance equations for:
  - Transport of dissolved radionuclide species and radionuclide species that are reversibly sorbed onto three types of colloids: iron oxyhydroxide, waste form, and groundwater
  - Transport of irreversibly sorbed radionuclide species on iron oxyhydroxide colloids
  - Transport of embedded radionuclide species on waste form colloids
  - Sorbed radionuclide species on stationary corrosion products in the waste package.

These mass balance equations are implemented in a framework that discretizes the EBS into the following:

- A waste form domain, consisting of SNF rods or HLW glass and DOE SNF
- A waste package corrosion products domain, composed of corroded steel from the internal components of the waste package
- The invert domain
- The EBS-unsaturated zone interface domain to establish a boundary condition for calculating the diffusive and advective radionuclide fluxes from the invert to the unsaturated zone, and to compute the partitioning of the radionuclide mass flux between the unsaturated zone fracture and matrix continua.

2.3.7.14 General References

Abraitis, P.K.; Livens, F.R.; Monteith, J.E.; Small, J.S.; Trivedi, D.P.; Vaughan, D.J.; and Wogelius, R.A. 2000. “The Kinetics and Mechanisms of Simulated British Magnox Waste Glass Dissolution as a Function of pH, Silicic Acid Activity, and Time in Low Temperature Aqueous Systems.” *Applied Geochemistry*, *15* (9), 1399–1416. New York, New York: Pergamon. TIC: 254333.

Advocat, T.; Jollivet, P.; Minet, Y.; Luckscheiter, B.; Grambow, B.; Gens, R.; Lemmens, K.; Van Iseghem, P.; Aertsens, M.; Pirlet, V.; and Curti, E. 1999. *Experimental and Modelling Studies to Formulate a Nuclear Waste Glass Source Term in Representative Geological Disposal Conditions*. EUR 19120 EN. Luxembourg, Luxembourg: Commission of the European Communities. TIC: 254312.

Altman, W.D.; Donnelly, J.P.; and Kennedy, J.E. 1988. *Qualification of Existing Data for High-Level Nuclear Waste Repositories: Generic Technical Position*. NUREG-1298. Washington, D.C.: U.S. Nuclear Regulatory Commission. TIC: 200652.

Aronson, S. 1958. "Oxidation of UO_2 in Water Containing Oxygen." *Bettis Technical Review, Reactor Metallurgy.* 14th Edition. WAPD-BT-10. TID-4500. Pittsburgh, Pennsylvania: Westinghouse Electric Corporation, Bettis Atomic Power Division. ACC: NNA.19911025.0062.

Baes, C.F., Jr. and Mesmer, R.E. 1986. *The Hydrolysis of Cations*. Malabar, Florida: Krieger Publishing Company. TIC: 223481.

Bazan, F.; Rego, J.; and Aines, R.D. 1987. "Leaching of Actinide-Doped Nuclear Waste Glass in a Tuff-Dominated System." *Scientific Basis for Nuclear Waste Management X, Symposium Held December 1–4, 1986, Boston, Massachusetts*, Bates, J.K. and Seefeldt, W.B., eds. *84*, 447–458. Pittsburgh, Pennsylvania: Materials Research Society. TIC: 203663.

Bibler, N.E. and Jurgensen, A.R. 1988. "Leaching Tc-99 from SRP Glass in Simulated Tuff and Salt Groundwaters." *Scientific Basis for Nuclear Waste Management XI, Symposium Held November 30–December 3, 1987, Boston, Massachusetts*, Apted, M.J. and Westerman, R.E., eds. 112, 585–593. Pittsburgh, Pennsylvania: Materials Research Society. TIC: 203662.

Bickford, D.F. and Pellarin, D.H. 1987. "Large Scale Leach Testing of DWPF Canister Sections." *Scientific Basis for Nuclear Waste Management X, Symposium Held December 1–4, 1986, Boston, Massachusetts*, Bates, J.K. and Seefeldt, W.B., eds. *84*, 509–518. Pittsburgh, Pennsylvania: Materials Research Society. TIC: 203663.

Bitea, C.; Walther, C.; Kim, J.I.; Geckeis, H.; Rabung, T.; Scherbaum, F.J.; and Cacuci, D.G. 2003. "Time-Resolved Observation of ZrO_2-Colloid Agglomeration." *Colloids and Surfaces A: Physicochemical and Engineering Aspects*, *215*, 55–66. New York, New York: Elsevier. TIC: 257515.

Bourcier, W.L. 1994. *Critical Review of Glass Performance Modeling*. ANL-94/17. Argonne, Illinois: Argonne National Laboratory. TIC: 211862.

Bradbury, M.H. and Baeyens, B. 2005. "Modeling the Sorption of Mn(II), Co(II), Ni(II), Zn(II), Cd(II), Eu(III), Am(III), Sn(IV), Th(IV), Np(V) and U(VI) on Montmorillonite: Linear Free Energy Relationships and Estimates of Surface Binding Constants for Some Selected Heavy Metals and Actinides." *Geochimica et Cosmoschimica Acta, 69*, (4), 875–892. New York, New York: Elsevier. TIC: 259202.

Bradbury, M.H. and Baeyens, B. 2006. "Modelling Sorption Data for the Actinides Am(III), Np(V) and Pa(V) on Montmorillonite." *Radiochimica Acta*, 94, 619–625. München, Germany: Oldenbourg Wissenschaftsverlag. TIC: 259214.

Bruno, J.; Cera, E.; de Pablo, J.; Duro, L.; Jordana, S.; and Savage, D. 1997. *Determination of Radionuclide Solubility Limits to be Used in SR 97–Uncertainties Associated to Calculated Solubilities*. SKB TR-97-33. Stockholm, Sweden: Svensk Kärnbränsleförsörjning A.B. TIC: 239307.

BSC (Bechtel SAIC Company) 2003. *Atlas Breached Waste Package and Drip Shield Experiments: Breached Drip Shield Tests*. TDR-EBS-MD-000025 REV 00. Las Vegas, Nevada: Bechtel SAIC Company. ACC: DOC.20030619.0001.

BSC 2004a. *Aqueous Corrosion Rates for Waste Package Materials*. ANL-DSD-MD-000001 REV 01. Las Vegas, Nevada: Bechtel SAIC Company. ACC: DOC.20041012.0003.

BSC 2004b. *CSNF Waste Form Degradation: Summary Abstraction*. ANL-EBS-MD-000015 REV 02. Las Vegas, Nevada: Bechtel SAIC Company. ACC: DOC.20040908.0001.

BSC 2004c. *DSNF and Other Waste Form Degradation Abstraction*. ANL-WIS-MD-000004 REV 04. Las Vegas, Nevada: Bechtel SAIC Company. ACC: DOC.20041201.0007.

BSC 2004d. *Defense HLW Glass Degradation Model.* ANL-EBS-MD-000016 REV 02. Las Vegas, Nevada: Bechtel SAIC Company. ACC: DOC.20041020.0015.

BSC 2004e. *Evaluation of Potential Impacts of Microbial Activities on Drift Chemistry.* ANL-EBS-MD-000038 REV 01. Las Vegas, Nevada: Bechtel SAIC Company. ACC: DOC.20041118.0005.

BSC 2004f. *Seepage Model for PA Including Drift Collapse*. MDL-NBS-HS-000002 REV 03. Las Vegas, Nevada: Bechtel SAIC Company. ACC: DOC.20040922.0008.

Buck, E.C.; McNamara, B.K.; and Hanson, B.D. 2004. *Alternative Conceptual Model for Colloid Generation from Commercial Spent Nuclear Fuel*. PNNL-14306. Richland, Washington: Pacific Northwest National Laboratory. ACC: MOL.20040901.0242.

Buck, E.C.; Hanson, B.D.; and McNamara, B.K. 2004. "The Geochemical Behaviour of Tc, Np, and Pu in Spent Nuclear Fuel in an Oxidizing Environment." *Energy, Waste, and the Environment: A Geochemical Perspective*. Giere, R. and Stille, P.; eds. Geological Society of London Special Publications, 236. Pages 65-88. London, England: Geological Society of London. TIC: 256910.

Burns P.C. 1999. "Cs Boltwoodite Obtained by Ion Exchange from Single Crystals: Implications for Radionuclide Release in a Nuclear Repository." *Journal of Nuclear Materials, 265*, 218–223. Amsterdam, The Netherlands: Elsevier. TIC: 246432.

Burns, P.C.; Deely, K.M.; and Skanthakumar, S. 2004. "Neptunium Incorporation into Uranyl Compounds that Form as Alteration Products of Spent Nuclear Fuel: Implications for Geologic

Repository Performance." *Radiochimica Acta, 92*, 151–159. München, Germany: Oldenbourg Wissenschaftsverlag. TIC: 256456.

Chick, L.A. and Pederson, L.R. 1984. "The Relationship Between Reaction Layer Thickness and Leach Rate for Nuclear Waste Glasses." *Scientific Basis for Nuclear Waste Management VII, Symposium Held November 14–17, 1983, Boston, Massachusetts*, McVay, G.L., ed. 26, 635–642. New York, New York: Elsevier. TIC: 204393.

CRWMS M&O (Civilian Radioactive Waste Management System Management and Operating Contractor) 2000a. *Waste Packages and Source Terms for the Commercial 1999 Design Basis Waste Streams*. CAL-MGR-MD-000001 REV 00. Las Vegas, Nevada: Civilian Radioactive Waste Management System Management and Operating Contractor. ACC: MOL.20000214.0479.

CRWMS M&O 2000b. *Commercial Spent Nuclear Fuel Degradation in Unsaturated Drip Tests*. Input Transmittal WP-WP-99432.T. Las Vegas, Nevada: Civilian Radioactive Waste Management System Management and Operating Contractor. ACC: MOL.20000107.0209.

CRWMS M&O 2000c. *Measured Solubilities, Argon National Lab High Drip Rate Tests*. Input Transmittal 00333.T. Las Vegas, Nevada: Civilian Radioactive Waste Management System Management and Operating Contractor. ACC: MOL.20000919.0019.

CRWMS M&O 2001. *Colloid-Associated Radionuclide Concentration Limits: ANL*. ANL-EBS-MD-000020 REV 00 ICN 01. Las Vegas, Nevada: Civilian Radioactive Waste Management System Management and Operating Contractor. ACC: MOL.20010216.0003.

Cunnane, J.; Ebert, W.; Goldberg, M.; Finch, R.; and Mertz, C. 2003. *Yucca Mountain Project Report, Waste Form Testing Work*. Argonne, Illinois: Argonne National Laboratory, Chemical Technology Division. ACC: MOL.20030630.0418.

Da Cunha Belo, M.; Walls, M.; Hakiki, N.E.; Corset, J.; Picquenard, E.; Sagon, G.; and Noel, D. 1998. "Composition, Structure, and Properties of the Oxide Films Formed on the Stainless Steel 316L in a Primary Type PWR Environment." *Corrosion Science, 40*, (2/3), 447–463. New York, New York: Pergamon. TIC: 259108.

De Pablo, J.; Casas, I.; Giménez, J.; Molera, M.; Rovira, M.; Duro, L.; and Bruno, J. 1999. "The Oxidative Dissolution Mechanism of Uranium Dioxide. I. The Effect of Temperature in Hydrogen Carbonate Medium." *Geochimica et Cosmochimica Acta*, *63* (19–20), 3097–3103. New York, New York: Pergamon. TIC: 254443.

DOE (U.S. Department of Energy) 1985. *An Evaluation of Commercial Repository Capacity for the Disposal of Defense High-Level Waste*. DOE/DP/0020/1. Washington, D.C.: U.S. Department of Energy. ACC: MOL.20010730.0387.

DOE 2003. *Source Term Estimates for DOE Spent Nuclear Fuels*. DOE/SNF/REP-078, Rev. 0. Idaho Falls, Idaho: U.S. Department of Energy, Idaho Operations Office. TIC: 254275.

DOE 2004. *Source Term Estimates for DOE Spent Nuclear Fuels*. DOE/SNF/REP-078, Rev. 1. Three volumes. Idaho Falls, Idaho: U.S. Department of Energy, Idaho Operations Office. ACC: MOL.20040524.0451.

DOE 2008. *Monitored Geologic Repository Systems Requirements Document*. YMP/CM-0026, Rev. 2. Las Vegas, Nevada: U.S. Department of Energy, Office of Civilian Radioactive Waste Management. ACC: DOC.20080128.0001.

Douglas, M.; Clark, S.B.; Friese, J.I.; Arey, B.W.; Buck, E.C.; Hanson, B.D.; Utsunomiya, S.; and Ewing, R.C. 2005. "Microscale Characterization of Uranium(VI) Silicate Solids and Associated Neptunium(V)." *Radiochimica Acta*, 93, 265–272. München, Germany: Oldenbourg Wissenschaftsverlag. TIC: 257469.

Douglas, M.; Clark, S.B.; Utsunomiya, S.; and Ewing, R.C. 2002. "Cesium and Strontium Incorporation into Uranophane, Ca[(UO^2) (SiO_3 OH_2)]•$5H_2$ O]." *Journal of Nuclear Science and Technology, Supplement 3*, 504–507. Tokyo, Japan: Atomic Energy Society of Japan. TIC: 259213.

Dreyfus, D. 1995. "Proposed Mix of DOE-Owned High Level Waste and Spent Nuclear Fuel." Memorandum from D. Dreyfus (DOE/OCRWM) to J.E. Lytle (DOE/OEM), November 9, 1995, with attachment. ACC: MOL.19990319.0341.

Ebert, W.L.; Wolf, S.F.; and Bates, J.K. 1996. "The Release of Technetium from Defense Waste Processing Facility Glasses." *Scientific Basis for Nuclear Waste Management XIX, Symposium Held November 27–December 1, 1995, Boston, Massachusetts*, Murphy, W.M. and Knecht, D.A., eds. *412*, 221–227. Pittsburgh, Pennsylvania: Materials Research Society. TIC: 233877.

Efurd, D.W.; Runde, W.; Banar, J.C.; Janecky, D.R.; Kaszuba, J.P.; Palmer, P.D.; Roensch, F.R.; and Tait, C.D. 1998. "Neptunium and Plutonium Solubilities in a Yucca Mountain Groundwater." *Environmental Science & Technology, 32,* (24), 3893-3900. Easton, Pennsylvania: American Chemical Society. TIC: 243857.

EPA (U.S. Environmental Protection Agency) 1999a. *Understanding Variation in Partition Coefficient, K_d, Values*. EPA 402-R-99-004A&B. Two volumes. Washington, D.C.: U.S. Environmental Protection Agency. TIC: 249201.

EPA 1999b. "Review of Geochemistry and Available K_d Values for Cadmium, Cesium, Chromium, Lead, Plutonium, Radon, Strontium, Thorium, Tritium^3 H), and Uranium." Volume II of *Understanding Variation in Partition Coefficient, K_d, Values*. EPA 402-R-99-004B. Washington, D.C.: U.S. Environmental Protection Agency, Office of Radiation and Indoor Air. ACC: MOL.20040628.0034.

EPA 2004. "Review of Geochemistry and Available K_d Values for Americium, Arsenic, Curium, Iodine, Neptunium, Radium, and Technetium." Volume III of *Understanding the Variation in Partition Coefficient, K_d, Values.* EPA 402-R-04-002C. Washington, D.C.: U.S. Environmental Protection Agency. ACC: MOL.20041102.0060.

EPRI 2000. *Evaluation of the Candidate High-Level Radioactive Waste Repository at Yucca Mountain Using Total System Performance Assessment, Phase 5*. 1000802. Palo Alto, California: Electric Power Research Institute. TIC: 249555.

Evans, M.; Hastings, N.; and Peacock, B. 1993. *Statistical Distributions*. 2nd Edition. New York, New York: John Wiley & Sons. TIC: 246114.

Ewing, R.C. and Haaker, R.F. 1979. *Naturally Occurring Glasses: Analogues for Radioactive Waste Forms*. PNL-2776. Richland, Washington: Pacific Northwest Laboratory. ACC: NNA.19900315.0277.

Finn, P.A.; Buck, E.C.; Gong, M.; Hoh, J.C.; Emery, J.W.; Hafenrichter, L.D.; and Bates, J.K. 1994. "Colloidal Products and Actinide Species in Leachate from Spent Nuclear Fuel." *Radiochimica Acta*, 66/67, 197–203. Munchen, Germany: R. Oldenbourg Verlag. TIC: 238493.

Forsyth, R. 1997. *The SKB Spent Fuel Corrosion Program. An Evaluation of Results from the Experimental Programme Performed in the Studsvik Hot Cell Laboratory*. SKB TR-97-25. Stockholm, Sweden: Svensk Kärnbränsleförsörjning A.B. TIC: 246406.

Gislason, S.R. and Eugster, H.P. 1987. "Meteoric Water-Basalt Interactions. II: A Field Study in N.E. Iceland." *Geochimica et Cosmochimica Acta, 51*, 2841–2855. New York, New York: Pergamon. TIC: 259231.

Goldberg, M. 2003. *Rod Segment Test Data Report, CSNF Degradation Model: Q Data Input from ANL Testing*. Task Number: PAWC1M5. Argonne, Illinois: Argonne National Laboratory, Chemical Engineering Division. ACC: MOL.20030627.0221.

Gordon, S.J. and Brady, P.V. 2002. "In Situ Determination of Long-Term Basaltic Glass Dissolution in the Unsaturated Zone." *Chemical Geology, 190*, (1-4), 113–122. New York, New York: Elsevier. TIC: 258314.

Grambow, B.; Jercinovic, M.J.; Ewing, R.C.; and Byers, C.D. 1986. "Weathered Basalt Glass: A Natural Analogue for the Effects of Reaction Progress on Nuclear Waste Glass Alteration." *Scientific Basis for Nuclear Waste Management IX, Symposium Held September 9–11, 1985, Stockholm, Sweden*, Werme, L.O., ed. *50*, 263–272. Pittsburgh, Pennsylvania: Materials Research Society. TIC: 203664.

Grambow, B.; Loida, A.; Dressler, P.; Geckeis, H.; Gago, J.; Casas, I.; de Pablo, J.; Giménez, J.; and Torrero, M.E. 1996. *Long-Term Safety of Radioactive Waste Disposal: Chemical Reaction of Fabricated and High Burnup Spent UO_2 Fuel with Saline Brines*. FZKA 5702. Final Report. Karlsruhe, Germany: Forschungszentrum Karlsruhe GmbH. TIC: 246887.

Gray, W.J.; Strachan, D.M.; and Wilson, C.N. 1992. "Gap and Grain-Boundary Inventories of Cs, Tc and Sr in Spent LWR Fuel." *Scientific Basis for Nuclear Waste Management XV, Symposium Held November 4–7, 1991, Strasbourg, France*, Sombret, C.G., ed. 257, 353–360. Pittsburgh, Pennsylvania: Materials Research Society. TIC: 204618.

Gray, W.J. and Wilson, C.N. 1995. *Spent Fuel Dissolution Studies FY 1991–1994*. PNL-10450. Richland, Washington: Pacific Northwest Laboratory. ACC: MOL.19960802.0035.

Grenthe, I.; Fuger, J.; Konings, R.J.M.; Lemire, R.J.; Muller, A.B.; Nguyen-Trung, C.; and Wanner, H. 1992. *Chemical Thermodynamics of Uranium. Volume 1 of Chemical Thermodynamics*. Wanner, H. and Forest, I., eds. Amsterdam, The Netherlands: North-Holland Publishing Company. TIC: 224074.

Guillaumont, R.; Fanghänel, T.; Fuger, J.; Grenthe, I.; Neck, V.; Palmer, D.A.; and Rand, M.H. 2003. "Update on the Chemical Thermodynamics of Uranium, Neptunium, Plutonium, Americium and Technetium." Mompean, F.J.; Illemassene, M.; Domenech-Orti, C.; and Ben Said, K., eds. *Chemical Thermodynamics*, *5*. Amsterdam, The Netherlands: Elsevier. TIC: 255230.

Hamel, W.F. 2003. "Waste Treatment and Immobilization Plant (WTP) High-Level Waste (HLW) Canister Production Estimates to Support Analyses by the Yucca Mountain Project." Memorandum from W.F. Hamel (DOE) to W.J. Taylor, June 26, 2003, with attachment. ACC: MOL.20030828.0080.

Hem, J.D. 1985. *Study and Interpretation of the Chemical Characteristics of Natural Water*. 3rd Edition. Geological Survey Water-Supply Paper 2254. Washington, D.C.: U.S. Government Printing Office. ACC: NNA.19940427.0181.

Honeyman, B.D. and Ranville, J.F. 2002. "Colloid Properties and their Effects on Radionuclide Transport through Soils and Groundwaters." *Geochemistry of Soil Radionuclides*, Chapter 7. Zhang, P.-C. and Brady, P.V., eds. SSSA Special Publication Number 59. Madison, Wisconsin: Soil Science Society of America. TIC: 253952.

Honig, E.P.; Roebersen, G.J.; and Wiersema, P.H. 1971. "Effect of Hydrodynamic Interaction on the Coagulation Rate of Hydrophobic Colloids." *Journal of Colloid and Interface Science, 36*, (1), 97–109. New York, New York: Elsevier. TIC: 259212.

Hsu, W.P.; Rönnquist, L.; and Matijevic, E. 1988. "Preparation and Properties of Monodispersed Colloidal Particles of Lanthanide Compounds. 2. Cerium (IV)." *Langmuir*, 4 (1), 31–37. Washington, D.C.: American Chemical Society. TIC: 257454.

Hummel, W.; Berner, U.; Curti, E.; Pearson, F.J.; and Thoenen, T. 2002. *Nagra/PSI Chemical Thermodynamic Data Base 01/01*. Parkland, Florida: Universal Publishers. TIC: 253421.

Ilton, E.S.; Liu, C.; Yantasee, W.; Wang, Z.; Moore, D.A.; Felmy, A.R.; and Zachara, J.M. 2006. "The Dissolution of Synthetic Na-Boltwoodite in Sodium Carbonate Solutions." *Geochimica et Cosmochimica Acta, 70*, 4836–4849. New York, New York: Elsevier. TIC: 259016.

Jara, A.A.; Goldberg, S.; and Mora, M.L. 2005. "Studies of the Surface Charge of Amorphous Aluminosilicates Using Surface Complexation Models." *Journal of Colloid and Interface Science, 292*, 160–170. New York, New York: Elsevier. TIC: 259358.

Jegou, C.; Paul, J.L.; and Lucchini, J.F. 2001. "State of the Art of the Leaching and RN Release from Spent Fuel." Section 8.2 of *Synthesis on the Long Term Behavior of the Spent Nuclear Fuel*. Poinssot, C., ed. CEA-R-5958(E). II. Paris, France: Commissariat à l'Énergie Atomique. TIC: 253976.

Jerden, J.L. and Kropf, A.J. 2007. "Surface Complexation of Neptunium(V) with Goethite." *Scientific Basis for Nuclear Waste Management XXX, Symposium Held November 27–December 1, 2006, Boston, Massachusetts.* Dunn, D.S., Poinssot, C., and Begg, B., eds. *985*, 413–418. Warrendale, Pennsylvania: Materials Research Society. TIC: 259484.

Johnson, A.B., Jr. and Francis, B. 1980. *Durability of Metals from Archaeological Objects, Metal Meteorites, and Native Metals*. PNL-3198. Richland, Washington: Pacific Northwest Laboratory. TIC: 229619.

Kaminski, M.D.; Dimitrijevic, N.M.; Mertz, C.J.; and Goldberg, M.M. 2005. "Colloids from the Aqueous Corrosion of Uranium Nuclear Fuel." *Journal of Nuclear Materials, 347*, 77–87. New York, New York: Elsevier. TIC: 259210.

Kim, C-W.; Wronkiewicz, D.J.; Finch, R.J.; and Buck, E.C. 2006. "Incorporation of Cerium and Neodymium in Uranyl Phases." *Journal of Nuclear Materials, 353*, 147–157. New York, New York: Elsevier. TIC: 259209.

Kim, Y-J. 1999. "Analysis of Oxide Film Formed on Type 304 Stainless Steel in 288°C Water Containing Oxygen, Hydrogen, and Hydrogen Peroxide." *Corrosion, 55*, (1), 81–88. Houston, Texas: NACE International. TIC: 245184.

Knauss, K.G.; Bourcier, W.L.; McKeegan, K.D.; Merzbacher, C.I.; Nguyen, S.N.; Ryerson, F.J.; Smith, D.K.; Weed, H.C.; and Newton, L. 1990. "Dissolution Kinetics of a Simple Analogue Nuclear Waste Glass as a Function of pH, Time and Temperature." *Scientific Basis for Nuclear Waste Management XIII, Symposium Held November 27–30, 1989, Boston, Massachusetts*, Oversby, V.M. and Brown, P.W., eds. *176*, 371–381. Pittsburgh, Pennsylvania: Materials Research Society. TIC: 203658.

Langmuir, D. 1997. *Aqueous Environmental Geochemistry.* Upper Saddle River, New Jersey: Prentice Hall. TIC: 237107.

Lee, J.H.; Chambre, P.L.; and Andrews, R.W. 1996. "Mathematical Models for Diffusive Mass Transfer from Waste Package Container with Multiple Perforations." *Proceedings of the 1996 International Conference on Deep Geological Disposal of Radioactive Waste, September 16–19, 1996, Winnipeg, Manitoba, Canada*, 5-61 to 5-72. Toronto, Ontario, Canada: Canadian Nuclear Society. TIC: 233923.

Liang, L. and Morgan, J.J. 1990. "Chemical Aspects of Iron Oxide Coagulation in Water: Laboratory Studies and Implications for Natural Systems." *Aquatic Sciences*, *52* (1), 32–55. Basel, Switzerland: Birkhauser Verlag. TIC: 246125.

Lu, N.; Conca, J.; Parker, G.R.; Leonard, P.A.; Moore, B.; Strietelmeier, B.; and Triay, I.R. 2000. *Adsorption of Actinides onto Colloids as a Function of Time, Temperature, Ionic Strength, and Colloid Concentration—Waste Form Colloids Report for Yucca Mountain Program (Colloid Data Summary from 1999 to 2000 Research)*. LA-UR-00-5121. Los Alamos, New Mexico: Los Alamos National Laboratory. ACC: MOL.20031204.0108.

Lytle, J.E. 1995. "Disposal of DOE-owned High Level Waste and Spent Nuclear Fuel." Memorandum from J.E. Lytle (DOE) to D.A. Dreyfus (DOE/OCRWM), October 26, 1995. ACC: HQO.19951116.0015.

Madden, A.S.; Hochella, M.F., Jr.; and Luxton, T.P. 2006. "Insights for Size-Dependent Reactivity of Hematite Nanomineral Surfaces through Cu^{2}+ Sorption." *Geochimica et Cosmochimica Acta*, *70*, 4095–4104. New York, New York: Elsevier. TIC: 259420.

McEachern, R.J. and Taylor, P. 1998. "A Review of the Oxidation of Uranium Dioxide at Temperatures Below 400°C." *Journal of Nuclear Material*, *254*, 87–121. Amsterdam, The Netherlands: Elsevier. TIC: 246427.

McGrail, B.P.; Ebert, W.L.; Bacon, D.H.; and Strachan, D.M. 1998. *A Strategy to Conduct an Analysis of the Long-Term Performance of Low-Activity Waste Glass in a Shallow Subsurface Disposal System at Hanford*. PNNL-11834. Richland, Washington: Pacific Northwest National Laboratory. TIC: 249433.

McNamara, B.; Hanson, B.; Buck, E.; and Soderquist, C. 2005. "Corrosion of Commercial Spent Nuclear Fuel. 2. Radiochemical Analyses of Metastudtite and Leachates." *Radiochimica Acta, 93*, 169–175. München, Germany: Oldenbourg Wissenschaftsverlag. TIC: 257131.

Ménard, O.; Advocat, T.; Ambrosi, J.P.; and Michard, A. 1998. "Behavior of Actinides (Th, U, Np and Pu) and Rare Earths (La, Ce and Nd) During Aqueous Leaching of a Nuclear Waste Glass Under Geological Disposal Conditions." *Applied Geochemistry, 13,* 105–126. New York, New York: Pergamon. TIC: 256470.

Mertz, C.J.; Finch, R.J.; Fortner, J.A.; Jerden, J.L., Jr.; Yifen, T.; Cunnane, J.C.; and Finn, P.A. 2003. *Characterization of Colloids Generated from Commercial Spent Nuclear Fuel Corrosion*. Activity Number: PAWTP30A. Argonne, Illinois: Argonne National Laboratory. ACC: MOL.20030422.0337.

Mertz, C.; Fortner, J.; Goldberg, M.; and Shelton-Davis, C. 2000. *Colloid Generation from Metallic Uranium Fuel.* Argonne, Illinois: Argonne National Laboratory. TIC: 254296.

Murakami, T.; Ohnuki, T.; Isobe, H.; and Sato, T. 1997. "Mobility of Uranium During Weathering." *American Mineralogist, 82,* 888–899. Washington, D.C.: Mineralogical Society of America. TIC: 246053.

NCRP (National Council on Radiation Protection and Measurements) 1996. *Screening Models for Releases of Radionuclides to Atmosphere, Surface Water, and Ground*. NCRP Report No. 123 I. Bethesda, Maryland: National Council on Radiation Protection and Measurements. TIC: 225158.

Neck, V. and Kim, J.I. 2001. "Solubility and Hydrolysis of Tetravalent Actinides." *Radiochimica Acta, 89* (1), 1–16. München, Germany: Oldenbourg Wissenschaftsverlag. TIC: 250728.

Nitsche, H.; Gatti, R.C.; Standifer, E.M.; Lee, S.C.; Müller, A.; Prussin, T.; Deinhammer, R.S.; Maurer, H.; Becraft, K.; Leung, S.; and Carpenter, S.A. 1993. *Measured Solubilities and Speciations of Neptunium, Plutonium, and Americium in a Typical Groundwater (J-13) from the Yucca Mountain Region*. LA-12562-MS. Los Alamos, New Mexico: Los Alamos National Laboratory. ACC: NNA.19930507.0136.

Nitsche, H.; Roberts, K.; Prussin, T.; Muller, A.; Becraft, K.; Keeney, D.; Carpenter, S.A.; and Gatti, R.C. 1994. *Measured Solubilities and Speciations from Oversaturation Experiments of Neptunium, Plutonium, and Americium in UE-25 P#1 Well Water from the Yucca Mountain Region. Milestone Report 3329-WBS1.2.3.4.1.3.1*. LA-12563-MS. Los Alamos, New Mexico: Los Alamos National Laboratory. TIC: 210589.

Nordstrom, D.K. and Munoz, J.L. 1986. *Geochemical Thermodynamics*. Palo Alto, California: Blackwell Scientific Publications. TIC: 208228.

Nuclear Waste Policy Act of 1982. 42 U.S.C. 10101 et seq.

Nye, P.H. 1979. "Diffusion of Ions and Uncharged Solutes in Soils and Soil Clays." *Advances in Agronomy, 31,* 225–272. New York, New York: Academic Press. TIC: 255345.

Olesen, T.; Moldrup, P.; and Gamst, J. 1999. "Solute Diffusion and Adsorption in Six Soils along a Soil Texture Gradient." *Soil Science Society of America Journal, 63* (3), 519–524. Madison, Wisconsin: Soil Science Society of America. TIC: 249743.

Pabalan, R.T. and Turner, D.R. 1997. "Uranium(6+) Sorption on Montmorillonite: Experimental and Surface Complexation Modeling Study." *Aquatic Geochemistry, 2*, 203–226. Dordrecht, The Netherlands: Kluwer Academic Publishers. TIC: 237077.

Palache, C.; Berman, H.; and Frondel, C. 1944. *Elements, Sulfides, Sulfosalts, Oxides. Volume I of The System of Mineralogy of James Dwight Dana and Edward Salisbury Dana, Yale University 1837–1892*. 7th Edition. New York, New York: John Wiley & Sons. TIC: 209331.

Pirlet, V. 2001. "Overview of Actinides (Np, Pu, Am) and Tc Release from Waste Glasses: Influence of Solution Composition." *Journal of Nuclear Materials, 298*, 47–54. New York, New York: Elsevier. TIC: 257455.

Pruess, K.; Wang, J.S.Y.; and Tsang, Y.W. 1990. "On Thermohydrologic Conditions Near High-Level Nuclear Wastes Emplaced in Partially Saturated Fractured Tuff, 2. Effective Continuum Approximation." *Water Resources Research, 26*, (6), 1249-1261. (Washington, D.C.): American Geophysical Union. TIC: 224854.

Rai, D. 1984. "Solubility Product of Pu(IV) Hydrous Oxide and Equilibrium Constants of Pu (IV)/Pu (V), Pu (IV)/Pu (VI), and Pu (V)/Pu (VI) Couples." *Radiochimica Acta, 35*, 97-106. München, Germany: R. Oldenbourg Verlag. TIC: 219109.

Rai, D.; Moore, D.A.; Felmy, A.R.; Choppin, G.R.; and Moore, R.C. 2001. "Thermodynamics of the PuO_2^+-Na^+-OH^--Cl^--ClO_4^--H_2O System: Use of NpO_2^+ Pitzer Parameters for PuO_2^+." *Radiochimica Acta, 89*, (8), 491-498. München, Germany: Oldenbourg Wissenschaftsverlag. TIC: 255398.

Rai, D. and Ryan, J.L. 1982. "Crystallinity and Solubility of Pu(IV) Oxide and Hydrous Oxide in Aged Aqueous Suspensions." *Radiochimica Acta, 30*, 213–216. München, Germany: R. Oldenbourg Verlag. TIC: 219107.

Reimus, P.W.; Callahan, T.J.; Ware, S.D.; Haga, M.J.; and Counce, D.A. 2007. "Matrix Diffusion Coefficients in Volcanic Rocks at the Nevada Test Site: Influence of Matrix Porosity, Matrix Permeability, and Fracture Coating Minerals." *Journal of Contaminant Hydrology, 93*, 85-95. New York, New York: Elsevier. TIC: 259673.

Roberts, J.J. and Lin, W. 1997. "Electrical Properties of Partially Saturated Topopah Spring Tuff: Water Distribution as a Function of Saturation." *Water Resources Research, 33* (4), 577–587. Washington, D.C.: American Geophysical Union. TIC: 239736.

Röllin, S.; Spahiu, K.; and Eklund, U.B. 2001. "Determination of Dissolution Rates of Spent Fuel in Carbonate Solutions Under Different Redox Conditions with a Flow-Through Experiment." *Journal of Nuclear Materials*, *297* (3), 231–243. Amsterdam, The Netherlands: North-Holland. TIC: 254044.

S. Cohen & Associates 1999. *Effectiveness of Fuel Rod Cladding as an Engineered Barrier in the Yucca Mountain Repository*. McLean, Virginia: S. Cohen & Associates. TIC: 246541.

Sanchez, A.L.; Murray, J.W.; and Sibley, T.H. 1985. "The Adsorption of Plutonium IV and V on Goethite." *Geochimica et Cosmochimica Acta, 49, (11)*, 2297–2307. New York, New York: Pergamon Press. TIC: 224091.

Schindler, M.; Mutter, A.; Hawthorne, F.C.; and Putnis, A. 2004. "Prediction of Crystal Morphology of Complex Uranyl-Sheet Minerals. I. Theory." *The Canadian Mineralogist*, *42* (6), 1629–1649. Ottawa, Ontario, Canada: Mineralogical Association of Canada. TIC: 257517.

Schwertmann, U. and Taylor, R.M. 1995. "Iron Oxides." Chapter 8 of *Minerals in Soil Environments*. 2nd Edition. Dixon, J.B. and Weed, S.B., eds. SSSA Book Series, No. 1. Madison, Wisconsin: Soil Science Society of America. TIC: 237222.

Sené, M.R.; Baily, M.; Illerhaus, B.; Goebbels, J.; Haase, O.; Kulish, A.; Godon, N.; and Choucan, J.L. 1999. *Characterisation of Accessible Surface Area of HLW Glass Monoliths by High Energy Accelerator Tomography and Comparison with Conventional Techniques*. EUR 19119 EN. Luxembourg, Luxembourg: Commission of the European Communities. TIC: 254444.

Serrano, J.A.; Rondinella, V.V.; Glatz, J.P.; Toscano, E.H.; Quiñones, J.; Diaz-Arocas, P.P.; and Garcia-Serrano, J. 1998. "Comparison of the Leaching Behaviour of Irradiated Fuel, SIMFUEL, and Non-Irradiated UO_2 Under Oxic Conditions." *Radiochimica Acta*, *82* (1–4), 33–37. München, Germany: R. Oldenbourg Verlag. TIC: 254195.

Shibutani, T.; Shibutani, S.; and Yui, M. 1998. *Database Development of Chemical Thermodynamics of Protactinium for Performance Assessment of HLW Geological Disposal System*. Tokyo, Japan: Tokai Works, Power Reactor and Nuclear Fuel Development Corporation. TIC: 251126.

Shoesmith, D.W. 2000. "Fuel Corrosion Processes under Waste Disposal Conditions." *Journal of Nuclear Materials*, *282* (1), 1–31. Amsterdam, The Netherlands: North-Holland. TIC: 254043.

SNL (Sandia National Laboratories) 2007a. *EBS Radionuclide Transport Abstraction*. ANL-WIS-PA-000001 REV 03. Las Vegas, Nevada: Sandia National Laboratories. ACC: DOC.20071004.0001.

SNL 2007b. *Radionuclide Screening*. ANL-WIS-MD-000006 REV 02. Las Vegas, Nevada: Sandia National Laboratories. ACC: DOC.20070326.0003.

SNL 2007c. *MOX Spent Nuclear Fuel and LaBS Glass for TSPA-LA*. ANL-WIS-MD-000022 REV 01. Las Vegas, Nevada: Sandia National Laboratories. ACC: DOC.20070220.0007.

SNL 2007d. *Initial Radionuclide Inventories*. ANL-WIS-MD-000020 REV 01 ADD 01. Las Vegas, Nevada: Sandia National Laboratories. ACC: DOC.20070801.0001.

SNL 2007e. *In-Package Chemistry Abstraction*. ANL-EBS-MD-000037 REV 04 ADD 01. Las Vegas, Nevada: Sandia National Laboratories. ACC: DOC.20070816.0004.

SNL 2007f. *Qualification of Thermodynamic Data for Geochemical Modeling of Mineral-Water Interactions in Dilute Systems*. ANL-WIS-GS-000003 REV 01. Las Vegas, Nevada: Sandia National Laboratories. ACC: DOC.20070619.0007.

SNL 2007g. *In-Drift Precipitates/Salts Model*. ANL-EBS-MD-000045 REV 03. Las Vegas, Nevada: Sandia National Laboratories. ACC: DOC.20070306.0037.

SNL 2007h. *Dissolved Concentration Limits of Elements with Radioactive Isotopes*. ANL-WIS-MD-000010 REV 06. Las Vegas, Nevada: Sandia National Laboratory. ACC: DOC.20070918.0010.

SNL 2007i. *Waste Form and In-Drift Colloids-Associated Radionuclide Concentrations: Abstraction and Summary*. MDL-EBS-PA-000004 REV 03. Las Vegas, Nevada: Sandia National Laboratories. ACC: DOC.20071018.0019.

SNL 2007j. *Radionuclide Transport Models Under Ambient Conditions*. MDL-NBS-HS-000008 REV 02 ADD 01. Las Vegas, Nevada: Sandia National Laboratories. ACC: DOC.20070718.0003.

SNL 2007k. *Cladding Degradation Summary for LA*. ANL-WIS-MD-000021 REV 03 ADD 01. Las Vegas, Nevada: Sandia National Laboratories. ACC: DOC.20070614.0002.

SNL 2007l. *Engineered Barrier System: Physical and Chemical Environment*. ANL-EBS-MD-000033 REV 06. Las Vegas, Nevada: Sandia National Laboratories. ACC: DOC.20070907.0003.

SNL 2008. *Total System Performance Assessment Model/Analysis for the License Application*. MDL-WIS-PA-000005 REV 00 ADD 01. Las Vegas, Nevada: Sandia National Laboratories. ACC: DOC.20080312.0001.

So, H.B. and Nye, P.H. 1989. "The Effect of Bulk Density, Water Content and Soil Type on the Diffusion of Chloride in Soil." *Journal of Soil Science, 40* (4), 743–749. Oxford, England: Blackwell Scientific. TIC: 255392.

Stout, R.B. and Leider, H.R. 1998. *Waste Form Characteristics Report, CD-ROM Version*. UCRL-ID-132375. Livermore, California: Lawrence Livermore National Laboratory. TIC: 246106.

Tachi, Y.; Shibutani, T.; Sato, H.; and Yui, M. 2001. "Experimental and Modeling Studies on Sorption and Diffusion of Radium in Bentonite." *Journal of Contaminant Hydrology, 47*, 171–186. New York, New York: Elsevier. TIC: 259205

Tait, J.C. and Luht, J.L. 1997. *Dissolution Rates of Uranium from Unirradiated UO_2 and Uranium and Radionuclides from Used CANDU Fuel Using the Single-Pass Flow-Through Apparatus*. 06819-REP-01200-0006 R00. Toronto, Ontario, Canada: Ontario Hydro. TIC: 243164.

Taylor, P.; Wood, D.D.; Duclos, A.M.; and Owen, D.G. 1989. "Formation of Uranium Trioxide Hydrates on UO_2 Fuel in Air-Steam Mixtures Near 200°C." *Journal of Nuclear Materials*, *168* (1–2), 70–75. Amsterdam, The Netherlands: Elsevier. TIC: 246601.

Thibault, D.H.; Sheppard, M.I.; and Smith, P.A. 1990. *A Critical Compilation and Review of Default Soil Solid/Liquid Partition Coefficients, K_d, for Use in Environmental Assessments*. AECL-10125. Pinawa, Manitoba, Canada: Atomic Energy of Canada Limited. TIC: 237236.

Thomas, E. 2003. "Transmittal of Unsaturated Testing of Bare Spent UO_2 Fuel Fragments: Data Report, Argonne National Laboratory." Interoffice memorandum from E. Thomas (BSC) to J.C. Cunnane, July 2, 2003, 0702037939, with attachment. ACC: MOL.20030702.0116; MOL.20030311.0097.

Tombácz, E.; Abraham, I.; Gilde, M.; and Szanto, F. 1990. "The pH-Dependent Colloidal Stability of Aqueous Montmorillonite Suspensions." *Colloids and Surfaces, 49*, 71–80. Amsterdam, The Netherlands: Elsevier. TIC: 246046.

Torstenfelt, B.; Andersson, K.; and Allard, B. 1982. "Sorption of Strontium and Cesium on Rocks and Minerals." *Chemical Geology*, *36*, 128–137. Amsterdam, The Netherlands: Elsevier. TIC: 256583.

Turney, G.L. 1986. *Quality of Ground Water in the Columbia Basin, Washington, 1983*. Water-Resources Investigations Report 85-4320. Tacoma, Washington: U.S. Geological Survey. ACC: LLR.20070321.0001.

van Middlesworth, P.E. and Wood, S.A. 1998. "The Aqueous Geochemistry of the Rare Earth Elements and Yttrium. Part 7. REE, Th and U contents in Thermal Springs Associated with the Idaho Batholith." *Applied Geochemistry*, *13* (7), 861–884. New York, New York: Pergamon. TIC: 256470.

Vernaz, E. and Godon, N. 1992. "Leaching of Actinides from Nuclear Waste Glass: French Experience." *Scientific Basis for Nuclear Waste Management XV, Symposium held November 4–7, 1991, Strasbourg, France*. Sombret, C.G., ed. *257*, 37–48. Pittsburgh, Pennsylvania: Materials Research Society. TIC: 204618.

Wang, X.Y.; Wu, Y.S.; Zhang, L.; and Yu, Z.Y. 2001. "Atomic Force Microscopy and X-Ray Photoelectron Spectroscopy Study on the Passive Film for Type 316L Stainless Steel." *Corrosion Science, 57* (6), 540–546. Houston, Texas: NACE International. TIC: 259109.

White, A.F. and Brantley, S.L. 2003. "The Effect of Time on the Weathering of Silicate Minerals: Why Do Weathering Rates Differ in the Laboratory and Field?" *Chemical Geology*, *202* (3–4), 479–506. New York, New York: Elsevier. TIC: 255730.

Wilson, C.N. 1990a. *Results from NNWSI Series 2 Bare Fuel Dissolution Tests*. PNL-7169. Richland, Washington: Pacific Northwest Laboratory. ACC: NNA.19900814.0048.

Wilson, C.N. 1990b. *Results from NNWSI Series 3 Spent Fuel Dissolution Tests*. PNL-7170. Richland, Washington: Pacific Northwest Laboratory. ACC: NNA.19900329.0142.

Wolery, T.J. 1992. EQ3NR, *A Computer Program for Geochemical Aqueous Speciation-Solubility Calculations: Theoretical Manual, User's Guide, and Related Documentation (Version 7.0)*. UCRL-MA-110662 PT III. Livermore, California: Lawrence Livermore National Laboratory. ACC: 19980717.0626.

Wolery, T.J. and Daveler, S.A. 1992. *EQ6, A Computer Program for Reaction Path Modeling of Aqueous Geochemical Systems: Theoretical Manual, User's Guide, and Related Documentation (Version 7.0)*. UCRL-MA-110662 PT IV. Livermore, California: Lawrence Livermore National Laboratory. ACC: MOL.19980701.0459.

Wronkiewicz, D.J.; Bates, J.K.; Wolf, S.F.; and Buck, E.C. 1996. "Ten-Year Results from Unsaturated Drip Tests with UO_2 at 90°C: Implications for the Corrosion of Spent Nuclear Fuel." *Journal of Nuclear Materials*, *238* (1), 78–95. Amsterdam, The Netherlands: North-Holland. TIC: 243361.

Yui, M.; Azuma, J.; and Shibata, M. 1999. *JNC Thermodynamic Database for Performance Assessment of High-Level Radioactive Waste Disposal System*. JNC TN8400 99-070. Tokyo, Japan: Tokai Works, Japan Nuclear Cycle Development Institute. TIC: 251129.

Zarrabi, K.; McMillan, S.; Elkonz, S.; and Cizdziel, J. 2003. *Corrosion and Mass Transport Processes in Carbon Steel Miniature Waste Packages.* Document TR-03-003, Rev. 0. Task 34. Las Vegas, Nevada: University of Nevada, Las Vegas. ACC: MOL.20040202.0079.

Zheng, Z.; Wan, J.; Song, X.; and Tokunaga, T.K. 2006. "Sodium Meta-Autunite Colloids: Synthesis, Characterization, and Stability." *Colloids and Surfaces A: Physicochemical Engineering Aspects*, *274*, 48–55. New York, New York: Elsevier. TIC: 259203.

Zoitos, B.K.; Clark, D.E.; Lodding, A.R.; and Wicks, G.G. 1989. "Correlation of Laboratory and Stripa Field Leaching Studies." *Scientific Basis for Nuclear Waste Management XII, Symposium held October 10–13, 1988, Berlin, Germany.* Lutze, W. and Ewing, R.C., eds. *127*, 145–151. Pittsburgh, Pennsylvania: Materials Research Society. TIC: 203660.

INTENTIONALLY LEFT BLANK

Table 2.3.7-1. Included FEPs Addressed in Section 2.3.7

Number and FEP Name	Description	Summary of Technical Basis/Approach for FEP Inclusion
1.2.02.01.0A Fractures	Groundwater flow in the Yucca Mountain region and transport of any released radionuclides may take place along fractures. The rate of flow and the extent of transport in fractures are influenced by characteristics such as orientation, aperture, asperity, fracture length, connectivity, and the nature of any linings or infills.	The EBS-unsaturated zone interface domain is included beneath the invert domain to establish a boundary condition for calculating the diffusive flux from the invert to the unsaturated zone and to compute the radionuclide mass flux fraction going into each of the unsaturated zone fracture and matrix continua (Section 2.3.7.12.3).
2.1.01.01.0A Waste inventory	The waste inventory includes all potential sources of radio toxicity and chemical toxicity. It consists of the radionuclide inventory (typically in units of curies), by specific isotope, and the nonradionuclide inventory (typically in units of density or concentration), including chemical waste constituents. The radionuclide composition of the waste will vary due to initial enrichment, burn-up, the number of fuel assemblies per waste package, and the decay time subsequent to discharge of the fuel from the reactor.	Table 2.2-5 provides the screening decisions for FEPs related to radiotoxicity and chemical toxicity (3.3.06.00.0A and 3.3.07.00.0A). TSPA models three representative waste form inventories: commercial SNF, DOE SNF, and HLW (Section 2.3.7.3). Naval SNF is represented by commercial SNF (Section 2.3.7.4.1.1). More than 100 radionuclides (e.g., fission products, actinides, and activation products) are screened for importance to expected dose (Section 2.3.7.4.1.2). The abstraction is treated with uncertainty ranges for each waste form (Section 2.3.7.4.3).
2.1.01.02.0B Interactions between co-disposed waste	Codisposal refers to the disposal of different waste types within the same waste package. Codisposal might affect chemical interactions or radionuclide mobilization. At Yucca Mountain, the DOE SNF will be combined with HLW canisters within a waste package. This codisposal with HLW within a waste package is unique to the DOE SNF and does not apply to the commercial SNF placement within waste packages. The DOE SNF will be contained within canisters that will be placed within the waste packages. Some DOE SNF waste packages may contain only DOE SNF canisters, while others may contain both DOE SNF and HLW canisters.	The in-package chemistry model (Section 2.3.7.5) provides the interaction between codisposed wastes. The DOE SNF degradation is modeled as insensitive to in-package chemistry and is modeled as instantaneous. The degradation rate of HLW depends on pH, which in turn is dependent on all materials within the package. Degradation of HLW tends to raise the in-package pH while degradation of disposal canisters and other in-package metals tends to lower the pH. Degradation of DOE SNF and surface complexation on corrosion products tends to bring the pH back toward neutral.

Table 2.3.7-1. Included FEPs Addressed in Section 2.3.7 (Continued)

Number and FEP Name	Description	Summary of Technical Basis/Approach for FEP Inclusion
2.1.01.03.0A Heterogeneity of waste inventory	Commercial SNF, DOE SNF, and HLW shipped to the repository may contain quantities of radionuclides that vary from waste package to waste package, fuel assembly to fuel assembly, and canister to canister. The composition of each of these waste forms may vary due to initial uranium enrichment, possible plutonium enrichment, and fuel burnup, among other factors. The physical state within the waste form may also vary. For example, damaged fuel pellets or extremely high-burnup fuels may have greater surface area exposed to any water penetrating a waste package than undamaged, low-burnup SNF. Given these potential differences in isotopic composition and physical condition, the mass of radionuclides available for transport may vary significantly among waste packages. The different physical (structure, geometry), chemical, and radiological properties of the many forms of commercial SNF, DOE SNF, and HLW could result in differences in the corrosion and alteration rates based on waste package composition. This could affect repository chemistry, breach times, dissolution rates, and availability of radionuclides for transport.	TSPA considers the gross heterogeneity between the waste form types: commercial SNF, DOE SNF, and HLW. Radionuclide inventory and degradation rates for each waste form type are discussed (Sections 2.3.7.4, 2.3.7.6, 2.3.7.7, 2.3.7.8, and 2.3.7.9). In-package chemistries and radionuclide solubilities are defined for each waste package type: commercial SNF and codisposal (Section 2.3.7.5 and 2.3.7.10). Heterogeneity is acknowledged in uncertainty parameters in each of these models.
2.1.01.04.0A Repository-scale spatial heterogeneity of emplaced waste	Waste placed in Yucca Mountain will have physical, chemical, and radiological properties that will vary spatially, resulting in variation in the mass of radionuclides available for transport from different parts of the repository.	Waste form heterogeneity is addressed through several approaches: (1) the waste form physical, chemical, and radiological properties are addressed through the degradation models for the commercial SNF waste form (Section 2.3.7.7), the DOE SNF waste form (Section 2.3.7.8), and the HLW form (Section 2.3.7.9); (2) waste package radionuclide inventory heterogeneity is addressed through uncertainty parameters (Section 2.3.7.4); and (3) effects of waste package heterogeneity as a result of differing waste form contents is addressed in the in-package chemistry model (Section 2.3.7.5) and the multiscale thermal-hydrologic model (Section 2.3.5.4.1).

Table 2.3.7-1. Included FEPs Addressed in Section 2.3.7 (Continued)

Number and FEP Name	Description	Summary of Technical Basis/Approach for FEP Inclusion
2.1.02.01.0A DSNF degradation (alteration, dissolution, and radionuclide release)	DOE SNF to be disposed in Yucca Mountain contains a variety of fuel types that include metallic uranium fuels; oxide and mixed oxide fuels; Three Mile Island rubble; and heterogeneous fuels such as UAl_x, $U\text{-}ZrH_x$, and graphite fuels. In general, the composition and structure of these spent fuels are significantly different from commercial SNF, and the degradation, alteration, and dissolution may be different from the commercial SNF degradation. Processes to be considered in this FEP include alteration and dissolution of the various DOE SNF waste forms, phase separation, oxidation of spent fuels, leaching, and the effects of the high-integrity canister on DOE SNF degradation.	The degradation rate of DOE SNF except naval SNF is modeled in TSPA as instantaneous. Naval SNF is represented by commercial SNF (Section 2.3.7.8).
2.1.02.02.0A CSNF degradation (alteration, dissolution, and radionuclide release)	Alteration of the original commercial SNF mineralogy (under wet or dry conditions) and dissolution of the uranium-oxide matrix can influence the mobilization of radionuclides. The degradation of UO_2 could be affected by a number of variables, such as surface area, burnup, temperature, overall solution electrochemical potential (Eh), pH, and especially solutions containing significant concentrations of calcium, sodium, carbonate, and silicate ions, as well as availability of organic complexing materials. In turn, these water properties are affected by the alteration of the cladding, fuel matrix, and other waste package internals.	The model for commercial SNF degradation is described in Section 2.3.7.7.
2.1.02.03.0A HLW glass degradation (alteration, dissolution, and radionuclide release)	Glass waste forms are thermodynamically unstable over long time periods and will alter on contact with water. Radionuclides can be mobilized from the glass waste by a variety of processes, including degradation and alteration of the glass, phase separation, congruent dissolution, precipitation of silicates, coprecipitation of other minerals (including iron corrosion products), and selective leaching.	TSPA uses an empirical glass degradation rate model that is a function of surface area, temperature, and pH (Section 2.3.7.9.3).

Table 2.3.7-1. Included FEPs Addressed in Section 2.3.7 (Continued)

Number and FEP Name	Description	Summary of Technical Basis/Approach for FEP Inclusion
2.1.02.05.0A HLW glass cracking	Cracking of the HLW glass on cooling and during handling means that the surface area of the glass is greater than the surface area of a monolithic block. The increase in the surface area could affect the rate of glass alteration and radionuclide dissolution.	The increase in surface area due to cracking is included in the exposure factor, $f_{exposure}$ (Section 2.3.7.9.3). A range of values is applied to account for experimental evidence.
2.1.02.07.0A Radionuclide release from gap and grain boundaries	While in the reactor at high temperatures, radionuclides such as iodine and cesium may migrate and preferentially accumulate in cracks in the fuel matrix, grain boundaries of the UO_2, and in the gap between the fuel and cladding. After the waste package fails and the cladding perforates, the release rate of this fraction of the radionuclides could be rapid.	The fraction of cesium, iodine, technetium, and strontium that reside in the gap and grain boundaries are represented in TSPA by the instantaneous release fractions, f_i (Section 2.3.7.7.3.1). This fraction is released instantly upon breach of the waste package.
2.1.02.09.0A Chemical effects of void space in waste package	If waste packages and/or DOE SNF canisters are not completely filled, then the unfilled inert gas or air-filled volume could influence water-chemistry calculations.	Upon waste package breach, the inert gas escapes and is replaced with humid air. The reaction of this air with waste package internals and the resulting changes in water chemistry are modeled with the in-package chemistry model (Section 2.3.7.5.3.1).
2.1.02.12.0A Degradation of cladding prior to disposal	Certain aspects of cladding degradation may occur before the SNF arrives at Yucca Mountain. Possible mechanisms include rod cladding degradation during reactor operation, degradation during wet SNF pool storage, degradation during dry storage, and rod degradation during shipping (e.g., from creep, and from vibration and impact), and fuel handling.	The potential impacts of preclosure cladding failure are conservatively bounded by assuming all cladding is susceptible to failure upon breach by any mechanism (Section 2.3.7.6).
2.1.02.23.0A Cladding unzipping	In either dry or wet oxidizing conditions and with perforated fuel cladding, the UO_2 fuel can oxidize. The volume increase of the fuel as it oxidizes can create stresses in the cladding that may cause gross rupture of the fuel cladding (unzipping).	The maximum impacts of pre-disposal cladding failure are bounded by conservatively assuming that perforated cladding unzips rapidly. This means that once a waste package is breached, regardless of the mechanism, the commercial SNF waste form surface is exposed to the environment (whether vapor or liquid water) and can initiate degradation (Section 2.3.7.6).

Table 2.3.7-1. Included FEPs Addressed in Section 2.3.7 (Continued)

Number and FEP Name	Description	Summary of Technical Basis/Approach for FEP Inclusion
2.1.02.25.0B Naval SNF cladding	DOE SNF to be disposed of in Yucca Mountain has a variety of fuel types that may not be similar to the commercial SNF to be disposed. Some of the fuel types may have initial cladding-degradation characteristics that are different than those for the commercial SNF. Therefore, the effectiveness of DOE SNF cladding as a barrier to radionuclide mobilization might be different from commercial SNF. This FEP addresses naval SNF structure only.	Naval SNF cladding and SNF performance is discussed in Section 2.3.7 of the classified *Naval Nuclear Propulsion Program Technical Support Document for the License Application.* Waste packages containing naval SNF are conservatively modeled in TSPA as commercial SNF waste packages.
2.1.02.28.0A Grouping of DSNF waste types into categories	Several hundred distinct types of DOE SNF may potentially be stored in the repository. These represent many more types than can viably be examined for their individual effect on the repository. A limited number of representative or bounding degradation models must be selected and/or abstracted.	A bounding instantaneous degradation rate of all DOE SNF except naval SNF was used in TSPA (Section 2.3.7.8.3). Naval SNF is represented as commercial SNF.
2.1.03.11.0A Physical form of waste package and drip shield	The specific forms of the various drip shields, waste packages, and internal waste containers that are proposed for the Yucca Mountain repository can affect long-term performance. Waste package form may affect container strength through the shape and dimensions of the waste package and affect heat dissipation through waste package volume and surface area. Waste package and drip shield materials may affect physical and chemical behavior of the disposal area environment. Waste package and drip shield integrity will affect the releases of radionuclides from the disposal system. Waste packages may have both local effects and repository-scale effects. All types of waste packages and containers, including commercial SNF, DOE SNF, and DOE HLW, should be considered.	Effects of the physical form of waste packages and drip shields on long-term performance are included by considering several nominal waste package configurations. Two nominal waste package configurations are considered to represent the waste package configurations for commercial SNF, DOE-owned HLW and DOE-owned SNF (long and short waste packages) and Naval short and long packages (Section 2.3.7.5.3 and 2.3.7.12.3). They cover the range of waste package lengths and outer barrier thickness, and waste package diameters, and account for the majority of the waste package units.
2.1.06.06.0A Effects of drip shield on flow	The drip shield will affect the amount of water reaching the waste package. Effects of the drip shield on the disposal region environment (e.g., changes in relative humidity and temperature below the shield) should be considered for both intact and degraded conditions.	The EBS flow model accounts for the flow of water through and around the drip shield (Section 2.3.7.12.1). An algorithm referred to as the drip shield flux-splitting submodel is developed for calculating the fraction of flow diverted by the drip shield when breaches in the drip shield exist, and is directly included in TSPA.

Table 2.3.7-1. Included FEPs Addressed in Section 2.3.7 (Continued)

Number and FEP Name	Description	Summary of Technical Basis/Approach for FEP Inclusion
2.1.08.05.0A Flow through invert	The invert, a porous material consisting of crushed tuff, separates the waste package from the bottom of the drift. Flow and transport through and around the invert can influence radionuclide release to the unsaturated zone.	The EBS flow model explicitly models flow through the invert and the advective transport of radionuclides (Section 2.3.7.12). Flow through the invert consists of the fluxes diverted by the drip shield and waste package, the flux through the waste package, and the imbibition flux from the unsaturated zone. Each of these terms is accounted for in the EBS flow model, which is used directly in TSPA. The conceptual model for flow through the EBS assumes that water and radionuclides pass directly from the waste package to the invert.
2.1.08.06.0A Capillary effects (wicking) in EBS	Capillary rise, or wicking, is a potential mechanism for water to move through the waste and EBS.	Wicking of water from the host rock to the invert is accounted for in the EBS flow model through the prediction of the matrix saturation of the invert. Wicking is included in TSPA through water saturation, which is directly applied in the calculation of diffusion coefficient in both the waste package and the invert.
2.1.08.07.0A Unsaturated flow in the EBS	Unsaturated flow may occur along preferential pathways in the waste and EBS. Physical and chemical properties of the EBS and waste form, in both intact and degraded states, should be considered in evaluating pathways.	Unsaturated flow is implicit in the flow component of the EBS flow and transport model, in which no distinction is made between saturated and unsaturated flow (Section 2.3.7.12.3). Flow pathways that include the drip shield and waste package are modeled as quasi-steady state flows without regard to the detailed mechanisms of the flow. The calculated transport of radionuclides is bounded by fully saturated conditions, as modeled in the case of nonzero seepage flux. The output of these calculations is used as input in TSPA.
2.1.09.01.0A Chemical characteristics of water in drifts	When flow in the drifts is re-established following the peak thermal period, water may have chemical characteristics influenced by the near-field host rock and EBS. Specifically, the water chemistry (pH and dissolved species in the groundwater) may be affected by interactions with cementitious materials or steel used in the disposal region. These point source contaminated waters may coalesce to form a larger volume of contaminated water. This altered groundwater is referred to as the carrier plume because dissolution and transport will occur in this altered chemical environment as contaminants move through the EBS, and down into the unsaturated zone. (Note: there is no defining limit as to what volume of contaminated water constitutes a plume.)	The chemical composition of waters in the drift are estimated by considering a range of percolating fluid compositions, their respective interactions with minerals as they move toward the drift, and the degree to which they might be evaporatively modified in the drift (Section 2.3.5).

Table 2.3.7-1. Included FEPs Addressed in Section 2.3.7 (Continued)

Number and FEP Name	Description	Summary of Technical Basis/Approach for FEP Inclusion
2.1.09.01.0B Chemical characteristics of water in waste package	Chemical characteristics of the water in the waste packages (pH and dissolved species) may be affected by interactions with steel and other materials used in the waste packages or waste forms, as well as by the inflowing water from the drifts and near-field host rock. The in-package chemistry, in turn, may influence dissolution and transport as contaminants move through the waste, EBS, and down into the unsaturated zone.	The in-package chemistry is determined by the reaction of incoming water and air with the waste forms and metals within the waste package (Section 2.3.7.5).
2.1.09.02.0A Chemical interaction with corrosion products	Corrosion products produced during degradation of the waste form, metallic portions of the waste package, and metals in the drift (e.g., rock bolts, steel in the invert, gantry rails) may affect the mobilization and transport of radionuclides. Corrosion products may facilitate sorption/desorption and coprecipitation/dissolution processes. Corrosion products may form a “rind” around the fuel that could (1) restrict the availability of water for dissolution of radionuclides or (2) inhibit advective or diffusive transport of water and radionuclides from the waste form to the EBS. Corrosion products also have the potential to retard the transport of radionuclides to the EBS. Finally, corrosion products may alter the local chemistry, possibly enhancing dissolution rates for specific waste forms, or altering radionuclide solubility.	The chemical influence of corrosion products inside the package is modeled in the EBS transport abstraction (Section 2.3.7.12). Corrosion products also provide the diffusive pathway for radionuclide release from the waste form to the invert (Section 2.3.7.12.3). Sorption of radionuclides onto corrosion products will retard radionuclide migration (Section 2.3.7.12.3), while sorption onto corrosion product colloids may facilitate migration (Section 2.3.7.11).
2.1.09.04.0A Radionuclide solubility, solubility limits, and speciation in the waste form and EBS	Degradation of the waste form will mobilize radionuclides in the aqueous phase. Factors to be considered in this FEP include the initial radionuclide inventory, justification of the limited inventory included in evaluations of aqueous concentrations, and the solubility limits for those radionuclides.	In the TSPA model, inventory concentrations of radioactive elements released from the waste forms (commercial SNF, DOE SNF, and HLW glass) are calculated according to the dissolution or degradation rates of waste forms and the volume of water within the (breached) waste package and radionuclide inventory. Then the radioelement concentrations are compared against their solubility limits (Section 2.3.7.10.3). If the concentration is greater than its solubility limit, then the amount of that radioactive element in excess of the solubility limit will be kept in the inventory, potentially available for transport at a later time.

Table 2.3.7-1. Included FEPs Addressed in Section 2.3.7 (Continued)

Number and FEP Name	Description	Summary of Technical Basis/Approach for FEP Inclusion
2.1.09.05.0A Sorption of dissolved radionuclides in EBS	Sorption of dissolved radionuclides within the waste package may affect the aqueous concentrations of radionuclides released to the EBS.	Sorption of dissolved radionuclides in the EBS is captured through a linear isotherm submodel relating the mass concentration of a radionuclide component in a solid phase to the dissolved concentration of the same component in a contacting phase (Section 2.3.7.12.3). This submodel accounts for sorption of radionuclides onto corrosion products in the waste package and the crushed tuff invert. The proportionality constant in this submodel is the distribution coefficient (K_d), which is uncertain, and which has been used to build a competitive surface complexation model. The competitive surface complexation model is used as input to the radionuclide transport calculation in the TSPA. Sorption retards the transport of radionuclides through the EBS and thus has a direct impact on estimated releases of radionuclides from the EBS.
2.1.09.06.0A Reduction-oxidation potential in waste package	The redox potential in the waste package influences the oxidation of waste-form materials and the in-package solubility of radionuclide species. Local variations in the in-package redox potential can occur.	As long as there are reduced fuels and metals within the breached waste package, there will be strong redox gradients between them and the atmosphere, providing the driving force for the reactions calculated in the in-package chemistry model. The in-package chemistry model uses the bounding approximation that the bulk water within the package is in equilibrium with the atmosphere. (Section 2.3.7.5.3).
2.1.09.07.0A Reaction kinetics in waste package	Chemical reactions, such as radionuclide dissolution/precipitation reactions and reactions controlling the reduction–oxidation state, may not be at equilibrium within the waste package.	The in-package chemistry model calculates the resulting pH and ionic strength from the reaction of metals and waste forms with air and water within the package (Section 2.3.7.5.3).
2.1.09.08.0A Diffusion of dissolved radionuclides in EBS	Radionuclide transport of dissolved radionuclides by diffusion, in response to chemical gradients, may occur within the EBS. Physical and chemical properties of the EBS and waste form, in both intact and degraded states, should be considered in evaluating diffusive transport.	Diffusive transport of dissolved radionuclides in the EBS is a major component of the EBS transport model (Section 2.3.7.12.3). Uncertainty in diffusive transport is incorporated via parameters for invert diffusion coefficient uncertainty, stainless steel and carbon steel corrosion rates, diffusive path length through corrosion products inside a waste package, and the specific surface area of Fe_2O_3 corrosion products. These parameters are sampled in TSPA, and the model for diffusive transport of radionuclides is implemented directly in TSPA.

Table 2.3.7-1. Included FEPs Addressed in Section 2.3.7 (Continued)

Number and FEP Name	Description	Summary of Technical Basis/Approach for FEP Inclusion
2.1.09.08.0B Advection of dissolved radionuclides in EBS	Radionuclide transport of dissolved radionuclides by advection with the flowing groundwater may occur within the EBS. Physical and chemical properties of the EBS and waste form, in both intact and degraded states, should be considered in evaluating advective transport.	Advective transport, which depends on the fluxes through breaches in the drip shield and waste package, is directly included in TSPA (Section 2.3.7.12.3). The flux splitting submodel determines the fraction of the seepage flux that flows through the waste package.
2.1.09.16.0A Formation of pseudo-colloids (natural) in EBS	Pseudocolloids are colloid-sized assemblages (between approximately 1 nm and 1 μm in diameter) of nonradioactive material that have radionuclides bound or sorbed to them. Natural pseudocolloids include microbial colloids, mineral fragments (e.g., clay, silica, iron oxyhydroxides), and humic and fulvic acids. This FEP addresses radionuclide-bearing pseudocolloids formed from host-rock materials and all interactions of the waste and EBS with the host rock environment except corrosion.	Seepage water colloids included in the colloid model are modeled with reversible radionuclide attachment using linear sorption coefficients K_d. (Section 2.3.7.11.3).
2.1.09.17.0A Formation of pseudo-colloids (corrosion product) in EBS	Pseudocolloids are colloid-sized assemblages (between approximately 1 nm and 1 μm in diameter) of nonradioactive material that have radionuclides bound or sorbed to them. Corrosion product pseudocolloids include iron oxyhydroxides from corrosion and degradation of the metals in the EBS, and silica from degradation of cementitious materials.	Corrosion product colloids included in the colloid model are modeled with both reversible and irreversible radionuclide attachments (Section 2.3.7.12.3.2).
2.1.09.19.0B Advection of colloids in EBS	Transport of radionuclide-bearing colloids in the waste and EBS may occur by advection.	Advective transport of radionuclide-bearing colloids in the EBS is determined in the EBS transport model (Section 2.3.7.12.3). The advective transport moves colloids (and the associated radionuclides) at about the same velocity as the liquid flux through the EBS. The concentration of colloids in EBS components, together with the water flow rates through each component, determines the rate of advective releases of colloids from the EBS.

Table 2.3.7-1. Included FEPs Addressed in Section 2.3.7 (Continued)

Number and FEP Name	Description	Summary of Technical Basis/Approach for FEP Inclusion
2.1.09.23.0A Stability of colloids in EBS	For radionuclide-bearing colloids to affect repository performance, they must remain suspended in the groundwater (i.e., be stable) for time scales that are long relative to the time required for groundwater travel. Further, they must carry significant concentrations of radionuclides. The stability of smectite colloids (applicable for natural groundwater colloids and waste-form colloids) is determined primarily by ionic strength but also to an extent by pH. The stability of iron-(hydr)oxide colloids (applicable to corrosion-product colloids) is determined by both ionic strength and pH.	The stability of smectite colloids, which is applicable for the repository groundwater colloids and waste form colloids, is determined primarily by ionic strength but also to an extent by pH. The stability of iron-(hydr)oxide colloids, which is applicable to corrosion-product colloids, is determined by both ionic strength and pH (Section 2.3.7.11.3).
2.1.09.24.0A Diffusion of colloids in EBS	Colloidal particles, together with any associated actinides, that are sufficiently small may be transported through the EBS by diffusion.	The colloid-facilitated diffusive transport and its implementation in TSPA are described in Section 2.3.7.12.3. The concentration of colloids in each region of the EBS, specifically in the waste form, the waste package corrosion products, and the invert, is determined in part by the local chemical environment.
2.1.09.25.0A Formation of colloids (waste-form) by co-precipitation in EBS	Dissolved radionuclides and other ions may coprecipitate to form colloids. Coprecipitates may consist of radionuclides bound in the crystal lattice of a dominating mineral phase or may consist of radionuclides engulfed by a dominating mineral phase.	Colloids formed from the corrosion of HLW glass were found to contain embedded radionuclide-carrying phases (Sections 2.3.7.11.2.1 and 2.3.7.11.3.2). These radionuclides are modeled as irreversibly attached to the colloids.
2.1.11.08.0A Thermal effects on chemistry and microbial activity in the EBS	Temperature changes may affect chemical and microbial processes in the waste and EBS.	Test data show that the reaction rates for commercial SNF (Section 2.3.7.7) and HLW glass (Section 2.3.7.9) degradation are temperature dependent. Temperature dependence was included in both models. Temperature effects on individual radionuclide solubilities were conservatively omitted or bounded.
2.2.07.06.0B Long-term release of radionuclides from the repository	The release of radionuclides from the repository may occur over a long period of time, as a result of the timing and magnitude of the waste packages and drip shield failures, waste form degradation, and radionuclide transport through the invert.	The TSPA model imposes no restrictions or conditions on the duration of radionuclide transport. TSPA models the timing and magnitude of the waste package and drip shield breaches, waste form degradation, and radionuclide transport through the invert (Sections 2.3.6 and 2.3.7).

Table 2.3.7-1. Included FEPs Addressed in Section 2.3.7 (Continued)

Number and FEP Name	Description	Summary of Technical Basis/Approach for FEP Inclusion
2.2.08.12.0B Chemistry of water flowing into the waste package	Inflowing water chemistry may be used in analysis or modeling that requires initial water chemistry in the waste package.	Three different initial water compositions were used to represent the chemistry of the water flowing into the waste package. This inflowing water chemistry is one of the inputs used to determine the in-package chemistry (Section 2.3.7.5.3.2).
3.1.01.01.0A Radioactive decay and ingrowth	Radioactivity is the spontaneous disintegration of an unstable atomic nucleus that results in the emission of subatomic particles. Radioactive species (isotopes) of a given element are known as radionuclides. Radioactive decay of the fuel in the repository changes the radionuclide content in the fuel with time and generates heat. Radionuclide quantities in the system at any time are the result of the radioactive decay and the ingrowth of decay products as a consequence of that decay. Over a 10,000-year performance period, these processes will produce decay products that need to be considered in order to adequately evaluate the release and transport of radionuclides to the accessible environment.	Radioactive decay and ingrowth were considered in screening which radionuclides to include in the TSPA (Section 2.3.7.4). The TSPA accounts for decay and ingrowth in the EBS using built-in functions of GoldSim. During execution, the GoldSim model automatically calculates decay and ingrowth of the included isotopes.

Table 2.3.7-2. Results of the Screening Analysis

Radionuclide	Scenario Classes with Groundwater Transport		Igneous Eruptive Modeling Case	
	10^2 years to 10^4 years	**10^4 years to 10^6 years**	**10^2 years to 10^4 years**	**10^4 years to 10^6 years**
^{227}Ac	—	**^{227}Ac**	—	**^{227}Ac**
^{241}Am	^{241}Am	—	^{241}Am	—
^{243}Am	^{243}Am	^{243}Am	^{243}Am	^{243}Am
^{14}C	^{14}C	^{14}C	—	—
^{36}Cl	^{36}Cl	^{36}Cl	—	—
^{245}Cm	Added to ensure that the effect of its decay on the inventory of ^{241}Am are included			
^{135}Cs	^{135}Cs	^{135}Cs	—	—
^{137}Cs	^{137}Cs	—	^{137}Cs	—
^{129}I	^{129}I	^{129}I	—	^{129}I
^{237}Np	^{237}Np	^{237}Np	—	^{237}Np
^{231}Pa	^{231}Pa	^{231}Pa	—	^{231}Pa
^{210}Pb	—	^{210}Pb	—	^{210}Pb
^{238}Pu	^{238}Pu	—	^{238}Pu	—
^{239}Pu	^{239}Pu	^{239}Pu	^{239}Pu	^{239}Pu
^{240}Pu	^{240}Pu	^{240}Pu	^{240}Pu	^{240}Pu
^{241}Pu	Added to ensure that the effect of its decay on the inventory of ^{241}Am and ^{237}Np are included			
^{242}Pu	—	^{242}Pu	—	^{242}Pu
^{226}Ra	—	^{226}Ra	—	^{226}Ra
^{228}Ra	—	^{228}Ra	—	^{228}Ra
^{79}Se	^{79}Se	^{79}Se	—	–
^{126}Sn	^{126}Sn	^{126}Sn	^{126}Sn	^{126}Sn
^{90}Sr	^{90}Sr	—	^{90}Sr	—
^{99}Tc	^{99}Tc	^{99}Tc	—	^{99}Tc
^{229}Th	^{229}Th	^{229}Th	^{229}Th	^{229}Th
^{230}Th	—	^{230}Th	—	^{230}Th
^{232}Th	—	^{232}Th	—	^{232}Th
^{232}U	^{232}U	^{232}U	—	—

Table 2.3.7-2. Results of the Screening Analysis (Continued)

Radionuclide	Scenario Classes with Groundwater Transport		Igneous Eruptive Modeling Case	
	10^2 years to 10^4 years	**10^4 years to 10^6 years**	**10^2 years to 10^4 years**	**10^4 years to 10^6 years**
^{233}U	^{233}U	^{233}U	^{233}U	^{233}U
^{234}U	^{234}U	^{234}U	^{234}U	^{234}U
^{235}U	—	^{235}U	—	—
^{236}U	^{236}U	^{236}U	—	—
^{238}U	^{238}U	^{238}U	—	^{238}U
Isotopes	32		25	
Elements	18		15	

NOTE: The counts in the last two rows include ^{245}Cm and ^{241}Pu.

Source: SNL 2007b, Table 7-1.

Table 2.3.7-3. Nominal Initial Radionuclide Inventory for Each Waste Form

Radionuclide	Grams per Waste Package		
	Commercial SNF	DOE SNF	HLW
^{227}Ac	2.47×10^{-6}	1.22×10^{-3}	1.91×10^{-4}
^{241}Am	8.18×10^{3}	2.18×10^{2}	3.75×10^{1}
^{243}Am	1.24×10^{3}	6.73×10^{0}	5.75×10^{-1}
^{14}C	1.35×10^{0}	1.81×10^{0}	0
^{36}Cl	3.23×10^{0}	4.23×10^{0}	0
^{245}Cm	1.75×10^{1}	9.25×10^{-2}	5.43×10^{-2}
^{135}Cs	4.36×10^{3}	9.74×10^{1}	1.27×10^{2}
^{137}Cs	5.90×10^{3}	9.72×10^{1}	3.02×10^{2}
^{129}I	1.73×10^{3}	3.56×10^{1}	7.27×10^{1}
^{237}Np	4.57×10^{3}	8.14×10^{1}	9.95×10^{1}
^{231}Pa	9.17×10^{-3}	2.14×10^{0}	1.53×10^{0}
^{210}Pb	0	3.35×10^{-7}	3.40×10^{-10}
^{238}Pu	1.52×10^{3}	1.25×10^{1}	3.91×10^{1}
^{239}Pu	4.32×10^{4}	2.21×10^{3}	5.58×10^{2}
^{240}Pu	2.05×10^{4}	4.35×10^{2}	4.61×10^{1}
^{241}Pu	2.66×10^{3}	2.92×10^{1}	1.22×10^{0}
^{242}Pu	5.28×10^{3}	3.02×10^{1}	3.89×10^{0}
^{226}Ra	0	4.57×10^{-5}	2.42×10^{-5}
^{228}Ra	0	1.51×10^{-5}	6.00×10^{-6}
^{79}Se	4.19×10^{1}	6.82×10^{0}	7.01×10^{0}
^{126}Sn	4.63×10^{2}	9.40×10^{0}	1.70×10^{1}
^{90}Sr	2.49×10^{3}	5.22×10^{1}	1.74×10^{2}
^{99}Tc	7.55×10^{3}	1.58×10^{2}	1.01×10^{3}
^{229}Th	0	3.24×10^{-1}	3.30×10^{-3}
^{230}Th	1.52×10^{-1}	1.18×10^{-1}	8.12×10^{-4}
^{232}Th	0	2.17×10^{4}	2.98×10^{4}
^{232}U	1.02×10^{-2}	1.28×10^{0}	4.08×10^{-4}
^{233}U	5.76×10^{-2}	5.38×10^{2}	1.94×10^{1}

Table 2.3.7-3. Nominal Initial Radionuclide Inventory for Each Waste Form (Continued)

Radionuclide	Grams per Waste Package		
	Commercial SNF	**DOE SNF**	**HLW**
^{234}U	1.75×10^{3}	4.73×10^{2}	2.33×10^{1}
^{235}U	6.26×10^{4}	2.51×10^{4}	1.41×10^{3}
^{236}U	3.84×10^{4}	1.25×10^{3}	5.99×10^{1}
^{238}U	7.82×10^{6}	6.84×10^{5}	2.37×10^{5}

NOTE: The commercial SNF quantities are those at 2067, and the DOE SNF and HLW quantities are those at 2030.

Source: SNL 2007d, Table 7-1[a].

Table 2.3.7-4. Nominal Initial Radionuclide Inventories for MOX and LaBS HLW

Radionuclide	Grams Added per Commercial SNF Waste Package	Grams Added per Codisposal Waste Package
^{227}Ac	1.11×10^{-10}	0
^{241}Am	1.90×10^{1}	2.78×10^{1}
^{243}Am	4.82×10^{1}	0
^{14}C	2.52×10^{-2}	0
^{36}Cl	2.42×10^{-7}	0
^{245}Cm	1.36×10^{0}	0
^{135}Cs	7.00×10^{1}	0
^{137}Cs	1.64×10^{2}	0
^{129}I	3.02×10^{1}	0
^{237}Np	1.44×10^{1}	4.77×10^{-1}
^{231}Pa	3.99×10^{-6}	0
^{210}Pb	1.13×10^{-12}	0
^{238}Pu	1.46×10^{1}	3.43×10^{0}
^{239}Pu	1.00×10^{3}	3.48×10^{3}
^{240}Pu	7.09×10^{2}	3.10×10^{2}
^{241}Pu	4.20×10^{2}	1.26×10^{1}
^{242}Pu	1.79×10^{2}	6.09×10^{0}
^{226}Ra	8.79×10^{-11}	0
^{228}Ra	5.89×10^{-17}	0
^{79}Se	5.30×10^{-1}	0
^{126}Sn	1.13×10^{1}	0
^{90}Sr	3.57×10^{1}	0
^{99}Tc	9.75×10^{1}	0
^{229}Th	2.68×10^{-9}	0
^{230}Th	4.29×10^{-6}	0
^{232}Th	1.15×10^{-6}	1.56×10^{1}
^{232}U	9.85×10^{-6}	0
^{233}U	2.28×10^{-5}	0
^{234}U	8.91×10^{-1}	4.24×10^{0}

Table 2.3.7-4. Nominal Initial Radionuclide Inventories for MOX and LaBS HLW (Continued)

Radionuclide	Grams Added per Commercial SNF Waste Package	Grams Added per Codisposal Waste Package
^{235}U	5.48×10^{1}	2.61×10^{2}
^{236}U	2.18×10^{1}	0
^{238}U	7.99×10^{4}	8.58×10^{2}

NOTE: The MOX quantities are those at 2035, and the LaBS HLW quantities are those at 2003.

Source: SNL 2007d, Table 7-1[a].

Table 2.3.7-5. Initial Radionuclide Inventories and Initial Radionuclide Activities Per Waste Package Type in the TSPA Model

Per Waste Package Inventory and Activity at Closure, 2117							
Radionuclide	**Specific Activity Ci/g**	**Commercial SNF w/ Mixed Oxide added, g/pkg**	**Commercial SNF w/Mixed Oxide added, Ci/pkg**	**DOE SNF, g/pkg**	**DOE SNF, Ci/pkg**	**HLW w/LaBS added, g/pkg**	**HLW w/LaBS added, Ci/pkg**
^{227}Ac	7.22×10^{1}	6.27×10^{-6}	4.53×10^{-4}	1.39×10^{-3}	1.00×10^{-1}	9.47×10^{-4}	6.84×10^{-2}
^{241}Am	3.43	1.02×10^{4}	3.51×10^{4}	2.15×10^{2}	7.37×10^{2}	6.77×10^{1}	2.32×10^{2}
^{243}Am	2.00×10^{-1}	1.28×10^{3}	2.56×10^{2}	6.68	1.34	5.70×10^{-1}	1.14×10^{-1}
^{14}C	4.46	1.37	6.09	1.79	7.98	0.00	0.00
^{36}Cl	3.30×10^{-2}	3.23	1.07×10^{-1}	4.23	1.40×10^{-1}	0.00	0.00
^{245}Cm	1.72×10^{-1}	1.88×10^{1}	3.23	9.18×10^{-2}	1.58×10^{-2}	5.39×10^{-2}	9.27×10^{-3}
^{135}Cs	1.15×10^{-3}	4.43×10^{3}	5.09	9.74×10^{1}	1.12×10^{-1}	1.27×10^{2}	1.46×10^{-1}
^{137}Cs	8.67×10^{1}	1.88×10^{3}	1.63×10^{5}	1.31×10^{1}	1.14×10^{3}	4.07×10^{1}	3.53×10^{3}
^{129}I	1.77×10^{-4}	1.76×10^{3}	3.12×10^{-1}	3.56×10^{1}	6.30×10^{-3}	7.27×10^{1}	1.29×10^{-2}
^{237}Np	7.05×10^{-4}	5.38×10^{3}	3.79	1.12×10^{2}	7.90×10^{-2}	1.11×10^{2}	7.81×10^{-2}
^{231}Pa	4.72×10^{-2}	1.22×10^{-2}	5.76×10^{-4}	2.14	1.01×10^{-1}	1.53	7.22×10^{-2}
^{238}Pu	1.71×10^{1}	1.03×10^{3}	1.76×10^{4}	6.28	1.07×10^{2}	2.10×10^{1}	3.59×10^{2}
^{239}Pu	6.21×10^{-2}	4.41×10^{4}	2.74×10^{3}	2.20×10^{3}	1.37×10^{2}	4.03×10^{3}	2.50×10^{2}
^{240}Pu	2.27×10^{-1}	2.11×10^{4}	4.79×10^{3}	4.31×10^{2}	9.78×10^{1}	3.52×10^{2}	7.98×10^{1}
^{241}Pu	1.03×10^{2}	2.48×10^{2}	2.56×10^{4}	4.49×10^{-1}	4.62×10^{1}	7.22×10^{-2}	7.44
^{242}Pu	3.94×10^{-3}	5.46×10^{3}	2.15×10^{1}	3.02×10^{1}	1.19×10^{-1}	9.98	3.93×10^{-2}
^{226}Ra	9.89×10^{-1}	1.29×10^{-4}	1.28×10^{-4}	1.80×10^{-4}	1.78×10^{-4}	2.76×10^{-5}	2.73×10^{-5}
^{228}Ra	2.72×10^{2}	1.90×10^{-11}	5.17×10^{-9}	8.77×10^{-6}	2.39×10^{-3}	1.20×10^{-5}	3.27×10^{-3}

Table 2.3.7-5. Initial Radionuclide Inventories and Initial Radionuclide Activities Per Waste Package Type in the TSPA Model (Continued)

Per Waste Package Inventory and Activity at Closure, 2117							
Radionuclide	**Specific Activity Ci/g**	**Commercial SNF w/ Mixed Oxide added, g/pkg**	**Commercial SNF w/Mixed Oxide added, Ci/pkg**	**DOE SNF, g/pkg**	**DOE SNF, Ci/pkg**	**HLW w/LaBS added, g/pkg**	**HLW w/LaBS added, Ci/pkg**
^{79}Se	1.53×10^{-2}	4.24×10^{1}	6.49×10^{-1}	6.82	1.04×10^{-1}	7.01	1.07×10^{-1}
^{126}Sn	1.13×10^{-2}	4.74×10^{2}	5.36	9.40	1.06×10^{-1}	1.70×10^{1}	1.92×10^{-1}
^{90}Sr	1.38×10^{2}	7.51×10^{2}	1.04×10^{5}	6.43	8.87×10^{2}	2.14×10^{1}	2.95×10^{3}
^{99}Tc	1.70×10^{-2}	7.65×10^{3}	1.30×10^{2}	1.58×10^{2}	2.69	1.01×10^{3}	1.72×10^{1}
^{229}Th	2.14×10^{-1}	2.08×10^{-5}	4.46×10^{-6}	5.22×10^{-1}	1.12×10^{-1}	1.05×10^{-2}	2.25×10^{-3}
^{230}Th	2.06×10^{-2}	4.33×10^{-1}	8.92×10^{-3}	2.33×10^{-1}	4.80×10^{-3}	1.07×10^{-2}	2.21×10^{-4}
^{232}Th	1.10×10^{-7}	5.64×10^{-2}	6.20×10^{-9}	2.17×10^{4}	2.39×10^{-3}	2.98×10^{4}	3.28×10^{-3}
^{232}U	2.21×10^{1}	6.20×10^{-3}	1.37×10^{-1}	5.39×10^{-1}	1.19×10^{1}	1.72×10^{-4}	3.80×10^{-3}
^{233}U	9.65×10^{-3}	1.38×10^{-1}	1.33×10^{-3}	5.38×10^{2}	5.19	1.94×10^{1}	1.87×10^{-1}
^{234}U	6.21×10^{-3}	2.25×10^{3}	1.40×10^{1}	4.79×10^{2}	2.97	4.86×10^{1}	3.02×10^{-1}
^{235}U	2.16×10^{-6}	6.28×10^{4}	1.36×10^{-1}	2.51×10^{4}	5.42×10^{-2}	1.68×10^{3}	3.63×10^{-3}
^{236}U	6.47×10^{-5}	3.85×10^{4}	2.49	1.25×10^{3}	8.09×10^{-2}	6.40×10^{1}	4.14×10^{-3}
^{238}U	3.36×10^{-7}	7.90×10^{6}	2.65	6.84×10^{5}	2.30×10^{-1}	2.38×10^{5}	7.99×10^{-2}

NOTE: There is no line for ^{210}Pb, which is screened in, because the biological effect of that radionuclide is included in the effect of its parent radionuclide.

Source: SNL 2008, Table 6.3.7-5

Table 2.3.7-6. Uncertainty Multipliers for the Initial Radionuclide Inventory for Each Waste Form Type

	Commercial SNF	**DOE SNF**	**HLW**
Isotopes	All except ^{238}U	All except ^{238}U	All
Distribution	Uniform	Triangular	Triangular
Minimum	0.85	0.45	0.70
Best Estimate	NA	0.62	1
Maximum	1.40	2.90	1.5

NOTE: NA = not applicable.

Source: SNL 2007d, Table 7-2.

Table 2.3.7-7. Estimated Curies Per Canister for Savannah River Site Batches (Year 2030)

	Batch 1A	Batch 1B	Batches 2 and 3	Batches 4 to 10
^{227}Ac	6.4196×10^{-8}	4.6920×10^{-8}	8.5283×10^{-8}	6.8448×10^{-8}
^{241}Am	4.1273	4.5983	2.2002×10^{1}	7.1435×10^{1}
^{243}Am	2.3323×10^{-2}	3.5501×10^{-2}	3.6707×10^{-1}	4.2980×10^{-9}
^{14}C	—	—	—	—
^{36}Cl	—	—	—	—
^{245}Cm	3.4999×10^{-4}	—	2.6618×10^{-3}	6.1466×10^{-3}
^{135}Cs	3.2400×10^{-4}	5.1600×10^{-4}	7.4399×10^{-4}	1.2400×10^{-1}
^{137}Cs	1.7272×10^{1}	4.5063×10^{1}	1.0212×10^{2}	1.7020×10^{4}
^{129}I	—	7.2900×10^{-5}	5.2200×10^{-6}	—
^{237}Np	8.6761×10^{-3}	1.0542×10^{-2}	9.3651×10^{-3}	2.1704×10^{-2}
^{231}Pa	1.6097×10^{-7}	1.3325×10^{-7}	2.5896×10^{-7}	2.0920×10^{-7}
^{210}Pb	1.1539×10^{-8}	4.4721×10^{-8}	8.1881×10^{-9}	7.7802×10^{-9}
^{238}Pu	2.7255×10^{1}	4.6471×10^{1}	2.1417×10^{1}	5.4948×10^{2}
^{239}Pu	4.1858	3.3772	5.2864	1.1291×10^{1}
^{240}Pu	1.1210	1.1747	1.6894	5.3319
^{241}Pu	3.6146	6.8403	5.2572	9.6093×10^{1}
^{242}Pu	9.8616×10^{-4}	1.9614×10^{-3}	3.1613×10^{-3}	1.1502×10^{-2}
^{226}Ra	4.1214×10^{-8}	1.4139×10^{-7}	3.5806×10^{-8}	3.8956×10^{-8}
^{228}Ra	6.9194×10^{-13}	1.1175×10^{-4}	2.4904×10^{-5}	9.0666×10^{-4}
^{79}Se	6.7775×10^{-3}	5.8681×10^{-2}	4.3088×10^{-2}	—
^{126}Sn	4.0090×10^{-3}	2.3095×10^{-2}	3.0894×10^{-2}	—
^{90}Sr	1.6010×10^{2}	1.2159×10^{3}	1.6155×10^{3}	1.4104×10^{4}
^{99}Tc	1.3598×10^{-1}	1.2399×10^{-1}	8.6792×10^{-2}	7.8193
^{229}Th	1.3297×10^{-4}	1.7108×10^{-4}	1.8785×10^{-5}	8.3143×10^{-5}
^{230}Th	5.5935×10^{-6}	1.4574×10^{-5}	6.2142×10^{-6}	8.6012×10^{-6}
^{232}Th	9.0127×10^{-13}	1.1500×10^{-4}	2.5900×10^{-5}	9.4400×10^{-4}
^{232}U	—	—	—	1.2826×10^{-4}
^{233}U	1.5999×10^{-2}	3.0197×10^{-2}	7.3702×10^{-3}	3.2899×10^{-2}
^{234}U	1.9137×10^{-2}	2.7487×10^{-2}	2.6428×10^{-2}	5.8085×10^{-2}

Table 2.3.7-7. Estimated Curies Per Canister for Savannah River Site Batches (Year 2030) (Continued)

	Batch 1A	Batch 1B	Batches 2 and 3	Batches 4 to 10
^{235}U	2.1615×10^{-4}	2.1310×10^{-4}	4.5314×10^{-4}	3.6930×10^{-4}
^{236}U	5.1916×10^{-4}	7.3003×10^{-4}	6.5233×10^{-4}	1.5442×10^{-3}
^{238}U	6.7800×10^{-3}	5.3300×10^{-3}	1.7400×10^{-2}	1.6500×10^{-2}
Number of Canisters	**495**	**726**	**705**	**3,134**

NOTE: The five significant figures shown in this table are the same as the source document. This level of precision should not be taken as an uncertainty estimate; uncertainties are presented in Table 2.3.7-6.

Source: SNL 2007d, Section 4.1, Table 4-9.

Table 2.3.7-8. Hanford HLW Canister Production Estimates for Alternative Canister Waste Loading and Canister Fill Levels

Canister Fill Scenario	Canister (Percent Fill)	Canister Glass Volume (m^3)	Number of Canisters		
			Program Case	Planning Case	Technology Case
Maximum Canister Fill	100	1.19	11,484	8,744	7,071
Contract Fill	95	1.14	12,085	9,202	7,442
Minimum Canister Fill	87	1.04	13,205	10,054	8,131

Source: SNL 2007d, Table 4-11.

Table 2.3.7-9. Yucca Mountain Pore Water Compositions

Parameter	Units	SD9	T17	P35	P33
Ca	mg/L	19	62	59.9	97
Mg	mg/L	0.7	7.9	16.7	17.4
Na	mg/L	59	45	123	62
K	mg/L	4.8	14.4	13.8	9
SiO_2	mg/L	42	52	Not measured	75
NO_3	mg/L	16	44	57.4	10
HCO_3	mg/L	142	126	149	Not measured
Cl	mg/L	23	67	146	123
F	mg/L	2.2	1.4	1.3	0.76
SO_4	mg/L	16	82	126	120
pH	pH	8.2	7.7	Not measured	8.31

Source: SNL 2007e, Table 4-2[a].

Table 2.3.7-10. A Basalt Groundwater Sample (SP 01) from Iceland

Parameter	Units	BI
Na	ppm	15.8
SiO_2	ppm	18.1
Ca	ppm	4.35
K	ppm	1.11
Mg	ppm	2.44
F	ppm	0.28
Cl	ppm	2.30
C	ppm as CO_2	35.6
SO_4	ppm	8.6
pH	Standard units	9.00
Temperature	Celsius	4.4

NOTE: ppm = parts per million.

Source: Gislason and Eugster 1987, Table 3

Table 2.3.7-11. Two Basalt Water Compositions from the Columbia Basin, Washington

Parameter	Unite	BW	BS
pH	Standard units	8.6	8.0
Temperature	Celsius	25.9	17.7
Ca	mg/L	3.9	36
Mg	mg/L	0.5	21
Na	mg/L	76	22
K	mg/L	8.0	6.4
HCO_3	mg/L	166	193
SO_4	mg/L	21	55
Cl	mg/L	13	17
F	mg/L	1.9	0.4
SiO_2	mg/L	73	58
$NO_2 + NO_3$	mg/L as N	< 0.1[a]	2.0

NOTE: [a]One half of the detection limit is used in the simulations.

Source: BW: Sample19/31E-27G01D1 from Wanapum/Grande Ronde formations (Turney 1986, pp. 49 to 53). BS: Sample 14/31E-19B01 from Saddle Mountain/Wanapum formations (Turney 1986, pp. 74 to 78).

Table 2.3.7-12. Triangular Probability Distribution Functions of Instantaneous Release Fraction (%)

	^{137}Cs	^{129}I	^{99}Tc	^{90}Sr
Apex	3.63	11.24	0.10[a]	0.09
Minimum	0.39	2.04	0.01[b]	0.02
Maximum	11.06	26.75	0.26	0.25

NOTE: [a]Rounded up from 0.06.
[b]Changed from zero to provide a nonzero minimum.

Source: BSC 2004b, Table 8-1.

Table 2.3.7-13. Parameter Values and Associated Characteristic Values of the Uncertainty Distributions for the Alkaline Conditions Model

Model Parameter	Parameter Value	Uncertainty Distribution Characteristic Values[a]
log(*A*)	–6.7	Triangular distribution: Minimum = –7.3 Apex = –6.7 Maximum = –5.4
a_0	4.705	0.601
a_1	–1,093.826	186.829
a_2	–0.102	0.0471
a_3	–0.338	0.0506

NOTE: [a]Estimated standard errors from regression analyses performed using Microsoft Excel.
Parameter values are regression coefficients. The large number of significant figures in regression coefficients should not be taken to indicate a corresponding precision of rate prediction.
NA = not applicable.

Source: BSC 2004b, Table 8-2.

Table 2.3.7-14. Parameter Values and Associated Characteristic Values of the Uncertainty Distributions for the Acidic Conditions Model

Model Parameter	Parameter Value	Uncertainty Distribution Characteristic Values[a]
log(*A*)	–6.70	Triangular distribution: Minimum = –7.3 Apex = –6.7 Maximum = –5.4
a_0	6.60	0.446
a_1	–1,093.826	186.829
a_3	–0.338	0.0506
a_4	–0.340	0.110

NOTE: [a]Estimated standard errors.
The uncertainties in the regression coefficients are also related through the covariance matrix provided in *CSNF Waste Form Degradation: Summary Abstraction* (BSC 2004b, Attachment II). Values for parameters a_1 and a_3 have been taken from the analysis for the alkaline conditions model and have no associated standard errors in the context of the acid conditions analysis; the standard errors obtained from the alkaline side regression analysis are used. Parameter values are regression coefficients. The large number of significant figures in the latter should not be taken to indicate a corresponding precision of rate prediction.
NA = not applicable.

Source: BSC 2004b, Table 8-3.

Table 2.3.7-15. Commercial SNF Flow-Through Test Dissolution Data (Alkaline Conditions)

Run No.	Burnup (MWd/kg U)	Specific Surface Area (m^2/g)	Temp (°C)	Total Carbonate (mol/L)	0_2 Partial Pressure (atmospheres)	pH	Dissolution Rate Normalized to Surface Area ($mg/m^2/day$)	Standard Deviation for DIssolution Rate ($mg/m^2/day$)	Slope of the Cumulative Release Curve (fraction released/day)
1	30	0.0858	49	2.0×10^{-3}	0.2	9.06	7.58	0.35	6.476×10^{-4}
2	30	0.0858	51	2.0×10^{-3}	0.2	9.06	8.55	0.76	7.194×10^{-4}
3	30	0.0858	50	2.0×10^{-3}	0.2	9.06	6.31	0.97	5.177×10^{-4}
4	30	0.0858	24	2.0×10^{-2}	0.2	8.18	4.15	0.33	3.426×10^{-4}
5	30	0.0858	73	2.0×10^{-2}	0.2	10.14	13.81	1.36	1.124×10^{-3}
5A	30	0.0858	77	2.0×10^{-2}	0.2	10.03	21.38	2.39	1.878×10^{-3}
6	30	0.0858	75	2.0×10^{-4}	0.2	8.13	10.52	1.60	9.265×10^{-4}
6A	30	0.0858	72	2.0×10^{-4}	0.2	8.13	9.90	0.82	8.683×10^{-4}
7	30	0.0858	23	2.0×10^{-4}	0.2	10.07	0.58	0.22	4.751×10^{-5}
7A	30	0.0858	20	2.0×10^{-4}	0.2	10.02	1.08	0.29	8.653×10^{-5}
8	30	0.0858	24	2.0×10^{-2}	0.2	9.12	3.25	0.31	2.755×10^{-4}
9	30	0.0858	24	2.0×10^{-3}	0.2	10.11	2.47	0.25	2.128×10^{-4}
10	30	0.0858	27	2.0×10^{-4}	0.02	8.00	2.12	0.16	1.819×10^{-4}
11	30	0.0858	78	2.0×10^{-4}	0.02	9.86	1.77	0.15	1.552×10^{-4}
12	30	0.0858	26	2.0×10^{-2}	0.02	10.04	2.46	0.21	2.082×10^{-4}
13	30	0.0858	77	2.0×10^{-2}	0.02	8.10	3.57	0.34	3.027×10^{-4}
14	30	0.0858	23	2.0×10^{-2}	0.002	8.25	2.94	0.09	2.494×10^{-4}

Table 2.3.7-15. Commercial SNF Flow-Through Test Dissolution Data (Alkaline Conditions) (Continued)

Run No.	Burnup (MWd/kg U)	Specific Surface Area (m^2/g)	Temp (°C)	Total Carbonate (mol/L)	0_2 Partial Pressure (atmospheres)	pH	Dissolution Rate Normalized to Surface Area ($mg/m^2/day$)	Standard Deviation for DIssolution Rate ($mg/m^2/day$)	Slope of the Cumulative Release Curve (fraction released/day)
15	30	0.0858	75	2.0×10^{-2}	0.002	10.12	0.95	0.32	8.624×10^{-5}
16	30	0.0858	76	2.0×10^{-4}	0.002	8.00	1.41	0.15	1.225×10^{-4}
17	30	0.0858	20	2.0×10^{-4}	0.002	10.00	0.76	0.19	6.042×10^{-5}
18	30	0.0858	50	2.0×10^{-2}	0.002	10.05	1.20	0.16	1.076×10^{-4}
19	30	0.0858	22	2.0×10^{-3}	0.002	8.97	1.95	0.33	1.808×10^{-4}
20	30	0.0858	74	2.0×10^{-2}	0.02	10.11	5.65	1.05	4.569×10^{-4}
21	31	0.0984	50	2.0×10^{-3}	0.2	9.05	6.61	0.54	6.578×10^{-4}
22	50	0.277	26	2.0×10^{-2}	0.2	8.27	1.63	0.32	4.376×10^{-4}
23	31	0.0678	23	2.0×10^{-2}	0.2	8.02	4.04	0.87	2.837×10^{-4}
24	31	0.0678	76	2.0×10^{-2}	0.2	8.04	9.41	2.82	6.457×10^{-4}
25	31	0.0678	23	2.0×10^{-4}	0.2	7.93	2.64	0.34	1.805×10^{-4}
26	31	0.0678	75	2.0×10^{-4}	0.2	7.75	10.99	1.72	7.918×10^{-4}
27	44	0.136	23	2.0×10^{-2}	0.2	8.27	3.62	0.64	4.453×10^{-4}
28	50	0.1023	25	2.0×10^{-2}	0.2	8.30	3.83	0.22	3.873×10^{-4}
29	50	0.1023	76	2.0×10^{-2}	0.2	8.30	6.90	1.04	6.939×10^{-4}
30	50	0.1023	25	2.0×10^{-4}	0.2	7.56	2.85	0.56	2.737×10^{-4}
31	50	0.1023	74	2.0×10^{-4}	0.2	7.56	9.45	1.37	9.902×10^{-4}
33	50	0.1023	75	2.0×10^{-2}	0.002	8.06	1.35	0.36	1.552×10^{-4}

Table 2.3.7-15. Commercial SNF Flow-Through Test Dissolution Data (Alkaline Conditions) (Continued)

Run No.	Burnup (MWd/kg U)	Specific Surface Area (m^2/g)	Temp (°C)	Total Carbonate (mol/L)	0_2 Partial Pressure (atmospheres)	pH	Dissolution Rate Normalized to Surface Area ($mg/m^2/day$)	Standard Deviation for DIssolution Rate ($mg/m^2/day$)	Slope of the Cumulative Release Curve (fraction released/day)
34	50	0.1023	27	2.0×10^{-4}	0.002	7.76	2.03	0.20	2.071×10^{-4}
35	50	0.1023	74	2.0×10^{-4}	0.002	7.74	3.50	0.46	3.612×10^{-4}
36	15	0.0837	27	2.0×10^{-2}	0.2	8.02	3.24	0.54	2.739×10^{-4}
37	15	0.0837	76	2.0×10^{-2}	0.2	7.96	11.94	3.97	9.558×10^{-4}
38	15	0.0837	27	2.0×10^{-4}	0.2	7.62	3.74	0.47	3.050×10^{-4}
61	65	0.133	26	2.0×10^{-2}	0.2	8.14	3.94	0.52	5.262×10^{-4}
62	65	0.133	76	2.0×10^{-2}	0.2	8.12	5.61	1.56	7.769×10^{-4}
63	65	0.133	26	2.0×10^{-4}	0.2	7.63	2.49	0.89	2.908×10^{-4}
64	65	0.133	76	2.0×10^{-4}	0.2	7.16	6.77	1.49	9.008×10^{-4}
65	65	0.133	76	2.0×10^{-2}	0.002	8.07	0.85	0.19	1.217×10^{-4}

Source: BSC 2004b, Table 4-2.

Table 2.3.7-16. Unirradiated UO_2 Flow-Through Test Dissolution Data (Alkaline Conditions)

Sample	T (°C)	Total CO_3 (mmol/L)	O_2 (%)	pH	DR (mg/M^2d)
4	25	20	20	8.7	2.42
5	75	20	20	10.3	77.4
6	75	0.2	20	9.1	10.9
7	25	0.2	20	9	2.55
8	25	20	20	9.4	6.72
9	25	2	20	9.3	9.34
10	26	0.2	2	7.8	0.12
11	75	0.2	2	9.7	9.21
12	26	20	2	10.1	1.87
13	75	20	2	8.5	5.11
14	25	20	0.2	8	0.22
15	75	20	0.2	9.8	5.61
16	75	0.2	0.2	8.7	0.51
17	26	0.2	0.2	9.3	0.23
18	50	20	0.2	9.9	4.6
19	26	2	0.2	9	1.52
21	50	2	2	8.9	12.3
22	50	2	2	8.8	7.96
23	50	2	2	8.9	10.4
24	75	0.2	20	9.5	6.48
25	75	2	20	9.6	23.3
26	75	20	20	8.5	54

Source: BSC 2004b, Table 4-3.

Table 2.3.7-17. Commercial SNF Flow-Through Test Dissolution Data (Acidic Conditions)

Test Identification	Burnup (MWd/kg M)	Temp (°C)	0_2 Partial Pressure (atmospheres)	pH	Dissolution Rate Normalized to Surface Area ($mg/m^2/day$)	Standard Deviation for DIssolution Rate	Slope of the Cumulative Release Curve (fraction released/day)
Y6-A2B	50	27	0.2	2.02	5.02×10^{1}	6.21	1.406×10^{-2}
Y6-A3B	50	27	0.2	3.01	3.45×10^{1}	5.37	1.045×10^{-2}
Run #66	31	24	0.2	3.25	1.09×10^{2}	6.35	9.043×10^{-3}
Y6-A4B	50	27	0.2	3.80	5.39×10^{1}	1.66×10^{1}	1.756×10^{-2}
Y6-A5B	50	26	0.2	5.07	7.18	7.24×10^{1}	2.019×10^{-3}
Y6-A6B	50	26	0.2	5.82	3.80	1.17	8.932×10^{-4}
Y6-A7B	50	26	0.2	7.29	3.45	1.04	8.381×10^{-4}

Source: BSC 2004b, Table 4-4.

Table 2.3.7-18. Summary of the Nevada Nuclear Waste Storage Investigations Series 3 Fractional Release Rate (d^{-1}) Results for Last Sampling Period

Isotope	H. B. Robinson Fuel (25°C)	H. B. Robinson Fuel (85°C)	Turkey Point Fuel (85°C)
^{90}Sr	5.79×10^{-7}	4.82×10^{-7}	4.79×10^{-7}
^{137}Cs	9.29×10^{-7}	1.07×10^{-6}	8.67×10^{-7}
^{99}Tc	6.87×10^{-7}	3.09×10^{-6}	1.17×10^{-6}
Average	7.32×10^{-7}	1.55×10^{-6}	1.02×10^{-6}
Base-Case Model Calculated Fractional Release Rates (d^{-1})	7.32×10^{-7}	3.02×10^{-6}	3.02×10^{-6}
Error Metric	0.0	0.3	0.5

Source: BSC 2004b, Table 7-8.

Table 2.3.7-19. Average Fractional Release Rates (d^{-1}) Measured in the Series 11 Tests on Fuel Rod Segments with Different Burnups and in the Series 3 Tests on Fuel Fragments

Element	Rod Segments[a]			Fragments[b]
	Burnup Range (27 to 30 MWD/kgU)	Burnup Range (35 to 46 MWD/kgU)	Burnup Range (46 to 49 MWD/kgU)	Burnup (42 MWd/kgU)
Strontium	2.07×10^{-7}	3.19×10^{-7}	3.12×10^{-7}	2.03×10^{-6}
Cesium	5.61×10^{-7}	6.69×10^{-7}	7.90×10^{-7}	3.53×10^{-6}
Molybdenum	1.85×10^{-6}	2.25×10^{-6}	1.28×10^{-6}	3.82×10^{-6}
Technetium	1.61×10^{-6}	$1.80- \times 10^{-6}$	1.35×10^{-6}	2.56×10^{-6}
Average	1.06×10^{-6}	1.26×10^{-6}	9.33×10^{-7}	2.99×10^{-6}
Base-Case Model Calculated Fractional Release Rates (d^{-1})	8.42×10^{-7}	8.42×10^{-7}	8.42×10^{-7}	8.42×10^{-7}
Error Metric	–0.1	–0.2	–0.0	–0.5

NOTE: [a]Forsyth 1997, Table 6-11.
[b]Data shown here are the average fractional release rates for the 3.23 and 3.24 tests (Forsyth 1997, Table 6-12).

Source: BSC 2004b, Table 7-9.

Table 2.3.7-20. Fractional DOE SNF Waste Form Dissolution Rates at 50°C, pH 8.5, 0.002 Molar CO_3^{2-}, and 0.20 Atmospheres Oxygen Calculated for Best-Estimate Models

DOE SNF Group	Best-Estimate Release Rate (mg/m^2 day)	Exposed Specific Surface Area (m^2/g)	Exposed Total Surface Area (m^2)	Fractional Corrosion Rate (d^{-1})
Group 2—Plutonium/Uranium Alloy	492	1.2×10^{-3}	1.02×10^{4}	5.9×10^{-4}
Group 3—Plutonium/Uranium Carbide	1.09×10^{5}	2.7×10^{-3}	2.61×10^{2}	0.174
Group 4—Mixed Oxide and Plutonium Oxide	5.41	4.0×10^{-3}	4.63×10^{4}	2.2×10^{-5}
Group 5—Thorium/Uranium Carbide	0.025	2.2×10^{-2}	0.54×10^{5}	5.5×10^{-7}
Group 6—Thorium./Uranium Oxide	0.034	3.6×10^{-4}	1.69×10^{4}	1.2×10^{-8}
Group 7—Uranium Metal-Based	1.1×10^{5}	7.0×10^{-5}	1.39×10^{5}	7.7×10^{-3}
Group 8a—Intact Uranium Oxide	4.83	4.0×10^{-3}	6.65×10^{5}	1.9×10^{-5}
Group 8b—Damaged Uranium Oxide	483	4.0×10^{-1}	—	0.19
Group 9—Alumium-based	0.19 at 25°C	6.5×10^{-3}	1.27×10^{5}	1.2×10^{-6}
Group 10—Miscellaneous SNF	492	4.0×10^{-1}	1.69×10^{6}	0.2
Group 11—Uranium-Zirconium Hydride	0.33	1.0×10^{-4}	1.51×10^{2}	3.3×10^{-8}

Source: BSC 2004c, Table 6-9.

Table 2.3.7-21. Glass Degradation Rate Parameters

Parameter Name	Parameter Description	Value	Distribution
η_{acidic}	pH coefficient for acidic solutions	–0.49	Single value
$\eta_{alkaline}$	pH coefficient for alkaline solutions	0.49	Single value
E_{a_acidic}	Temperature coefficient for acidic solutions	31 kJ/mol	Single value
$E_{a\_alkaline}$	Temperature coefficient for alkaline solutions	69 kJ/mol	Single value
k_{E_acidic}	Glass degradation rate coefficient for acidic solutions	Minimum: 8.41×10^3 g/(m^2·day) Maximum: 1.15×10^7 g/(m^2·day) Most probable: 8.41×10^3 g/(m^2·day)	Triangular
$k_{E\_alkaline}$	Glass degradation rate coefficient for alkaline solutions	Minimum: 2.82×10^1 g/(m^2·day) Maximum: 3.47×10^4 g/(m^2·day) Most probable: 2.82×10^1 g/(m^2·day)	Triangular
$f_{exposure}$	Glass exposure factor	Minimum: 4 Maximum: 17 Most probable: 4	Triangular
S_{sp}	Specific surface area of a glass log	2.70×10^{-3} m^2/kg	Single value
M_0	Initial mass of a glass log	2,710 kg[a]	Single value
Φ	Porosity of glass rind	0.17	Single value

NOTE: [a]2,710 kg is a weighted average of mass of glass in a canister expected to range from 1,560 to 3,360 kg (Table 1.5.1-15).

Source: BSC 2004d, Table 8-1.

Table 2.3.7-22. Chemical Composition of Reference Water (J-13 Well Water)

Component	Concentration (mg/L)	Uncertainty (±)
Na^+	45.8	2.29
K^+	5.04	0.61
Ca^{2+}	13.0	0.99
Mg^{2+}	2.01	0.21
Si (SiO_2(aq))	28.5 (60.97)	1.85
Cl^-	7.14	0.61
F^-	2.18	0.29
NO_3^-	8.78	1.03
SO_4^{2-}	18.4	1.03

NOTE: The measured pH for J-13 well water is 7.41 ±0.44. The alkalinity for J-13 well water is 128.9 ±8.6 mg/L as HCO_3^-. The conversion of silicon to SiO_2 is 1 mg/L silicon = 2.14 mg/L SiO_2.

Source: SNL 2007h, Table 4-2.

Table 2.3.7-23. Developed Sorption Coefficients for Smectite and Uranophane Colloids

Radionuclide	Colloid	K_d Value Range (ml/g)
Pu	Smectite	10^3 to 10^5
	Uranophane	5 to10^4
Am, Th, Pa	Smectite	10^4 to 10^7
	Uranophane	5 to10^4
Cs	Smectite	50 to 5000
	Uranophane	10 to 1000
Np	Smectite	10 to 500
	Uranophane	10 to 500
U	Smectite	500 to 50,000
Sn	Smectite	10^5 to 10^6
	Uranophane	1 to 100
Ra	Smectite	100 to 5000
	Uranophane	10 to 1000

Source: SNL 2007i, Tables 6-9 and 6-15.

Table 2.3.7-24. Modeled K_d Values for Plutonium, Americium, Thorium, Neptunium, and Uranium Sorption onto Yucca Mountain-Vicinity Colloids

Radionuclide Sorbate and Oxidation State(s) at YMP	**K_d Values (mL/g)**
U(VI)	2×10^0 to 7×10^2
Np(V)	9 to 2×10^2
Pu(V)	9×10^2 to 2×10^4
Th(IV)	2×10^3 to 9×10^4
AM(III)	1×10^4 to 1×10^7

Source: Honeyman and Ranville 2002, estimated from Figure 7-5 in reference.

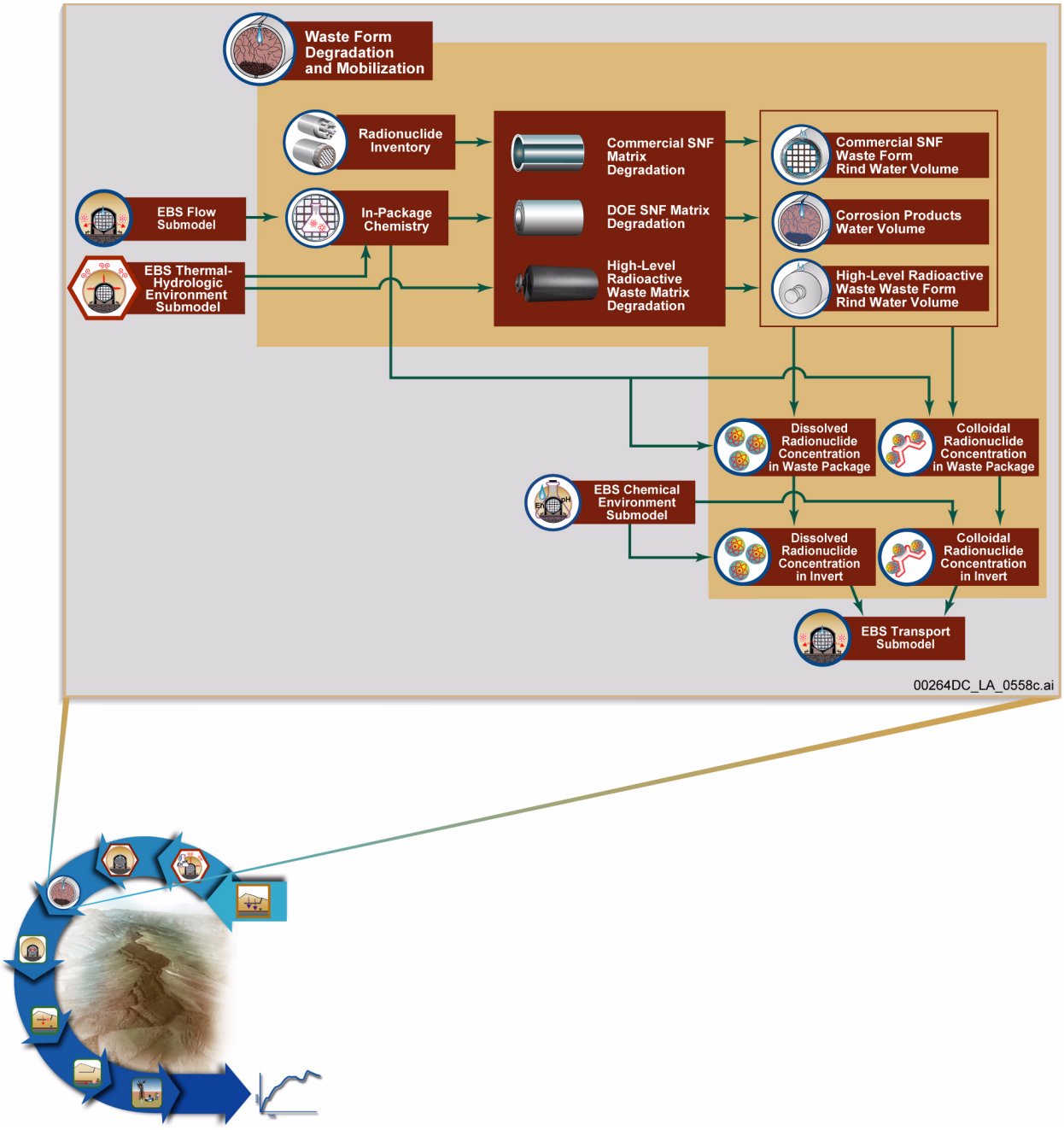

Figure 2.3.7-1. Information Flow Diagram for Waste Form Degradation and Mobilization

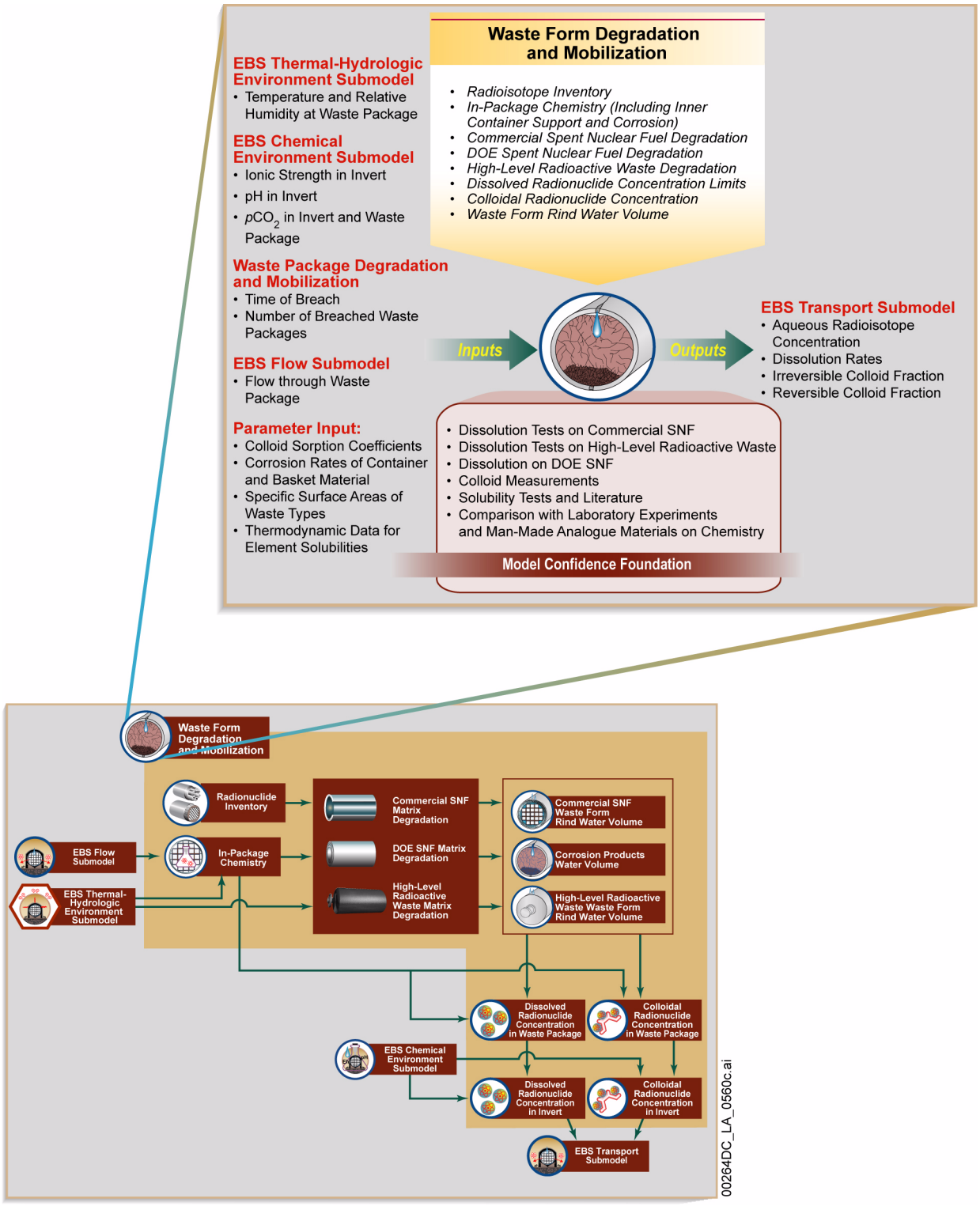

Figure 2.3.7-2. Inputs and Outputs for the Waste Form Degradation and Mobilization Component of TSPA

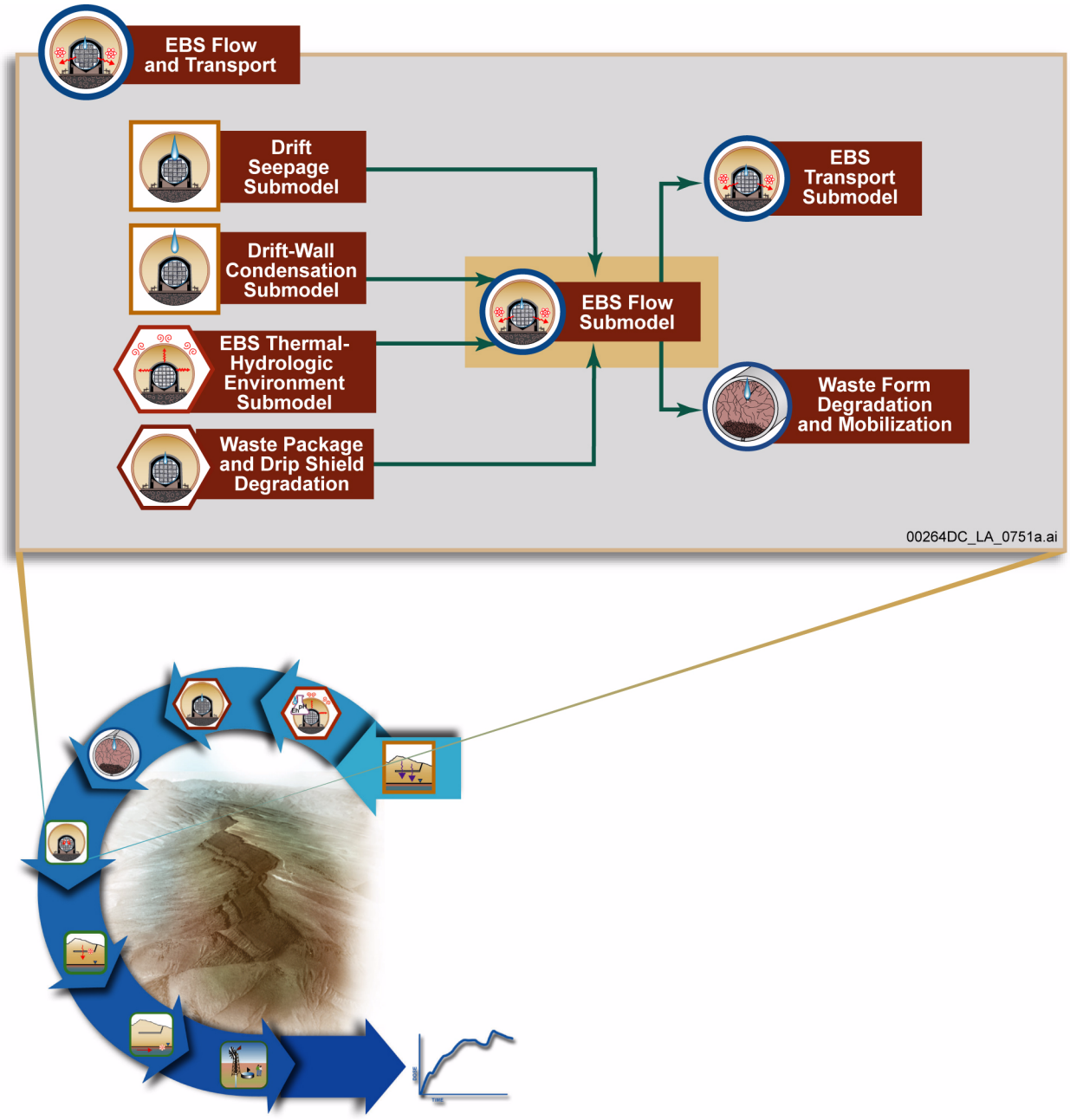

Figure 2.3.7-3. Information Flow Diagram for the Engineered Barrier System Flow Submodel

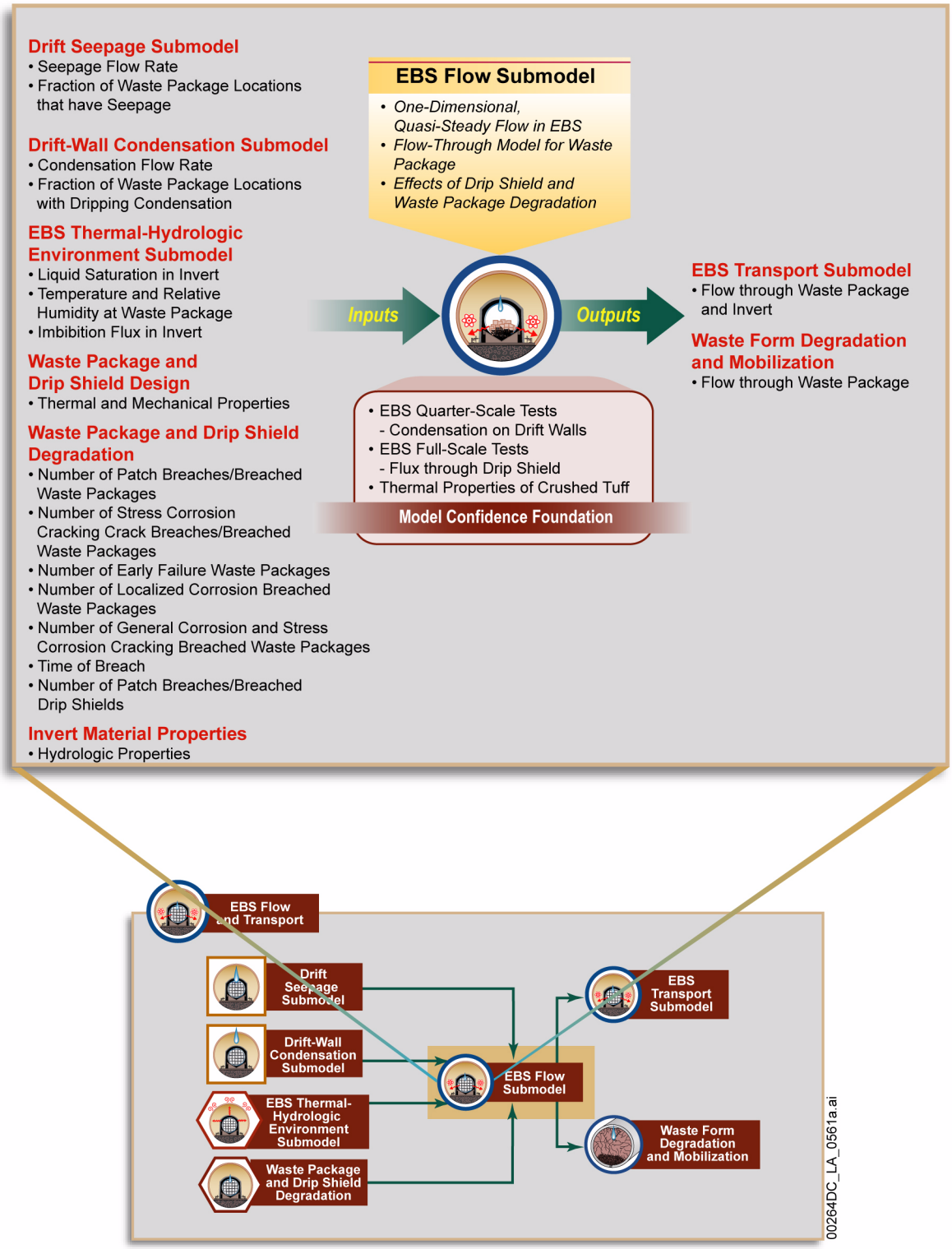

Figure 2.3.7-4. Inputs and Outputs for the Engineered Barrier System Flow Submodel

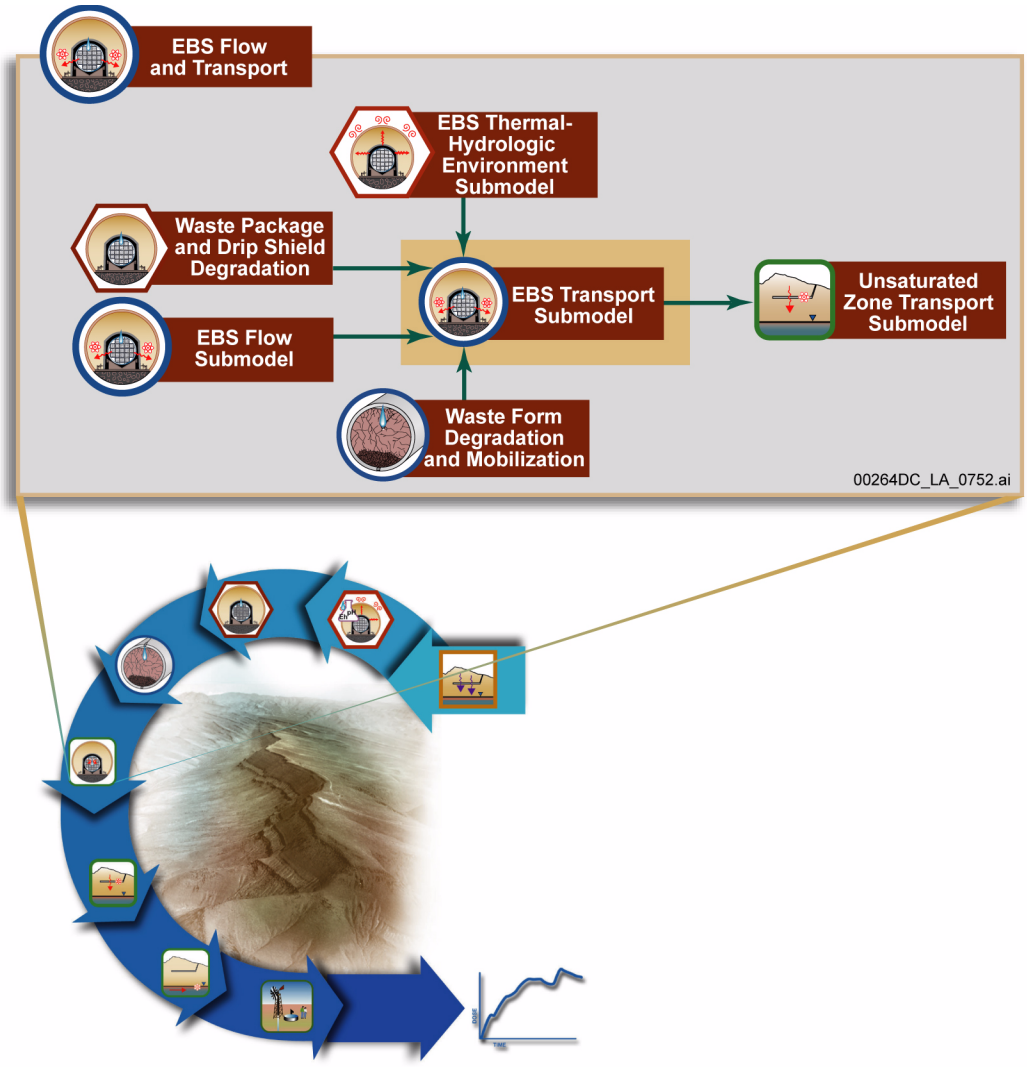

Figure 2.3.7-5. Information Flow Diagram for the Engineered Barrier System Transport Submodel

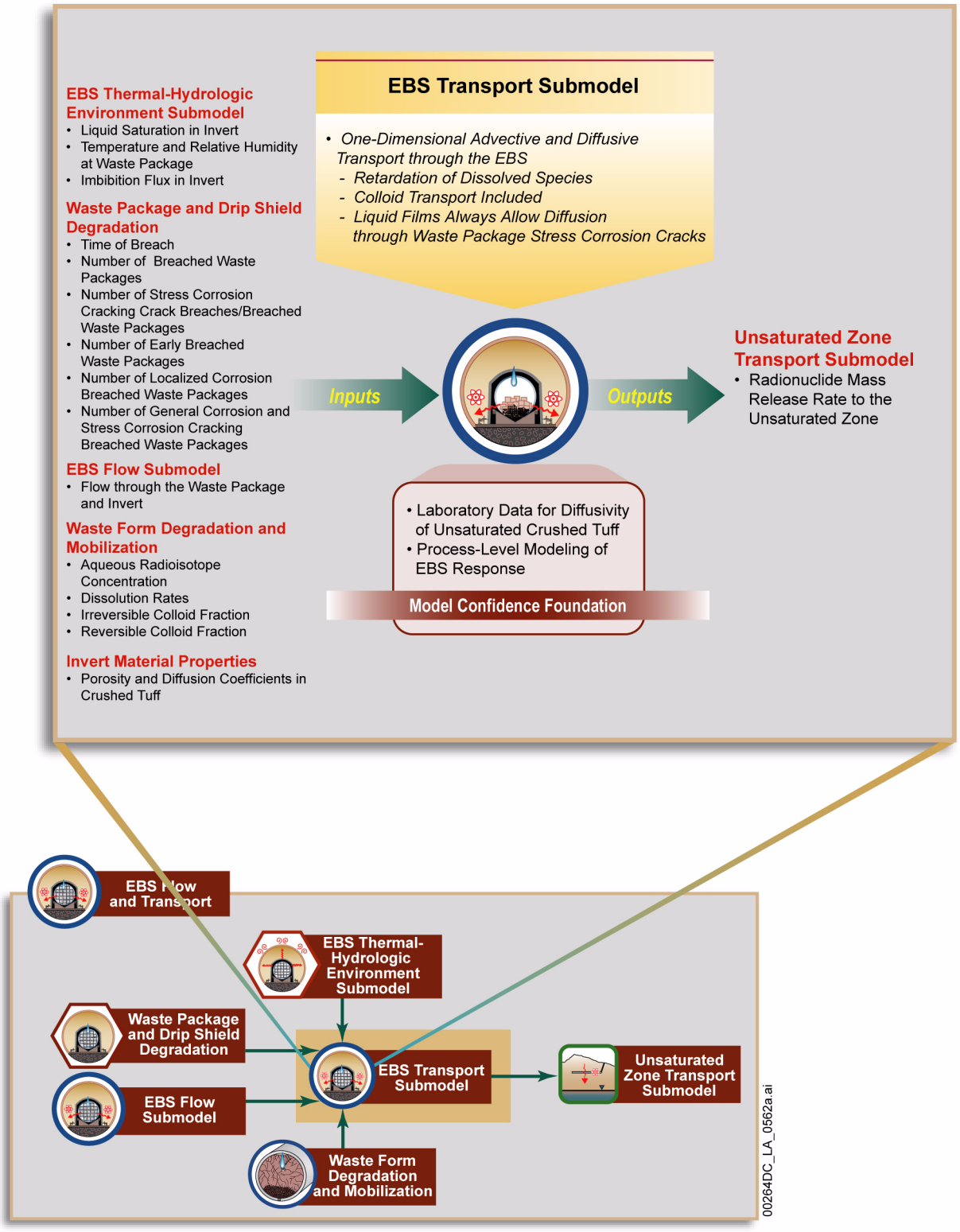

Figure 2.3.7-6. Inputs and Outputs for the Engineered Barrier System Transport Submodel

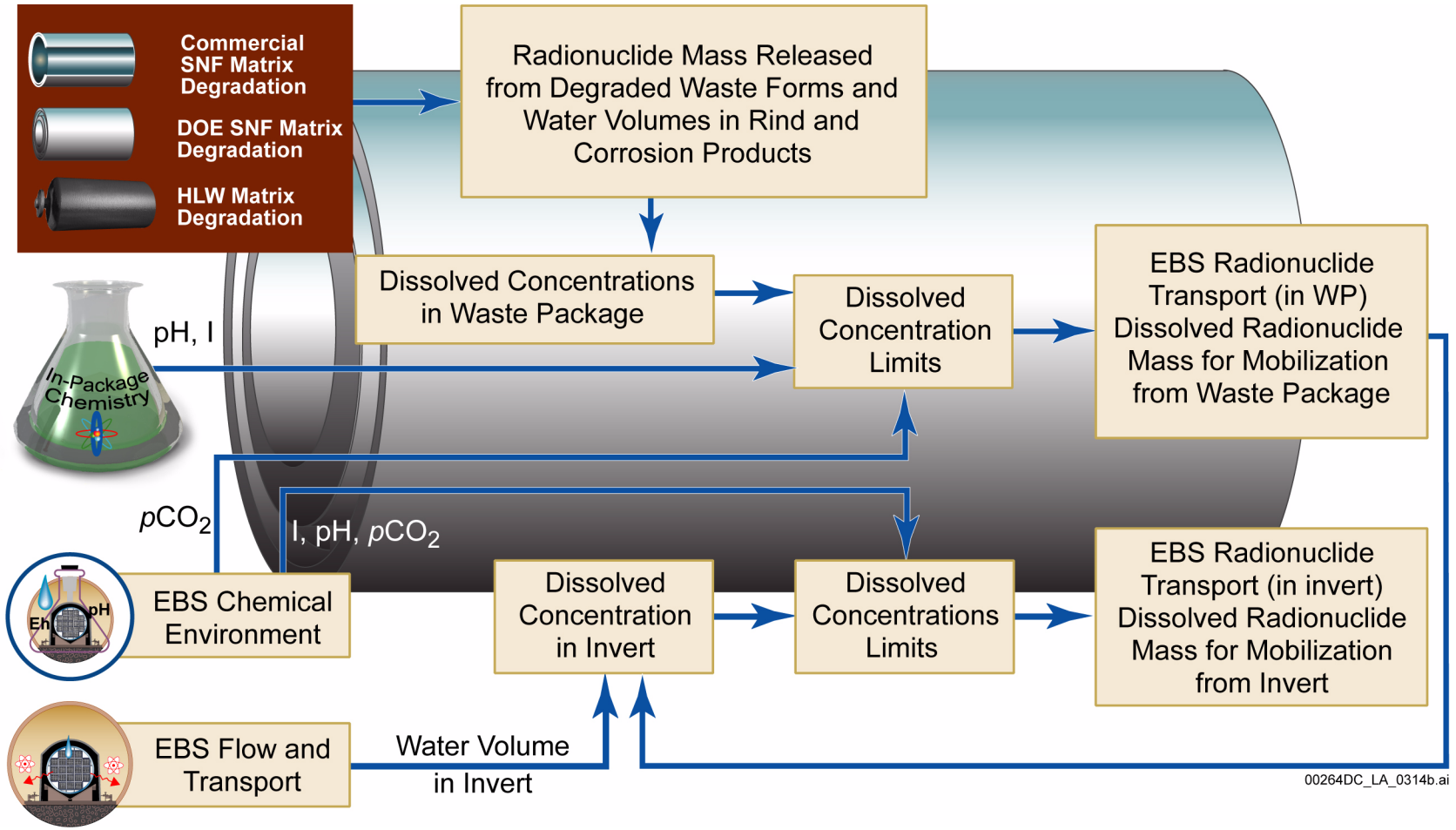

Figure 2.3.7-7. Linkage of Submodels in the Waste Form Degradation and Mobilization Component Model with Those in the EBS Radionuclide and Transport Component Model

NOTE: WP = waste package.

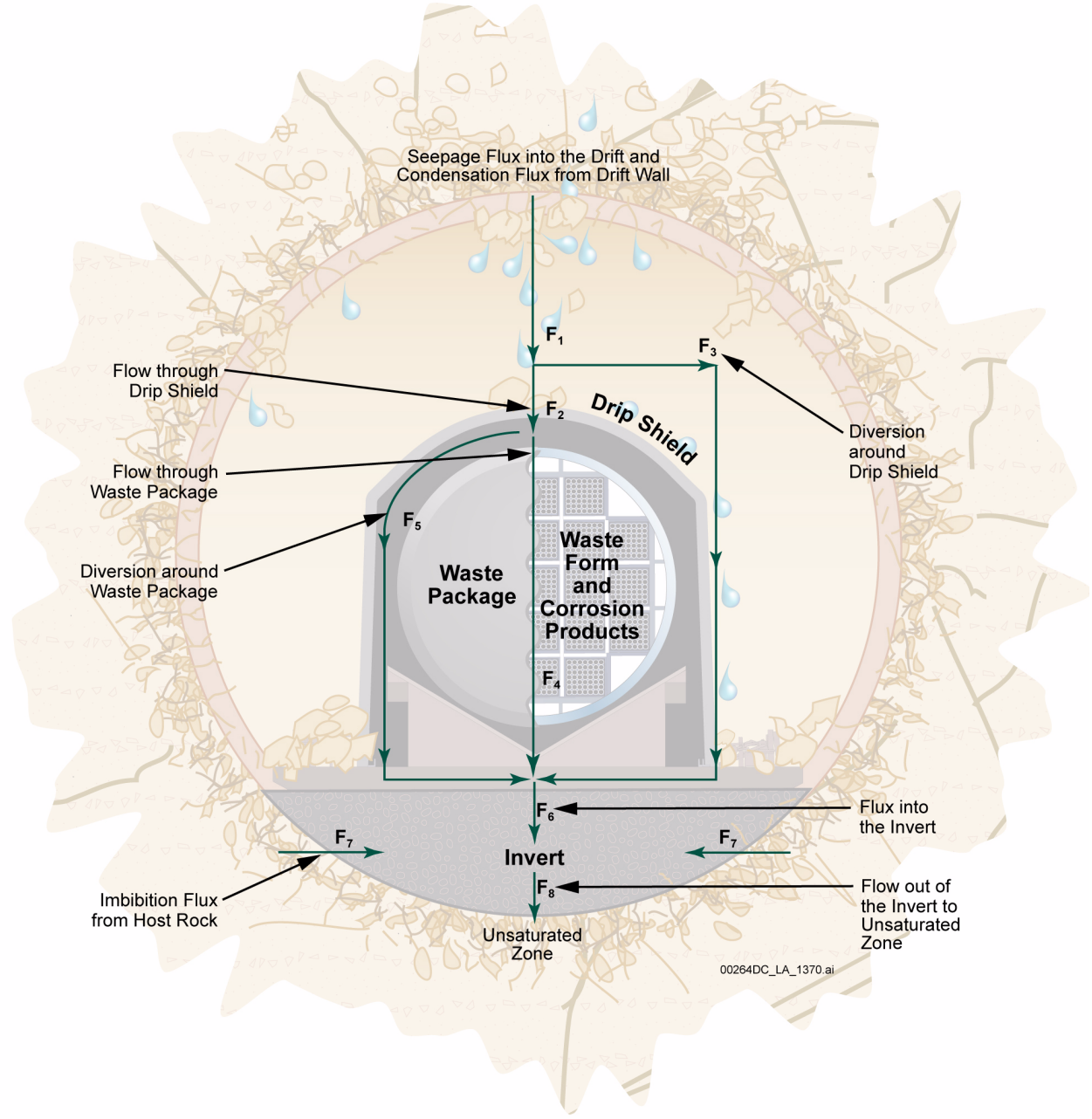

Figure 2.3.7-8. Potential Flow Pathways in the Engineered Barrier System

NOTE: Flow paths are labeled F_1 to F_8.

Source: SNL 2007a, Figure 6.3-1.

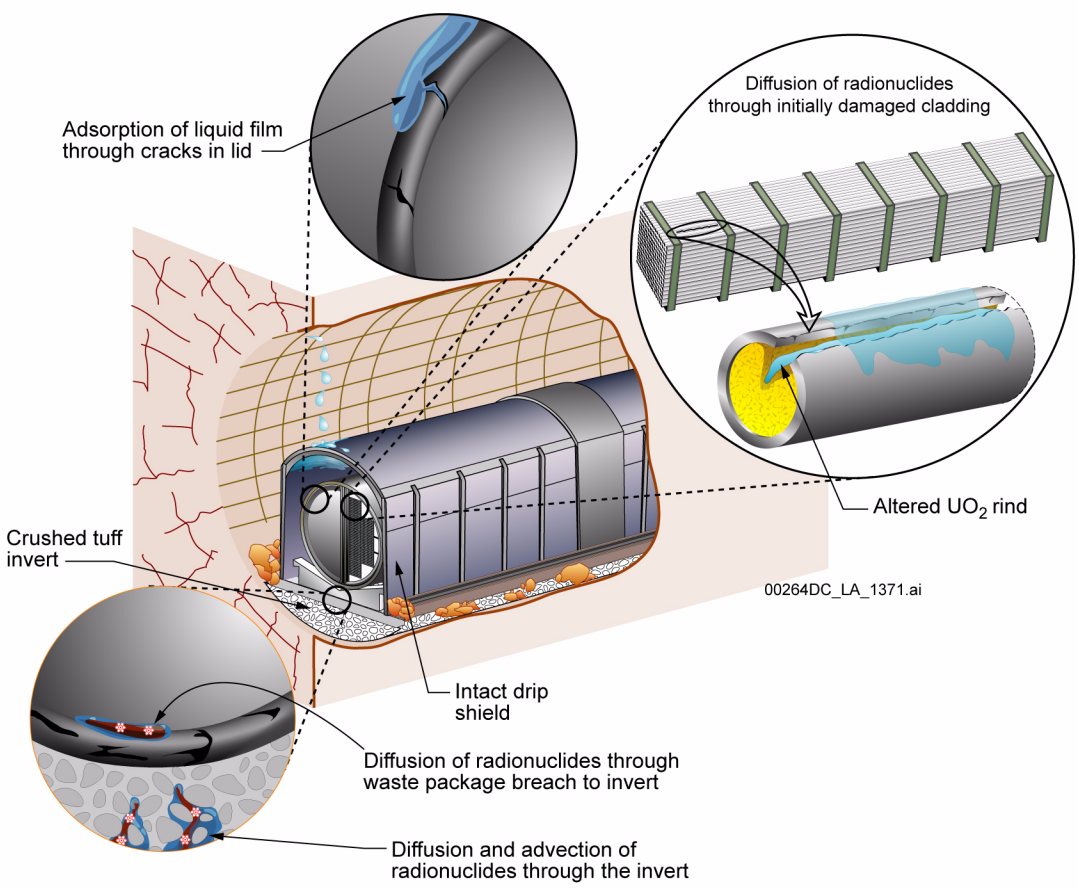

Figure 2.3.7-9. Degradation of Waste Form under Nominal Scenario Class

NOTE: For the nominal and seismic scenario class, waste form degradation is limited, and only diffusive release occurs while the drip shield remains intact for several hundred thousand years.

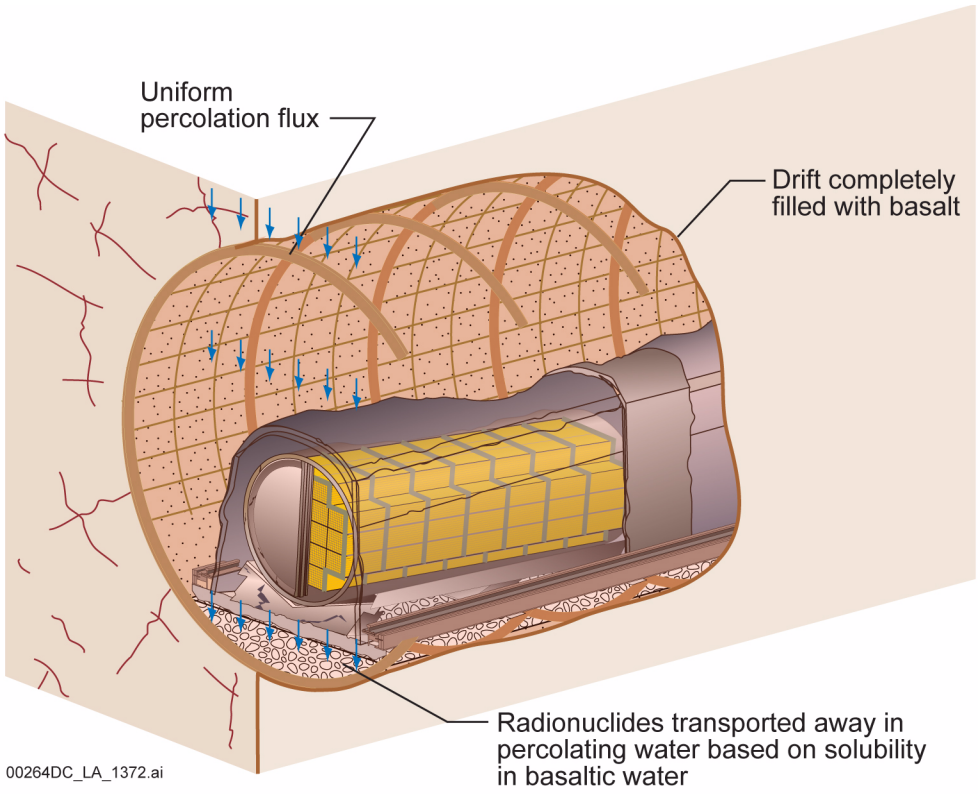

Figure 2.3.7-10. Degradation under the Igneous Intrusion Modeling Case

NOTE: In the igneous intrusion modeling case, the drip shield, waste package, and integrity of the waste form are completely destroyed in the entire repository.

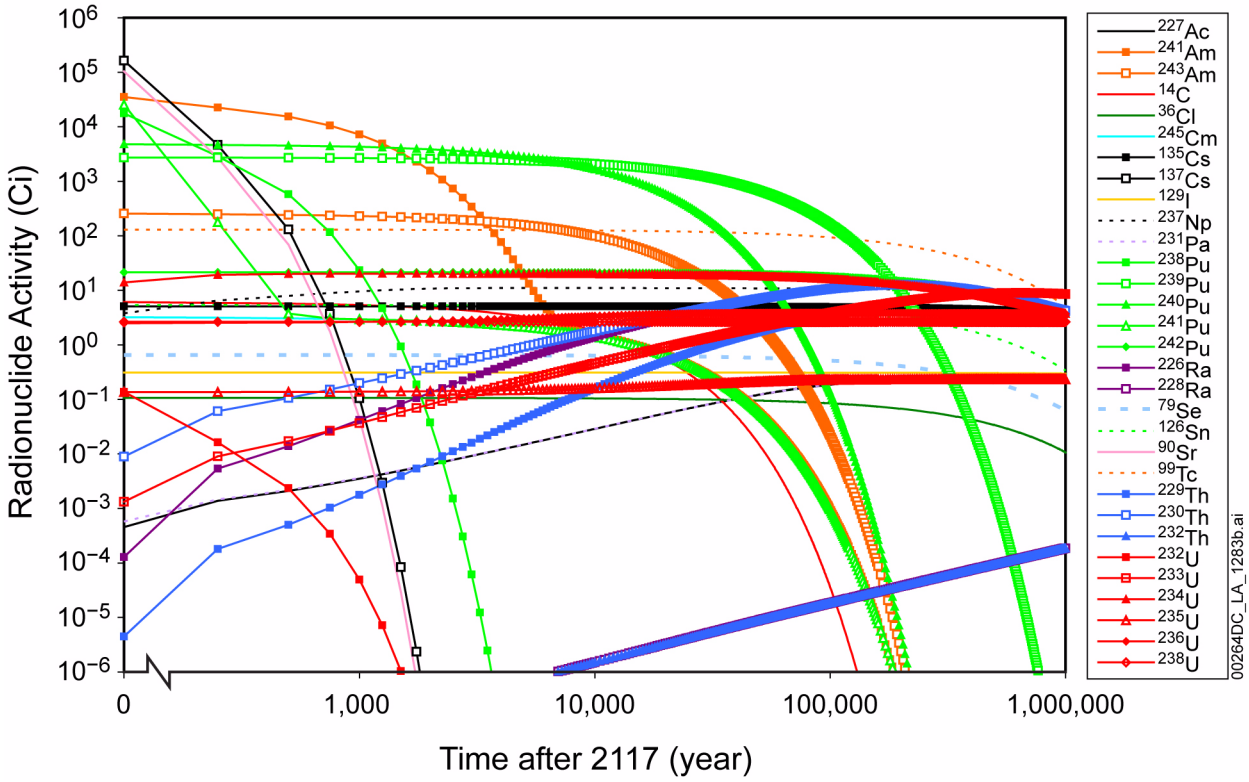

Figure 2.3.7-11. Radionuclide Inventory Decay for the Waste in a Commercial SNF Waste Package

NOTE: ^{210}Pb is not shown in the figure because TSPA assumes that radionuclide is in secular equilibrium with its parent, is transported with its parent, and therefore that its biological dose conversion factor can be included in that of the parent.

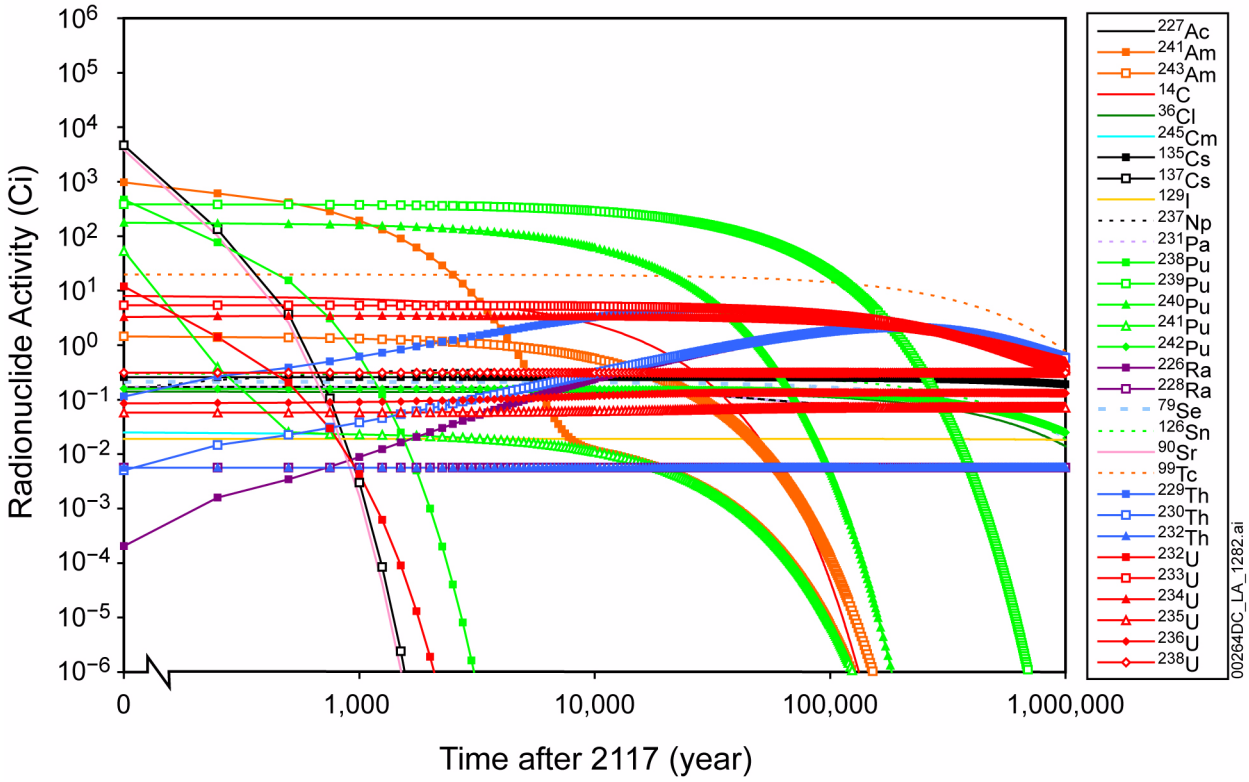

Figure 2.3.7-12. Radionuclide Inventory Decay for the Waste in a Codisposal Waste Package

NOTE: ^{210}Pb is not shown in the figure because TSPA assumes that radionuclide is in secular equilibrium with its parent, is transported with its parent, and therefore that its biological dose conversion factor can be included in that of the parent.

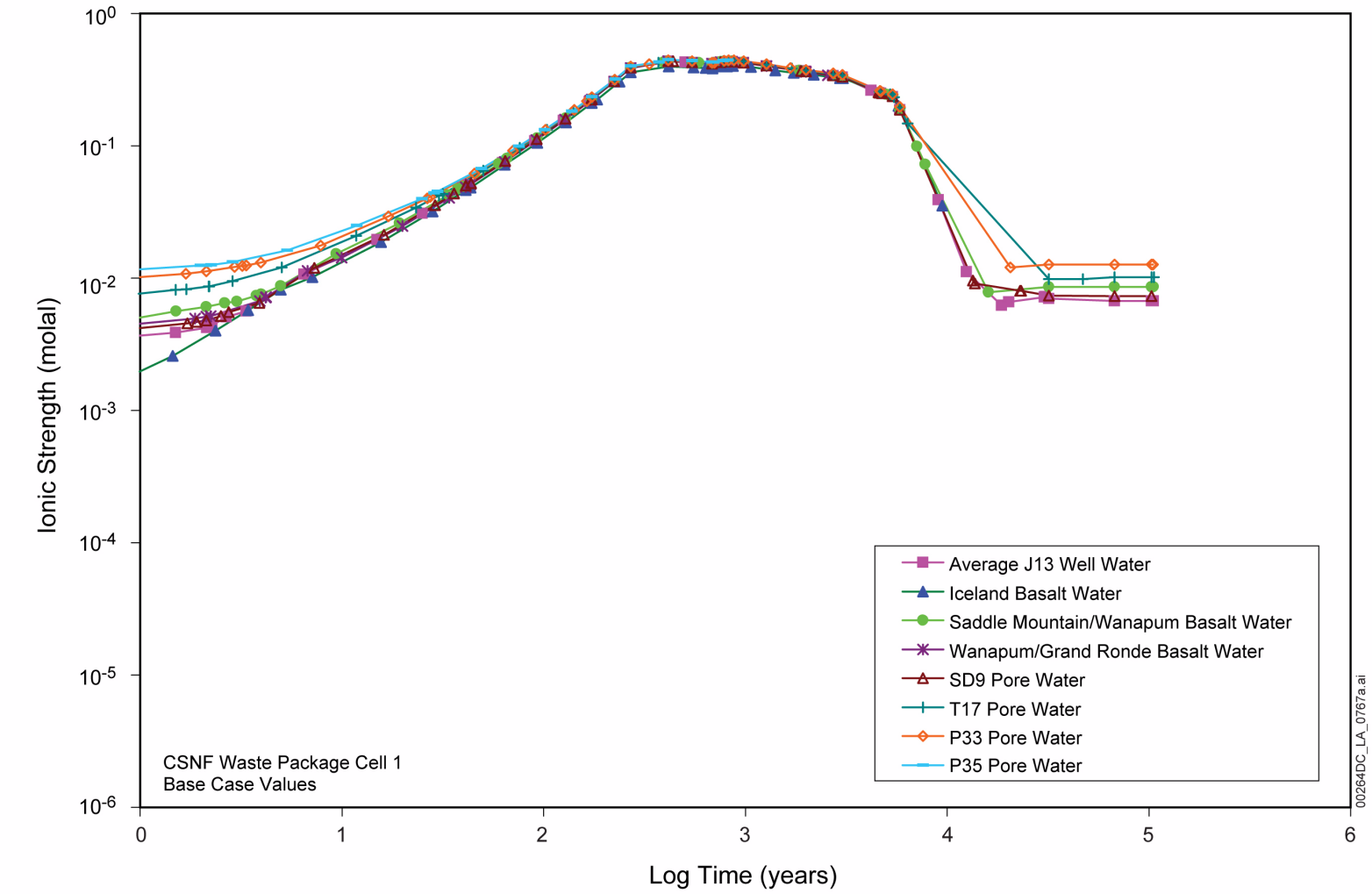

Figure 2.3.7-13. Commercial SNF Liquid-Influx Base Case Ionic Strength over Time for Various Seepage Compositions

NOTE: The base case involves a liquid flux of 1 L/yr and P_{CO_2} = 0.001 atmospheres.

Source: SNL 2007e, Figure 6-6[a]

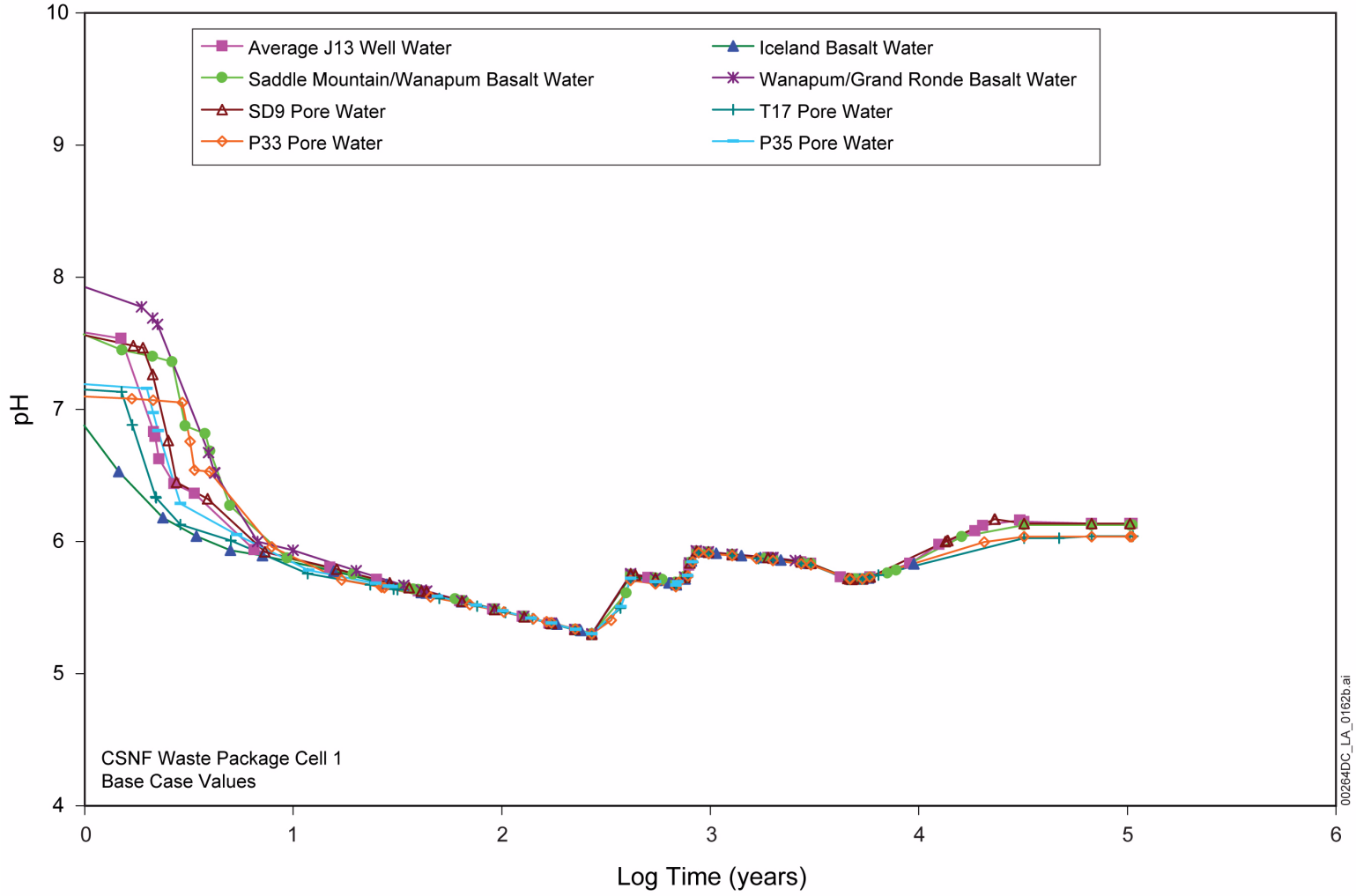

Figure 2.3.7-14. Commercial SNF Liquid-Influx Base Case pH over Time for Various Seepage Compositions

NOTE: The base case involves a liquid flux of 1 L/yr and P_{CO_2} = 0.001 atmospheres.

Source: SNL 2007e, Figure 6-5[a].

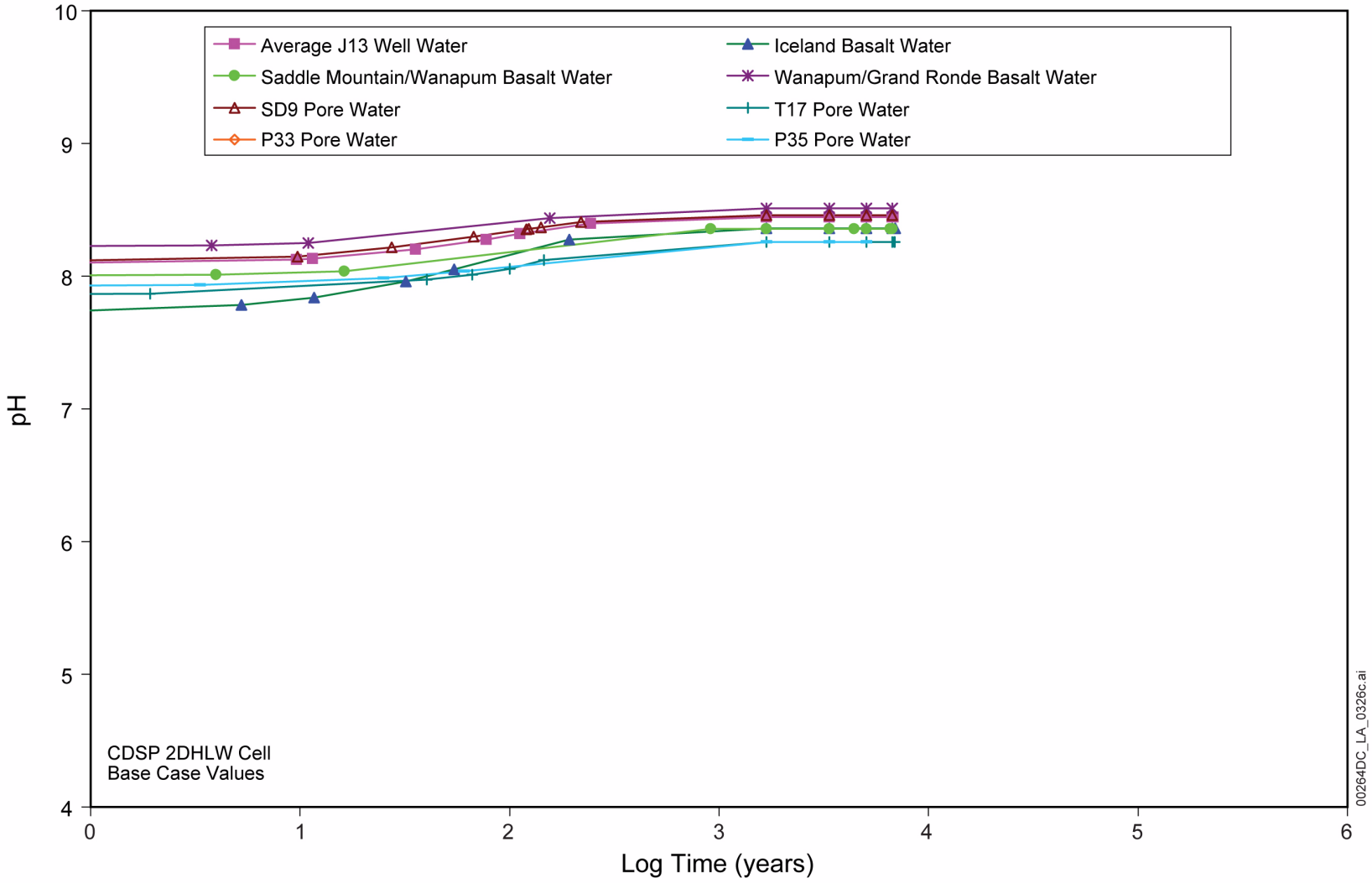

Figure 2.3.7-15. 2-DHLW Liquid-Influx Base Case pH over Time for Various Seepage Compositions

Source: SNL 2007e, Figure 6-8[a].

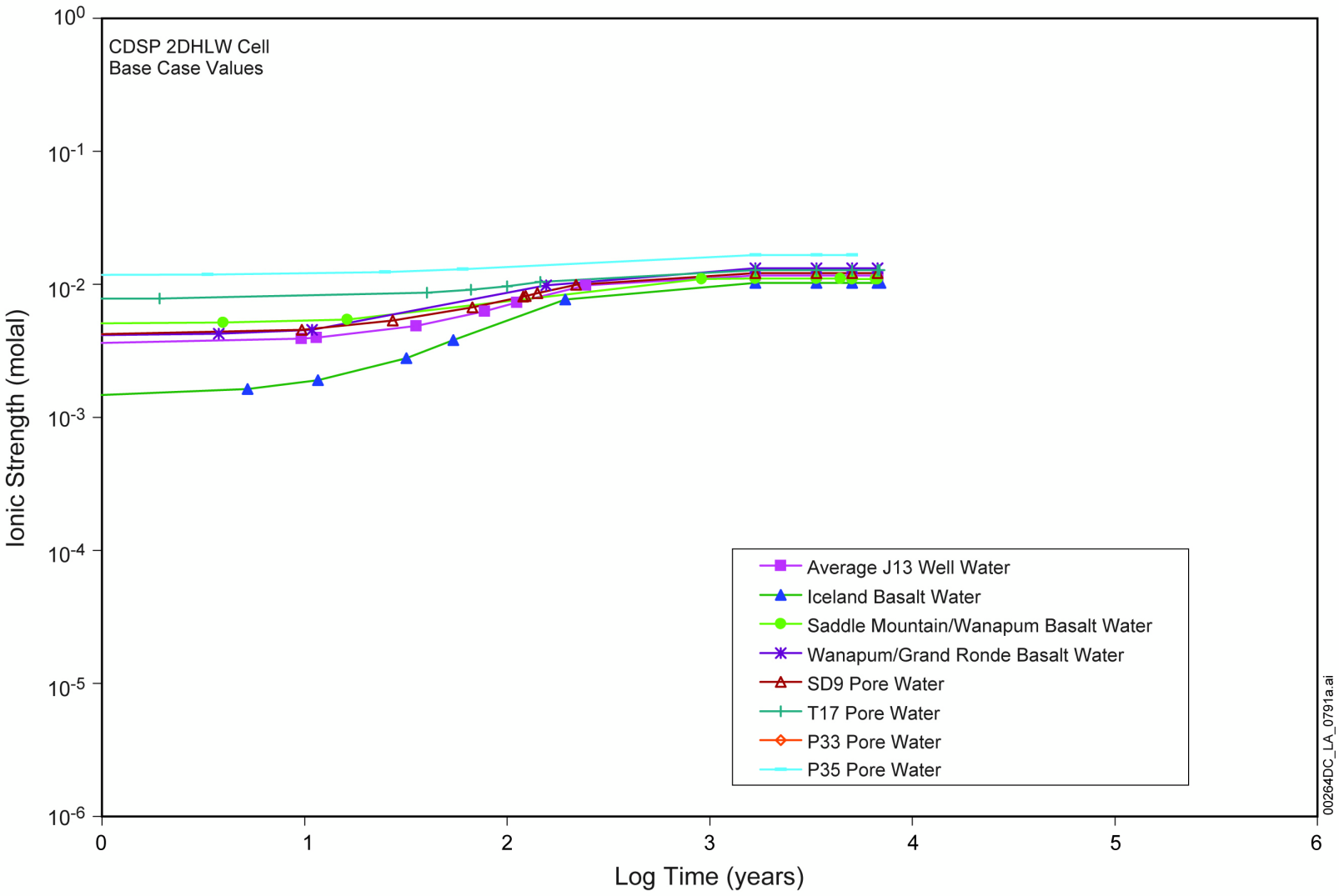

Figure 2.3.7-16. 2-DHLW Liquid-Influx Base Case Ionic Strength over Time for Various Seepage Compositions

Source: SNL 2007e, Figure 6-9[a].

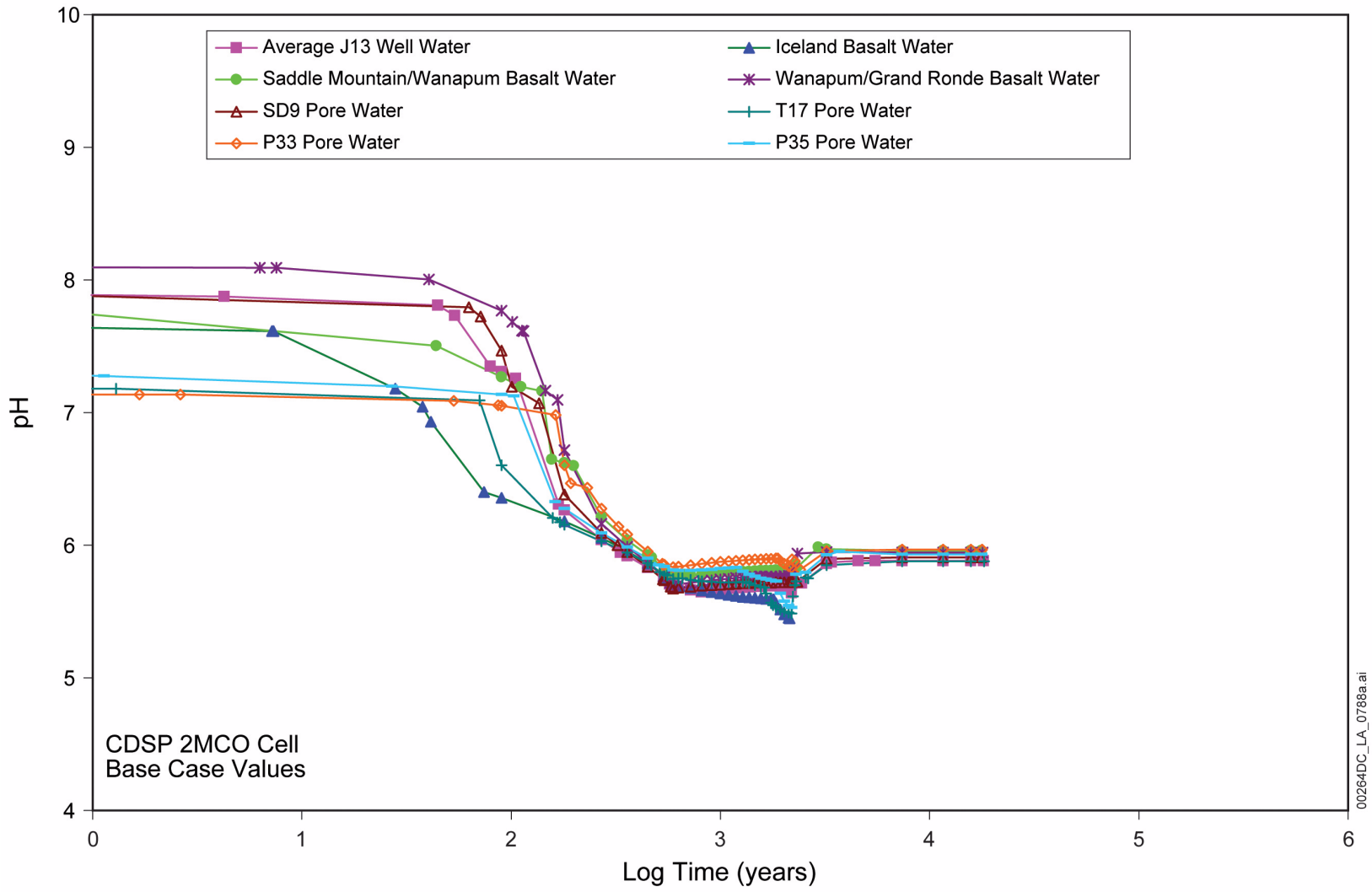

Figure 2.3.7-17. 2-MCO Liquid-Influx Base Case pH over Time for Various Seepage Compositions

Source: SNL 2007e, Figure 6-11[a].

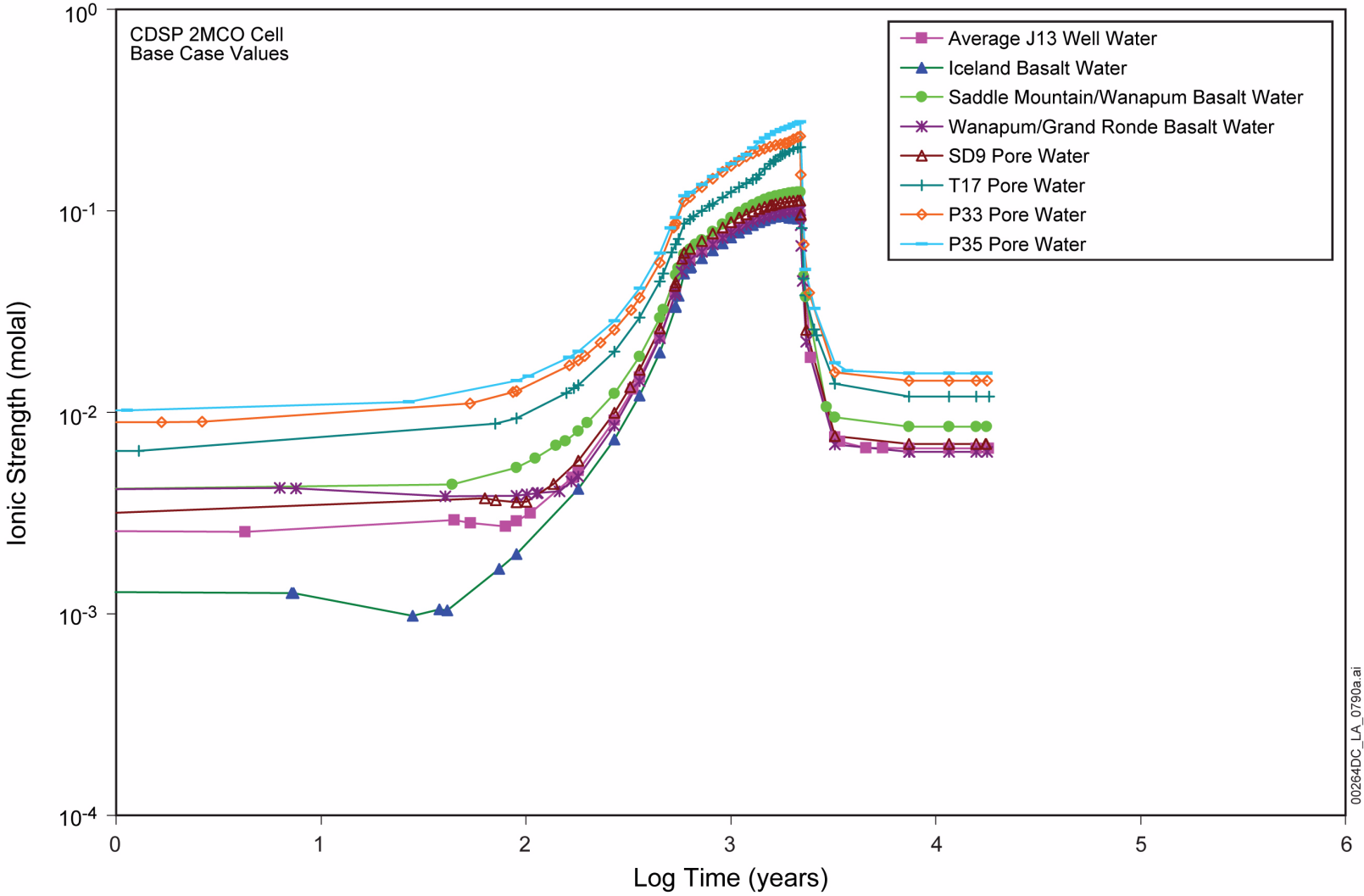

Figure 2.3.7-18. 2-MCO Liquid-Influx Base Case Ionic Strength over Time for Various Seepage Compositions

Source: SNL 2007e, Figure 6-12[a].

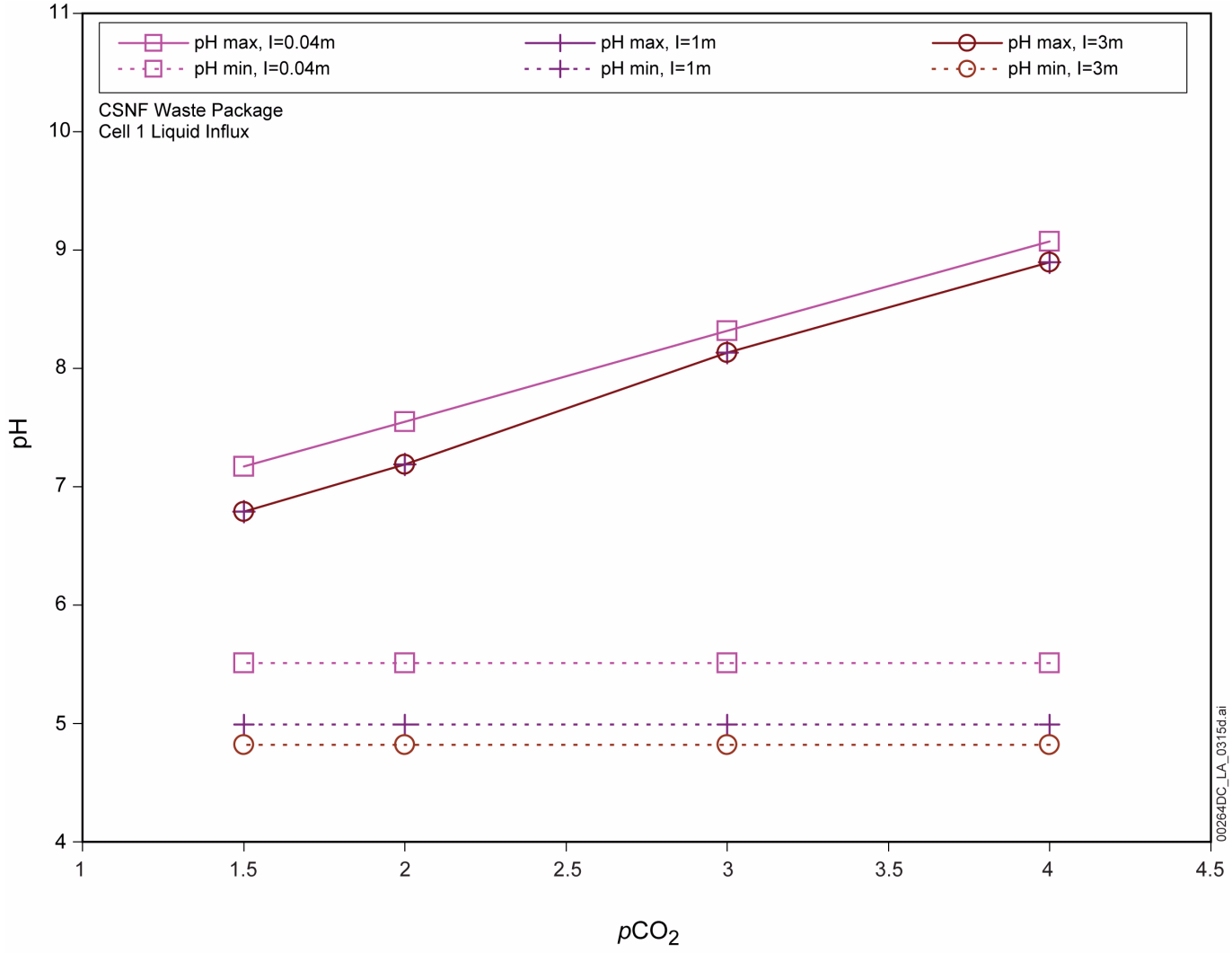

Figure 2.3.7-19. Commercial SNF Liquid-Influx Minimum and Maximum pH Values Versus pCO_2 for Various Ionic Strengths

Source: SNL 2007e, Figure 6-41[a].

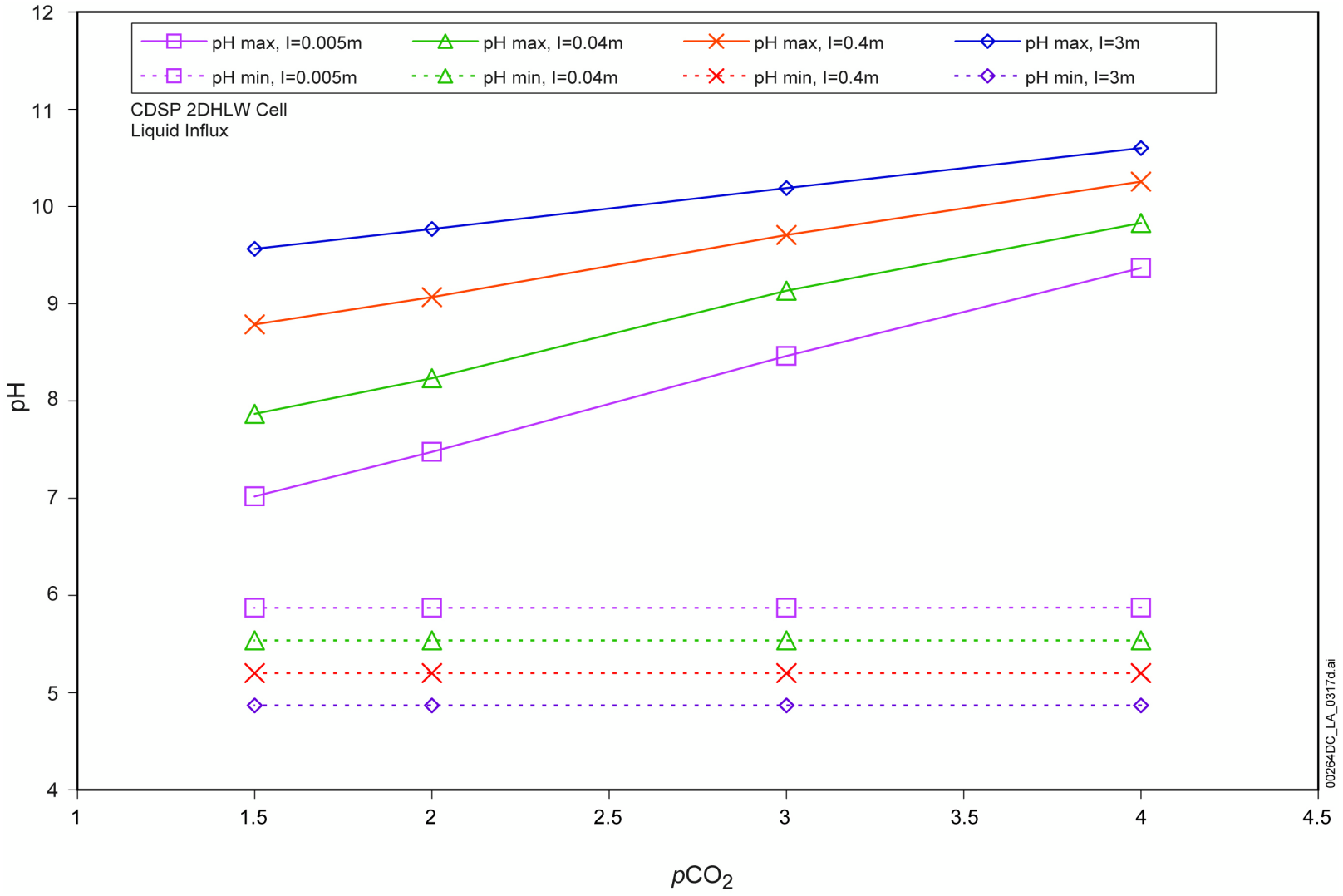

Figure 2.3.7-20. 2-DHLW Liquid-Influx Minimum and Maximum pH Values Versus pCO_2 for Various Ionic Strengths

Source: SNL 2007e, Figure 6-42[a].

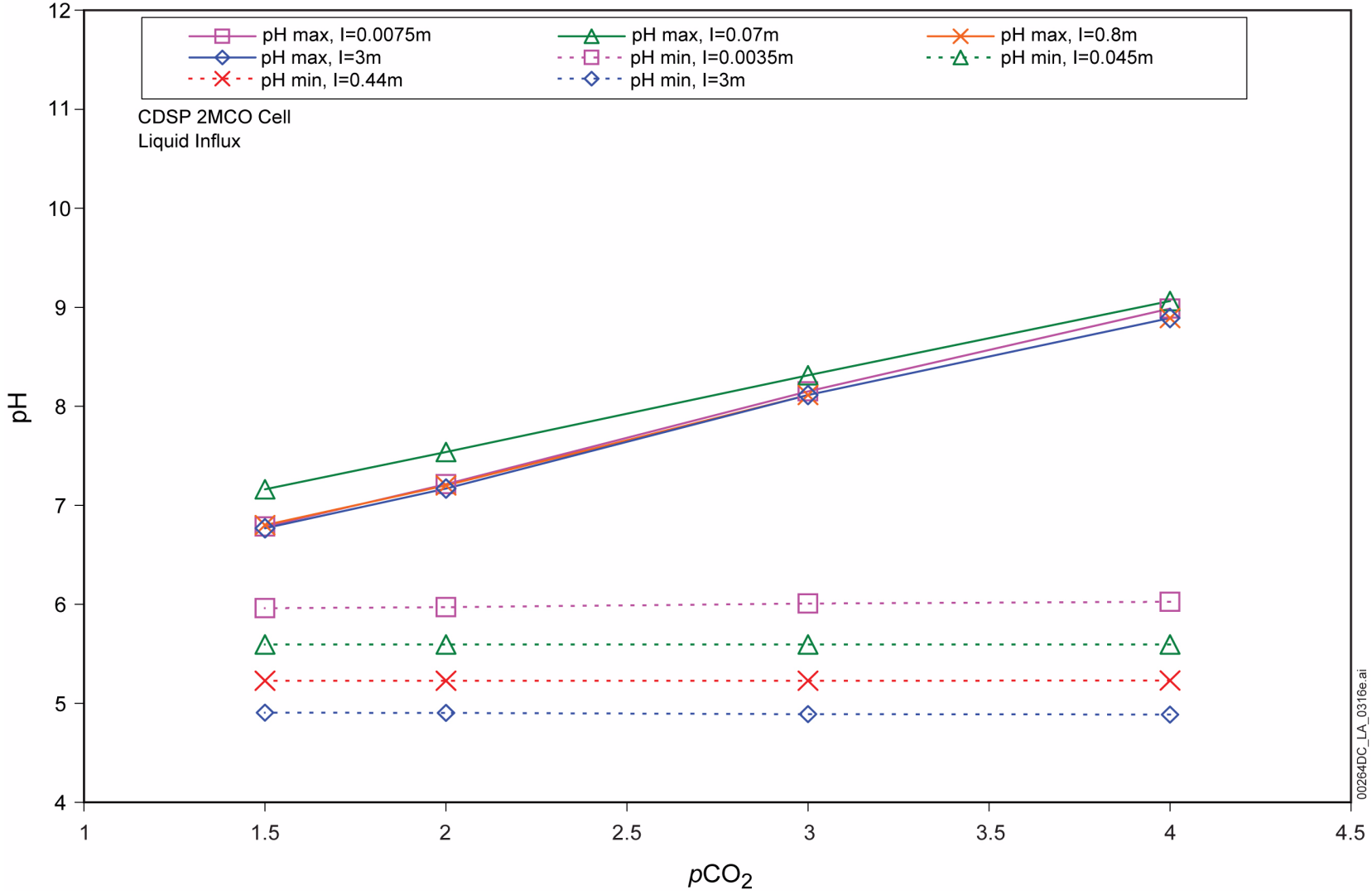

Figure 2.3.7-21. 2-MCO Liquid-Influx Minimum and Maximum pH Values Versus pCO_2 for Various Ionic Strengths

Source: SNL 2007e, Figure 6-43[a].

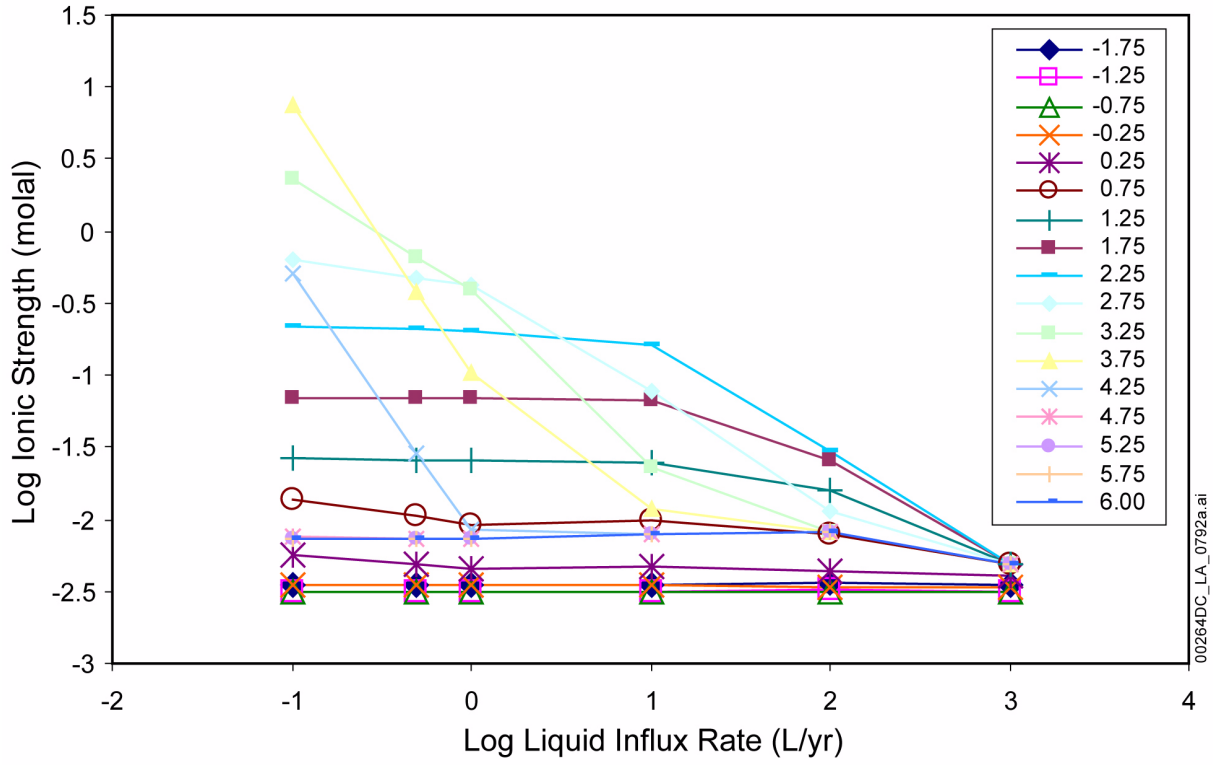

Figure 2.3.7-22. Commercial SNF Ionic Strength Versus Liquid-Influx Rate at Various Values of Log time (year)

Source: SNL 2007e, Figure 6-47[a].

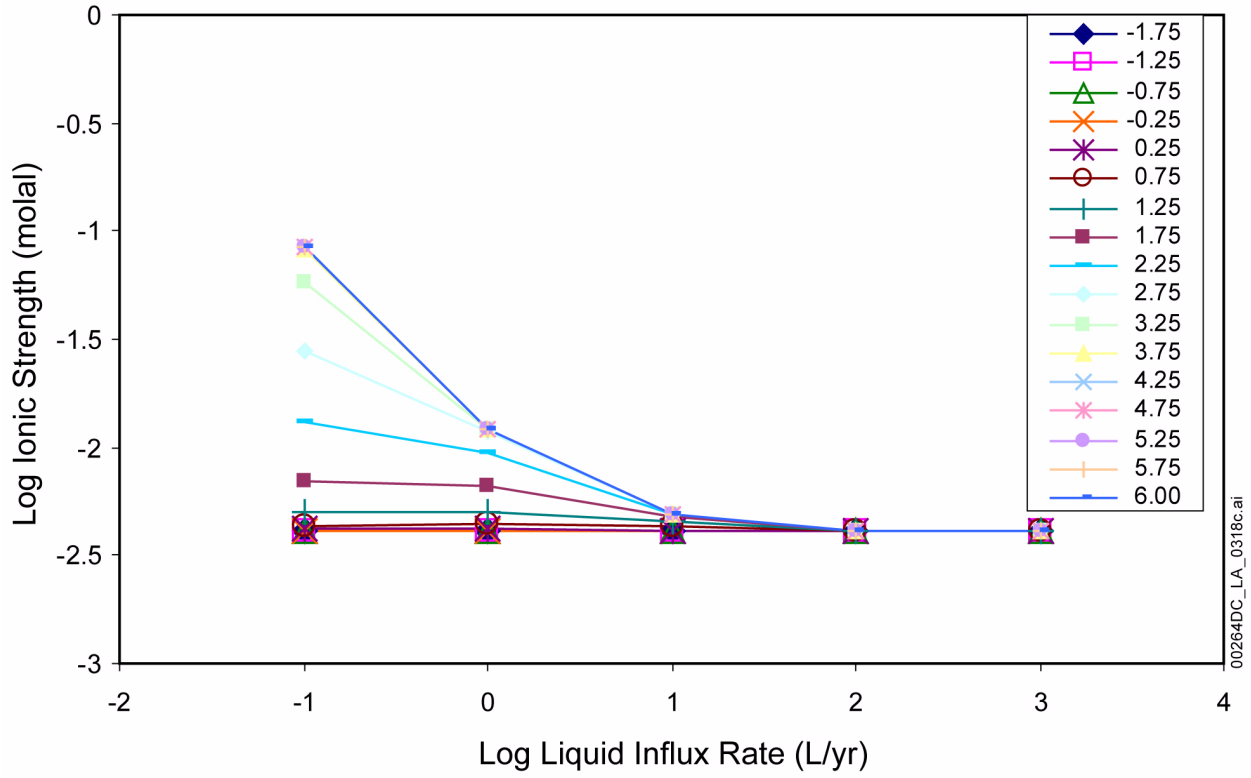

Figure 2.3.7-23. 2-DHLW Ionic Strength Versus Liquid-Influx Rate at Various Values of Log time (year)

Source: SNL 2007e, Figure 6-48[a].

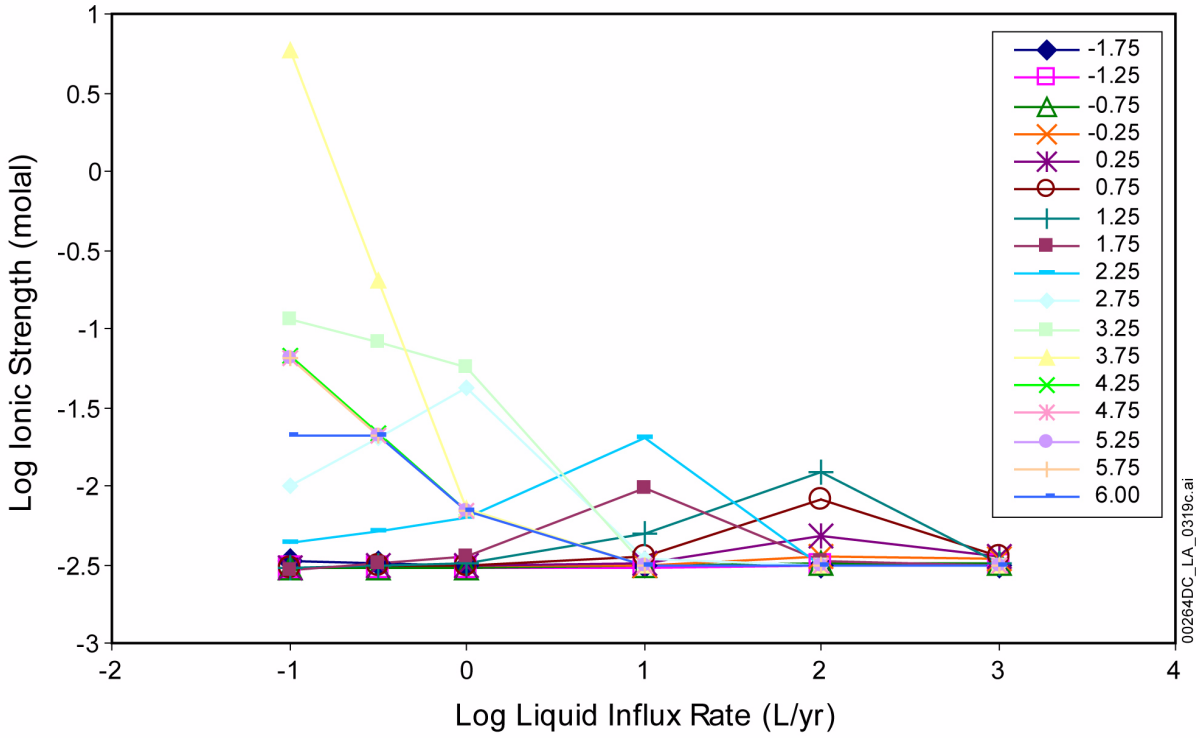

Figure 2.3.7-24. 2-MCO Ionic Strength Versus Liquid-Influx Rate at Various Values of Log time (year)

Source: SNL 2007e, Figure 6-49[a].

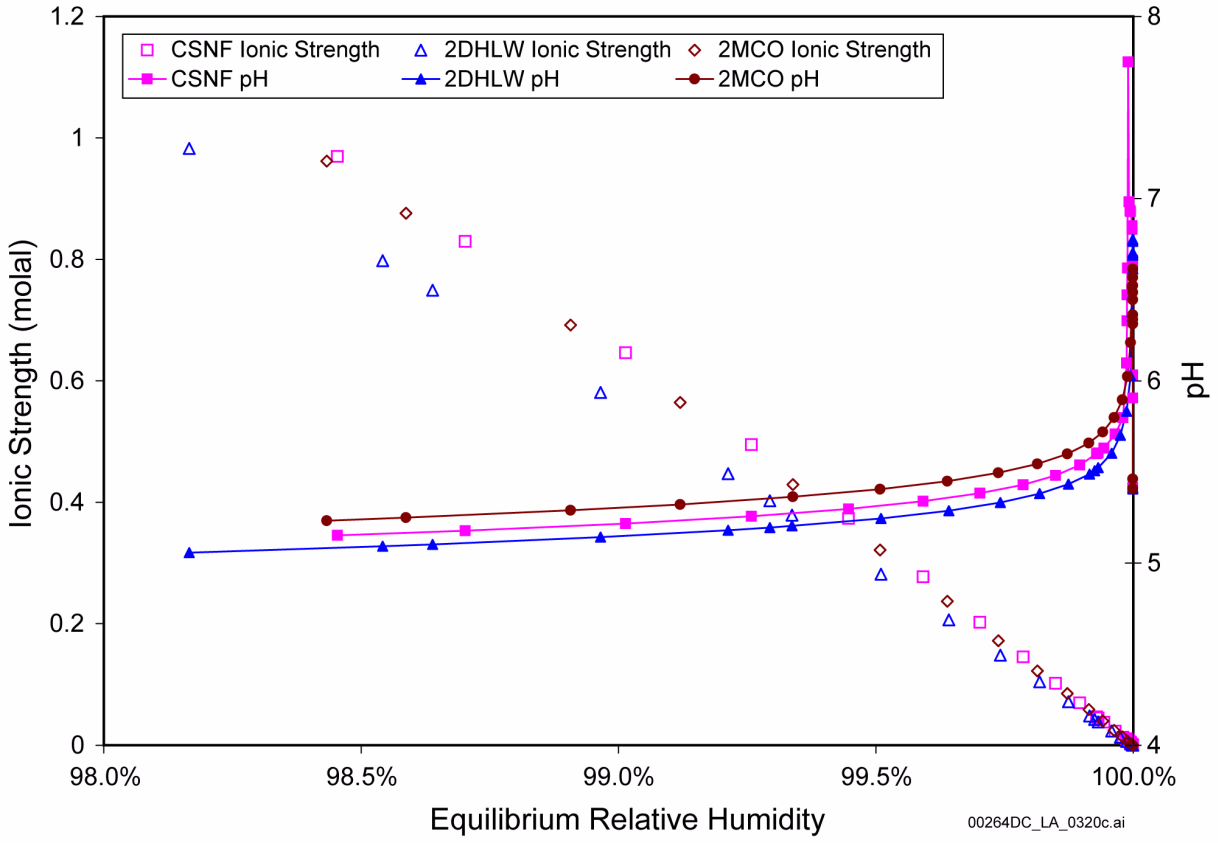

Figure 2.3.7-25. Vapor-Influx Base Case pH and Ionic Strength Versus Equilibrium Relative Humidity

Source: SNL 2007e, Figure 6-13[a].

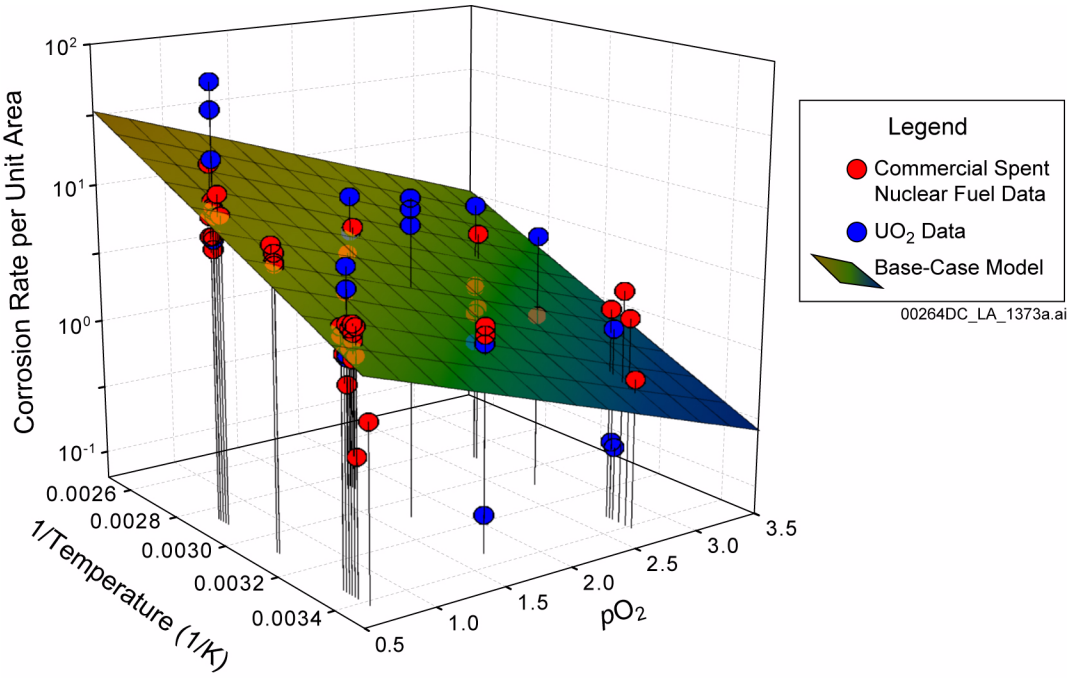

Figure 2.3.7-26. Comparison of the Base-Case Alkaline Conditions Model (pCO_3 = 2.7) to the Input Commercial SNF and UO_2 Data

Source: BSC 2004b, Figure 6-3.

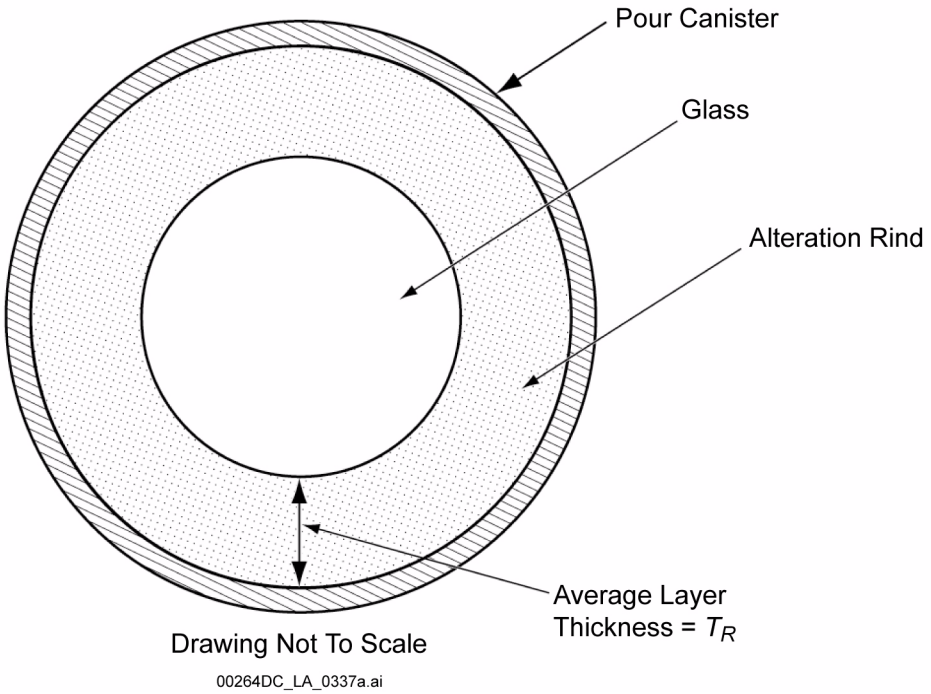

Figure 2.3.7-27. Schematic Drawing of Canister Cross Section Showing Conceptual Model of Degradation of High-Level Radioactive Waste Glass Logs

Source: BSC 2004d, Figure D-1.

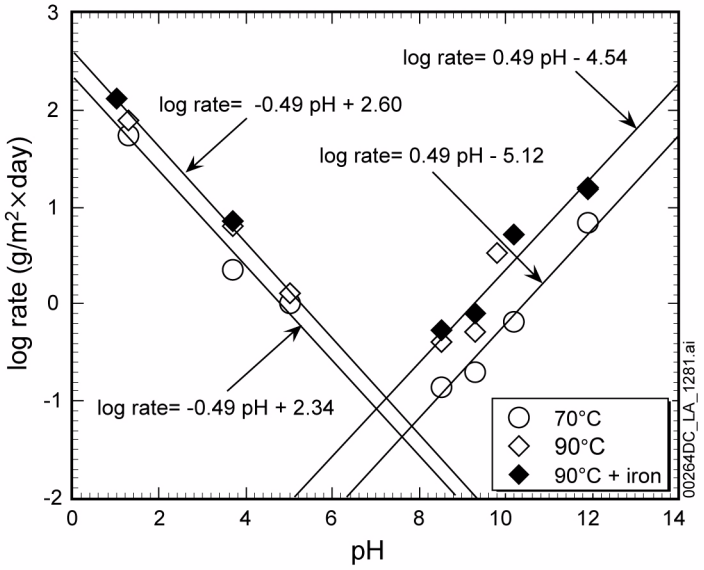

Figure 2.3.7-28. The pH and Temperature-Dependent Glass Degradation Rates

Source: BSC 2004d, Figure 6-2.

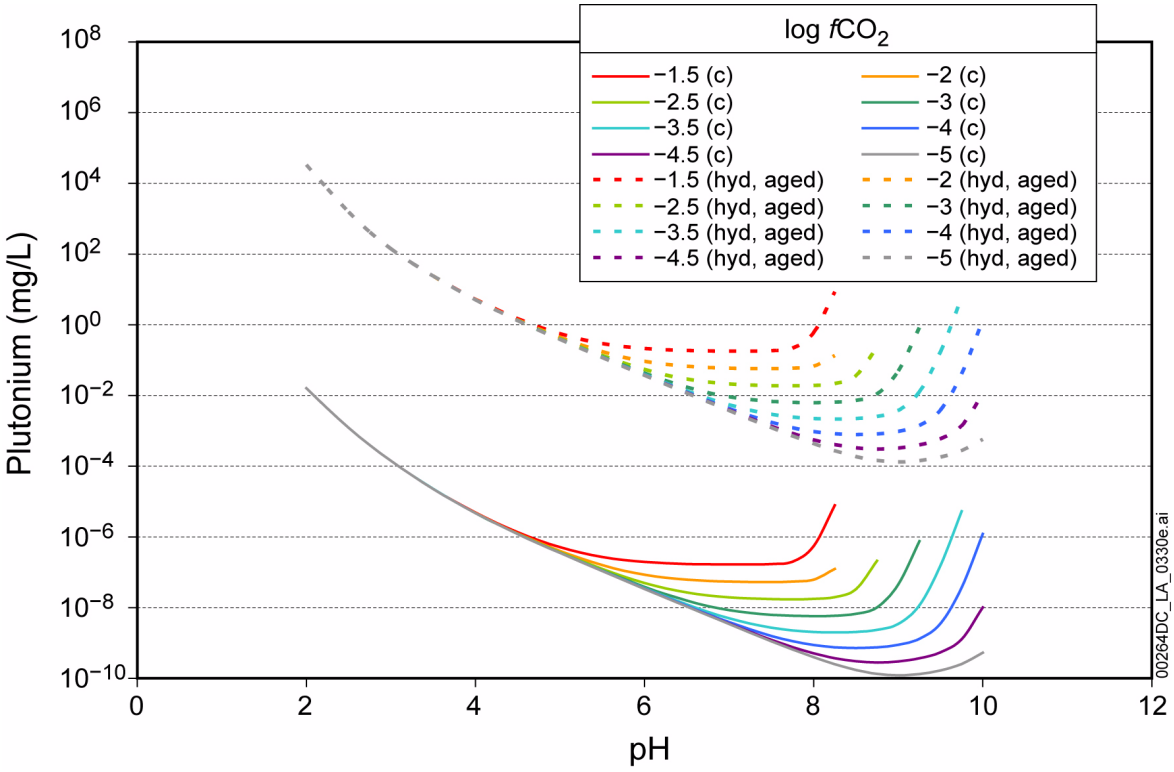

Figure 2.3.7-29. Base-Case Plutonium Solubility (Adjusted Eh Model) for Crystalline PuO_2(c) and PuO_2(hyd,aged)

Source: SNL 2007h, Table 6.5-1.

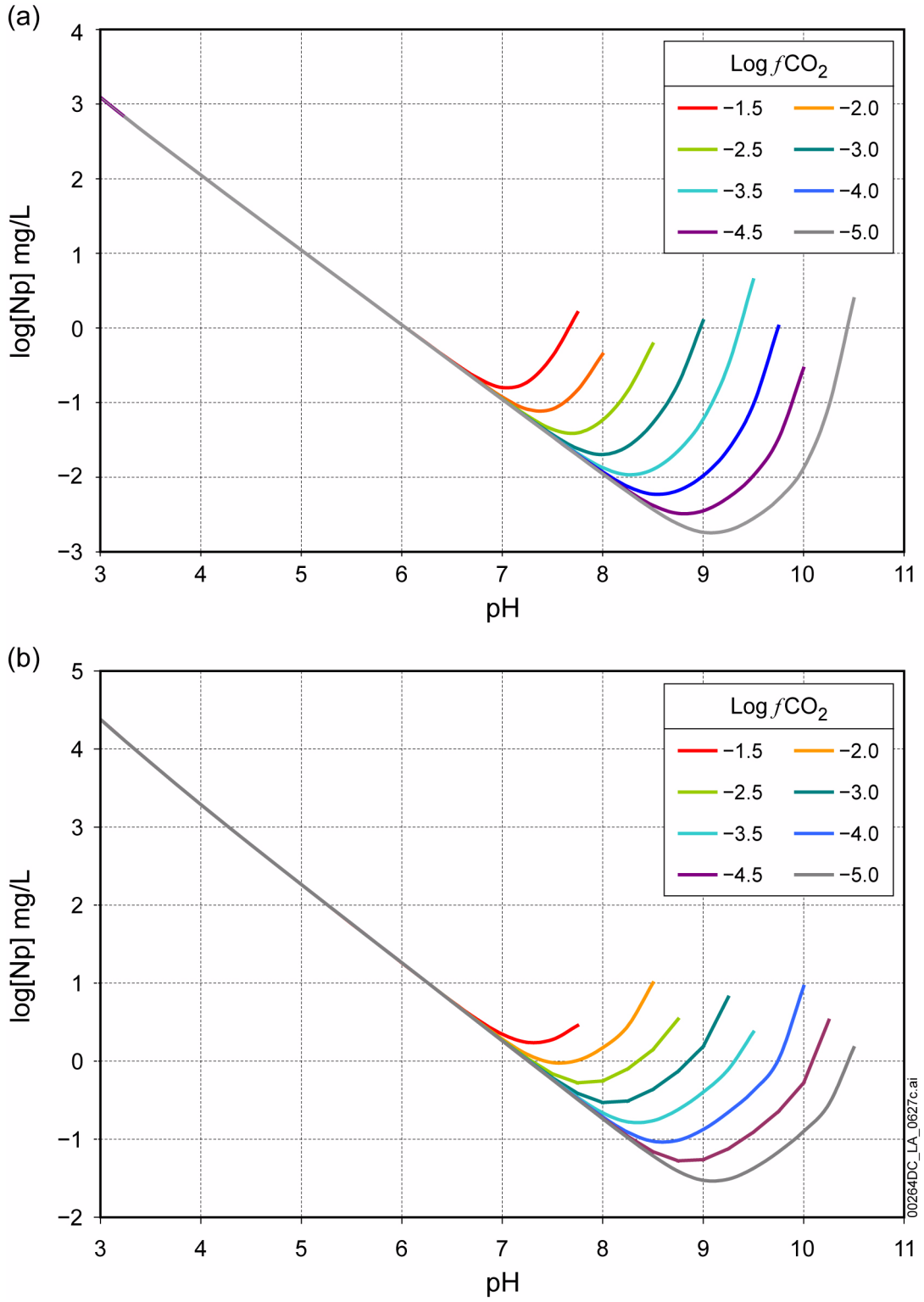

Figure 2.3.7-30. (a) Base-Case Neptunium Solubility Inside the Corroding Waste Package (NpO_2); (b) Base-Case Neptunium Solubility for the Invert (Np_2O_5)

Source: (a) SNL 2007h, Figure 6.6-1; (b) SNL 2007h, Figure 6.6-2.

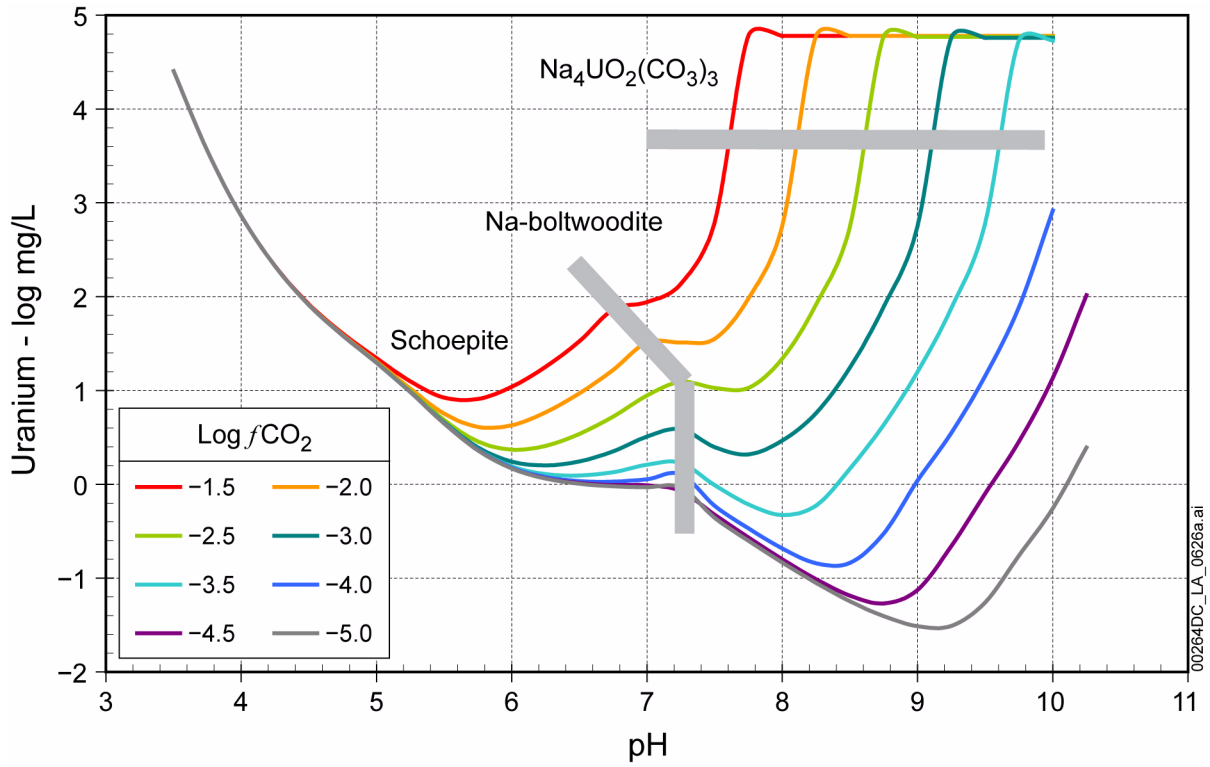

Figure 2.3.7-31. Uranium Solubility Modeled as a Function of fCO_2 and pH for Commercial SNF Waste Packages Breached by a Hypothetical Igneous Intrusive Event, Codisposal Waste Packages Under Any Breach Scenario, and Waters in the Invert

NOTE: Shaded areas are between pH-fCO_2 regions controlled by indicated minerals.

Source: SNL 2007h, Figure 6.7-2.

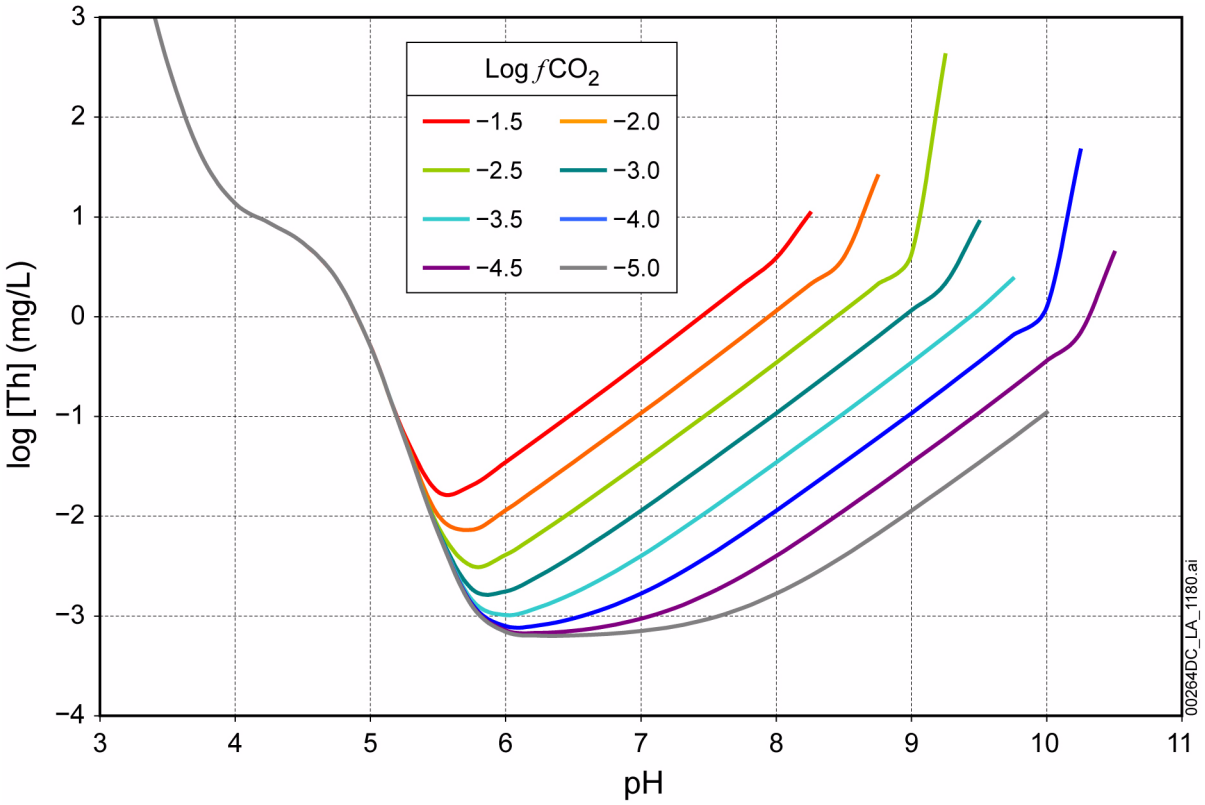

Figure 2.3.7-32. ThO_2(am) Solubility Modeled as a Function of fCO_2 and pH

Source: SNL 2007h, Figure 6.8-1.

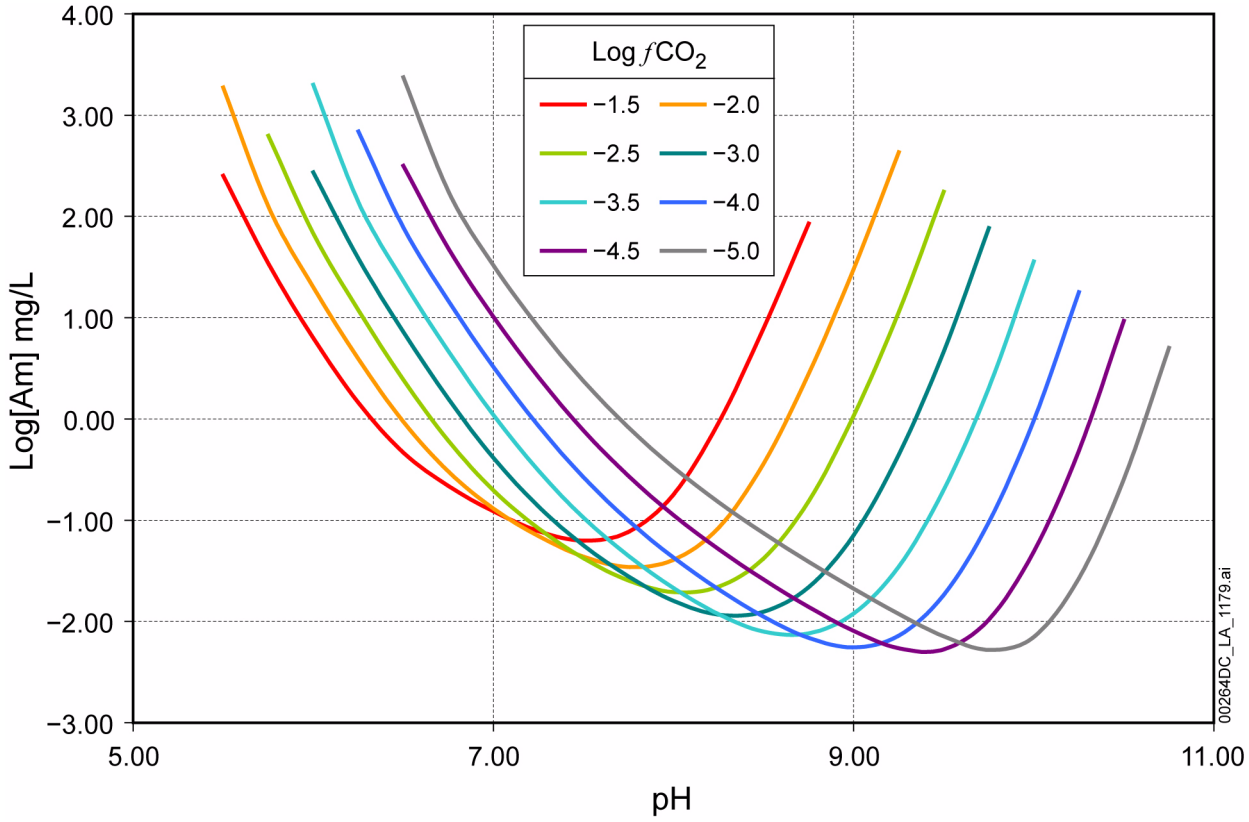

Figure 2.3.7-33. $AmOHCO_3$ Solubility Modeled as a Function of fCO_2 and pH

Source: SNL 2007h, Figure 6.9-3.

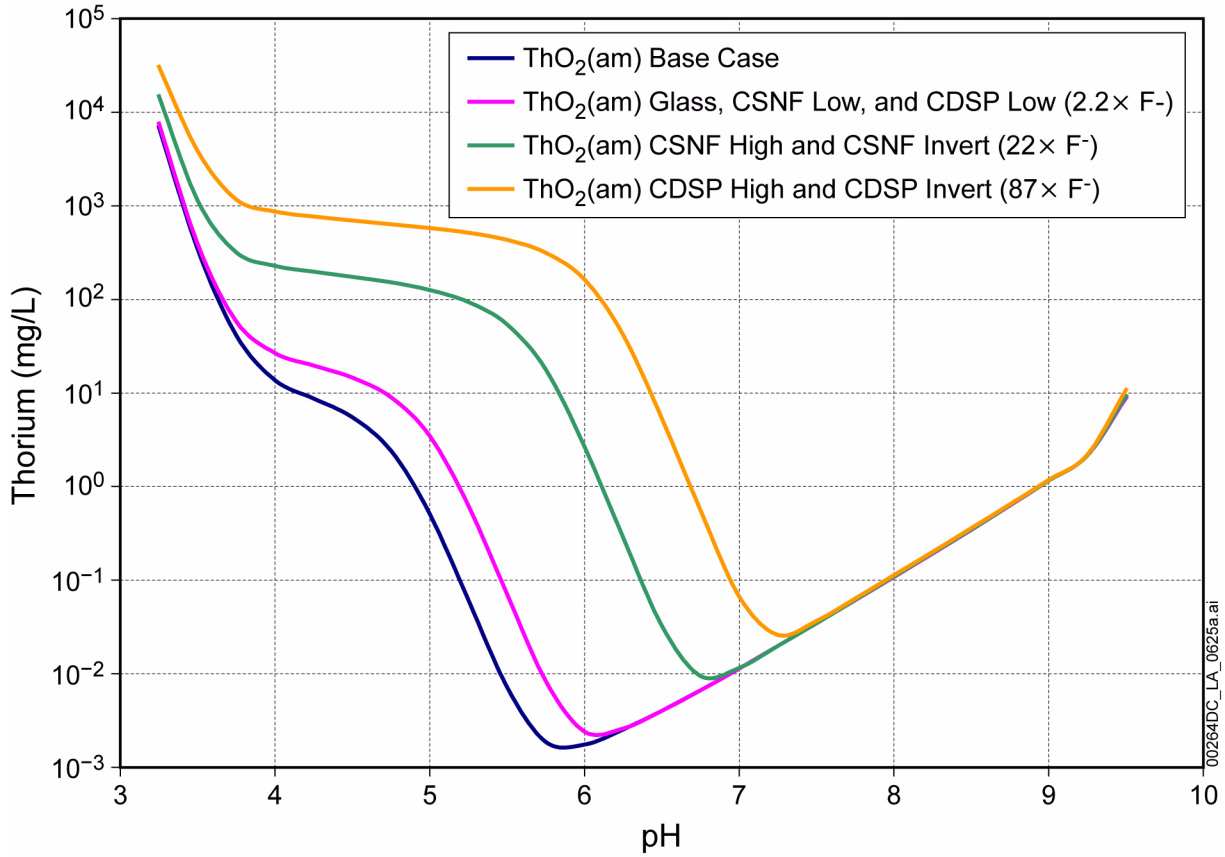

Figure 2.3.7-34. ThO_2(am) Solubility at log(fCO_2) = –3.0 as a Function of pH and F^- Concentration

Source: SNL 2007h, Figure 6.8-5.

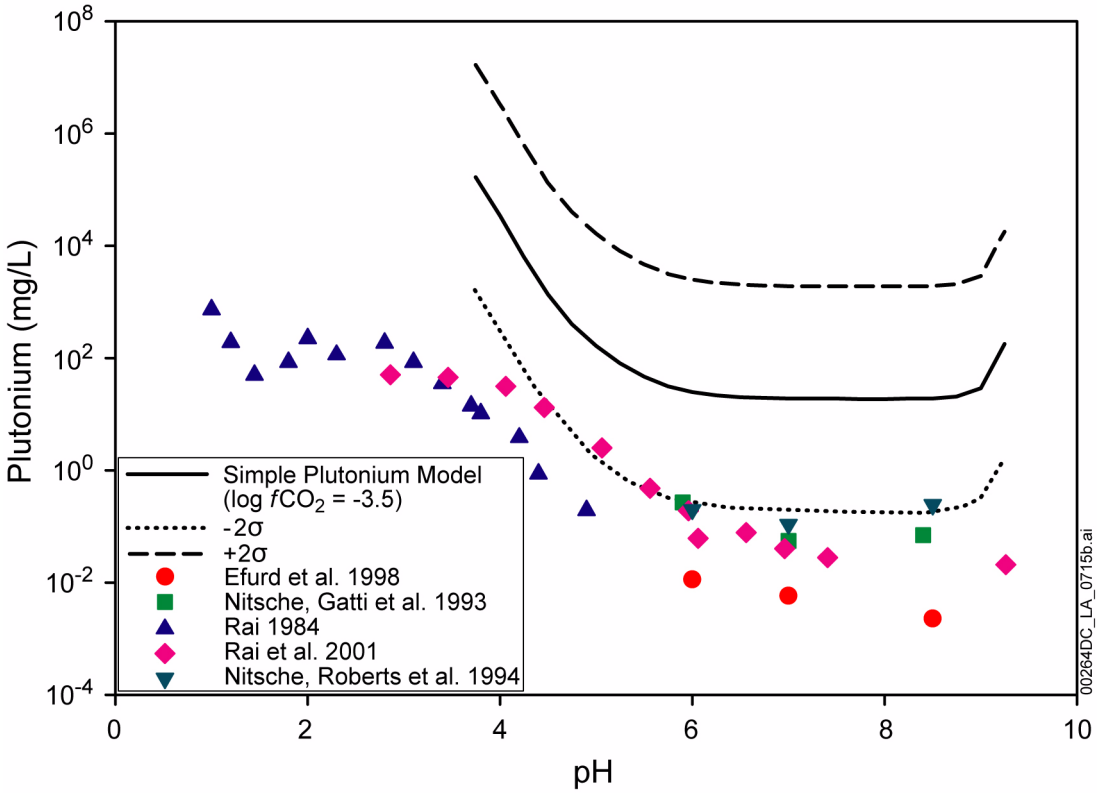

Figure 2.3.7-35. Comparison of the Theoretical (Atmospheric) fCO_2, PuO_2 (hyd,aged) Model with Plutonium Solubility Measurements

NOTE: Modeled results are for log fCO_2 = –3.5 bars and fO_2 = 0.2 along with plutonium-solubility measurements from five experiments (Rai 1984;Nitsche, Gatti et al. 1993; Nitsche, Roberts et al. 1994; Efurd et al. 1998; Rai et al. 2001).

Source: SNL 2007h, Figure V-2.

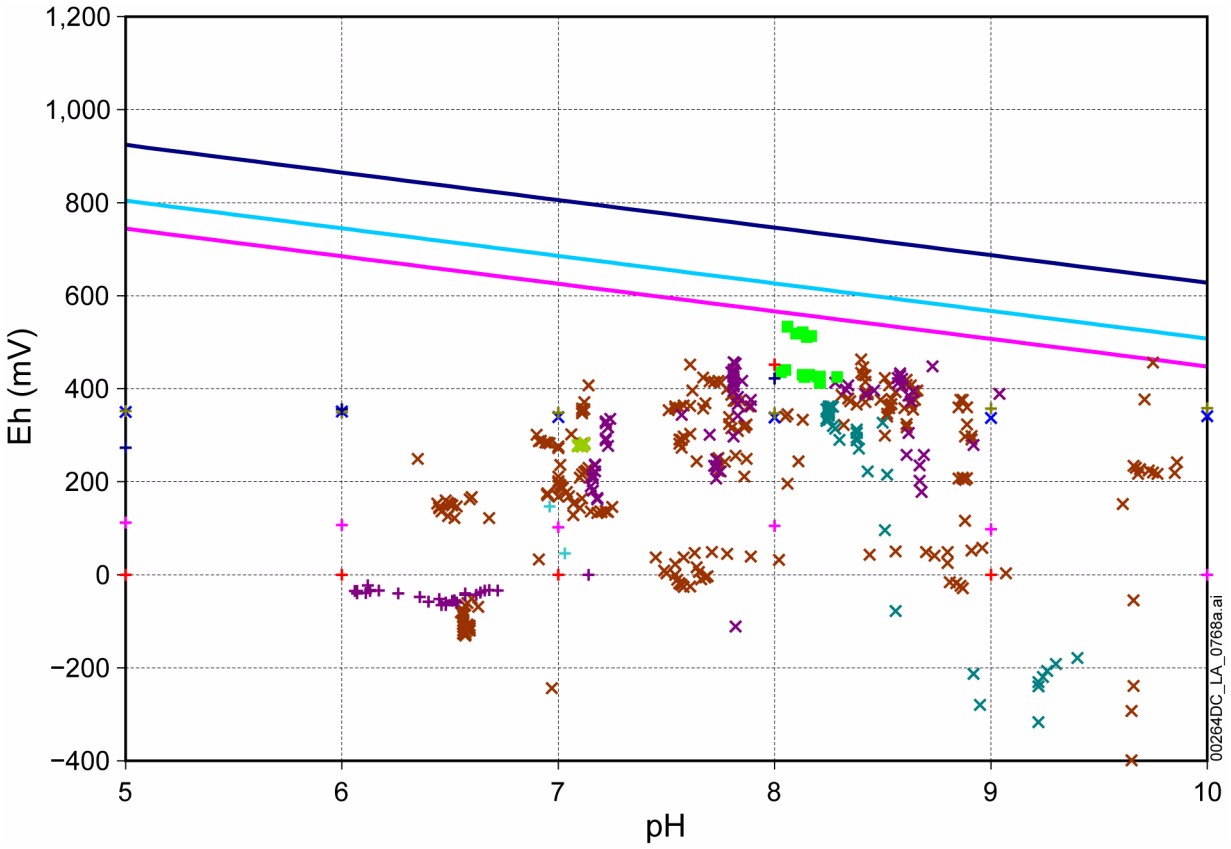

Figure 2.3.7-36. Eh-pH Measurements at Yucca Mountain Compared Against Theoretically Calculated Eh-pH Relationships

NOTE: The upper line shows the theoretical oxidation potential at fO_2 = 0.2 bars and the lower line shows the upper limit for empirical Eh measurements in natural waters. The middle line shows the adjusted Eh. Modeled results are for log fCO_2 = –3.5.

Source: SNL 2007h, Figure V-6.

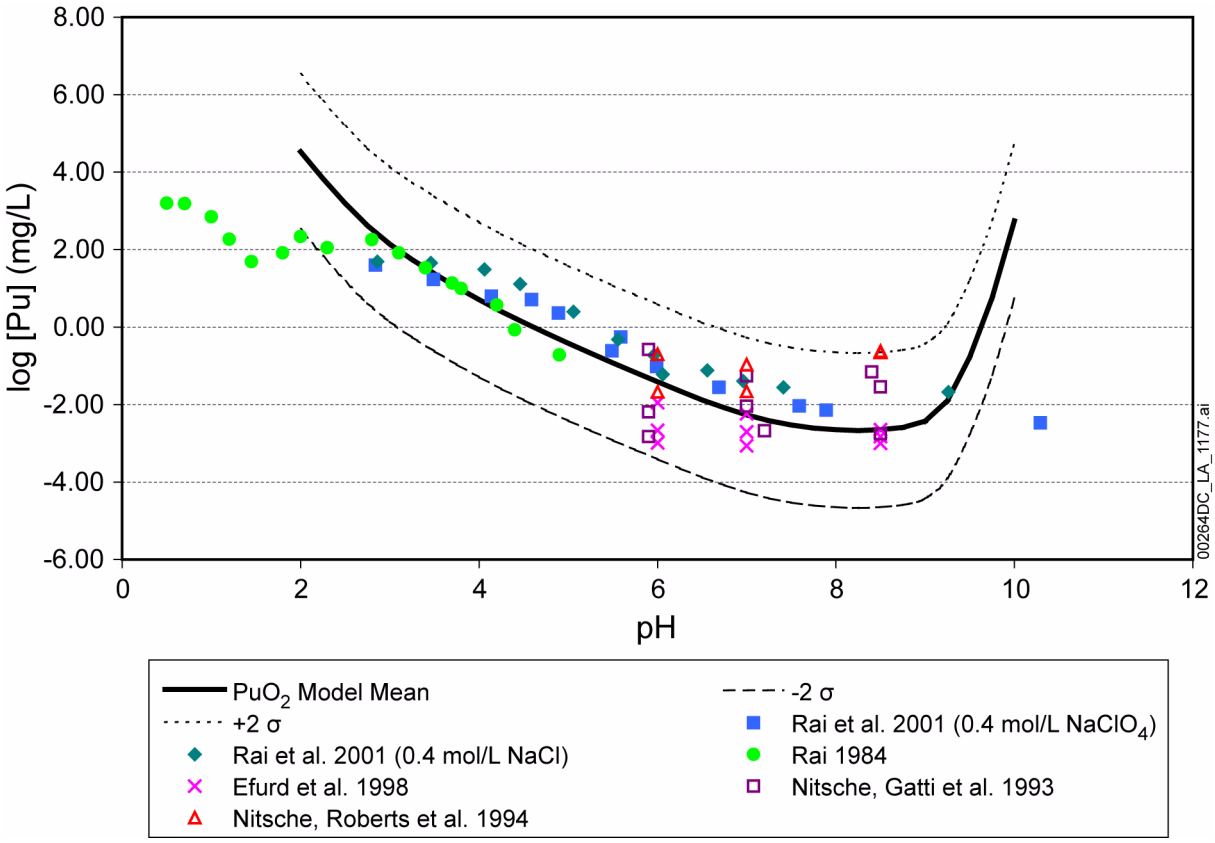

Figure 2.3.7-37. Comparison of Experimental Data with the Predictions of the Plutonium-Solubility Using Equation 2.3.7-11 to Calculate Eh

NOTE: These calculations were carried out at log P_{CO2} of -3.5 along with plutonium-solubility measurements from six experiments (Rai 1984; Nitsche, Gatti et al. 1993; Nitsche, Roberts et al. 1994; Efurd et al. 1998; Rai et al. 2001).

Source: SNL 2007h, Figure 6.5-6.

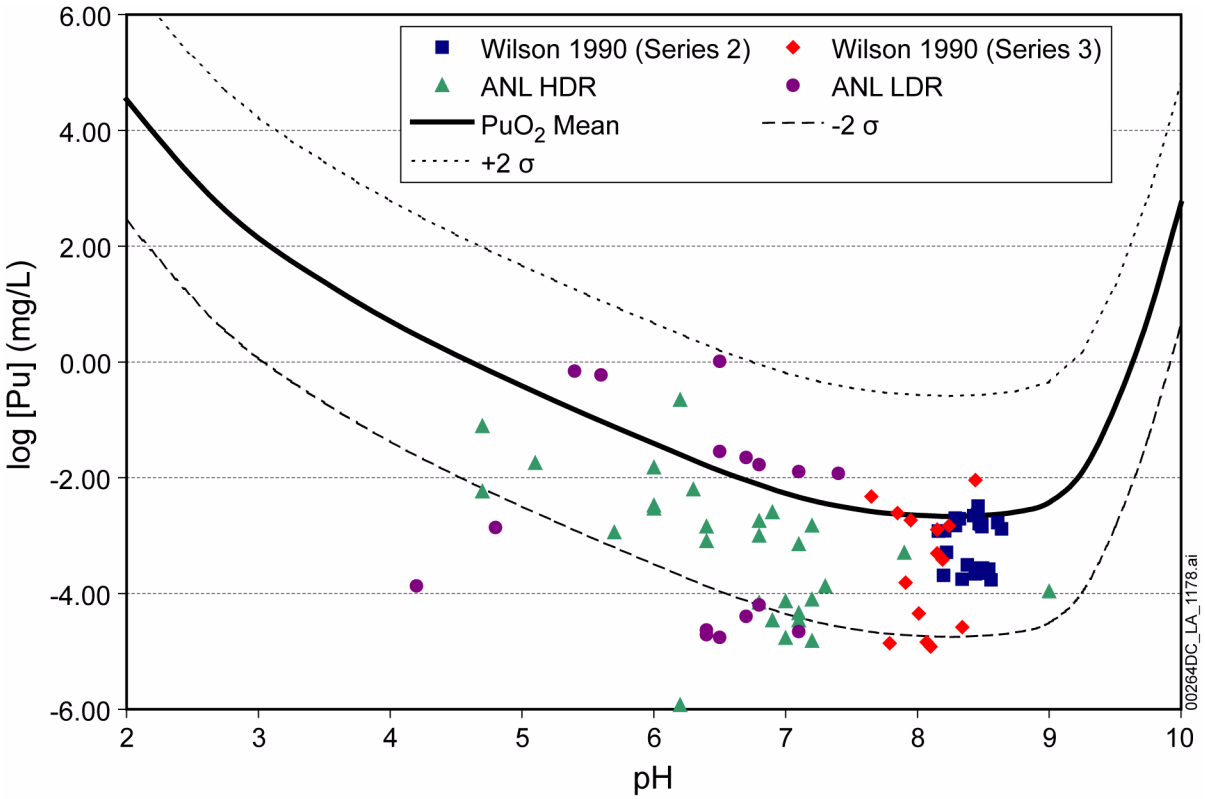

Figure 2.3.7-38. Comparison of the PuO_2 (hyd,aged) Model with Spent Fuel Leaching Measurements

NOTE: Wilson 1990; Wilson 1990 (Series 2 and Series 3 tests, respectively); CRWMS M&O 2000b; CRWMS M&O 2000c for ANL high-drip rate and low-drip rate tests.
HDR = high-drip rate; LDR = low-drip rate.

Source: SNL 2007h, Figure 7-1.

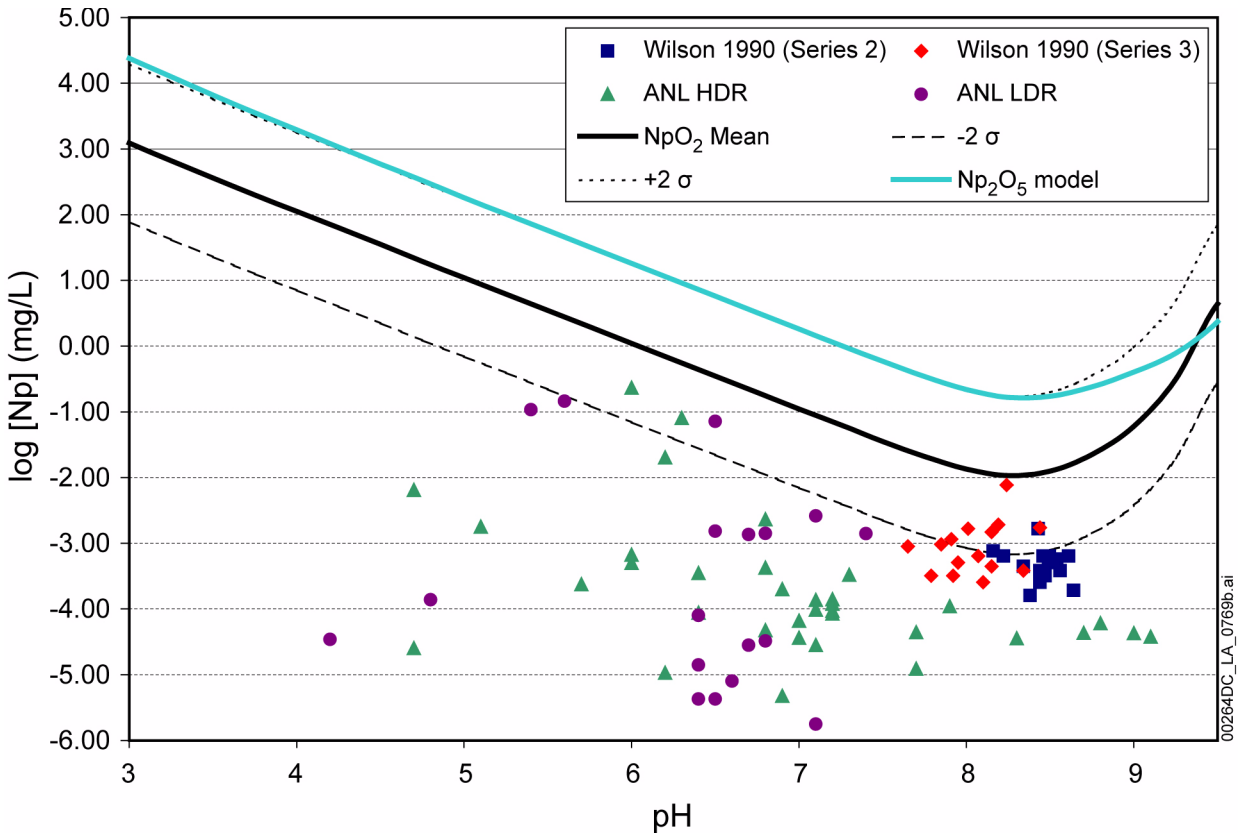

Figure 2.3.7-39. Comparison of Neptunium-Solubility Models at log fCO_2 = -3.5 bars with Laboratory Measurements

NOTE: In-package (NpO_2) and ex-package (e.g., invert) (Np_2O_5) models are shown. The NpO_2 and Np_2O_5 models include $NaNpO_2CO_3$ at high pH values. Wilson 1990; Wilson 1990 (Series 2 and Series 3 tests, respectively); CRWMS M&O 2000b; CRWMS M&O 2000c; Thomas 2004 for ANL high-drip rate and low-drip rate tests. HDR = high-drip rate; LDR = low-drip rate.

Source: SNL 2007h, Figure 7-3.

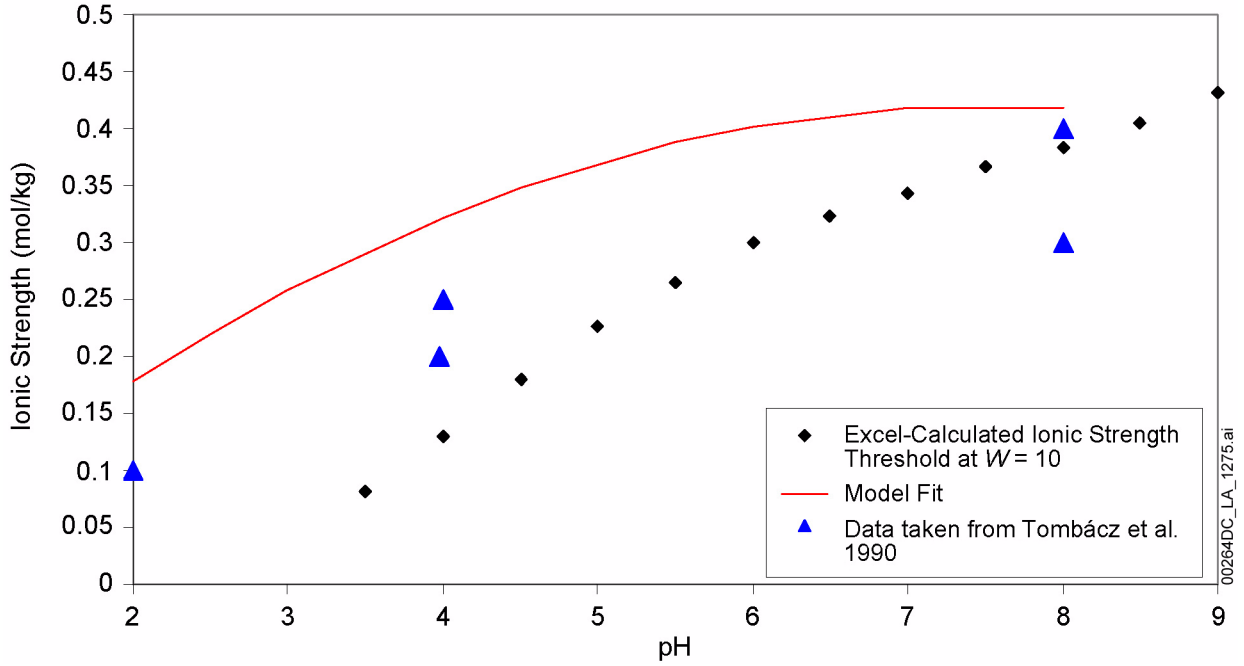

Figure 2.3.7-40. Plot showing the Derjaguin, Landau, Verwey, and Overbeek Model-Calculated Stability of Montmorillonite Colloids at W = 10 with a Quadratic Fit to the Model and Experimental Values

NOTE: Experimental values from Tombácz et al. (1990).

Source: SNL 2007i, Figure 6-9.

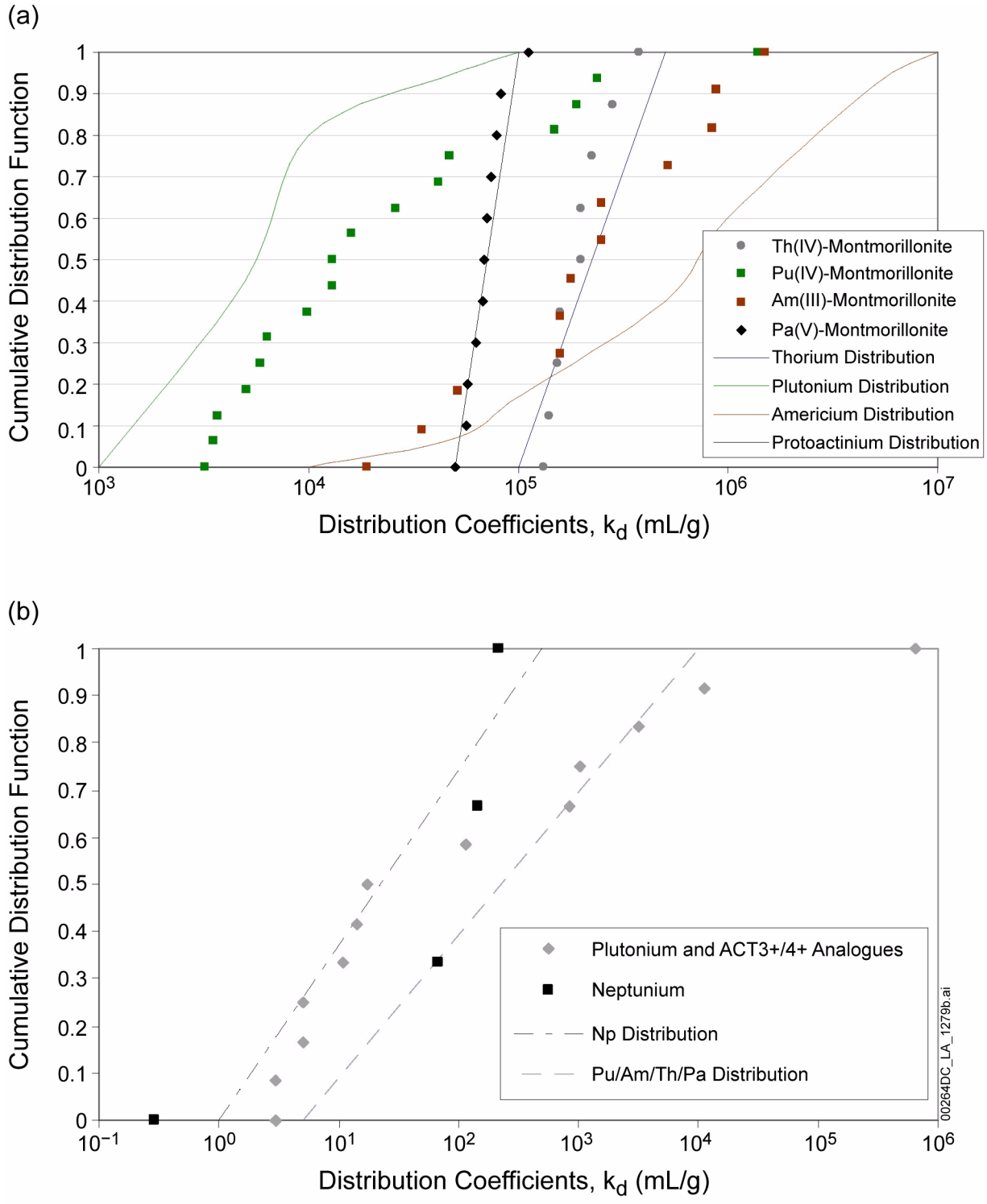

Figure 2.3.7-41. Radionuclide Sorption Distribution Coefficients on Montmorillonite (a) and Uranophane (b)

Source: SNL 2007i, Figures 6-24c and 6-16.

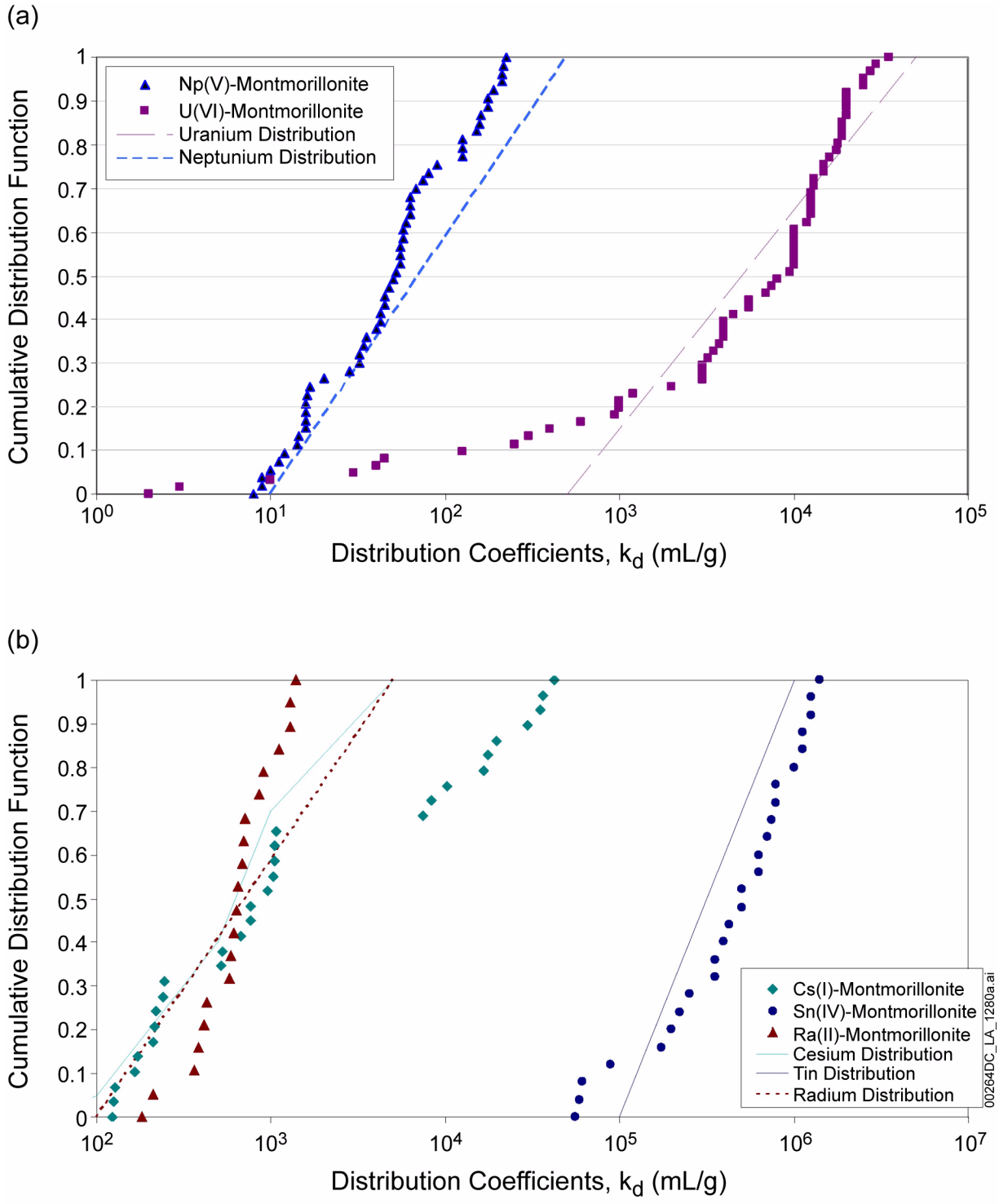

Figure 2.3.7-42. Radionuclide Sorption Distribution Coefficients on Montmorillonite (Smectite)

Source: SNL 2007i, Figures 6-24a and 6-24b.

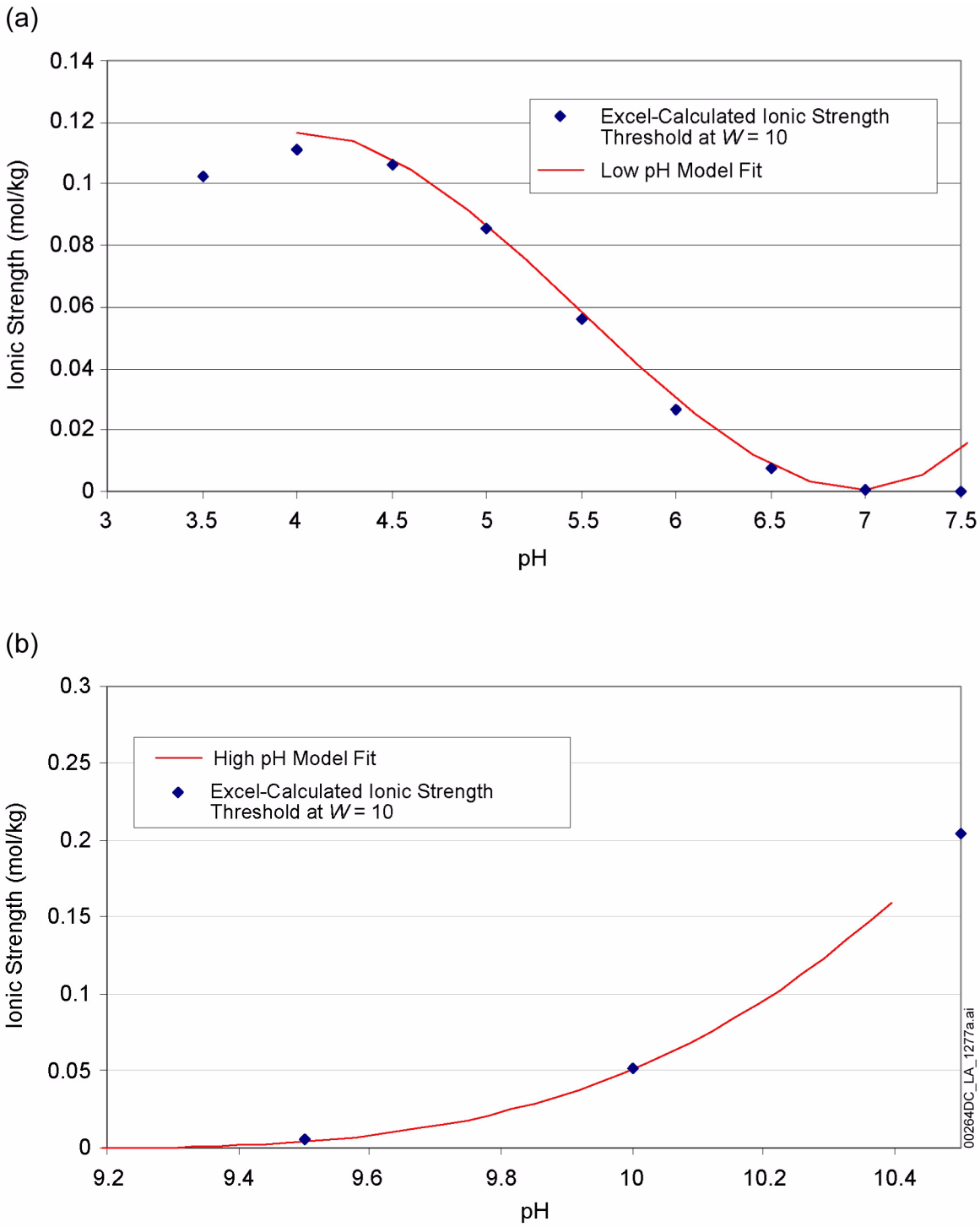

Figure 2.3.7-43. Calculated Derjaguin, Landau, Verwey, and Overbeek Model-Stability Plots with Polynomial Fit to the Model for ZrO_2 Colloids Suspensions at High pH

Source: SNL 2007i, Figures 6-12a and 6-12b.

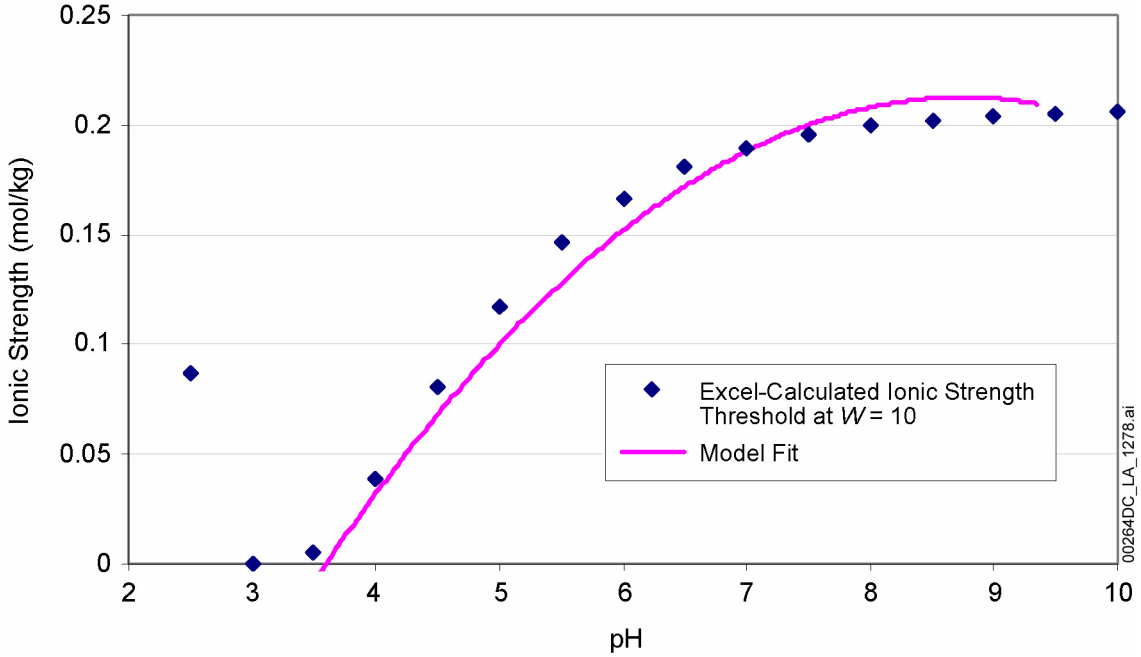

Figure 2.3.7-44. Calculated Stability Plots with a Polynomial Fit to the Derjaguin, Landau, Verwey, and Overbeek Model for Uranophane Colloid Suspensions

Source: SNL 2007i, Figure 6-14.

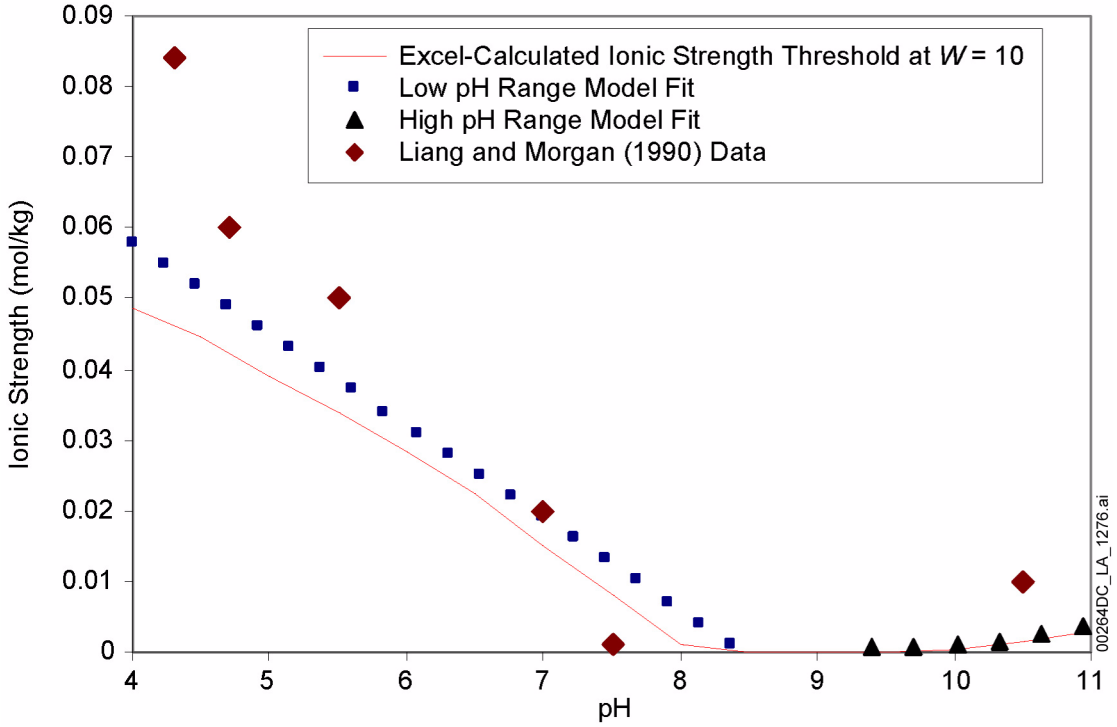

Figure 2.3.7-45. Calculated Stability Plot for Hematite with Fits to the Derjaguin, Landau, Verwey, and Overbeek Model at the Low and High pH Regions and Experimental Values from Liang and Morgan (1990, Figure 1, p. 40)

Source: SNL 2007i, Figure 6-5.

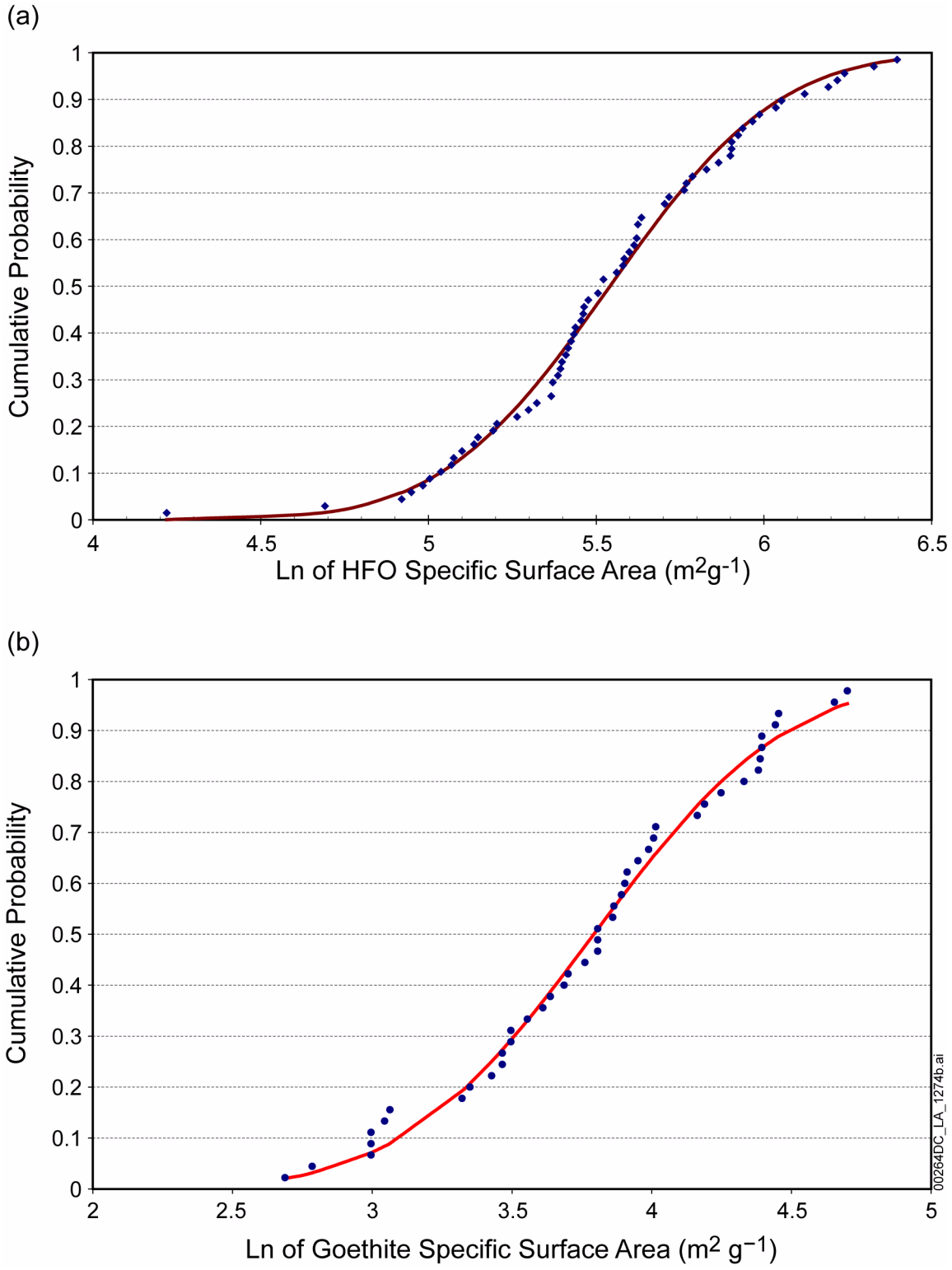

Figure 2.3.7-46. Iron Oxide Surface Area Distributions

NOTE: Dots are observed. Lines are fits of a log normal distribution to the data.

Source: SNL 2007a, Appendix K, Figures K-4 and K-5.

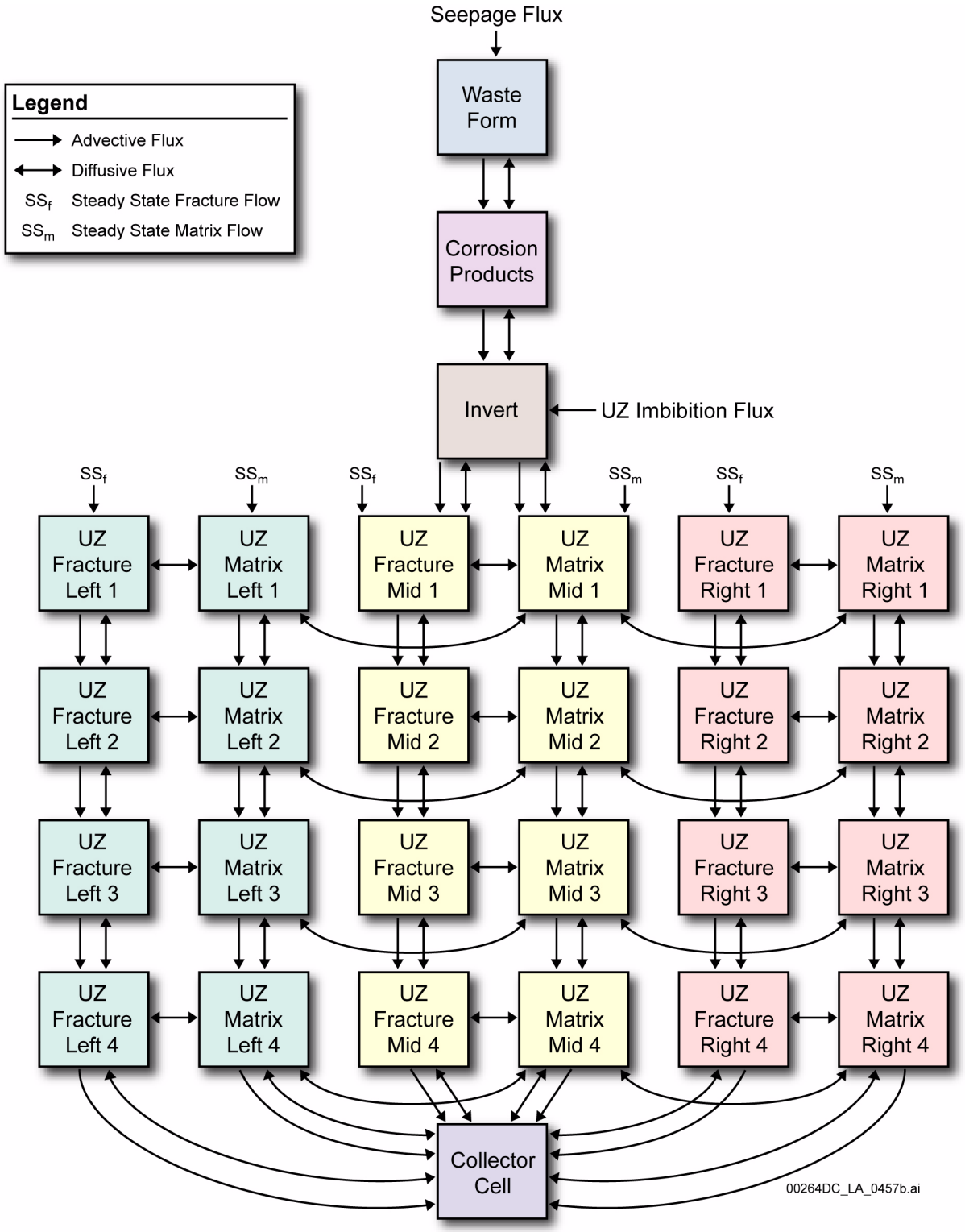

Figure 2.3.7-47. Computational Grid in the Engineered Barrier System–Unsaturated Zone Interface Model

Source: SNL 2007a, Figure 6.5-20.

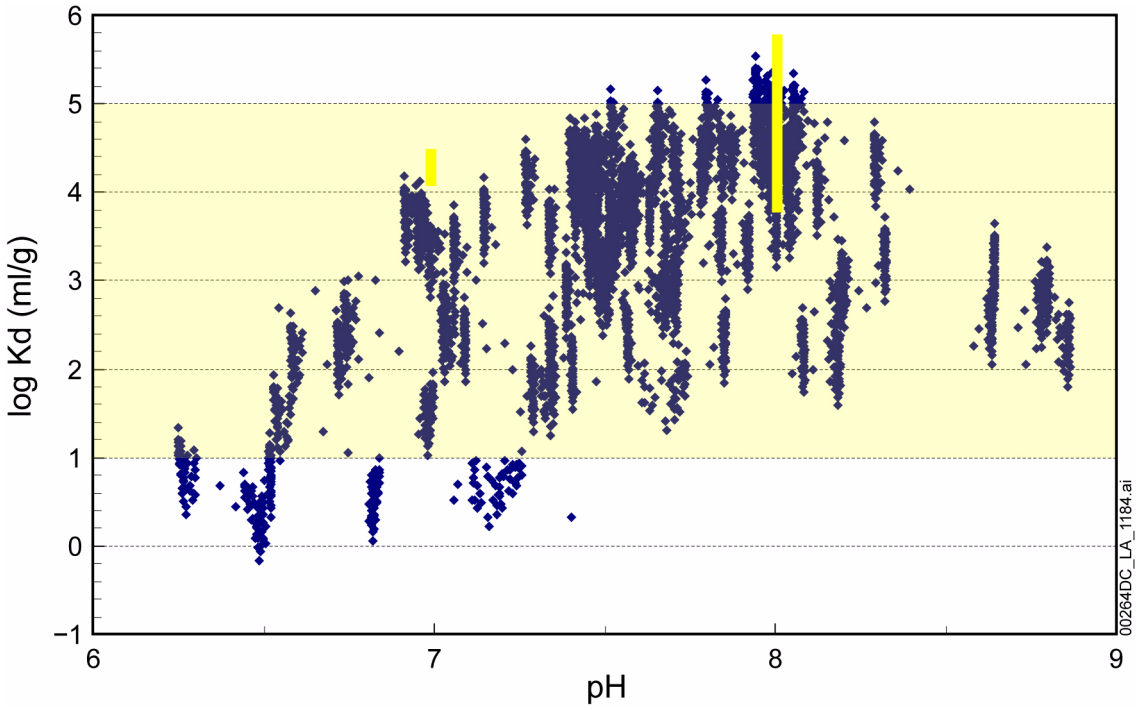

Figure 2.3.7-48. EPA Plutonium Soil *Kd*s and Competitive Surface Complexation Model Iron Oxide K_ds

NOTE: The yellow bar at pH 8 is the range of plutonium K_ds measured on hematite colloids by Lu et al. (2000); pH varied by roughly a unit. The yellow bar at pH 7 shows estimated plutonium K_ds from Sanchez et al. (1985). The blue dots are competitive surface complexation model predicted K_ds, and the broad horizontal pale yellow band is the EPA K_ds.